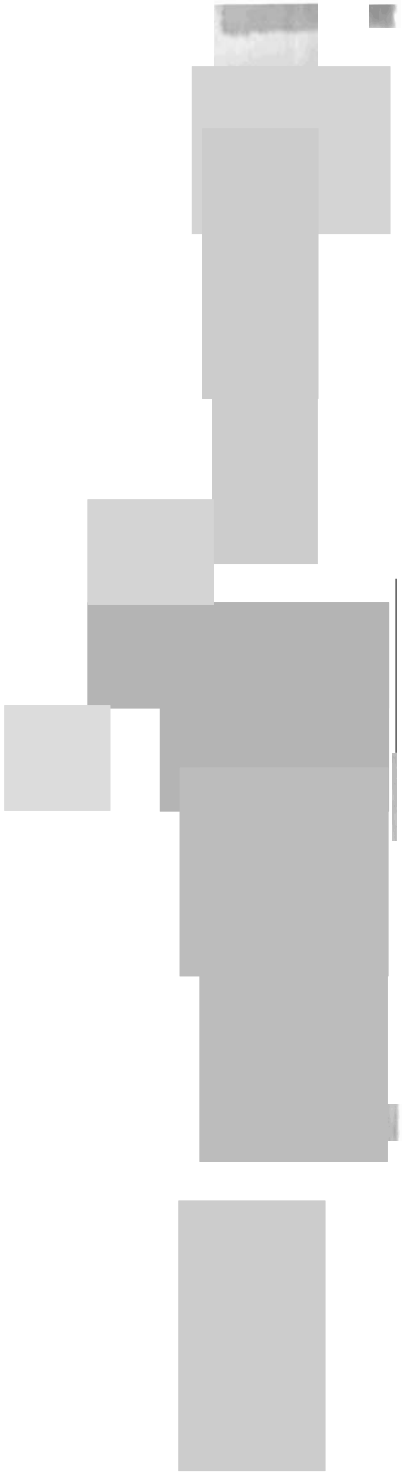

SOLIDIFICATION AND CASTING

G. J. DAVIES

Department of Metallurgy and Materials Science
University of Cambridge
Fellow of St. Catharine's College

APPLIED SCIENCE PUBLISHERS LTD
LONDON

SOLIDIFICATION AND CASTING

G. J. DAVIES

Department of Metallurgy and Materials Science
University of Cambridge
Fellow of Sr. Catharine's College

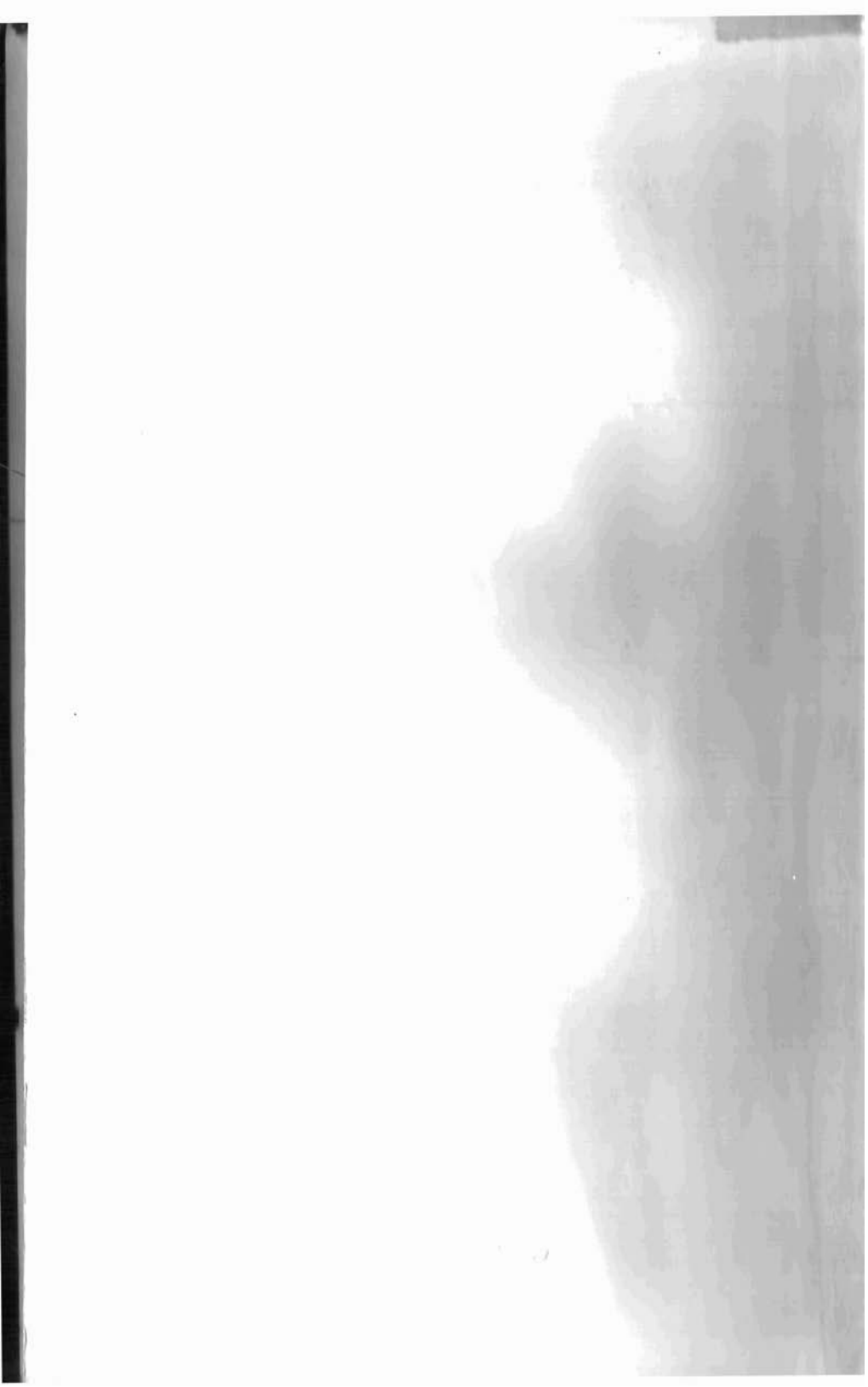

APPLIED SCIENCE PUBLISHERS LTD
LONDON

APPLIED SCIENCE PUBLISHERS LTD
RIPPLE ROAD, BARKING, ESSEX, ENGLAND

ISBN: 0 85334 556 2

WITH 13 TABLES AND 138 ILLUSTRATIONS

Printed in Great Britain by Galliard Limited, Great Yarmouth, Norfolk, England.

Preface

The study of the solidification of metals has assumed considerable proportions in recent years. This is incontrast to theneglect this subject suflered in earlier years. This neglect was particularly unfortunate since essentially all metals undergo the liquid-to-solid transformation at some stage. Only those few metals which are produced and used in powder form can be excepted. In many cases peculiaritiesof grain structure, composition and phase distribution result from solidification and these seriously influence subsequent treatments and properties.

It is essential for the metallurgist and the engineer to understand the underlying mechanisms involved in solidification if they are to be able to exercise some control over the structure and composition of the solidified metal. It must bc admitted that in many cases complete details of meclianisms arc not yet known. Nevertheless sufficient information is available to allow the making of predictions with a degree of confidence.

The objective of this monograph is to present a coherent and continuous development of this information.

Initially the structure of liquid metals will be considered and then the development will progress through nucleation and growth to an understanding of the important parameters affecting solidification and the distribution of solute during solidification. Up to this stage the emphasis will mainly be on processes at an atomic or microlevel. Attention will then be given to the study of solidification processes at the macrolevel. This will involve the examination of multiphase solidification, segregation and the factors which determine the structure of castings. Particular emphasis will be placed on ways in which the structure can be controlled.

It is these macroscopic considerations that are probably of greatest importance to both students of metallurgy and engineering and to practising technologists. It would be unreasonable, however, to consider these technological aspects without the preceding consideration of the fundamentals of solidification.

Subsequently, current casting processes and procedures will be described and the nature of defects in castings and their cause and avoidance discussed.

The monograph is primarily intended for students of metallurgy, materials science and engineering in universities and technological colleges and institutes. However, it is also hoped that it will form a useful basis for practising metallurgists and engineers who wish to establish anew, or to refresh, their knowledge of solidification and casting.

In preparing the monograph a compromise has been attempted between the conflicting demands of comprehensiveness and conciseness. To enable ease of reading and to condense the subject matter, explanatory detail has been kept to the minimum compatible with adequate coverage of the different topics. To compensate for this each chapter is fully referenced so that readers know where further detailed information can be found should it be required. In addition, a bibliography is given in an appendix. This is intended as a guide to finding source material on both the fundamental and technological aspects of solidification and casting.

I am indebted to members of this department for their help during the preparation of the manuscript, and in particular to Dr John Garland for his constructive comments and to Miss Doreen Rawlinson for preparing the typescript. I must also thank those persons who have allowed the use of figures. Most particular acknowledgement must be made of the assistance provided by Mr G. C. May of the Institute of British Foundrymen during the compilation of Chapters 8 and 9.

Department of Metallurgy and Materials Science G. J. DAVIES
University of Cambridge

Contents

Acknowledgements

I would like to express my thanks to the following for granting permission for the use of figures and tables from copyrighted publications:

American Institute of Physics
American Society for Metals
Butterworths Scientific Publications
The Institute of British Foundrymen
The Institute of Metals
The Institution of Metallurgists
The Iron and Steel Institute
John Wiley and Sons Inc.
McGraw-Hill Publishing Company
The Macmillan Press Limited
North Holland Publishing Company
Pergamon Press
The Royal Society

[illegible] acknowledged in the captions to figures and [illegible]

CHAPTER 1

Liquid Metals

The solidification sequence during any casting process begins with the metal or alloy in a liquid form. To some extent the initial nucleation processes are influenced by the structure and properties of the liquid and therefore it is instructive to begin our study of solidification and casting by examining liquid metals.

Scientific understanding of the liquid state lagged far behind that of the gaseous and solid states of matter. Developments in the eighteenth and nineteenth centuries led to a relatively clear formulation for the gaseous state. The ideal gas was considered to be comprised of component atoms or molecules which behaved essentially as elastic spheres. At low and moderate pressures the components travel distances that are, on average, large when compared with the sizes of the individual components. Interactions between the individual atoms and molecules could be largely ignored and the overall properties of the gas could be determined by summing the behaviour of a representative individual component over the total number of components. This was the essence of the classical kinetic theory of gases. At high pressures, difficulties were encountered because interactions between the atoms could no longer be ignored; nor could the volume occupied by the components themselves. Several approaches to the problem were made and perhaps the best known is the van der Waals' formulation. In this, the classical equation of state,

$$pV = RT$$

was modified to

$$\left(p + \frac{a}{V^2}\right)(V - b) = RT$$

In both these equations, p is the pressure, V is the gram molecular volume, R is the universal gas constant and T is the absolute temperature. In the second equation, b is a constant which is related to the

volume of the component atoms or molecules and a/V^2 is a term which allows for interactions between these components. In this case the basic many-body problem of an aggregate of components was also overcome by considering it as a single-body problem with summation over a number of apparently identical components.

The understanding of the solid state, on the other hand, was beset with difficulties until early in the twentieth century, when diffraction procedures clearly established the structure of crystalline solids as one in which atoms or groups of atoms are arranged in regular geometrical patterns in space. Here it was clear that interactions, between individual atoms had necessarily to be taken into account, but since the relative atomic positions were defined† the interactions of an atom with its neighbours could be estimated. The overall properties of the assembly could then he determined by summation over the total of atoms. Here again the many-body problem was overcome by considering it as a sum of single-body problems.

The study of liquids encountered difficulty because it was essentially a true many-body problem. Interactions between neighbouring components needed to be taken into account, but the relative atomic positions were not well defined. In general the environment of any individual atom was more unlike than like that of another. The principal approaches to the study of liquids came from two directions. Liquids were considered as either dense gases or rather disordered solids. More recently a geometrical concept in which the liquid is considered as a 'heap' of atoms or molecules has been the subject of study.

Before turning our attention to an examination of these different theories it is useful to consider the experimental facts which these theories must account for as far as possible.

1.1 EXPERIMENTAL CONSIDERATIONS

1.1.1 The change in volume on melting

Table 1.1 lists a number of common metals together with their crystal structure, melting point and change in volume on melting. It can be seen that in most cases there is an expansion of from 3 to 5 % except for a small number of metals with rather open structures in which there is a small contraction on melting.

† The atomic position can be simply considered as the mean position of the atomic centre. In practice this is only true on average since the atom is normally undergoing thermal vibrations. For a rigorous treatment it may be necessary to 'stop' the atoms by assuming the solid is at 0 K.

TABLE 1.1

THE CHANGE IN VOLUME ON MELTING OF SOME COMMON METALS[a]

Metal	*Crystal structure*	*Melting point* (°C)	*Change in volume on melting* (%)
Aluminium	f.c.c.	660	+6·0
Gold	f.c.c.	1 063	+5·1
Zinc	h.c.p.	420	+4·2
Copper	f.c.c.	1 083	+4·15
Magnesium	h.c.p.	650	+4·1
Cadmium	h.c.p.	321	+4·0
Iron	b.c.c./f.c.c.	1 537	+3·0
Tin	tetr.	232	+2·3
Antimony	rhombohedral	631	−0·95
Gallium	f.c. orthorhombic	30	−3·2
Bismuth	rhombohedral	271	−3·35
Germanium	dia. cubic	937	−5·0

[a] Data from Schneider and Heymer.[1]

TABLE 1.2

LATENT HEATS OF MELTING AND VAPORISATION OF SOME COMMON METALS[a]

Metal	*Crystal structure*	*Melting point* (°C)	*Latent heat*[b] *of melting* (L_m)	*Boiling point* °C	*Latent heat of vaporisation* (L_b)	$\frac{L_b}{L_m}$
Aluminium	f.c.c.	660	2·5	2 480	69·6	27·8
Gold	f.c.c.	1 063	3·06	2 950	81·8	26·7
Copper	f.c.c.	1 083	3·11	2 575	72·8	23·4
Iron	f.c.c./b.c.c.	1 536	3.63	3 070	81·3	22·4
Zinc	h.c.p.	420	1·72	907	27·5	16·0
Cadmium	h.c.p.	321	1·53	765	23·8	15·6
Magnesium	h.c.p.	650	2·08	1 103	32·0	15·4

[a] Data from Smithells.[2]
[b] Latent heats in kcal mol^{-1}.

1.1.2 The latent heat of melting

Table 1.2 gives data on the melting and boiling points of some common metals with corresponding values of the latent heats of melting and of vaporisation. From these, the ratio of the latent heat of vaporisation to the latent heat of melting has been calculated. In all cases this ratio is large. Consider, for instance, the face-centred cubic metal aluminium. Here it requires nearly 28 times as much energy to completely separate the atoms in the liquid to form the gaseous phase as it does to transform the solid to a liquid.

In the solid phase the atomic co-ordination number of aluminium is 12. In the gaseous phase it is zero. The latent heats involved in the change from solid to gas are responsible for destroying 12 nearest neighbour bonds. Of these, only approximately one-half of a nearest neighbour bond disappears on melting. It follows that the change in co-ordination on melting is small. The situation is undoubtedly more complicated for the semi-metals or non-metals with open structures, and for complex solids. Nevertheless, the conclusion is a reasonable one.

1.1.3 The entropy of melting

Table **1.3** gives a comparative list of the entropy change between room temperature and the melting point, and of the entropy of melting, for some of the metals considered above. These figures show that there is a relatively large increase in entropy on melting, particularly when the small change in co-ordination is taken into account. This indicates that there is a considerable loss of ***order*** on melting without a large

TABLE 1.3

ENTROPY CHANGES DURING THE HEATING OF SOME COMMON METALS[a]

Metal	*Change in entropy*[b] 298°K *to melting point* ΔS	*Entropy of melting* ΔS_m	$\frac{\Delta S_m}{\Delta S}$
Cadmium	4.53	2.46	0·54
Zinc	5·45	2·55	0.47
Aluminium	7.51	2.75	0.37
Magnesium	7.54	2.32	0.31
Copper	9.79	2.30	0.24
Gold	9.78	2.21	0.23
Iron	15.50	2·00	0·13

[a] Data from Hultgren *et al.*[3]
[b] Entropies in cal mole^{-1} °K^{-1}.

change in the separation of individual atoms or of the numbers of neighbour atoms.

1.1.4 Diffraction studies of liquid structure

Diffraction studies have been carried out on liquids using both x-rays and neutrons (*see*, for example, the survey by Gingrich[4]). The results

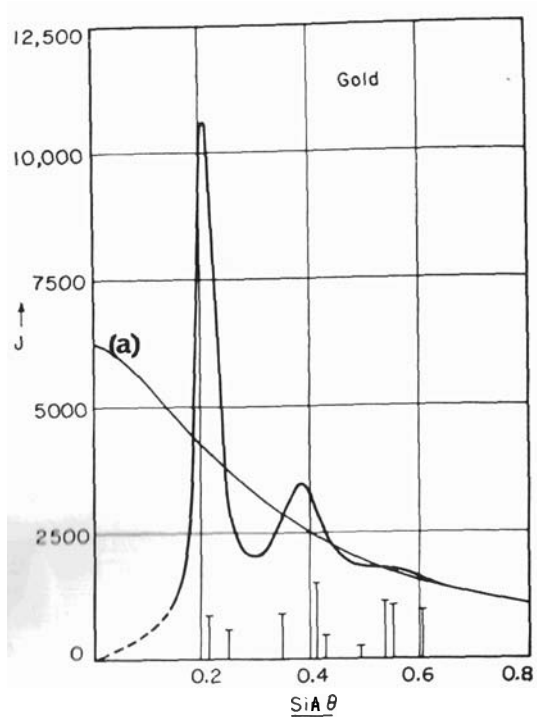

Fig. 1.1 ***X-ray diffraction intensity for liquid gold at*** 1100°C. ***Curve (a) is the*** *square* ***of the atomic structure factor. Lines in the powder pattern from crystalline gold are*** *shown* ***at the bottom of the figure (Vineyards after*** *Hendus*[6]).

are in agreement and we will confine our attention to results obtained by x-ray diffraction.

X-ray photographs from liquids, using monochromatic radiation, consist of a series of rather diffuse haloes. The intensity of the diffracted beam can be determined as a function of $\sin\theta/\lambda$ by densitometry. More usually it is determined directly using a crystal diffractometer (Fig. 1.1). This figure shows two reasonably well-defined peaks. It should be noted that these show a degree of correspondence with

the positions of the diffraction lines obtained in a powder photograph of the same material in solid form. It is possible, using defined analytical procedures[7] and making the necessary corrections for incoherent scattering,' to determine the radial distribution function, $\rho(r)$, for the liquid metal. The radial distribution function gives the number of atoms per unit volume at a radial distance r from a reference atom.

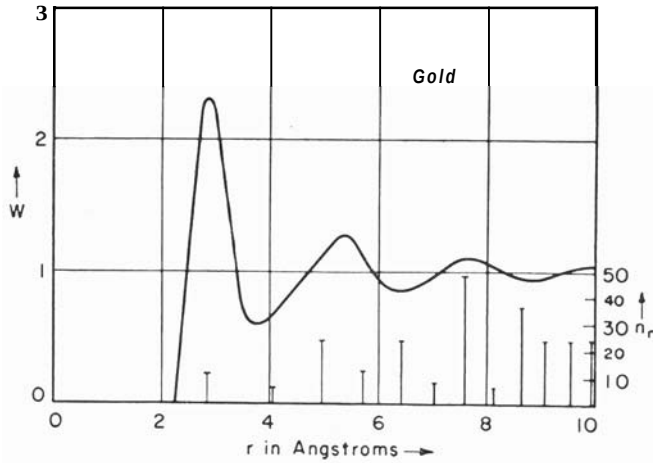

Fig. 1.2 *Radial density function for liquid gold. W is the ratio of the radial distribution function density, $\rho(r)$, to the bulk density, ρ_0. The radial density for crystalline gold is indicated by the vertical lines at the bottom of the figure (Vineyard[5] after Hendus[6]).*

Figure 1.2 gives the radial distribution function derived from Fig. 1.1. This figure also shows correspondence between the principal peaks and the radial density for the solid crystal. Because of repulsive interactions between atoms, $\rho(r)$ has zero magnitude out to a radius nearly equal to the atomic radius. At large radii, $\rho(r)$ is equal to the bulk density of the liquid. The mean co-ordination number for the liquid can be determined from this curve by integration.[9] Table 1.4 gives some comparisons of data obtained from diffraction studies on liquids with the corresponding data for the crystalline solids. In general it is found that

(a) the average interatomic separation in the iiquid is slightly greater than in the solid, and
(b) the co-ordination number in the liquid is less than in the solid and is usually in the range 8–11.

These data are direct experimental measurements relating to the liquid structure. It is instructive to note the good correlation with

TABLE 1.4

COMPARISON OF STRUCTURAL DATA FOR LIQUID AND SOLID METALS OBTAINED BY DIFFRACTION'

Metal	*Liquid*		*Solid*	
	atomic separation	*co-ordination number*	*atomic separation*	*co-ordination number*
Aluminium	2.96	10–11	2.86	12
Zinc	2.94	11	2.65	6
			2.94	6
Cadmium	3.06	8	2.97	6
			3.30	6
Gold	2.86	11	2.88	12

"Data abstracted from Vineyard.[5]

the conclusions drawn from the thermochemical data given in the preceding sections.

1.1.5 Transport properties

For completeness we should consider transport phenomena in liquid metals and particularly that important property, their lack of resistance to shearing stresses. Certainly, any satisfactory theory should deal with these properties. It is fair to say that in so far as *solidification processes* are concerned, the main consideration should be given to diffusivity and fluidity. However, these are inherent properties of the liquid which, while influencing events during solidification, do not have as marked an effect in the initial stages as do those factors dependent on the structural information considered above. The diffusivity has a considerable effect on solute redistribution during the growth phase. Fluidity is of greater importance when considered with reference to the casting process as a whole. Both of these factors will be examined in more detail in late- chapters. Meanwhile, the reader is referred to the monographs by Pryde[10] and March[11] for a full treatment of the transport properties of liquid metals.

1.2 THEORIES OF LIQUID STRUCTURE

As mentioned previously, theories of liquid structure can be divided into those which consider the liquid as a dense gas (condensation theories), those which consider the liquid as disordered solid (lattice theories) and the geometrical theories.

1.2.1 Condensation theories

These theories proceeded from the kinetic theory of gases through modified equations of state, such as the van der Waals' equation, in an attempt to correct for the effects of the interatomic or intermolecular forces resulting from the close proximity of the components in a dense gas. Born and Green,[12] following an approach initiated by Kirkwood,[13] developed a set of molecular distribution functions adequate for the formulation of a kinetic theory of liquids. The formulation is mathematically complex, however, and has not yielded much in the way of practical results.

1.2.2 Lattice theories

There theories all use as a starting point a crystal lattice into which defects are introduced in a variety of ways. Several possibilities have

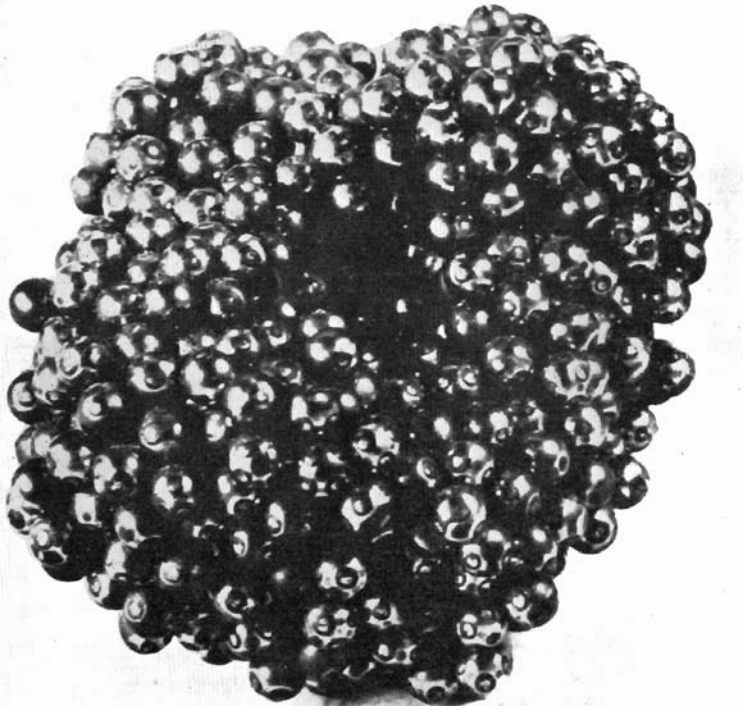

Fig. 1.3 A random close-packed heap of spheres (Bernal[20]).

been explored, the most relevant of which are

(a) the cell theory[14,15] in which melting is considered as a type of order–disorder reaction in which atoms continue to be confined to the vicinity of a lattice site, but are allowed to oscillate randomly and independently,

(b) the hole or free volume theory[16,17] which treated the liquid as a pseudo-lattice with a large number of vacant sites, and

(c) the significant structures theory[**] in which the liquid state involves partition between crystal-like and gas-like components.

A number of effective results follow from these different approaches, but the theories suffer because their basis on a lattice builds in a degree of long-range order which is absent in the liquid. For instance, lattice theories underestimate the entropy change resulting from melting. This is a consequence of the retention of long-range order.

1.2.3 Geometrical theories

The basic concept in this case is of a liquid as a 'heap' of atoms or molecules. Bernal[19], and Bernal and King[21] used models to construct random close-packed heaps of spheres (see Fig. 1.3). The method followed from the general hypothesis that the liquid was a homogeneous, coherent and essentially irregular assemblage of atoms or molecules containing no crystalline regions nor holes large enough to accommodate another atom. The approach was partially successful since it yielded a radial distribution function in agreement with that measured experimentally for a simple monatomic liquid (Fig. 1.4). Similar measurements were also carried out by Scott[22] with the same result. The data from both Bernal and Scott are given in Fig. 1.4. The model has not, however, been developed in mathematical form, although some work in this direction has been attempted.[23]

One interesting observation made in these model studies was the existence of regions of high density called 'pseudo-nuclei'. When the nucleation processes involved in the change from liquid to solid are considered (Chapter 2) the occurrence of ordered crystal-like regions (embryos) in the liquid is postulated. These pseudo-nuclei or the crystal-like components of the significant structures theory could satisfy this postulate.

In all it is clear that there is still a long way to go before the experimental observations given in Section 1.1 are accounted for by the different theoretical approaches. Some success has been achieved and more should follow as the approaches are co-ordinated.

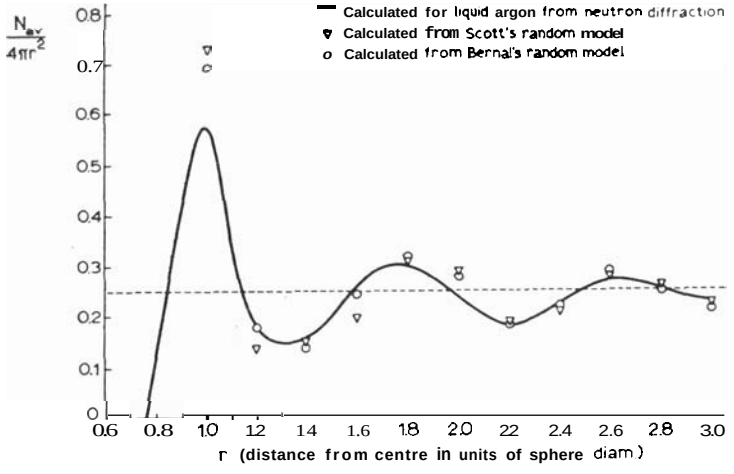

Fig. 1.4 The radial distribution of random close packing of equal spheres. N_{av} *is the average number of spheres in intervals of 0.2 of a sphere diameter* (Bernal[20]).

REFERENCES

1. Schneider, A. and Heymer, G. (1958). *The Physical Chemistry of Metallic Solutions and Intermetallic Compounds,* Vol. II, HMSO, London, Paper 4A.
2. Smithells, C. J. (1967). *Metals Reference Book,* 4th Edition, Butterworths, London, p. 224.
3. Hultgren, R., Orr, R. L., Anderson, P. D. and Kelley, K. K. (1963). *Selected Values of Thermodynamic Properties of Metals and Alloys,* John Wiley, New York.
4. Gingrich, N. S. (1965). *Liquids: Structures, Properties, Solid Interactions* (Ed. by *T*. J. Hughel), Elsevier, Amsterdam, p. 172.
5. Vineyard, G. H. (1958). *Liquid Metals and Solidification,* ASM, Cleveland, p. 1.
6. Hendus, H. (1947). Z. *Naturforsch,* **2A,** 505.
7. Zernicke, F. and Prins, J. A. (1927). *Z. Physik,* 41, 184.
8. Gingrich, N. S. (1943). *Rev. Mod. Physics,* **15,** 90.
9. Pings, C. J. (1968). *Physics of Simple Liquids* (*Ed.* by H. N. V. Temperley, J. S. Rowlinson and G. S. Rushbrooke), North-Holland, Amsterdam, p. 387.
10. Pryde, J. A. (1966). *The Liquid State,* Hutchinson, London.
11. March, N. H. (1968). *Liquid Metals,* Pergamon, Oxford.
12. Born, M. and Green, H. S. (1946). *Proc. Roy. Soc.*, **A188,** 10.
13. Kirkwood, J. G. (1935). J. *Chem. Phys., 3,* 300.
14. Lennard–Jones, J. E. and Devonshire, A. F. (1936). *Proc. Roy. Soc.*, **A163,** 53.

15. Lennard–Jones, J. E. and Devonshire, A. F. (1938). *Proc. Roy. Soc.*, **A165,** 1.
16. Eyring, H. (1936). J. *Chem. Phys., 4,* 283.
17. Cernuschi, F. and Eyring, H. (1939). J. *Chem. Phys., 7,* 547.
18. Eyring, H., Ree, T. and Hirai, N. (1958). *Proc. Nat. Acad. Sci., 44,* 683.
19. Bernal, J. D. (1964). *Proc. Roy. Soc.,* **A280,** 299.
20. Bernal, J. D. (1965). *Liquids: Structures, Properties, Solid Interactions* (Ed. by T. J. Hughel), Elsevier, Amsterdam, p. 25.
21. Bernal, J. D. and King, S. V. (1968). *Physics of Simple Liquids* (Ed. by *H*. N. V. Temperley, J. S. Rowlinson and G. S. Rushbrooke), North-Holland, Amsterdam, p. 231.
22. Scott, G. D. (1962). *Nature,* 194, 956.
23. Turnbull, D. (1965). *Liquids: Structure, Properties, Solid Interactions* (Ed. by T. J. Hughel), Elsevier, Amsterdam, p. 6.

CHAPTER 2

Nucleation

Nucleation may be defined as the formation of a new phase in a distinct region separated from the surroundings by a discrete boundary. During solidification, solid nuclei form in the liquid and subsequently grow until the whole of the volume is solid. We are concerned with a change from one position of stable or metastable equilibrium to another in response to a driving force. The existence of a driving force, namely a decrease in the free energy of the system, indicates that the transformation is favourable. This driving force is a necessary but not sufficient requirement. Whether or not the transformation takes place is determined by kinetic factors. First, we must ask can the transformation begin? This is a problem of nucleation and is dealt with in this chapter. Second, we must ascertain that after nucleation the transformation can continue. This involves the study of growth and is considered in Chapter 3. Before we can examine the different processes of nucleation we must examine the nature of the driving force.

2.1 THERMODYNAMIC ASPECTS

When considering the development of microstructure we are concerned with heterogeneous equilibrium, *i.e.* equilibrium involving more than one phase. The free energy, G, of a component phase is defined by

$$G = H - TS \qquad (2.1)$$

where H is the enthalpy, T the absolute temperature and S the entropy. For most metallurgical systems, pressure can be considered to be constant, so that

$$\left(\frac{\partial G}{\partial T}\right)_{p=\text{constant}} = -S$$

Thus the free energy decreases with increasing temperature.

The variation of the free energies of the different pure metal phases is shown schematically in Fig. 2.1. The change in free energy on transformation at constant temperature from one phase to another is given by

$$AG = AH - TAS$$

At equilibrium between two phases,

$$AG = 0$$

and this defines the equilibrium melting point, T_m, and boiling point, T_b. At other temperatures, the equilibrium phase is that which has

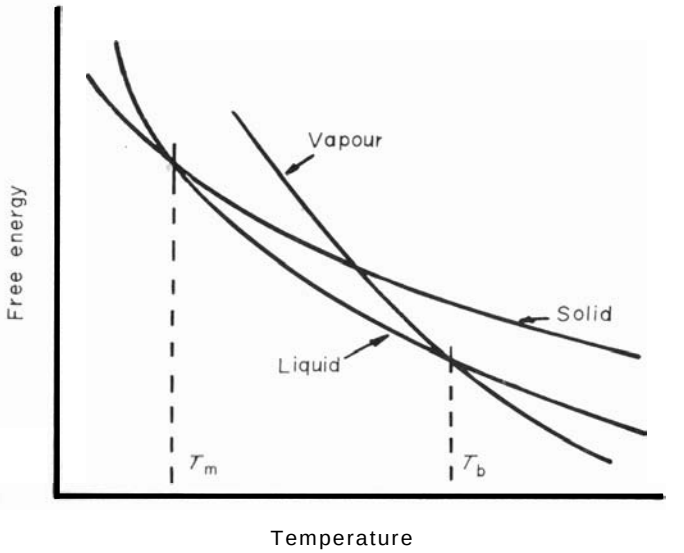

Fig. **2.1** *The variation in free energy* ***of metallic phases with temperature (schematic).***

the minimum free energy; AG, the difference between the free energies, provides the driving force for transformation.

With simple binary alloys the free energy can vary with composition in several ways, as shown in Fig. 2.2. The free energy curves for the component phases move relatively as the temperature changes. For a particular composition the equilibrium phase or phases at a given temperature are those which give the minimum overall free energy at that temperature.† The difference between the free energies

† **A full description of the free-energy composition diagram and its relation to the equilibrium phase diagram can be found in the books by Cottrell[1] and Darken and Gurry.[2]**

of the component phases before and, after transformation is the driving force.

In many cases the final equilibrium state is not reached and the system rests in a state of metastable equilibrium.

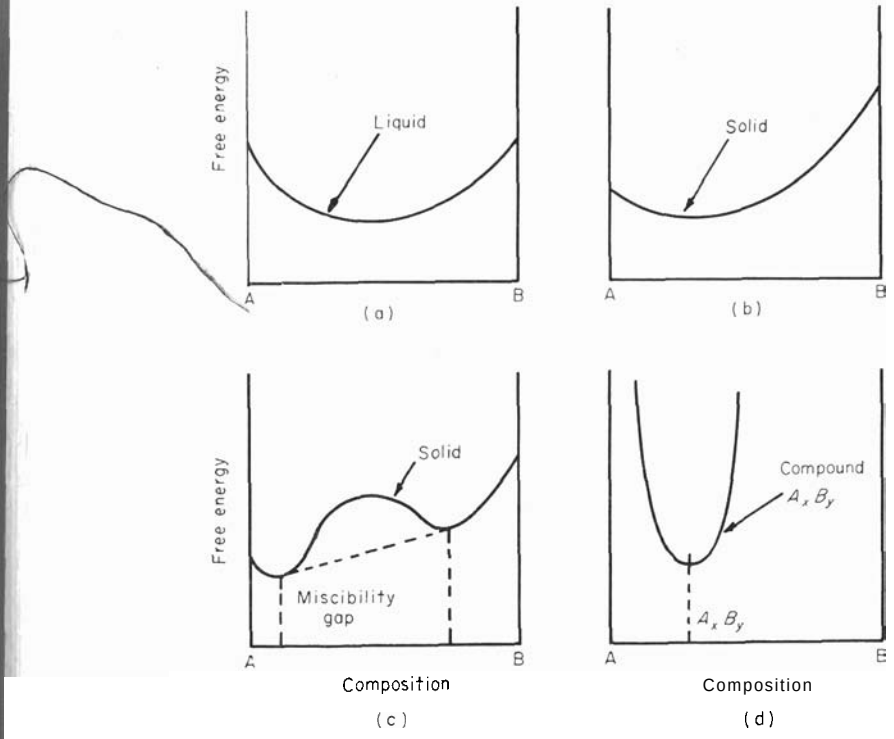

Fig. 2.2 Free-energy composition diagrams for different binary alloys: (a) liquid; (6) solid; (c) solid with a miscibility gap; and (d) an intermetallic compound.

For the transformation from liquid to solid the volume free energy chance AG, is

$$\Delta G_v = G_L - G_S$$

where G, and G_S are the free energies of the liquid and solid respectively. From eqn. (2.1)

$$\Delta G_v = (H_L - H_S) - T(S_L - S_S)$$

If we assume that the temperature dependence of the changes of enthalpy and entropy are small, then

$$H_L - H_S = L_m$$

where L_m is the latent heat of melting. At the equilibrium melting boint, since AG is zero, the entropy of melting is given by

$$S_L - S_S = \frac{L_m}{T_m}$$

Thus

$$\Delta G_v = L_m \left(1 - \frac{T}{T_m}\right)$$

$$= \frac{L_m \cdot \Delta T}{T_m} \qquad (2.2)$$

In this equation AT is the temperature interval between the equilibrium melting point and the temperature of transformation and is known as the supercooling.

2.2 HOMOGENEOUS NUCLEATION

2.2.1 Energetics of nucleation

The classical theory of nucleation was developed by Volmer and Weber,[3] and Becker and Doring[4] for the condensation of a pure vapour to form a liquid. The subsequent theory[5,6] for the liquid–solid transformation was based on this earlier work. The theory considered homogeneous nucleation, *i.e.* the formation of one phase by the aggregation of components of another phase without change of composition and without being influenced by impurities or external surfaces. Impurity particles and external surfaces are taken into account in heterogeneous nucleation theory (Section 2.3). Modifications to the classical theory are necessary to allow for the effects of compositional changes.

Consider the free energy changes which occur if a spherical embryo of solid is formed within a uniform liquid. First, there will be a change in free energy associated with the difference in volume free energy of the atoms in the solid and the liquid.? Second, there will be a term introduced because a number of the atoms occur in the transition region between liquid and solid. These atoms will be in a high energy state and are the origin of the surface free energy of the embryo.

† One of the inherent difficulties of nucleation theory is associated with the use of macroscopic thermodynamic properties, ***e.g.*** volume free energy and surface energy, in microscopic situations. This is unavoidable but does not normally introduce serious numerical error.

For a spherical embryo of radius r, the overall change in free energy, AG, is given by

$$AG = 4\pi r^2 \gamma_{LC} + (\tfrac{4}{3})\pi r^3 \cdot AG, \qquad (2.3)$$

where γ_{LC} is the surface free energy (erg cm^{-2}). As above, ΔG_v is the volume free energy change (erg cm^{-3}). Above the melting point.

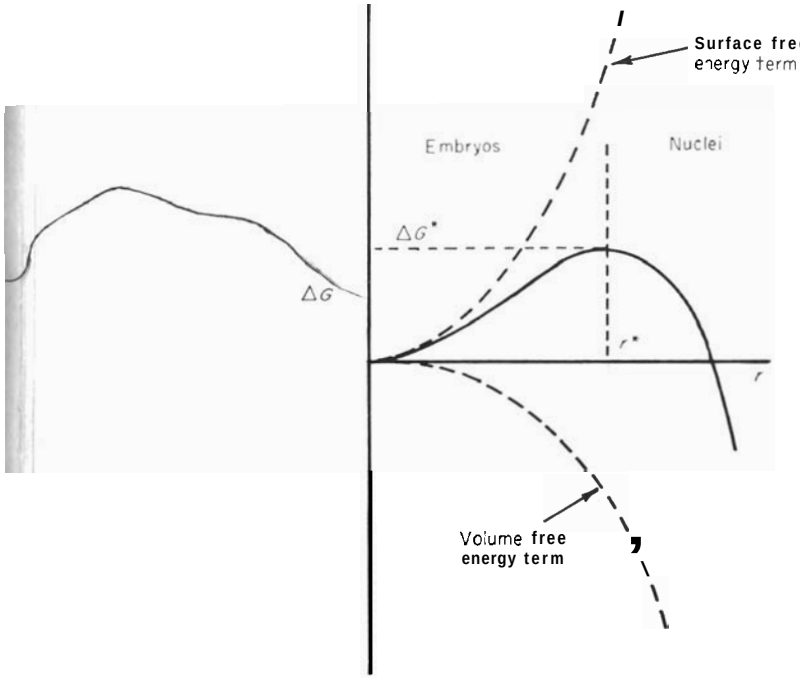

Fig. **2.3** ***The change in free energy resulting from the formation of a spherical embryo of solid in the liquid.***

AG, is positive and below it AG, is negative. The variation of the different free energy terms below T_m and the overall change in free energy are shown in Fig. 2.3. Any embryos which form above T_m will rapidly disperse. On the other hand, below T_m, provided the embryo reaches a critical size with radius r*, at which $(\partial(\Delta G)/\partial r) = 0$, it is equally probable that it will disperse or that it will grow as a stable nucleus. To form this critical nucleus a random fluctuation producing a localised energy change AG* is required. Differentiating eqn. (2.3) and allowing for the sign of AG, we find

$$r^* = \frac{2\gamma_{LC}}{\Delta G_v}$$

This is the critical nucleus size. Substituting from Eqn. (2.2) gives

$$r^* = \frac{2\gamma_{LC} \cdot T_m}{L_m \cdot \Delta T} \qquad (2.4)$$

The localised energy change, AG*, can then be determined by introducing r* into eqn. (2.3):

$$\Delta G^* = \frac{16\pi\gamma_{LC}^3 \cdot T_m^2}{3(L_m \cdot \Delta T)^2} \qquad (2.5)$$

AG* is often referred to as 'the work of nucleation'. Since ΔG_v increases approximately linearly as the temperature falls, the critical radius decreases rapidly as does the work of nucleation (Fig. 2.4).

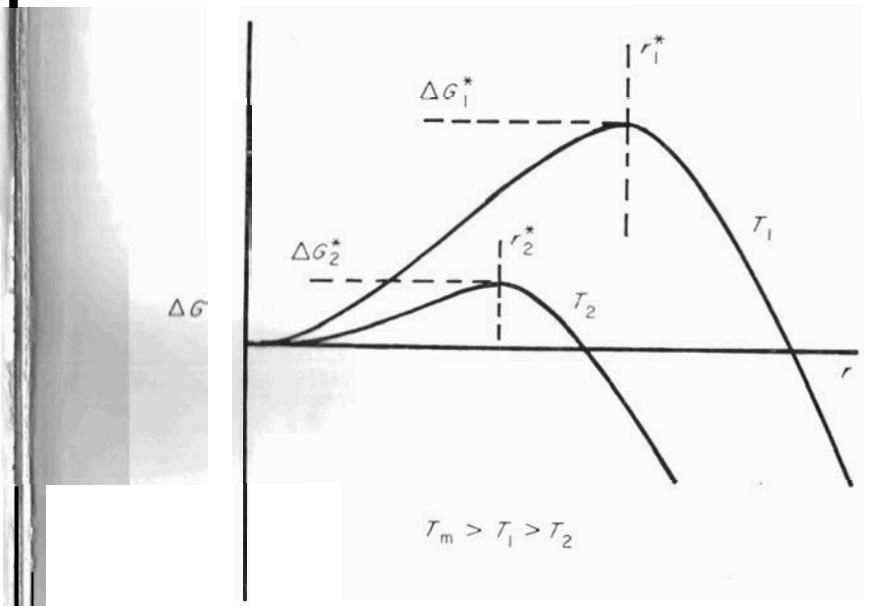

Fig. **2.4** ***The effect of decreasing temperature on the critical radius for nucleation and on the work of nucleation.***

2.2.2 Rate of nucleation

The theory for the rate of nucleation also follows from that derived for vapours. Becker[7] originally proposed that the nucleation rate, **I**, in condensed systems, such as are involved in the liquid–solid transformation, was determined by an expression of the type

$$I = K \exp(-(AG^* + \Delta G_A)/kT)$$

where ΔG^* is the work of nucleation (*i.e.* the maximum fluctuation in free energy necessary for nucleus formation) and **AG,** is the energy of activation for diffusion across the boundary separating the phases: k is Boltzmann's constant. Thus, the rate was a combination of the probability of having the required energy fluctuation with the probability of having an atom add itself to the embryonic nucleus.

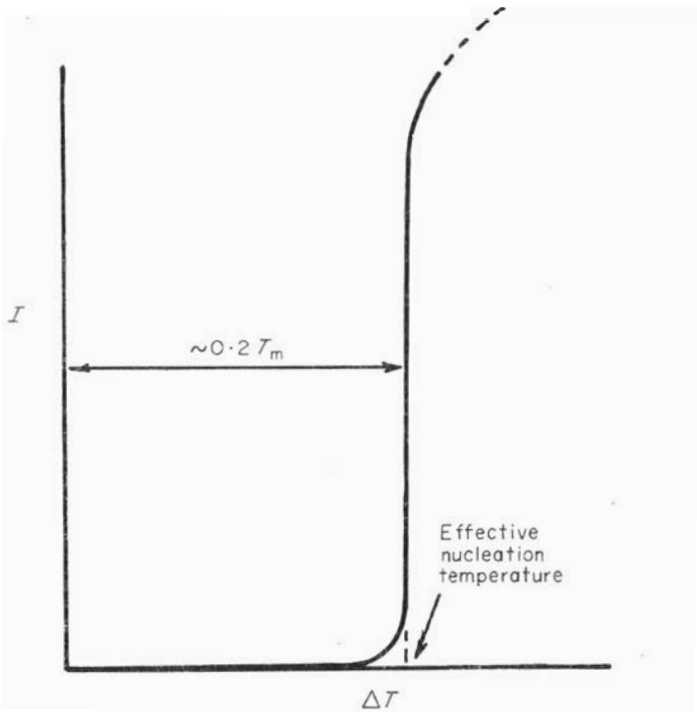

Fig. 25 *The dependence of the rate of nucleation on the undercooling.*

A formal derivation for the constant K was made by Turnbull and Fisher,[5] using the theory of absolute reaction rates. This treatment gave a rate of nucleation

$$I = \frac{NkT}{h} \exp\left(-\frac{\Delta G_A}{kT}\right) \exp\left[-\frac{16\pi\gamma_{LC}^3 T_m^2}{3L_m^2(\Delta T)^2 kT}\right] \qquad (2.6)$$

where N is the total number of atoms, h is Planck's constant and the other symbols are as defined earlier. In this expression the result contained in eqn. (2.5) has been introduced for ΔG^*. The form of eqn. (2.6) means that the rate of nucleation will be extremely sensitive

to the undercooling, AT. It also follows that the rate of nucleation will be dependent on the size of the system under examination.

It is found that there is a temperature at which the rate of nucleation increases rapidly, as shown in Fig. 2.5. Substitution of acceptable values for the terms in the equation for nucleation rate indicates that undercoolings of $-0.2\,T_m$ are to be expected for the homogeneous

TABLE 2.1

SUMMARY OF DATA ON THE SUPERCOOLING OF SMALL DROPLETS OF METALS[a]

Metal	*Melting point,* T_m(°K)	*Undercooling,* ΔT (°C)	T/T_m
Mercury	234.3	58	0·287
Gallium	303	76	0.250
Tin	505.7	105	0.208
Bismuth	544	90	0.166
Lead	600.7	80	0.133
Antimony	903	135	0·150
Aluminium	931.7	130	0.140
Germanium	1 231.7	227	0.184
Silver	1 233.7	227	0·184
Gold	1 336	230	0.172
Copper	1 356	236	0.174
Manganese	1 493	308	0.206
Nickel	1 725	319	0.185
Cobalt	1 763	330	0.187
Iron	1 803	295	0.164
Palladium	1 828	332	0.182
Platinum	2 043	370	0·181

[a] Data from Turnbull.[8]

nucleation of solids from liquids. This has been verified experimentally for many metals. In the experiments of Turnbull[8,9] the solidification of dispersions of fine droplets of liquid metals was observed dilatometrically. The experimental undercoolings were of the order of $0{\cdot}2\,T_m$, as shown in Table 2.1.

At this undercooling, the critical radius is $\sim 10^{-7}$ cm and the nucleus would contain approximately 200 atoms.

Homogeneous nucleation in alloys is a more complex process since the phase diagram requires equilibrium between a solid nucleus and liquid of different compositions. In this situation diffusional processes

in the liquid will play an important part.† There is at present no theoretical treatment for this problem. However, experimental observations[10] on copper–nickel alloys showed that the undercooling required for homogeneous nucleation was −0.2 of the liquidus temperature.

The form of the nucleation rate equation is such that at very large undercoolings there should be a decrease in the rate of nucleation resulting from a decreased mobility of atoms. We might thus expect the curve of Fig. 2.5 to tend towards a maximum as indicated. For most metallic systems, however, it is not possible to cool through the range of temperature at which copious nucleation occurs at a rate fast enough to suppress nucleation. Quench rates of the order of 10^6 °C sec^{-1} have been used unsuccessfully with melts of pure liquid metals. In binary alloy systems where redistribution of solute must occur as part of the nucleation process, some amorphous solids have been produced using rapid quenching techniques.[11–13]

The occurrence of amorphous phases results from the combined influence of two exponential factors, one related to the transfer of

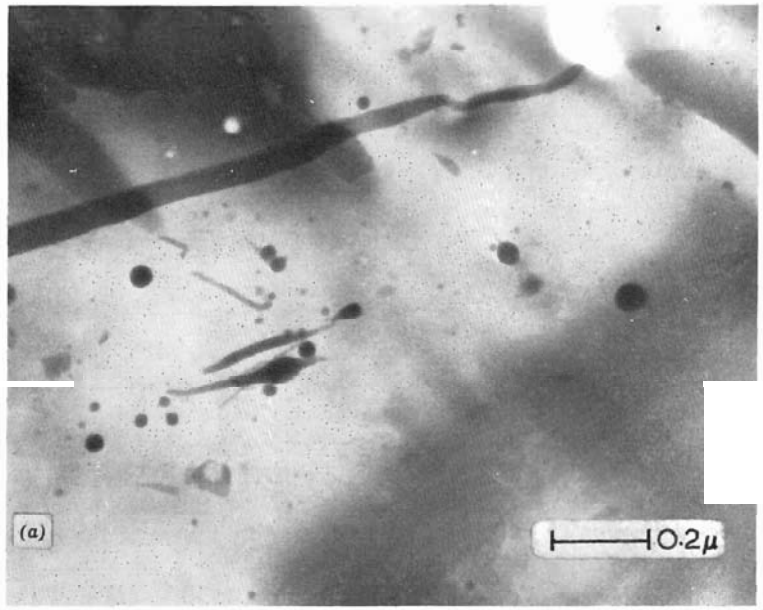

Fig. 2.6 (*a*)

† **There is some evidence that in special cases the *earliest* stages of nucleation and growth take place without solute** redistribution.[35]

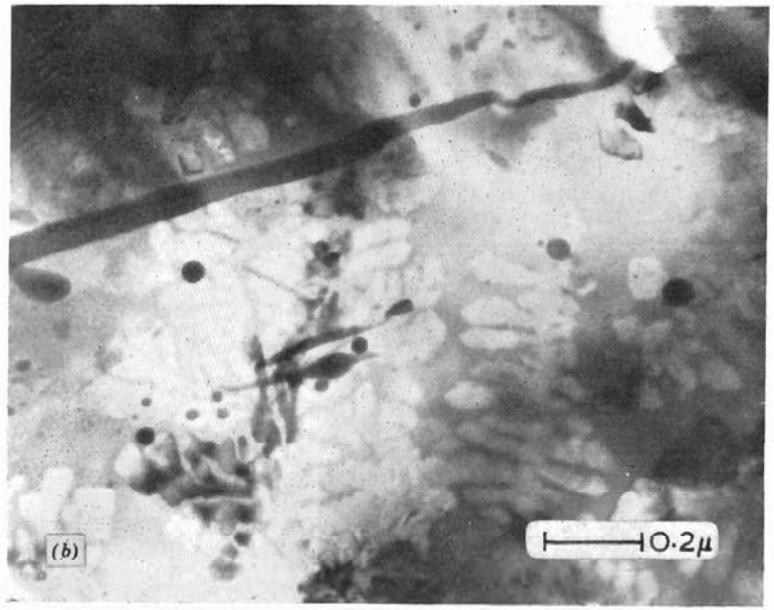

Fig. 2.6 *The electron microstructure of splat-cooled tellurium–15* **at.** *90 germanium in* **(a) the amorphous state** *and* **(b)** *after heating.* **The growth** *of dendrites can be* **seen clearly in the latter micrograph** (*Willens*[13]).

atoms from the liquid to the solid and the other associated with bulk diffusion in the liquid. On reheating, transformation to the crystalline state occurs quite rapidly, as shown in Fig. 2.6.

It should be noted that the treatment given assumed a spherical nucleus. Simple modifications result from considering nuclei of other shapes. One of the more realistic shapes may be that described by Chalmers[14] in which it was proposed that the nucleus was bounded by planes of high atomic density (Fig. 2.7).

Before considering heterogeneous nucleation it is interesting to question how the liquid structure affects homogeneous nucleation. This has been considered by Walton.[15] The structure of the liquid influences the nucleation rate firstly throdgh ΔG^*, since this term contains the volume free energy change ΔG_v. If clustering occurs in the liquid this will aid nucleation. Oriani and Sundquist[16] have estimated that for most metals supercoolings of more than 10°C will be sufficient to promote embryo formation as the liquid structure orders. The structure of the liquid also has a direct effect on ΔG_v, the diffusion term, and on the liquid–crystal interfacial energy, γ_{LC}.

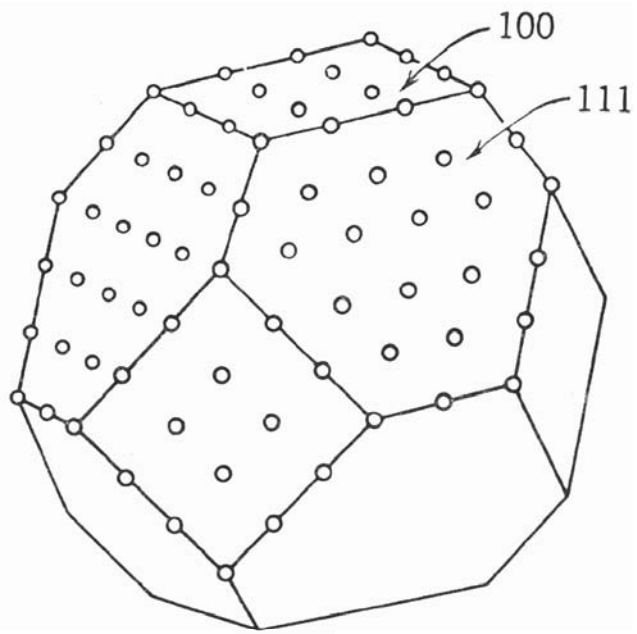

Fig. 2.7 **Possible structure for** *the critical nucleus* **of a cubic metal** (*Chalmers*[14]).

2.3 HETEROGENEOUS NUCLEATION

2.3.1 Theory

In practice, the majority of nucleation phenomena in liquids take place at undercoolings significantly less than those predicted by theories of homogeneous nucleation. For example, whereas undercoolings of the order of 0.2 T_m (−200°C for most metals) would be expected in solidifying pure metals, it is found experimentally that most metal melts nucleate at temperatures only tens of degrees below the melting point. This discrepancy is attributed to the presence of a suitable surface in contact with the liquid. The nucleation is considered to be heterogeneous and to take place on the surface of the container or on particles present in the system. Heterogeneous nucleation can occur provided some preferential sites exist.

The theory has been developed by Turnbull,[17] following Volmer,[18] for the simple case in which a spherical cap of solid forms on a planar substrate (Fig. 2.8). A critical factor is the contact angle, 8. For a spherical cap as shown, the volume and surface areas are given by:

$$\text{volume} = \tfrac{1}{3}\pi h^2(3r - h) = \tfrac{1}{3}\pi r^3(2 - 3\cos 8 + \cos^3\theta)$$

$$\text{surface area} = 2\pi rh = 2\text{nr}^2(1 - \cos 0)$$

Under stable conditions the contact angle θ is a function of the surface energies of the liquid-crystal interface γ_{LC}, the crystal–suhstrate interface γ_{CS} and the liquid–substrate interface γ_{LS}, namely

$$\cos\theta = \frac{\gamma_{LS} - \gamma_{CS}}{\gamma_{LC}} \tag{2.7}$$

This can be proved rigorously using a virtual displacement method. The proof is given in Appendix 1.

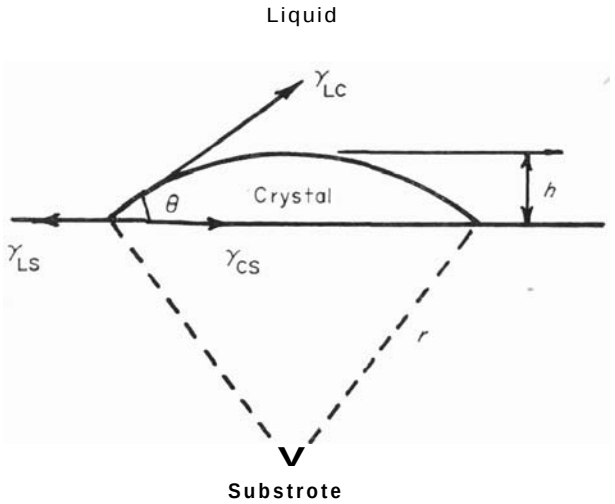

Fig. 2.8 *Spherical cap of solid formed on a planar substrate.*

Following a procedure similar to that of the theory of homogeneous nucleation leads to an equation analogous to eqn. (2.3):

$$\Delta G = \gamma_{LC} \cdot 2\pi r^2(1 - \cos\theta) + \tfrac{1}{3}\pi r^2(2 - 3\cos\theta + \cos^3\theta)\Delta G_v + (\gamma_{CS} - \gamma_{SL})\pi r^2(1 - \cos^2\theta)$$

The latter term arises because of the change in energy resulting from the substrate being in contact with crystal rather than liquid. Differentiating, putting $[\partial(\Delta G)/\partial r] = 0$ and substituting in eqn. (2.7) gives

$$r^* = \frac{2\gamma_{LC}}{\Delta G_v}$$

as before, and the work of nucleation

$$\Delta G^* = \frac{4\pi\gamma_{LC}{}^3(2 - 3\cos\theta + \cos^3\theta)}{3\Delta G_v{}^2}$$

This differs from the value obtained in considering homogeneous nucleation by the factor

$$\$(2 - 3\cos 8 + \cos^3 8)$$

For $\theta = 180$" the energy fluctuation required is the same as for homogeneous nucleation, but for all other cases in which $0 \leq \theta < 180^\circ$ heterogeneous nucleation is a more energetically favourable process.

For systems in which the contact angle is small, it is clear that the barrier to nucleation is also small, and this can satisfactorily account for the low undercoolings observed in practice.

The theory can also be modified to allow for different nucleus geometries, ***e.g.*** disc-shaped caps, without substantially affecting the overall result. If the substrate is allowed to have curvature, or if the formation of nuclei in cavities on the surface is considered, it is found that the barrier to nucleation is reduced even further.[17]

For low contact angles it is desirable to have the crystal–substrate interface significantly less energetic than the liquid–substrate interface. A number of criteria have been postulated for this to be so. One of the most promising approaches was that of Turnbull and Vonnegut[19] which related the undercooling necessary for heterogeneous nucleation to the disregistry between the lattices of the crystal nucleus and the substrate at the interface. More recently, Sundquist and Mondolfo[20,21] have questioned this approach and the evidence they put forward strongly suggests that the nucleation process is much more complex (***see*** Section 2.3.2).

Nonetheless, it is well established that the energy fluctuation required for heterogeneous nucleation, AC*, is much less than that for homogeneous nucleation, and proceeding as before it is possible to obtain[22] an expression for the rate of nucleation that is similar in form to that for homogeneous nucleation. The smaller value of AG* leads to higher rates of nucleation at smaller undercoolings and a much less sharp transition from low rates to high rates of nucleation. In addition, since the heterogeneous nucleation process depends on the presence of suitable sites, it is concluded that the rate of nucleation will pass through a maximum and show a cut-off at higher undercoolings. This results from lateral spread of nuclei across the substrate and the consequent reduction in the surface area available for new nuclei. As with homogeneous nucleation, it is not common for diffusion in the liquid to act as a limiting factor which reduces the nucleation rate at larger undercoolings. Figure 2.9 summarises schematically the relative difference between the two forms of nucleation.

Recently, attention has been paid to heterogeneous nucleation in alloy systems, and in particular in eutectic alloys.[23] Although the

general features of the nucleation process in this case are similar to those for pure metals, one important difference concerns the strong dependence of the structure on the nucleation conditions.

In some cases, ***e.g.*** growth from dilute solutions, where the supply of atoms may exert a limiting effect it is common for surface imperfections such as emergent screw dislocations, grain boundaries or

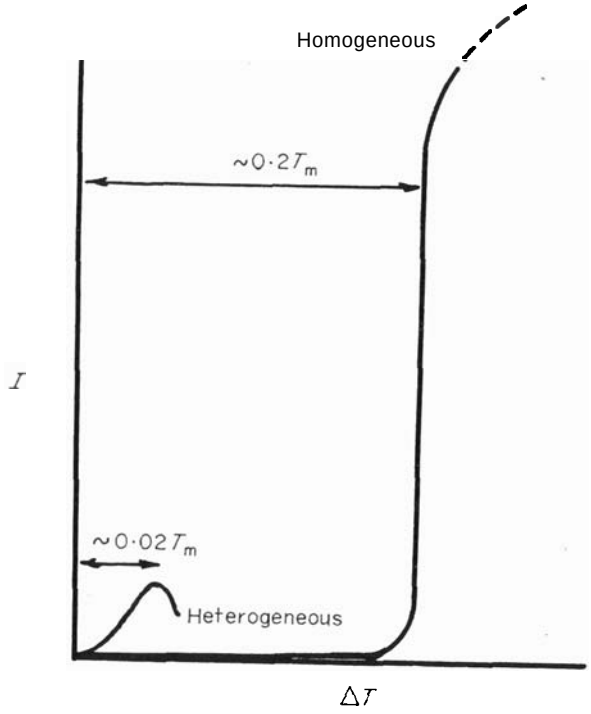

Fig. 2.9 ***The relative rates of nucleation at decreasing temperatures for heterogeneous and homogeneous nucleation processes.***

steps to act as preferred sites for heterogeneous nucleation. The subsequent growth structure usually reflects the influence of these modes of nucleation.

2.3.2 Nucleating agents

So far we have discussed both homogeneous and heterogeneous nucleation as processes occurring without being specifically influenced by external perturbations. In practice, one of the most important technical aspects of casting is the control of nucleation. As discussed in detail in later chapters, it is found that the grain size and grain

shape together with segregation effects occurring during casting can have a significant influence on the physical, mechanical and chemical properties of the cast product. Most commonly, control is exerted by the use of nucleating agents (inoculants). The nature of heterogeneous nucleation and its relation to inoculant effectiveness has been reviewed by Chadwick.[24] As described above, the nucleation potency is strongly dependent on the contact angle (Fig. 2.8). For

TABLE 2.2

COMPOUNDS USED TO STUDY THE HETEROGENEOUS NUCLEATION OF ALUMINIUM FROM ITS MELT[a]

Compound	*Crystal structure*	*S for close-packed planes*	*Nucleating effect*
VC	Cubic	0·014	Strong
TiC	Cubic	0·060	Strong
TiB_2	Hexagonal	0·048	Strong
AlB_2	Hexagonal	0·038	Strong
ZrC	Cubic	0·145	Strong
NbC	Cubic	0·086	Strong
W_2C	Hexagonal	0·035	Strong
Cr_3C_2	Complex	—	Weak or nil
Mn_3C	Complex		Weak or nil
Fe_3C	Complex		Weak or nil

[a] Data from Chadwick.[24]

easy nucleation, low contact angles are required and evidence[19,25] supports the view that when the chemical parameters (bond type and bond strength) of the crystal and the substrate are similar the lattice mismatch between crystal and substrate is important. The lattice mismatch is defined as

$$\delta = \frac{\Delta a}{a}$$

where a is lattice parameter of the crystal being nucleated and Δa is the difference in the lattice parameters of crystal and substrate. Table 2.2 gives data for the heterogeneous nucleation of aluminium from its melt. It is apparent from this table that the chemical parameters have a greater effect than originally anticipated.[19] Nevertheless, despite the fundamental difficulties, efficient inoculants have been determined for most metals, for the most part by processes of trial and error. The results of Cibula,[25] Reynolds and Tottle[26] and Hall and Jackson[27] (*see* Fig. 2.10) are good examples of the practical development of effective inoculation procedures.

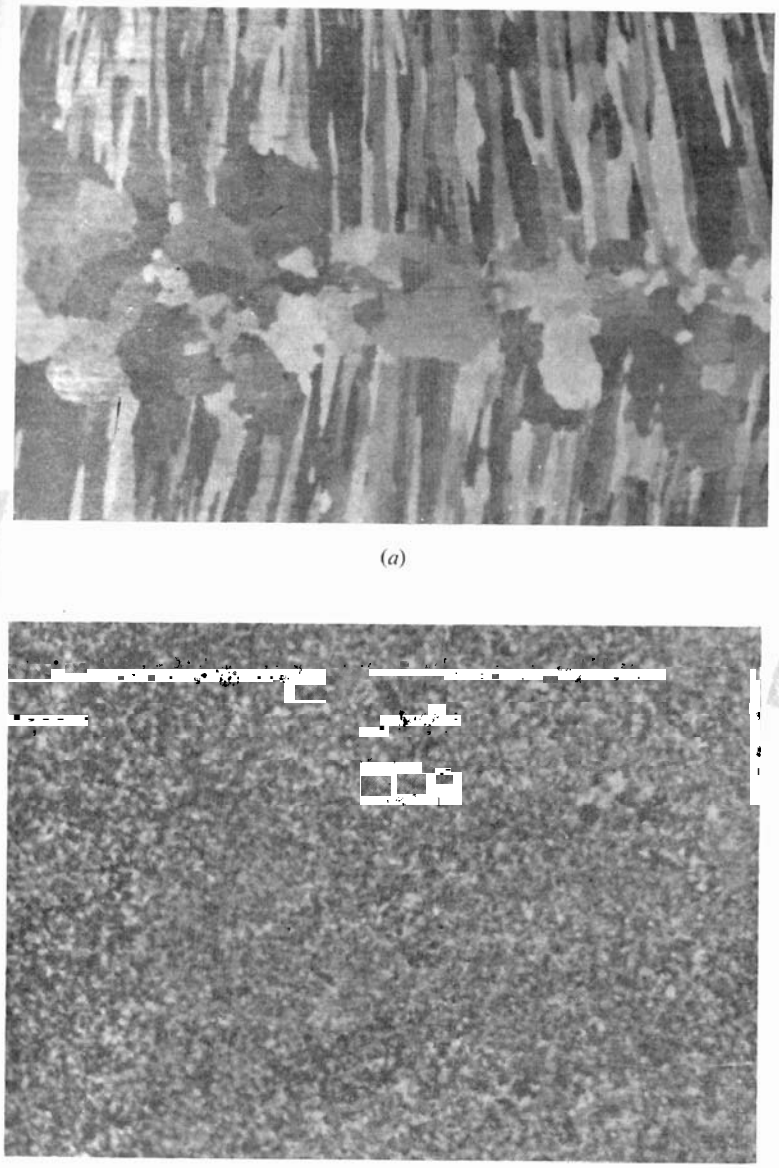

(*a*)

(*b*)

Fig. **2.10** (*a*) ***Normal coarse-grained structure in 18% chromium–12% nickel steel.*** (*b*) ***Same steel as (a) refined by inoculation*** (*Hall and Jackson*[27]).

2.4 DYNAMIC NUCLEATION

So far we have considered nucleation in an essentially static situation. Only temperature and the potency of nucleating substrates have been considered as having any effect. It is possible to induce nucleation by subjecting the liquid metal to dynamic stimuli. Two distinct forms can be identified:

(i) an initial nucleation phenomenon induced mechanically, and
(ii) a grain-refining action which is a consequence of crystal multiplication, and is not a nucleation event in the normal sense.

The latter form is usually the result of fragmentation of existing solid. It is an important means of exerting control over the grain structure and we will examine this in some detail in Chapter 6.

There are few reliable data concerning true dynamic nucleation [(i) above]. Walker,[27] Stuhr[29] and Frawley and Childs[30] have all shown how mechanical vibrations can cause nucleation to occur at lower supercoolings than normally required. It was proposed by Chalmers[31] that cavitation followed by internal evaporation was responsible. This was disproved, however, by Hickling.[32] The most feasible hypothesis is that of Vonnegut,[33] who argued that the positive pressure wave generated by the collapse of an internal cavity in the liquid could be large enough to raise the melting point for metals which contract on freezing by an amount sufficient to increase the effective supercooling of the melt and thus to produce nucleation. Nucleation in systems which expand on freezing would be affected similarly by the rarefaction following the initial pressure pulse. The hypothesis has some support from both calculation[30] and experiment.[34]

REFERENCES

1. Cottrell, A. H. (1955). *Theoretical Structural Metallurgy,* Arnold, London, p. 139 *et seq.*
2. Darken, *L.* S. and Gurry, R. W. (1953). ***Physical Chemistry of Metals,*** McGraw-Hill, New York, p. 326 *et sec;.*
3. Volmer, *M.* and Weber, A. (1926). ***Z. Phys. Chem., 119,*** 227.
4. Becker, R. and Döring, W. (1935). *Ann.* ***Phys.,*** 24, 719.
5. Turnbull, D. and Fisher, J. C. (1949). **J. *Chem. Phys.,* 17,** 71.
6. Holloman, J. H. and Turnbull, D. (1953). ***Progress. Met. Physics,* 4,** 333.
7. Becker, R. (1938). ***Ann. Phys.,* 32,** 128.
8. Turnbull, D.,' 1950). **J. *Metals,* 188,** 1144.

9. Turnbull, D. (1950). ***J. Appl. Phys., 21,*** 1022.
10. Tarshis, L. A., Walker, J. L. and Rutter, J. W. (1971). ***Met. Trans.,* 2,** 2589.
11. Duwez, P., Willens, R. H. and Klements, W., Jr. (1960). **J. *Appl. Phys.,* 31,** 1136.
12. Duwez, P. and Willens, R. H. (1963). ***Trans. Met. Soc. AIME,* 227,** 362.
13. Willens, R. H. (1962). **J. *Appl. Phys., 33,*** 3269.
14. Chalmers, B. (1959). ***Physical Metallurgy,*** John Wiley, New York, p. 246.
15. Walton, A. G. (1969). *Nucleation* (Ed. by A. *C.* Zettlemoyer), Dekker, New York, p. 225.
16. Briani, R. A. and Sundquist, B. E. (1962). **J. *Chem. Phys., 36,*** 2604.
17. Turnbull, D. (1950). J. *Chem.* ***Phys.,* 18,** 198.
18. Volmer, M. (1929). Z. *Electrochem.,* **35,** 555.
19. Turnbull, **D.** and Vonnegut, B. (1952). *Ind. Eng. Chem., 44,* 1292.
20. Sundquist, R. E. and Mondolfo, L. F. (1961). *Trans.* ***Met. Soc. AIME,*** 221, 157.
21. Sundquist, R. E. and Mondolfo, L. F. (1961). *Trans.* ***Met Soc. AIME,*** 221, 607.
22. Turnbull, D. (1952). J. *Chem. Phys.,* **20,** 411.
23. Mondolfo, L. F. (1965). J. *Aust. Inst. Met.,* **10,** 169.
24. Chadwick, G. A. (1969). *Met. and Materials,* **3,** 77.
25. Cibula, A. (1949). *J. Inst. Metals,* **76,** 321.
26. Reynolds, J. A. and Tottle, C. R. (1951). *J. Inst. Metals,* **80,** 93.
27. Hall, H. T. and Jackson, W. J. (1968). *The Solidification* ***of Metals,*** Publication 110, p. 115.
28. [illegible] (1959). *Physical Chemistry of* ***Process Metallurgy*** (Ed. [illegible]), Interscience, New York, p. 845.
29. [illegible] M.S. Thesis, Rensselaer Polytechnic Institute, New [illegible]
30. [illegible] and Childs, W. J. (1968). ***Trans. Met. Soc. AIME,* 242,** [illegible]
31. [illegible] (1965). *Liquids: Structures,* ***Properties, Solid Interactions,*** [illegible] by P. J. Hughel), Elsevier, Amsterdam, p. 308.
32. Hickling, R. (1965). *Liquids: Structures,* ***Properties, Solid Interactions,*** (Ed. by P. J. Hughel), Elsevier, Amsterdam, p. 324.
33. Vonnegut, B. (*see* Turnbull, ***D.)*** (1950). ***Thermodynamics*** *in* ***Physical*** *Metallurgy,* ASM, Cleveland, p. 282.
34. Hunt, J. D. and Jackson, K. A. (1966). **J. *Appl. Phys.,* 37,** 254.
35. Biloni, H. and Chalmers, B. (1965). ***Trans. Met. Soc. AIME,* 233,** 373.

CHAPTER 3

Growth

After nucleation a first step is to consider the growing nucleus. This reauires an examination of the nature of the interface between the growing solid and the liquid.

The structure and form of this interface influences both the microstructural morphology of the resultant solid and also the number and distribution of imperfections within the solid. It also has an effect on thermal and constitutional changes in the adjacent liquid, and the interaction between these effects can in turn lead to growth modifications. The nature and extent of these modifications can be studied by an examination of the behaviour of single-phase materials during solidification. This is done in Chapter 4.

3.1 THE STRUCTURE OF THE INTERFACE

The interface can broadly be defined as the boundary between the liquid and the solid. It is normally described as 'smooth' when the boundary is discrete and 'rough' when the transition extends over a number of atomic layers. Jackson,[1] following a suggestion of Burton *et al.*,[2] carried out an examination of the equilibrium structure of a solid interface in contact with a liquid. It was shown that starting with an atomically smooth surface and adding atoms at random the relative change in surface free energy, ΔF_s,† was given by

$$\frac{\Delta F_s}{NkT_m} = \alpha \cdot x(1-x) + x \ln x + (1-x)\ln(1-x) \quad (3.1)$$

where N is the number of possible sites on the interface, k is Boltzmann's constant, T_m is the equilibrium melting temperature, x is the

† It should be noted that the symbol F is used for free energy instead of G, as previously, to conform with Jackson's original treatment.

fraction of sites occupied and

$$\alpha = \frac{L_m \xi}{kT_m} \quad (3.2)$$

In eqn. (3.2) L_m is the latent heat of solidification and ξ is a crystallographic factor. It is a measure of the fraction of the total binding energy which binds an atom in a layer parallel to the plane face to other atoms in the layer. ξ is always less than unity and is largest for

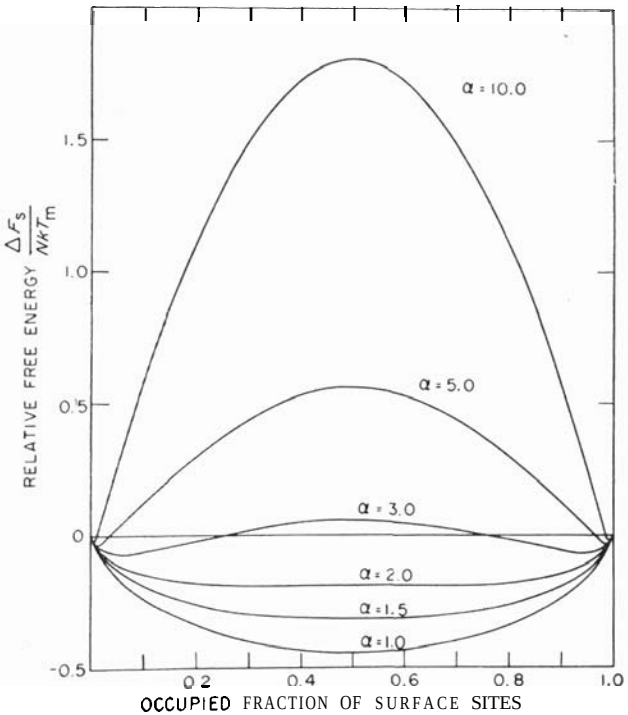

Fig. **3.1** ***Relative change in surface free energy as a function of the fraction of surface sites which are occupied. α depends on the crystal face, the type of crystal and the phase from which the crystal is growing (Jackson[1]).***

the most closely packed planes of the crystal; for these it is invariably greater than or equal to 0.5. α depends on the material and the phase from which the crystal is growing. Figure 3.1 shows the expression of eqn. (3.1) plotted against x for various values of a. Two distinct types of interface can be deduced from this figure. First, for $\alpha \lesssim 2$ the interface has a minimum energy when approximately half the sites are occupied. On the other hand, for a $\gtrsim 5$ the relative free energy is at a minimum when there are only a few occupied sites

or a few unoccupied sites. The first type of interface was classified as 'rough' and the second type of interface as 'smooth' or 'faceted'. Further analysis showed that most metals had a $\lesssim 2$, in which case they were expected to grow with a rough interface whose position was approximately determined by the isotherm fractionally below T_m. Inorganic and organic liquids normally have a $\gtrsim 5$, in which case the growing nucleus rapidly becomes bounded by crystallographic faces. A small group of materials exist, ***e.g.*** silicon, bismuth, which occupy the middle ground in that a = 2–5 for different faces. In these materials the behaviour is more complex and often a mixed growth form results.[3,4] It must be emphasised that the analysis of Jackson considers the relative free energy change with the fraction of sites occupied on the surface, and thus in essence it does not predict the true minimum energy form of a stationary equilibrated interface. This latter point has been examined by Miller and Chadwick.[5]

Nevertheless. the treatment has been of considerable value in increasing the understanding of the factors influencing the interface form during solidification. The studies of Jackson and Hunt[6] and Jackson ***et*** *al.*[4]—in which transparent organic crystals, chosen with a range of α-factors and thus analogous to a range of materials both metallic and non-metallic, were observed during solidification—were largely in agreement with Jackson's original predictions.' Figure 3.2 shows examples of the different types of interface.

There are inadequacies in the theory of Jackson, particularly those associated with kinetic influences and related to details of the crystal structure, ***e.g.*** the anisotropy of growth.

One approach to the problem of the relation between the interface structure and the growth of the interface was that of Cahn[7] ***(see also*** Cahn ***et*** *al.*[8]) who considered in detail the 'diffuseness' of the interface, ***i.e.*** the number of atomic layers comprising the transition from solid to liquid. Cahn concluded that the degree of diffuseness was dependent on both the material and the driving force for transformation. The driving force is determined by the undercooling at the interface. As a result it was predicted that at low driving forces the interface would be discrete and propagation would take place by the transverse motion of interface steps, while at large driving forces the growth would be normal with the interface diffuse. This theory was examined in detail by Jackson ***et*** *al.*,[4] who compared the predictions with experimental data for a considerable range of materials. The examination showed that the evidence did not support the predictions.

Jackson[9] followed up his earlier work with a more general theory of crystal growth which related both structure and growth rate. This led to reasonable predictions for growth rate anisotropy. The theory

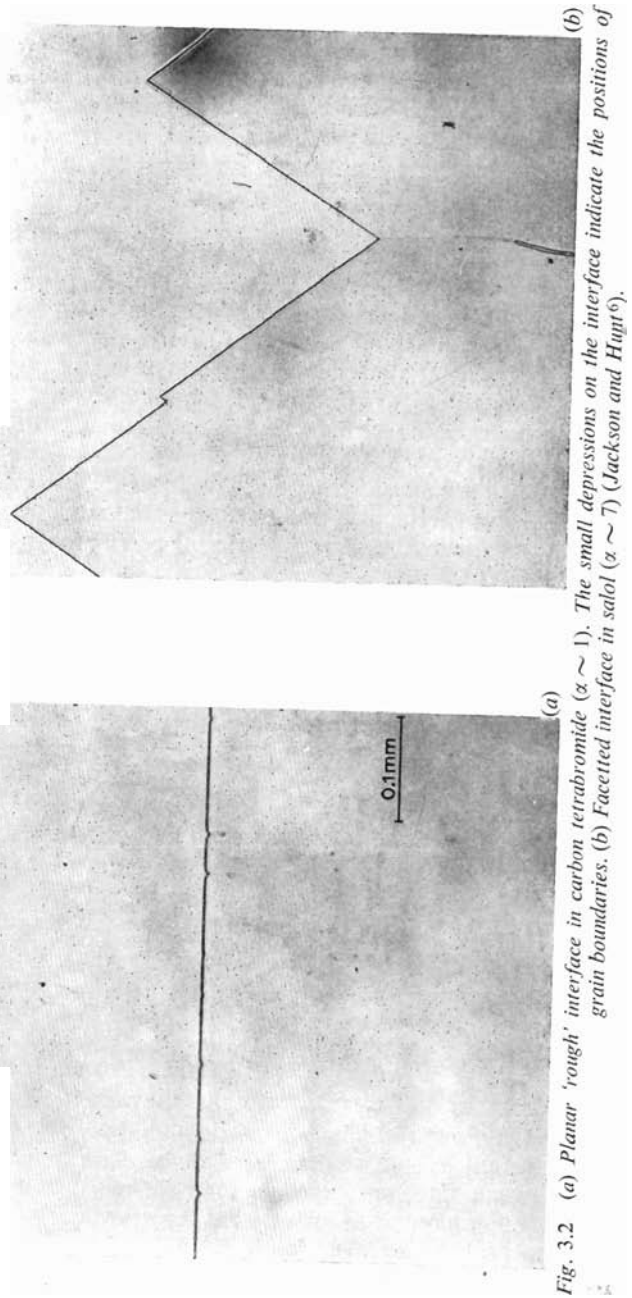

Fig. 3.2 (a) Planar 'rough' interface in carbon tetrabromide (α ~ 1). The small depressions on the interface indicate the positions of grain boundaries. (b) Facetted interface in salol (α ~ 7) (Jackson and Hunt[6]).

predicted interface structures which correlated well with the previous predictions[1] based on the α-factor (eqn. 3.2). This theory was extended by the development of a fundamental rate equation for crystal growth[9,10] and this is examined further in the next section. It was, however, unable to explain the anisotropy of crystal growth for processes such as dendritic growth (see Section 4.6).

3.2 GROWTH OF THE INTERFACE

The growth rate of a crystal depends on the difference between the rate at which atoms add theniselves to the interface and the rate at which they leave the interface. In the previous section two principal forms of interface were characterised, one atomically rough and non-crystallographic in character and the other smooth and crystallographically faceted. Different mechanisms of interface advance can be attributed to these different interface forms. The normal procedure is to define a mechanism and calculate the mean rate of interface motion as a function of the undercooling AT. Three mechanisms will be considered:

(i) the normal growth mechanism;
(ii) growth by repeated surface nucleation; and
(iii) growth on imperfections.

The latter two mechanisms require the existence of growth steps on the interface.

3.2.1 Normal growth

In normal growth[11] all sites on the interface are considered to be equivalent and the interface advances by the continuous random addition of atoms. The theory was based on earlier work by Wilson[12] and Frenkel[13] and it predicts that the mean growth rate, $\bar{R}$, is proportional to the undercooling, *i.e.*

$$\bar{R} = \mu_1 \cdot \mathrm{AT} \tag{3.3}$$

where μ_1 is a constant.

For normal growth the growth rates can be quite high and the requirement of site equivalence implies the need for a rough interface. This is the growth mechanism considered applicable to most metals. The constant p, can be calculated to be $\sim$1 cm sec^{-1} K^{-1}. Thus high growth rates are expected for relatively small undercoolings. On the other hand, it follows that at the growth rates encountered in practice ($\sim 10^{-2}$ cm sec^{-1}, see Table 4.1) the undercoolings are immeasurably small. This makes experimental verification of the

normal growth theory difficult. The rate controlling mechanism is usually the rate of removal of latent heat. Since the materials with rough interfaces also tend to have low latent heats of melting, the rapid growth rates are comparatively easily sustained.

3.2.2 Growth by surface nucleation

This theory[14] (*see* also Hollomon and Turnbull[15]) assumes that the crystal interface is smooth (faceted) and that growth proceeds by the homogeneous nucleation of new layers in the form of disc nuclei which grow *laterally* until a complete layer is formed. This is shown

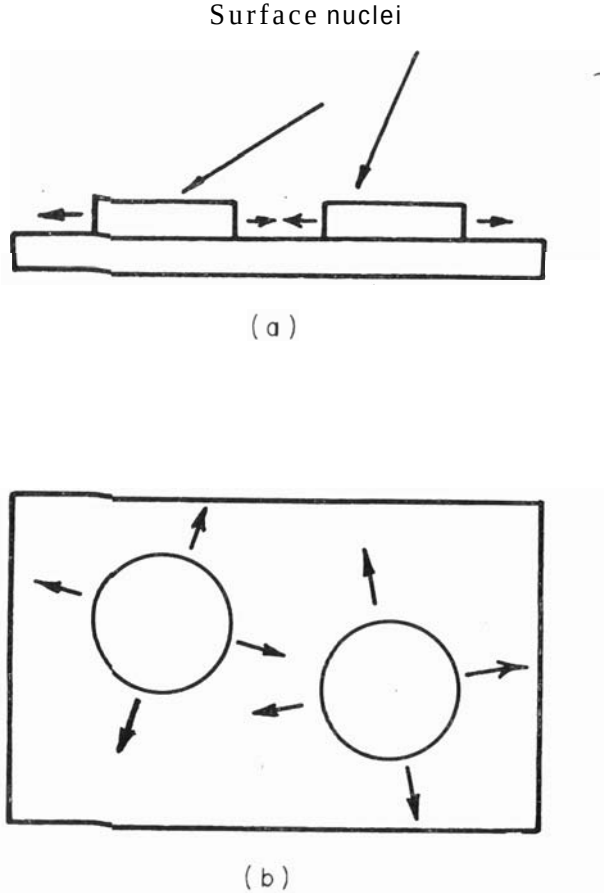

Schematic view of the formation of disc-shaped nuclei on a crystal (a) view parallel to the surface; and (b) view normal to the surface.

schematically in Fig. 3.3. The mode of growth leads to a rate equation of the form

$$\bar{R} = \mu_2 \cdot \exp\left(-\frac{b}{\Delta T}\right) \tag{3.4}$$

where μ_2 and b are constants. The theory predicts growth rates which are negligibly slow at low undercoolings. The evidence in support of this mechanism is very limited.[4]

3.2.3 Growth on imperfections

Here the assumption is that some form of continuous growth step exists at which atoms can be added. The simplest form of step is that formed when a screw dislocation emerges at a crystallographically smooth interface (Fig. 3.4). The theory of growth on screw dislocations has been treated by Frank[16] and Hillig and Turnbull.[17] This method of growth has a rate law

$$\bar{R} = \mu_3 \cdot \Delta T^2 \tag{3.5}$$

In this case the predicted growth rates are also very low and this is

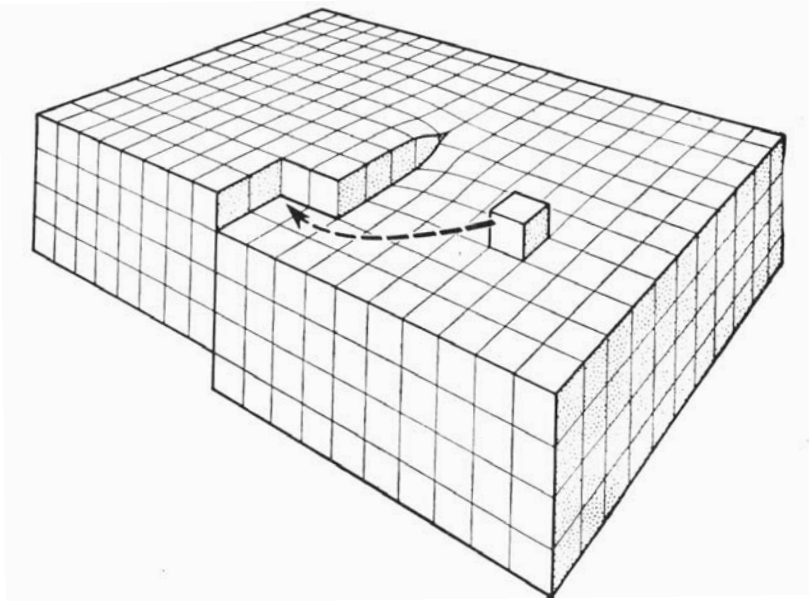

Fig. *3.4 Schematic view of a crystal containing a screw dislocation running normal to the upper surface. This surface is a spiral ramp and cannot be eliminated by adding atoms as shown (Read*[28]*).*

...ely a consequence of the restriction on the number of available ...wth sites. Nevertheless, the faceted growth of non-metals has ...n observed[18] to involve this mechanism. Spiral growth on screw ...locations is common during the growth of crystals from solution ... from the vapour (Fig. **3.5).**

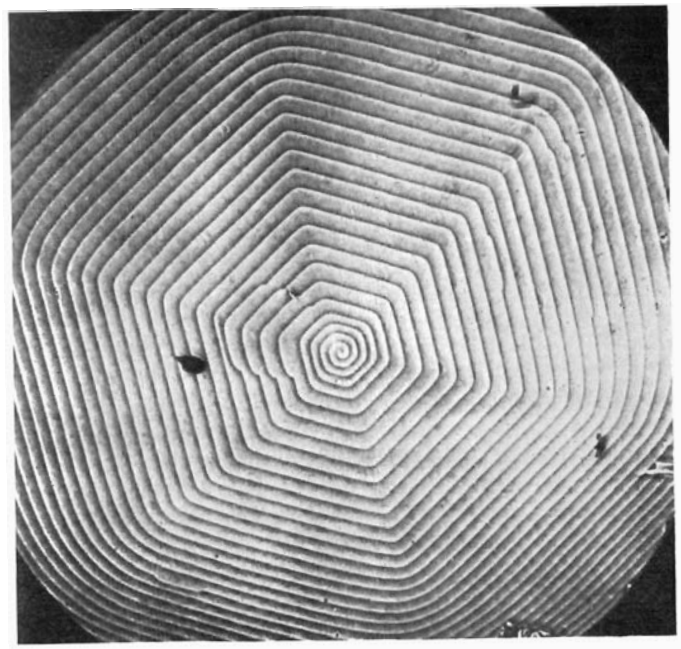

Fig. 3.5 A growth spiral on a crystal of SiC grown from the vapour (Verma[29]*).*

3.2.4 The generalised rate equation

As mentioned earlier, Jackson[10] developed a general formulation for the prediction of growth rate from a knowledge of the interface structure. This rigorous theory was shown to incorporate as limiting cases the previous growth rate theories described above.

3.3 GROWTH DEFECTS

Atomic scale defects, ***e.g.*** vacancies, dislocations, can be produced during crystal growth. Because of their contribution to increased entropy the different forms of point defect are thermodynamically stable.[19] The equilibrium concentration of vacancies in solids at temperatures near the melting temperature is of the order of 10^{-5}.

As shown by Chalmers,[20] they are readily produced during solidification, although it is not expected that a supersaturation should exist after solidification. The equilibrium concentration in the solid decreases exponentially as the temperature decreases and rapid cooling of the solid can lead to supersaturation. The presence of vacancy sinks, ***e.g.*** grain boundaries, will reduce the degree of supersaturation.

Under normal conditions of crystal growth the supersaturation should be small, and no clustering is expected.[21] In melt-grown crystals the influence of point defects will be limited.

The presence of dislocations can have marked effects. A number of factors can lead to the production of dislocations during growth from the melt. In the presence of impurities when cellular or dendritic interfaces are formed (***see*** Section 4.5), a well-developed dislocation substructure is produced.[22,23] On a large scale the trapping of foreign particles can produce dislocations both to accommodate mismatch at the particle–solid interface and as a result of misfit stresses.[24,25] The presence of impurity particles also leads to the development of the dislocation array of sub-boundaries produced during solidification, known as the lineage structure.[11]

The grown-in dislocation density can be multiplied by mechanical and thermal stresses. The usual densities are of the order of 10^7 cm cm^{-3} although with care very low densities can be produced in metals[27] (10^2 cm cm^{-3}), and in non-metals, such as silicon, dislocations can be eliminated altogether.[24]

REFERENCES

1. Jackson, K. A. (1958). *Liquid Metals and* ***Solidification,*** ASM, Cleveland, p. 174.
2. Burton, W. K., Cabrera, N. and Frank, F. C. (1951). ***Phil. Trans. Roy. Soc., A243,*** 249.
3. Wagner, R. S. (1965). *Trans.* ***Met. Soc. AIME, 224,*** 1182.
4. Jackson, K. A., Uhlmann, D. R. and Hunt, J. D. (1967). ***J. Crystal Growth, 1,*** 1.
5. Miller, W. A. and Chadwick, G. A. (1969). ***Proc.*** *Roy.* ***Soc., A312,*** 257.
6. Jackson, K. ***A.*** and Hunt, J. D. (1965). ***Acta Met., 13,*** 1212.
7. Cahn, J. W. (1960). ***Acta Met.,*** 8, 554.
8. Cahn, J. W., Hillig, W. B. and Sears, G. W. (1964). ***Acta Met., 12,*** 1421.
9. Jackson, K. A. (1968). ***J. Crystal Growth, 3–4,*** 507.
10. Jackson, K. A. (1969). ***J. Crystal Growth, 5,*** 13.
11. Jackson, K. A. and Chalmers, B. (1956). ***Can. J. Phys., 34,*** 473.
12. Wilson, H. A. (1900). *Phil Mag.,* **50,** 238.
13. Frenkel, J. (1932). ***Physik.*** *Z. Sowjet* ***Union, 1,*** 498.

Volmer, M. and Mander, M. (1931). Z. ***Physik. Chem., A154,*** 97.
Holloman, J. H. and Turnbull, D. (1953). ***Progr. Metal Physics, 4,*** 333.
Frank, F. C. (1949). ***Disc. Faraday Soc., 5,*** 48.
Hillig, W. B. and Turnbull, D. (1956). ***J. Chem. Phys., 24,*** 219.
Roveros, **H.** G. (1968). ***J. Crystal Growth, 2,*** 173.
Swalin, R. A. (1962). ***Thermodynamics of Solids,*** John Wiley, New York, p. 222.
Chalmers, B. (1954). ***Trans. AIME, 200,*** 519.
Jackson, K. A. (1962). ***Phil. Mag.,*** 7, 117.
Damiano, V. V. and Tint, D. S. (1961). ***Acta Met.,*** 9, 177.
Hunt, M. D., Spittle, J. A. and Smith, R. W. (1968). ***J. Crystal Growth, 3 4,*** 656.
Dash, W. C. (1959). ***J.*** Appl. ***Phys., 30,*** 459.
Jackson, **K.** A. (1962). ***Phil. Mag.,*** 7, 1615.
Jaffrey, D. and Chadwick, G. A. (1968). *Phil. Mag.,* ***18, 573.***
Young, F. W. and Savage, J. R. (1964). ***J. Appl. Phys., 35,*** 1917.
Read, W. T. (1953). ***Dislocations in Crystals,*** McGraw-Hill, New York.
Verma, A. R. (1953). ***Crystal Growth and Dislocations,*** Butterworths, London.

CHAPTER 4

Solidification of Single-phase Metals and Alloys

In this chapter we will be concerned with the effect of the different solidification variables ***(e.g.*** growth rate and temperature gradient in the liquid) on the structure and composition of the growing solid. In particular, when we consider single-phase alloys, the way in which the solute is redistributed during solidification will bccxarnined, as will the effects of this redistribution on the micro- and macro-structure of the solidifying alloy. Before examining the solidification processes it is essential to define clearly a terminology.

4.1 TERMINOLOGY

(a) The *growth* ***rate,*** R, is a measure of the rate of advance of the interface between the liquid and the solid. Sometimes the growth rate will refer to the rate averaged over several points on the interface and sometimes it will refer to a specific region of the interface. Growth rates are normally expressed in cm sec^{-1} or cm hr^{-1}. Some typical growth rates for a range of solidification processes are given in Table 4.1 .

TABLE 4.1

TYPICAL GROWTH RATES FOR DIFFERENT SOLIDIFICATION PROCESSES

Process	*Growth rate, cm* sec^{-1}
Growth of metal single crystals	10^{-3}
Directional growth studies in research	10^{-2}
Ingot solidification	10^{-2}
Initial dendritic growth ($\Delta T \sim 0.02\ T_m$)	5
Initial dendritic growth ($\Delta T \sim 0.2\ T_m$)	5 000

(b) The ***temperature gradient,*** G, is usually taken to refer to the gradient in the liquid away from the interface in the direction of growth. If the temperature increases as we go into the liquid, the temperature gradient is considered to be positive and vice versa. Commonly, temperature gradients vary from a few degrees Centigrade per centimetre during the growth of single crystals, to tens of

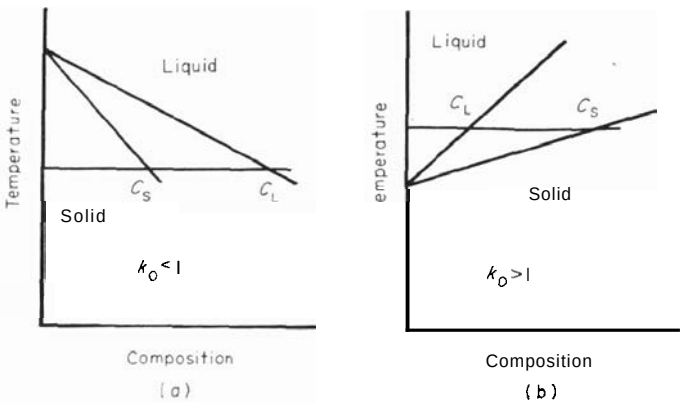

Fig. **4.1** ***(a) Portion of a phase diagram in which the distribution coefficient*** $k_0 < 1$. ***(b) Portion of a phase diagram in which the distribution coefficient*** $k_0 > 1$.

degrees Centigrade per centimetre in castings and ingots, and to hundreds of degrees Centigrade per centimetre during weld-pool solidification.

(c) The *diffusivity*, D, determines the rate at which atoms can move in the liquid. For virtually all metallic liquids D is of the order of 5×10^{-5} cm^2 sec^{-1}. Diffusion rates in the solid are much smaller, ***e.g.*** $\sim 10^{-8}$ cm^2 sec^{-1} for common metals just below their melting points. Thus solute redistribution in *the* solid is usually ignored in comparison to solute redistribution in the liquid.

(d) The equilibrium ***distribution*** *coefficient*, k_0, is defined by the phase diagram, assuming the liquidus and solidus lines to be straight. Figure 4.1 shows the two different forms of liquidus and solidus arrangement at the pure substance,end of a phase diagram. The equilibrium distribution coefficient is given by the ratio

$$k_0 = \frac{\text{solute concentration in the solid at temperature T}}{\text{solute concentration in the liquid at the same temperature}} = \frac{C_S}{C_L}$$

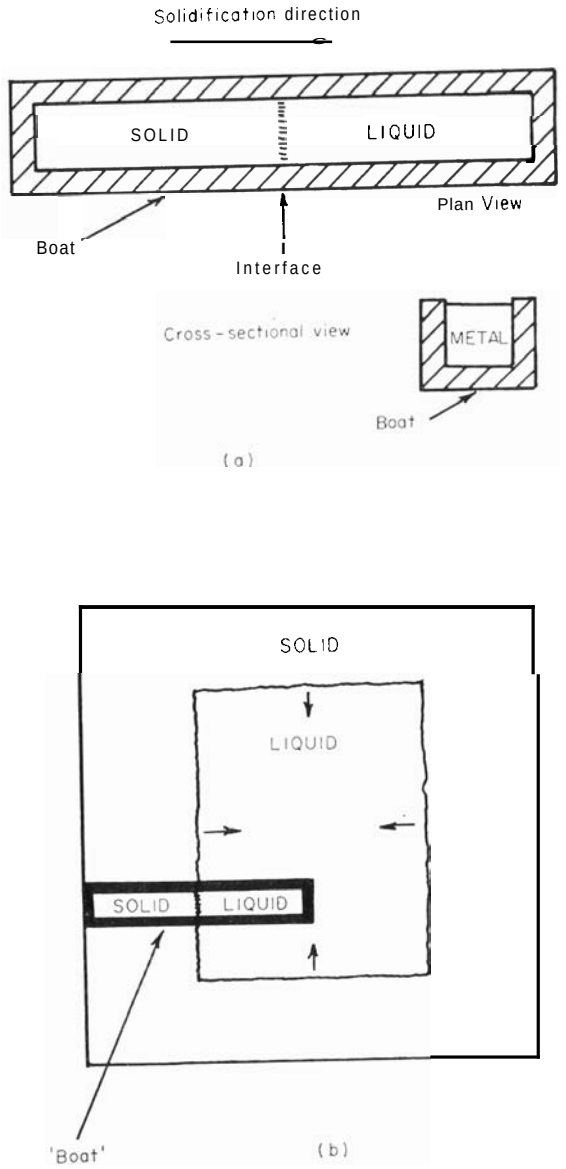

Fig. 4.2 (a) A casting boat used for controlled directional solidification (schematic). The metal is shown as partially solidified. (b) Schematic view of the cross section of a partially solidified ingot showing how the casting boat con be considered as a section of the ingot.

If the effect of the solute is to lower the liquidus temperature, then $k_0 < 1$ and vice versa.

It is sometimes convenient to define an 'effective' distribution, k_E, as

$$k_E = \frac{\text{instantaneous composition of solid formed}}{\text{average composition of the liquid at that time}}$$

This definition is of importance in Section 4.3 when we consider solute redistribution effects during solidification.

(e) The ***slope of the liquidus line*** is given the symbol m. In their classical paper on solute redistribution, Tiller ***et al.***[1] defined the liquidus slope shown in Fig. 1(a) as ***positive*** m and that shown in Fig. 1(b) as ***negative*** *m*. It should be noted that although this is contrary to normal mathematical practice, this convention has been adhered to throughout the literature on solidification and will be followed in this chapter.

(f) The earliest solidification studies of Chalmers and his co-workers involved the *unidirectional solidification* of metals and alloys under controlled conditions in casting 'boats' of graphite or a similar material. The solidification process in the boat was essentially treated as if it were a section from a larger ingot or casting undergoing solidification, as shown in Fig. 4.2. This approach yielded valuable fundamental data on solidification processes and has been widely adopted since. We will have frequent occasion to refer to this type of unidirectional solidification procedure throughout this chapter.

4.2 PURE METALS

4.2.1 Interface forms

The growth of pure metals in a region of positive temperature gradient is controlled by the flow of heat away from the interface through the solid. The interface is normally rough and isothermal, being at a temperature below the equilibrium temperature just necessary to provide sufficient kinetic driving force. This kinetic undercooling has been estimated as −0.01"K. Non-metallic materials of high purity are expected to behave in a similar way within the constraints conferred upon them by the need to fulfil the interface requirements outlined in the previous chapter. The growing interface for both groups of materials should progress in a stable form. Any localised instability formed on the interface would project into a region at a temperature higher than the melting temperature and would remelt to restore the isothermal interface. The sequence of events is illustrated schematically in Fig. 4.3.

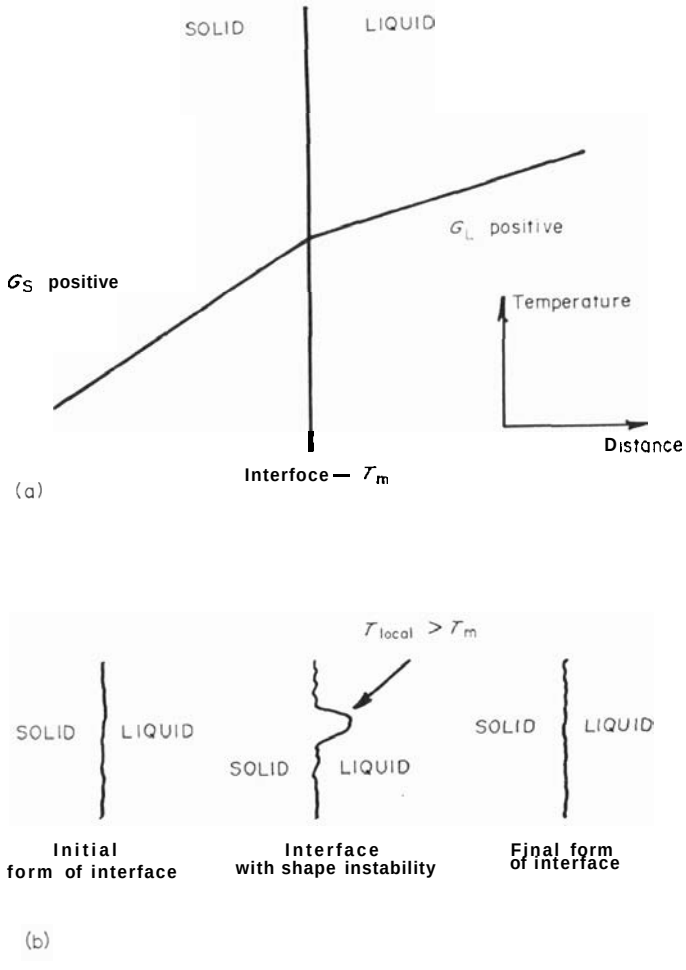

Fig. 4.3 (a) Area of solid and liquid adjacent to the interface showing positive temperature gradients in the liquid and solid (schematic). G_{solid} is steeper than G_{liquid} because of the higher thermal conductivity of the solid. (b) Schematic sequence showing the formation of an unstable protuberance which melts because the local tip temperature exceeds the melting temperature.

However, if a state of metastability or instability is created near the growing interface by the occurrence of an inverted gradient of free energy (this is normally achieved by inverting the temperature gradient), the growing interface will break down and grow as shown in Fig. 4.4. Usually these interface instabilities also break down laterally and develop side branches. The interface thus degenerates

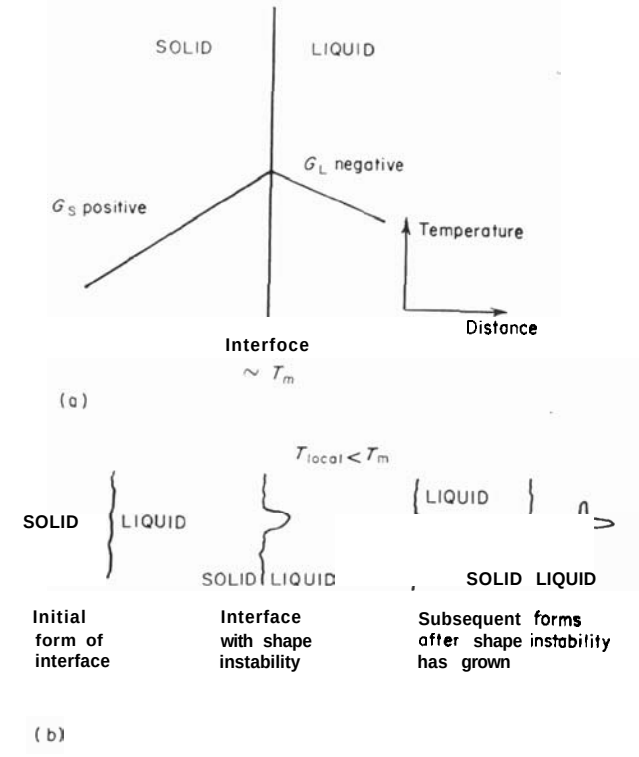

Fig. 4.4 (a) Area of solid and liquid adjacent to the interface showing a negative temperature gradient in the liquid and a positive temperature gradient in the solid (schematic). (b) Schematic sequence showing the formation and stabilisation of a protuberance on the interface when it projects into a region where the local tip temperature is below the melting temperature.

and grows dendritically.[2] In practice, these conditions will only exist in bulk pure materials during the period between the initial nucleation and the attainment of the transformation temperature at which the dendrite arms thicken. Thus, if we consider a typical form of cooling curve it can be divided into sections as shown in Fig. 4.5. Dendritic structures are considered in greater detail in Section 4.6.

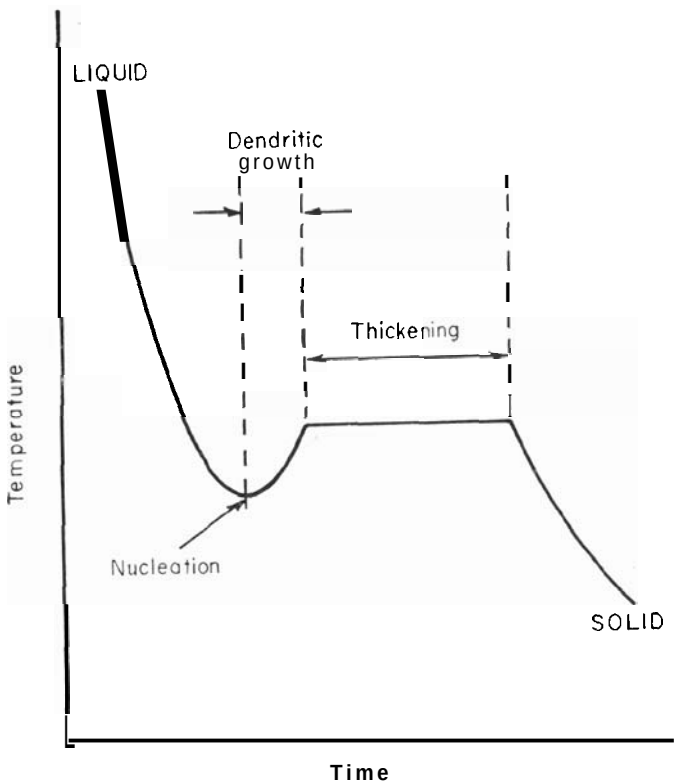

Fig. **4.5** *Typical form of* **cooling curve for** *pure metals showing* **the regions in** *which* **the different growth phenomena occur.**

4.2.2 Structural effects

From a structural point of view the important factors are those of grain size and shape. These are macrostructural variables and will be considered in Chapter 6. Of minor importance are the extent and nature of crystal defects, *e.g.* vacancies and dislocations. It is not expected that the concentrations of vacancies either singly or in clusters will be large under normal solidification conditions,[3] nor that properties will be significantly affected. Dislocations, however, can have a significant influence. The grown-in dislocation density is determined by interactions during growth and by subsequent multiplication processes. With care, the overall densities can be kept low for metals[4] and reduced to zero for non-metallic materials. Lineage structures, i.e. arrays of dislocation sub-boundaries,[5,6] also frequently

occur, but the available evidence indicates that they result from entrapped impurity particles.[7]

4.3 SOLUTE REDISTRIBUTION EFFECTS IN ALLOYS

The growth of impure metals is much more complex because of the redistribution of solute that occurs during solidification. This can

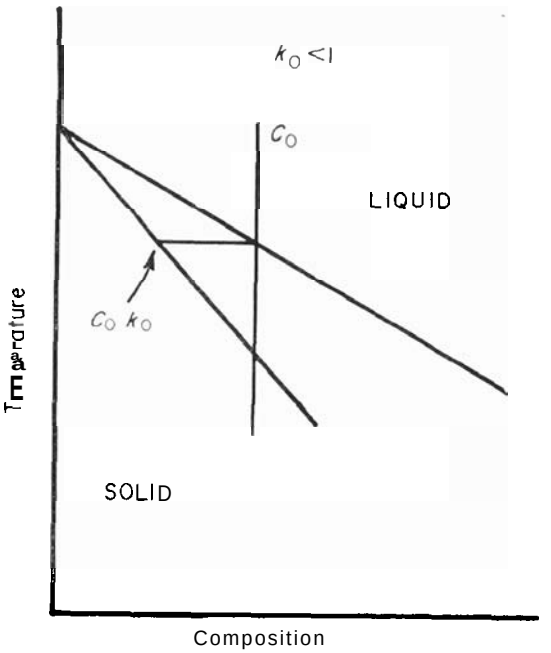

Fig. 4.6 *Portion of a phase* **diagram for an alloy of composition** C_0, **with** $k_0 < 1$, *showing* **initial** *compositional changes.*

produce changes in the growth morphology and lead to solute segregation on both a microscale and a macroscale. If we consider the initial sequence of events during the solidification of an alloy of composition, C_0, with distribution coefficient, $k_0 < 1$ (Fig. 4.6), it is clear from the phase diagram that the first solid to form will have composition $C_0 k_0$. Since $k_0 < 1$ there is a small localised increase in the solute content of the liquid. Two extreme cases should be considered. First, the solute increase may disperse in the liquid by diffusion only. Alternatively, conditions of complete mixing may exist in the liquid which rapidly spread the excess solute throughout

the bulk of the liquid. We will examine both of these and the intermediate case of redistribution by diffusion and partial mixing. In all cases it will be assumed that no concentration changes occur in the solid after solidification. For reasons outlined in Section 4.1(c), this assumption is reasonable.

4.3.1 Solute redistribution by diffusion

Reconsidering the alloy with $k_0 < 1$, it is clear that after the first solid of composition C_0k_0 has been formed, because of the local solute enrichment of the liquid the next element of solid deposited

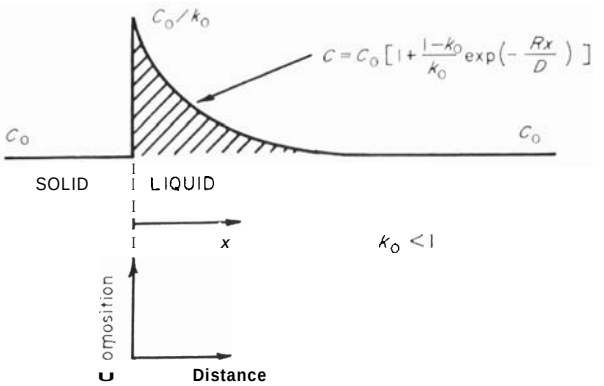

Fig. 4.7 The solute profile ahead of the interface during steady-state solidification with solute redistribution by diffusion only ($k_0 < 1$).

will have a composition $(C_s + \delta C_0)k_0$, where δC_0 represents the local enrichment, and so on. At the same time a layer of solute will build up at the interface and solute diffusion will take place down the concentration gradient. There will thus be an initial transient in concentration in the solid but, in due course, a steady-state will occur where the rate of rejection of solute at the interface just equals the rate of solute diffusion away from the interface.

It was shown by Tiller *et al.*[1] that the solute distribution in the liquid at the steady-state was given by the solution to the differential equation

$$D\frac{d^2C}{dx^2} + R\frac{dC}{dx} = 0$$

This equation has the general solution

$$C = A + B\exp\left(-\frac{Rx}{D}\right) \qquad (4.1)$$

where C is the solute concentration in the liquid at a distance x ahead of the interface, R and D have their usual meanings and A and B are constants determined by the boundary conditions. Simple deduction shows that the nature of the solute 'pile-up' ahead of the interface at the steady-state must be as shown in Fig. 4.7 since incremental movement of this profile puts out solid of composition $(C_0/k_0)k_0 = C_0$ and takes in liquid of composition C_0. The composition of the liquid in the regions remote from the interface will

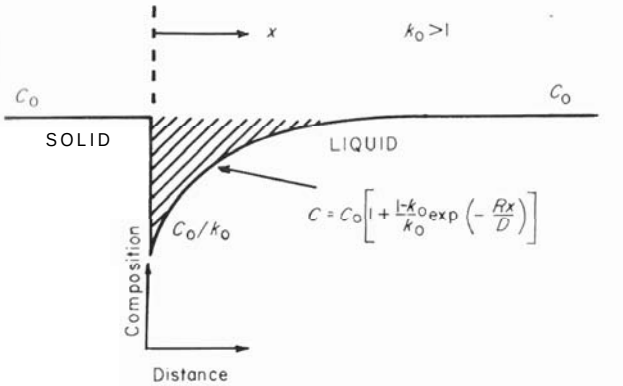

Fig. 4.8 The corresponding profile to that of Fig. 4.7 for $k_0 > 1$.

only differ significantly from C_0 at the later stages of solidification. This in its turn gives rise to a terminal transient.

For the steady-state the solute profile then has the boundary conditions,

$$x = 0, \quad C = C_0/k_0, \quad x = \infty, \quad C = C_0$$

Substitution in eqn. (4.1) gives the result

$$C = C_0\left[1 + \frac{1-k_0}{k_0}\exp\left(-\frac{Rx}{D}\right)\right] \qquad (4.2)$$

Treatment of the case of an alloy with $k_0 > 1$ leads to the same form of equation as in eqn. (4.2). The solute profile is, however, inverted (Fig. 4.8).

Figure 4.9 illustrates, schematically, the way the solute concentration profile changes in front of the interface with changes in the variables R, D and $k_0(<1)$, respectively.

It is seen that a short, steep pile-up is produced at high growth rates and for low solute diffusivities. Of particular importance are the extreme solute accumulations that can occur near the interface for systems in which k_0 is very small.

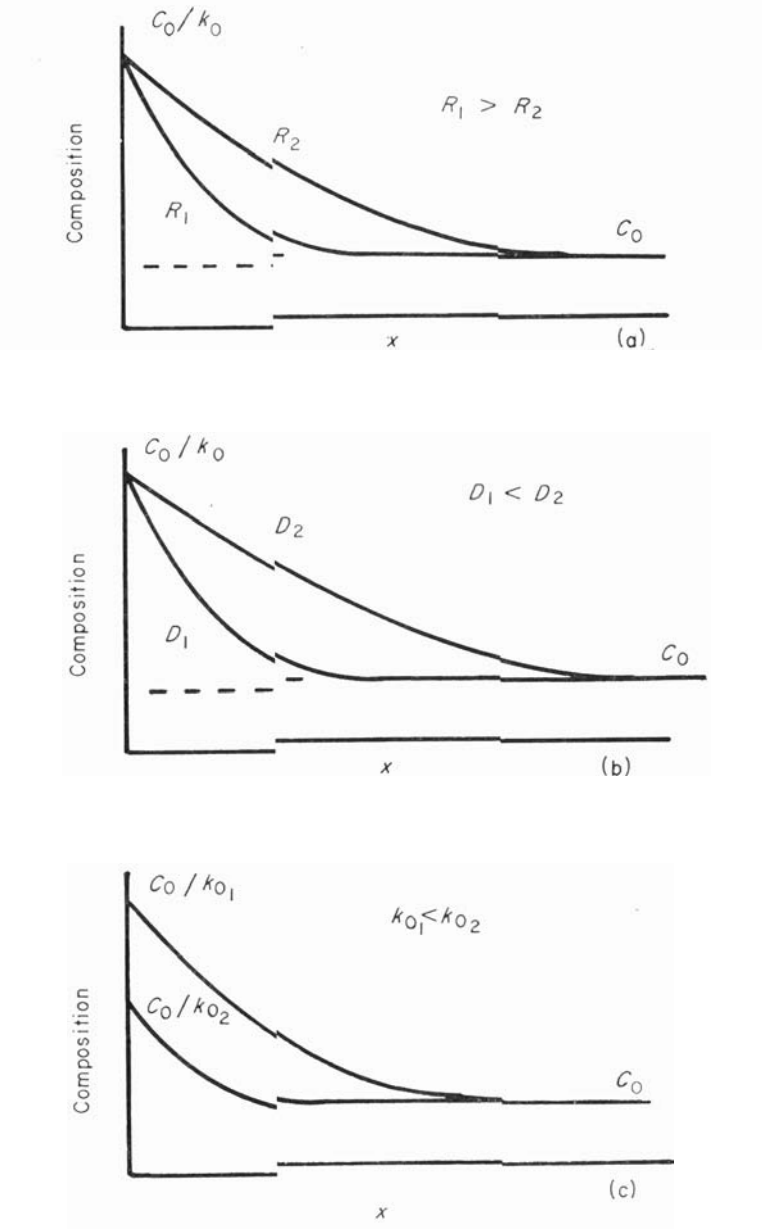

Fig. 4.9 Changes in the solute concentration ahead of a growing interface for changes in the growth parameters: (a) growth rate; (b) diffusivity; (c) distribution coefficient.

For solute concentrations higher than about 0·5% the solute pile-up effects are very marked and the physical nature of the interface differs to a non-planar configuration (this is considered in detail in the next section). Under these conditions, eqn. (4.2) is no longer valid, although it can be used to give some approximate indication

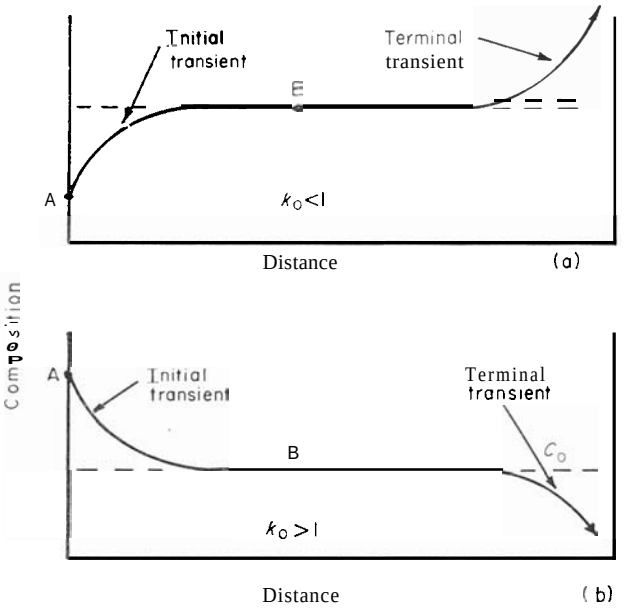

Fig. 4.10 Concentration–distance profiles for a bar solidified under conditions where solute transport in the liquid is by diffusion only: (a) $k_0 < 1$; *(b)* $k_0 > 1$.

of the solute distribution near the interface. Calculation shows that the solute pile-up would seldom exceed a thickness of 0·1 mm without a significant change in the interface form.

For a case in which eqn. (4.2) holds, if a boat full of liquid of initial composition C_0 is solidified to a bar under the conditions considered above, the final solute distribution is as shown in Fig. 4.10, making allowance for the initial and terminal transients. At points A and B on these two curves the compositions of the solid formed instantaneously are C_0k_0 and C_0, respectively. The average composition (ignoring the small *overall* average increase resulting from the localised interface pile-up) in both cases is C_0. Thus the *effective distribution coefficients* are k_e and 1 for the two cases. The distribution coefficient is therefore seen to vary from the equilibrium value k_0 to the value 1 as the steady-state is approached.

4.3.2 Complete mixing in the liquid

If conditions of complete mixing by convection or stirring exist within the liquid, then with $k_0 < 1$ the solute rejected at the interface is distributed evenly throughout the liquid. Thus in the initial stages, where the volume of liquid is large, the overall change in composition

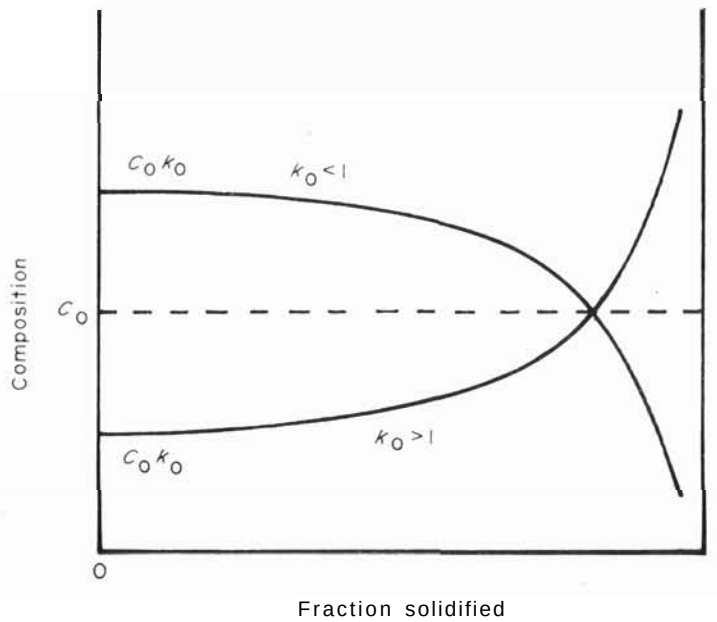

Fig. 4.11 *Concentration–distance* ***profiles for a bar*** *solidified under conditions of* ***complete solute mixing in the liquid.***

is small. As solidification proceeds, however, the compositional changes in the liquid become more marked. The form of the final solute distribution in the solid has been analysed by Pfann.[8] The solute profile is given by

$$C_s = C_0 k_0 (1 - x)^{k_0 - 1} \tag{4.3}$$

where C_s is the solute concentration in the bar at a point where a fraction x of the bar has solidified. The detailed analysis is given in Appendix 2. The form of the solute distribution is shown in Fig. 4.11. Since no diffusion in the solid is assumed, the average liquid composition after a fraction x has solidified must be

$$C = C_0 (1 - x)^{k_0 - 1}$$

4.3.3 Partial mixing in the liquid

The intermediate case in which partial mixing in the liquid is produced by the combined effect of diffusion and convection or stirring has been examined by Burton *et al.*[9] They treated the problem as one in which the solute layer at the interface was gradually broken down by the stirring effects (Fig. 4.12). In their analysis the thickness of the diffusion boundary layer, 6, decreased with increased mixing varying from about 10^{-2} mm for vigorous stirring to about 1 mm for natural convective stirring. They confirmed that the solute

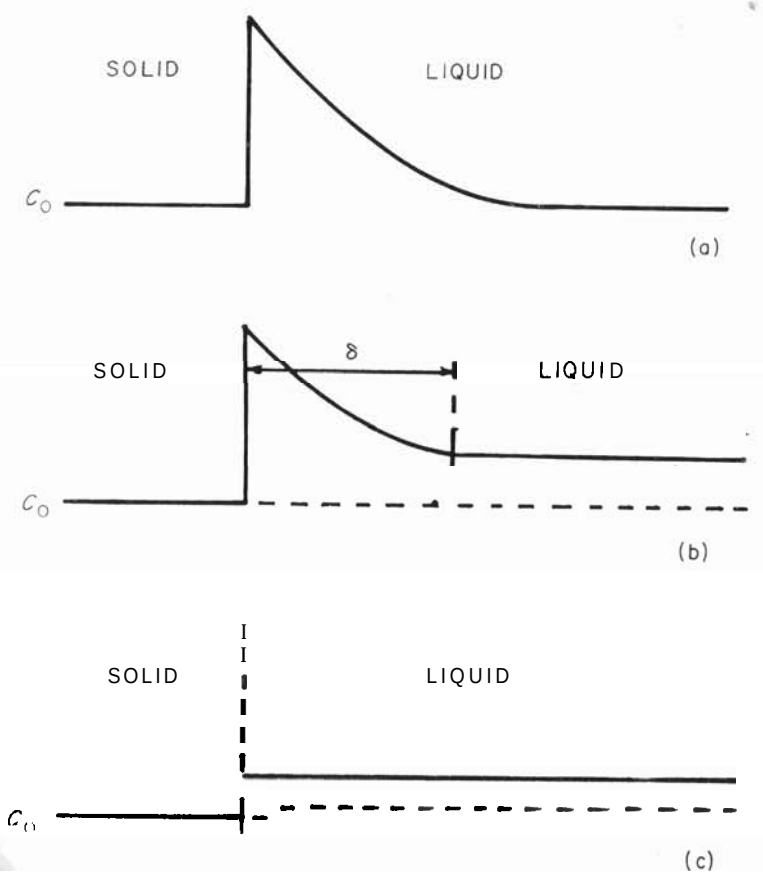

Fig. 4.12 *The effect* ***of the mixing conditions on the nature of the solute layer at the interface:*** *(a)* ***no mixing, diffusion only; (b) partial mixing; (c) complete mixing.***

distribution was given by an equation similar to eqn. (4.3), that is

$$C_s = C_0 k_E (1 - x)^{k_0 - 1} \qquad (4.4)$$

in which the *effective* distribution coefficient is given by

$$k_E = \frac{k_0}{k_0 + (1 - k_0)\exp[-(R\delta/D)]}$$

The solute distribution of eqn. (4.4) lies intermediate between the cases considered above. Figure 4.13 summarises the differences

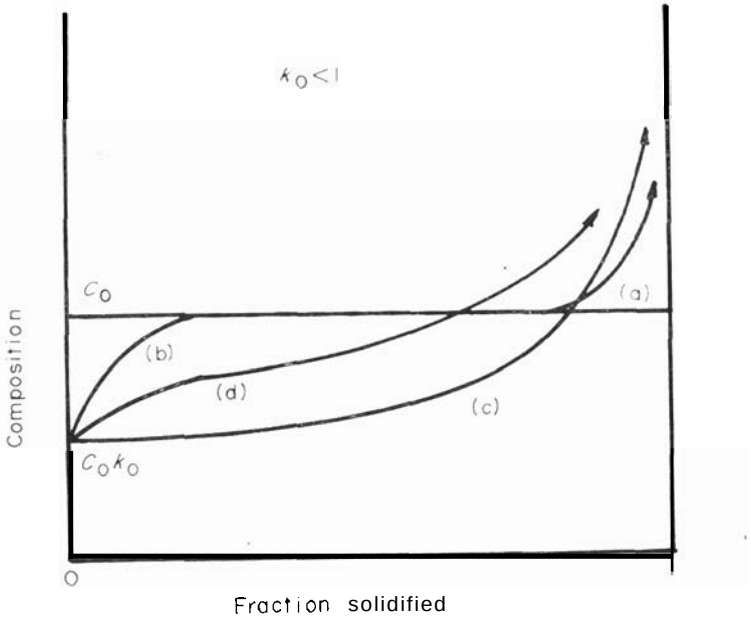

Fig. 4.13 *Solute distributions in a solid bar frozen from liquid of initial concentration* C_0*, for: (a) equilibrium freezing; (b) solute mixing in the liquid by diffusion only; (c) complete solute mixing in the liquid; (d) partial solute mixing in the liquid.*

between the solute profiles obtained for the different solidification conditions. Included in this figure is the profile obtained for equilibrium freezing.

4.3.4 The effect of growth rate changes

If we consider the solute profiles of Fig. 4.9(a), we can see that the *total* amount of solute incorporated into the diffusion boundary layer increases as the growth rate decreases and vice versa. Thus if a

fluctuation in the growth rate occurs during solidification of an alloy with $k_0 < 1$, the amount of solute in the interface pile-up will need to increase if the growth rate slows down or to decrease if the growth rate speeds up. These changes will lead to a localised deviation from the steady-state while the solute pile-up changes. The need for an increase in the amount of solute in the pile-up with a decreased growth rate means a local decrease in the amount of solute deposited in the solid as the growth rate changes. Thus a region depleted in solute will appear in the solid. The reverse is true if the growth rate is increased. The result in the two cases is shown in Fig. 4.14. Only

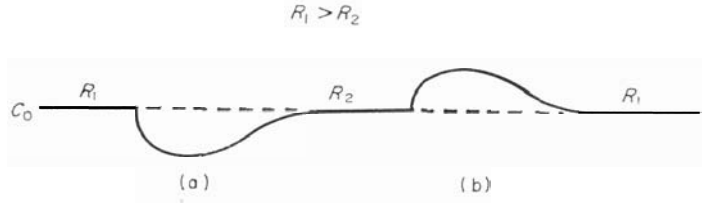

Fig. 4.14 ***The effect of changes in the growth rate on the localised solute distribution in the solid: (a) growth rate decreased; (b) growth rate increased.***

with complete mixing in the liquid is no solute banding to be expected as the growth rate fluctuates.

4.3.5 Practical consequences

The effects of solute redistribution in alloys are of great practical importance. On the one hand, there are the many difficulties generally considered under the heading 'segregation'; these are examined in detail in Chapter 7. On the other hand, there is the technique of *zone refining* in which the solute redistribution is used to advantage to produce materials of very high purity. The specialised field of zone refining has been the subject of excellent monographs by Pfann[10] and Schildknecht[11] and will not be considered further here.

4.4 CONSTITUTIONAL SUPERCOOLING IN ALLOYS

Originally, constitutional supercooling was analysed by Tiller *et al.*' Their treatment was as follows. From the parts of the phase diagrams shown in Fig. 4.1 and the definition of m (the slope of the liquidus line), the equilibrium liquidus temperature, T_L, is given by

$$T_L = T_m - mC$$

where T_m is the melting temperature of the pure metal and C is the

of the liquid. For the steady-state solidification of an alloy of initial composition, C_0, the interface temperature, T_i, is

$$T_i = T_m - \frac{mC_0}{k_0} \tag{4.5}$$

For a solute distribution given by eqn. (4.2), the equilibrium liquidus temperature corresponding to different points ahead of the interface will then be

$$T_L = T_m - mC_0\left[1 + \frac{1-k_0}{k_0}\exp\left(-\frac{Rx}{D}\right)\right]$$

Using eqn. (4.5) this can be rewritten as

$$T_L = T_i + \frac{mC_0(1-k_0)}{k_0}\left[1 - \exp\left(-\frac{Rx}{D}\right)\right] \tag{4.6}$$

The actual temperature in the liquid is given by

$$T = T_i + Gx$$

where G is the temperature gradient in the liquid ahead of the interface. As G varies, a situation can arise where the liquid ahead of the

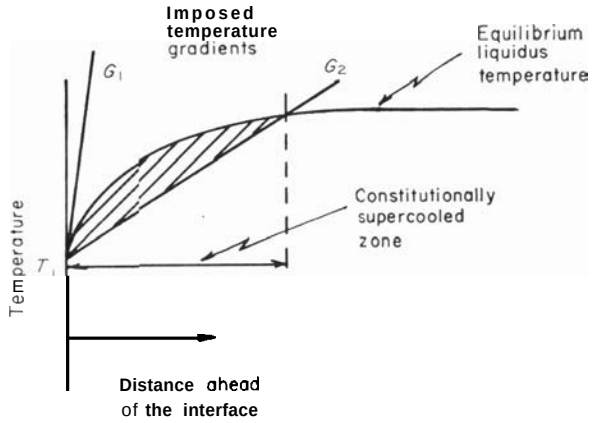

Fig. **4.15** *Constitutional supercooling ahead of an interface showing two applied temperature gradients.*

interface is at a temperature below its equilibrium liquidus temperature, in which case a region of supercooling exists ahead of the interface. This is shown in Fig. 4.15, and the temperature distributions are essentially the same for both $k_0 < 1$ and $k_0 > 1$. This phenomenon is known as ***ronstitutional*** *supercooling*. The limiting condition

, where the temperature gradient is just tangential to the liquidus ·urve at the interface. For steeper temperature gradients ***no*** constitutional supercooling will occur. Thus for no constitutional upercooling we require that

$$G > \left(\frac{dT_L}{dx}\right)_{x=0}$$

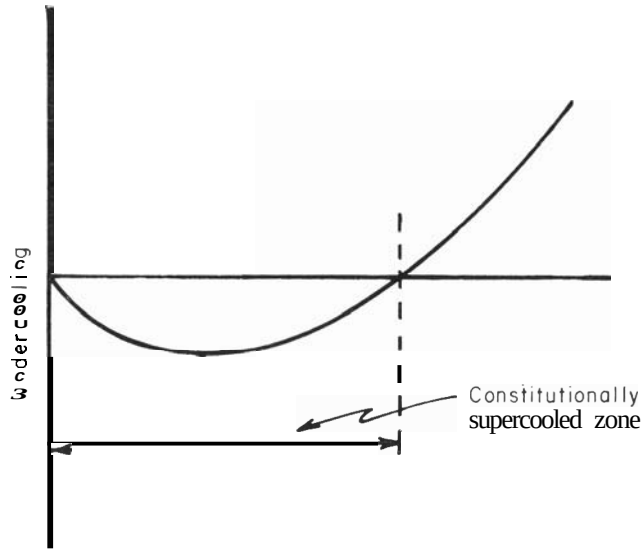

Fig. 4.16 *The magnitude of the undercooling ahead of an interface when* ***constitutional supercooling exists.***

Using cqn. (4.6) it is easily shown that this condition is

$$\frac{G}{R} > \frac{mC_0(1-k_0)}{D\,k_0} \tag{4.7}$$

The terms in eqn. (4.7) are grouped with growth parameters on the left-hand side and material and system parameters on the right-hand side. The nature of this equation allows us to define conditions which will *favour* constitutional supercooling. These are:

(i) low temperature gradients in the liquid;
(ii) fast growth rates;
(iii) steep liquidus lines;
(iv) high alloy contents;?

(v) typical values of the different parameters it can be shown that constitutional supercooling normally **exists** for $C_0 \gtrsim 0.2\%$.

(v) low diffusivity in the liquid;
(vi) very low k_0 for $k_0 < 1$ or very high k_0 for $k_0 > 1$.

In the presence of constitutional supercooling the undercooling is,

$$\Delta T = T_L - T$$

Thus

$$\Delta T = \frac{mC_0(1 - k_0)}{k_0}\left[1 - \exp\left(-\frac{Rx}{D}\right)\right] - Gx \qquad (4.8)$$

This is as shown in Fig. 4.16. The maximum undercooling can be determined from eqn. (4.8) and is,

$$\Delta T_{max} = \frac{mC_0(1 - k_0)}{k_0} - \frac{GD}{R}\left[1 + \ln\frac{(mC_0(1 - k_0)R)}{GDk_0}\right] \qquad (4.9)$$

This maximum undercooling occurs at a point given by

$$x = \frac{D}{R}\log_e\left[\frac{mC_0(1 - k_0)R}{GDk_0}\right] \qquad (4.10)$$

The above treatment assumes that solute mixing in the liquid is the result of diffusion only. It can be modified to allow for partial or complete mixing in the liquid (*see* Chalmers[12]). In these circumstances long-range segregation will still occur.

4.5 STRUCTURAL EFFECTS RESULTING FROM SOLUTE REDISTRIBUTION IN ALLOYS

In the absence of constitutional supercooling, the behaviour during growth is essentially the same as that of pure materials with the exception that long-range segregational effects occur which are associated with the initial and final transients in the solidification process (Fig. 4.13).

The existence of a zone of constitutional supercooling, and thus a negative gradient of free energy, ahead of the interface will make an initially planar interface unstable to perturbations in shape. At low degrees of supercooling a cellular interface develops (Fig. 4.17) from the planar interface after first becoming pock-marked and then showing elongated cells. The breakdown from the planar to the cellular form can be shown experimentally to be governed by eqn. (4.7).[13,14] As the degree of supercooling increases the cell caps becomes extended and eventually branch to form cellular dendrites

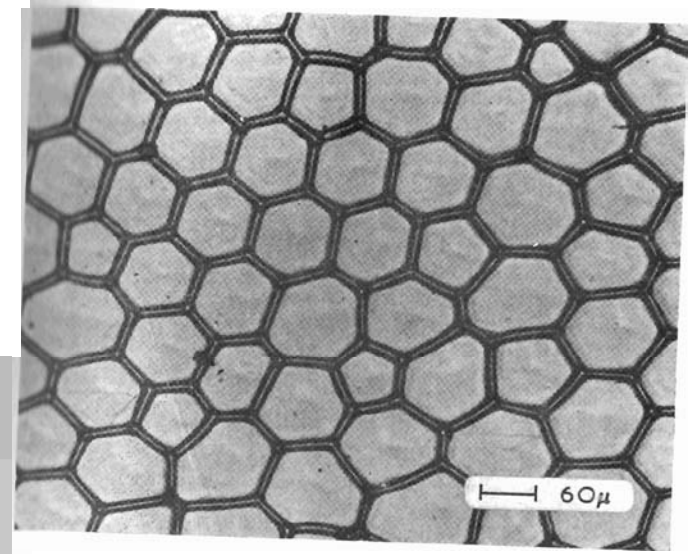

(*a*)

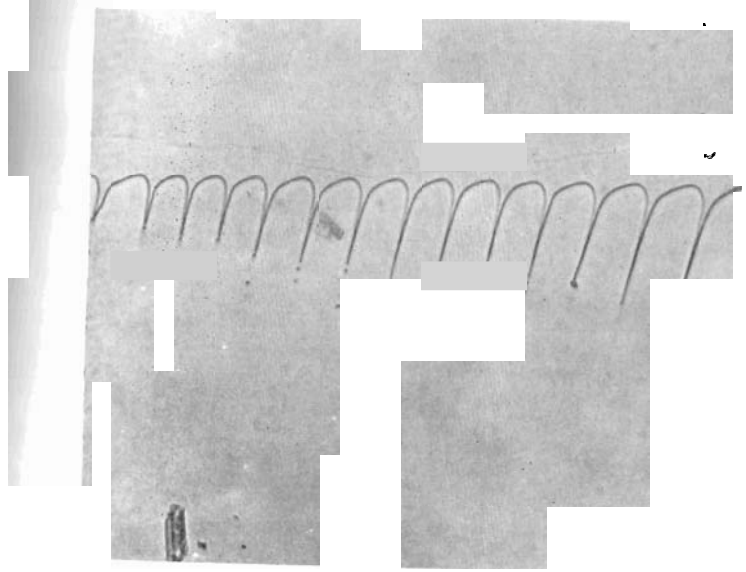

(*b*)

Fig. 4.17 *The cellular interface structure: (a) normal view of a decanted interface; and (b) view of growing interface in impure carbon tetrabromide (Jackson and Hunt*[15]*).*

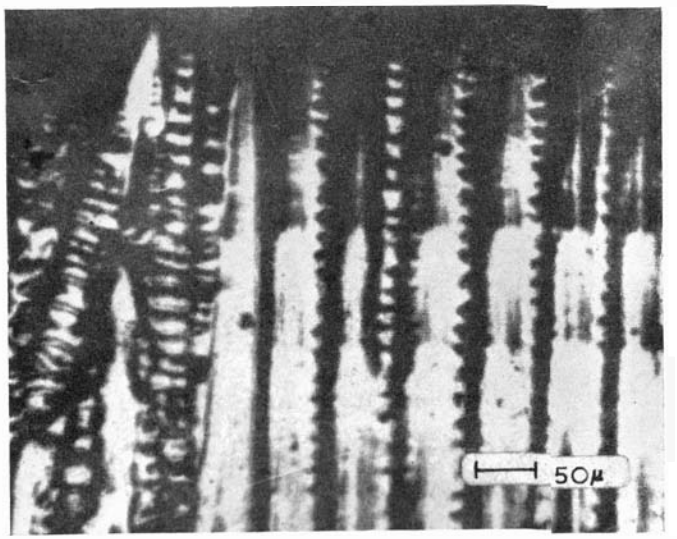

(*a*)

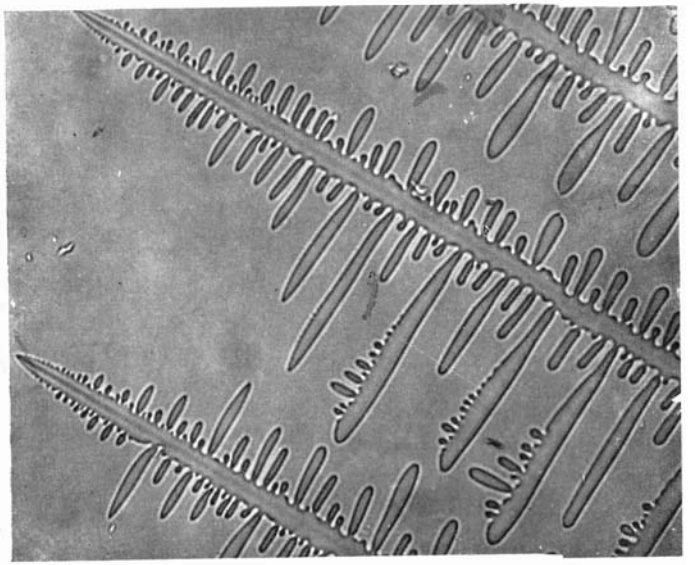

(*b*)

Fig. **4.18** *The cellular–dendritic interface: (a) top surface of an impure lead alloy showing the development of branches on elongated cells (Tiller and Rutter*[13]*); and (b) dendritic growth in cyclohexanol (Jackson and Hunt*[15]*).*

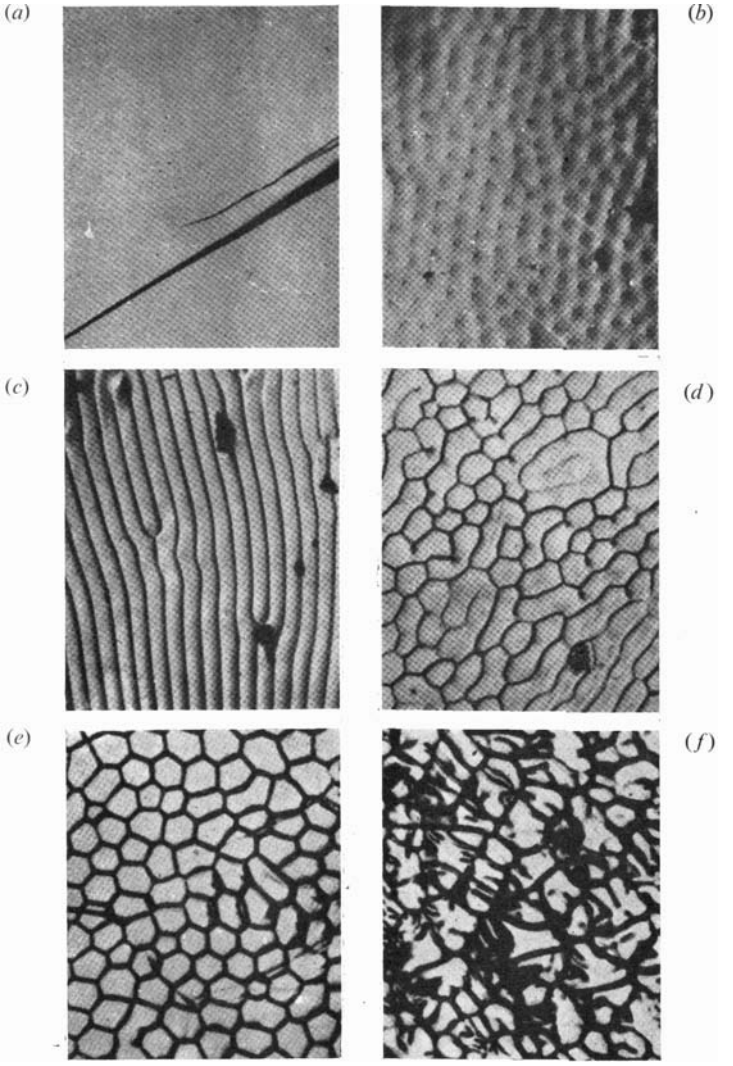

Fig. 4.19 *The transition in growth substructures in a tin–0.005 atom percent lead alloy with constitutional supercooling. In the sequence (a) to (e) G/R decreases from 2000°C cm−2 sec−1 to 350°C cm−2 sec−1. Photograph (f) is a tin–0·2 atom percent lead alloy. (a) Planar interface; (b) box structure; (c) elongated cells; (d) broken cells; (e) hexagonal cells; (f) cellular dendrites (Nutting and Baker*[30]*).*

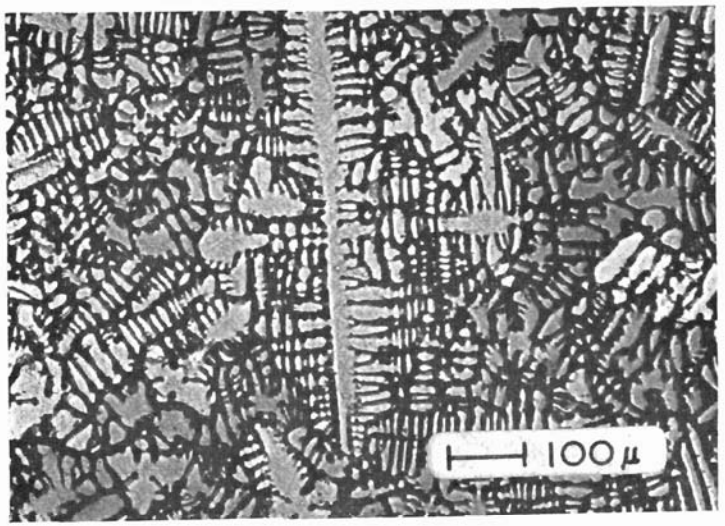

(*a*)

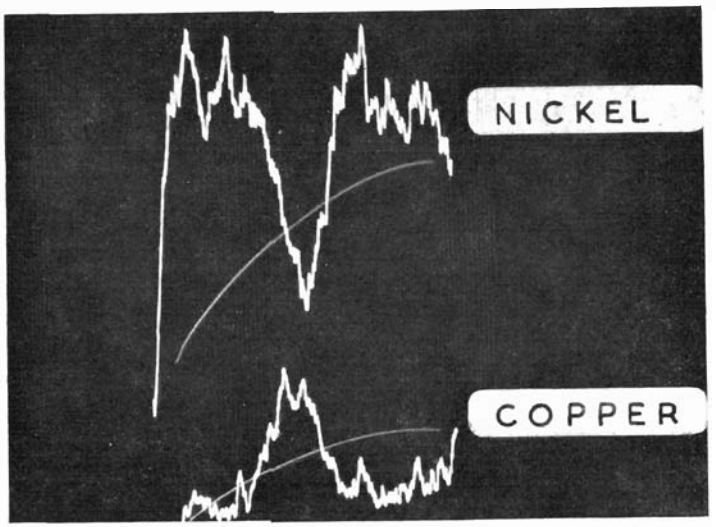

(*b*)

Fig. 4.20 ***Coring in chill-cast*** *cupronickel* ($k_0 < 1$): ***(a) as-cast*** *structure*; ***and*** (*b*) ***electron-beam*** *microanalyser* ***trace across the*** *boundary* ***between two*** *dendrite* ***arms. The*** *qualitative* ***nature of the segregation is*** *apparent* ***as a*** *maximum* *and* ***a*** *minimum* ***in the copper and nickel*** *respectively*.

4.18). There is no clear criterion for the transition from cells llular tlcndrites.[14] The overall transition sequence is as shown e. 4.19. In the case of both cells and cellular dendrites, micro- gation occurs. The intercellular regions are rich in solute for l and depleted of solute for $k_0 > 1$. Under these conditions, range segregation effects similar to those shown in Fig. 4.13 lso bound to occur.

n a macroscopic scale this mean that a dendrite will show a tion in composition from inside to out, ***i.e.*** the phenomenon of ng. This is illustrated in Fig. 4.20; in this figure the dendritic ture is clearly evident. Although it cannot be resolved, the den- arms would undoubtedly show microscopic cellular segrega- Both forms of segregation can be eliminated by a homogenising treatment although, of course, macrosegregation effects involve diffusion distances and thus long heat-treatment times. The of homogenisation is shown in Fig. 4.21.

A quite different approach to the problem of interface breakdown hat of Mullins and Sekerka,[16] who considered the stability of the terface in the presence of shape fluctuations. This treatment has me advantages, particularly since it predicts some of the para- ters, *e.g.* cell size, which were not treated in the original analysis constitutional supercooling. The treatment is mathematically mplex and details can be obtained from the original paper.

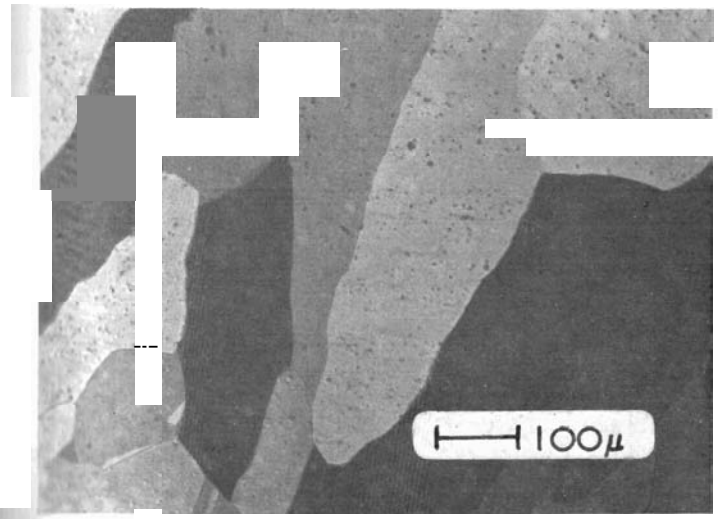

Fig. 4.21 ***(a)***

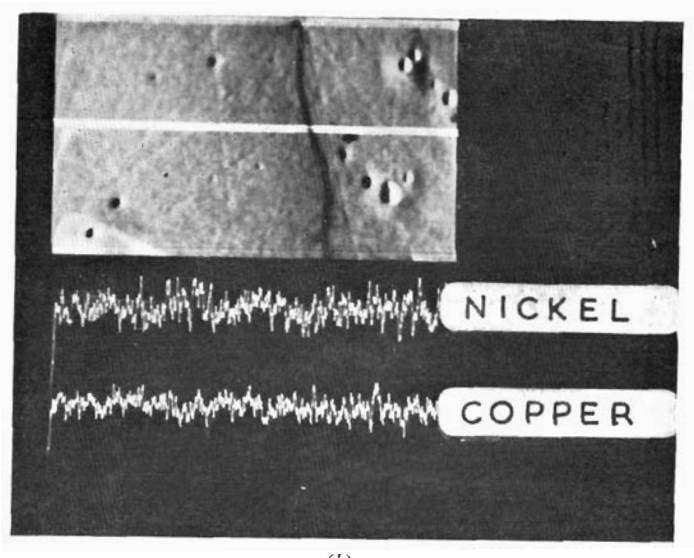

(*b*)

Fig. 4.21 The structure of Fig. 4.20 after homogenising: (a) grain structure. The small dark particles are intermetallic impurities. (b) Electron-beam microanalyser trace across a grain boundary. The boundary is the dark line in the electron image. The traces correspond to the white line in the electron image.

At this stage it would seem appropriate to point out that all the early studies of the interface of metals and alloys and the corresponding microstructural observations were handicapped by a basic experimental difficulty. This arose from the energetic constraints that ensured that a layer of liquid was retained when a solid–liquid interface was decanted. The recent direct observations of interface behaviour in organic analogues of metals,[15,17] and in thin films solidifying in the electron microscope,[18] have thus given valuable confirmation of the different theoretical mechanisms.

4.6 DENDRITIC STRUCTURES

Dendritic growth is strongly crystallographic. The primary arms and side branches have their arms parallel to specific crystallographic directions. For example, in face-centred cubic metals and alloys these are the <001> directions.[2,19] Table 4.2 gives details of the crystallography of dendrites of metals with different crystal structures.

No fully satisfactory theory has yet been advanced which reconciles the proposed rough and non-crystallographic form of the

TABLE 4.2

CRYSTALLOGRAPHY OF DENDRITES[a]

Structure	*Metal*	*Normal dendrite direction*
·entred cubic	Lead	<001>
·entred cubic	β-brass	<001>
·onal close-packed	Zinc	<10$\bar{1}$0>
·onal	Tin	<110>

[a] from Weinberg and Chalmers[2] and Hellawell and Herbert.[19]

·d liquid interface in a metallic melt (*see* Section 3.1) with the ·imental observations on the direction of dendritic growth.

·he growth forms are very varied. Normally each large branched ·drite grows from a single nucleus and has a single orientation. ·ll misorientations can be produced during growth by mechanical ·tortions brought about by turbulence.

When dendritic growth occurs continuously over a large volume ·material the resultant structure is strongly anisotropic. This ·sotropy can have quite deleterious effects on properties. For this ·son steps are normally taken to promote profuse nucleation and ·ure maximum isotropy. This important feature is considered ·ther in Chapter 6.

Although numerous measurements have been made of the dependence of the dendrite arm spacing on growth conditions,[20–22] the ·tors controlling side branching have not been identified. Morris and Winegard[23] have, however, given a striking illustration of the ·velopment of a dendrite tip instability in a metal analogue system ·uccinonitrile). The sequence is given in Fig. 4.22. This clearly ·hows that the dendrite tip does not grow with a constant shape ·ut fluctuates periodically as it propagates into the melt. It is ·ossible that the interface stability theory of Mullins and Sekerka[16] ·ay, with modifications,[24] be used to account for these observations.

An extensive series of studies by Fleming and his co-workers[25–27] ·s shown that cellular dendrites form a characteristic *plate-like* ·ay (Fig. 4.23) with an arm spacing determined by the local solidi·ation time. The effect of solute content, however, is far from clear ·s experimental results exist which show that increasing solute ·ntent increases,[13,28] decreases[22,29] and has no influence upon[25] ·he cellular dendrite arm spacing. The dendrite arm spacing is not ·mply determined by the initial growth behaviour, but is complicated by coarsening effects.[27]

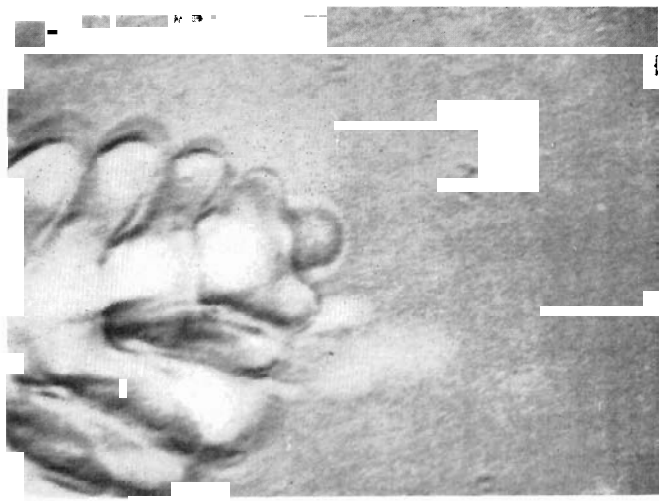

Fig. 4.22 (*a*)

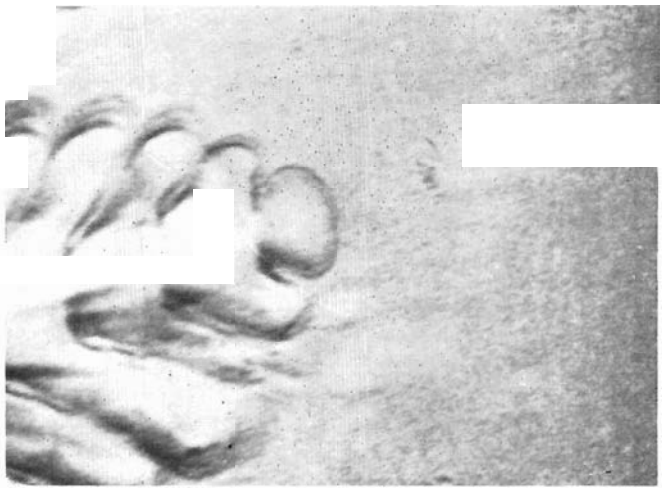

Fig. 4.22 (*b*)

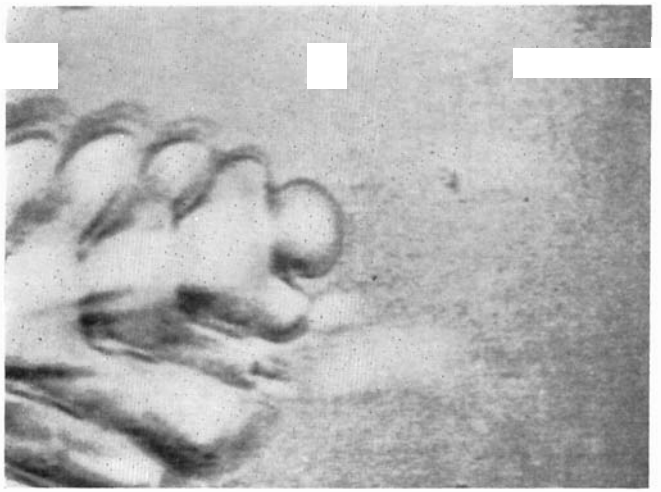

(*c*)

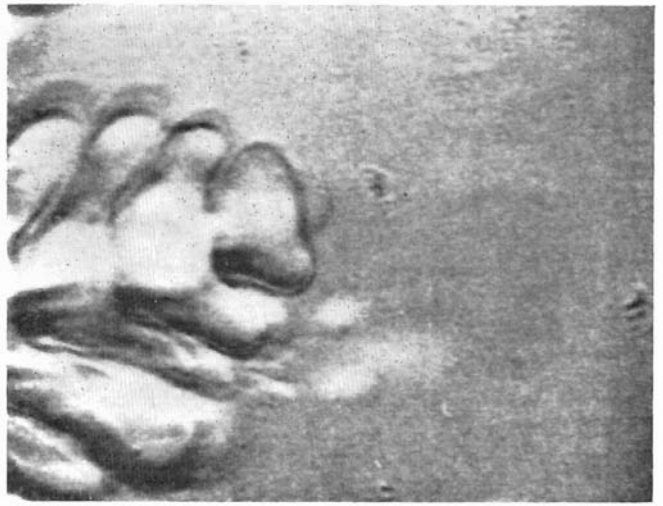

(*d*)

Fig. 4.22 *Tip of a growing dendrite showing progressive steps in tip morphology. The time interval between (a) and (b) was* 1·2 *sec; between (b) and (c) 1.2 sec; and between (c) and (d) 2.1 sec (Morris and Winegard*[23]).

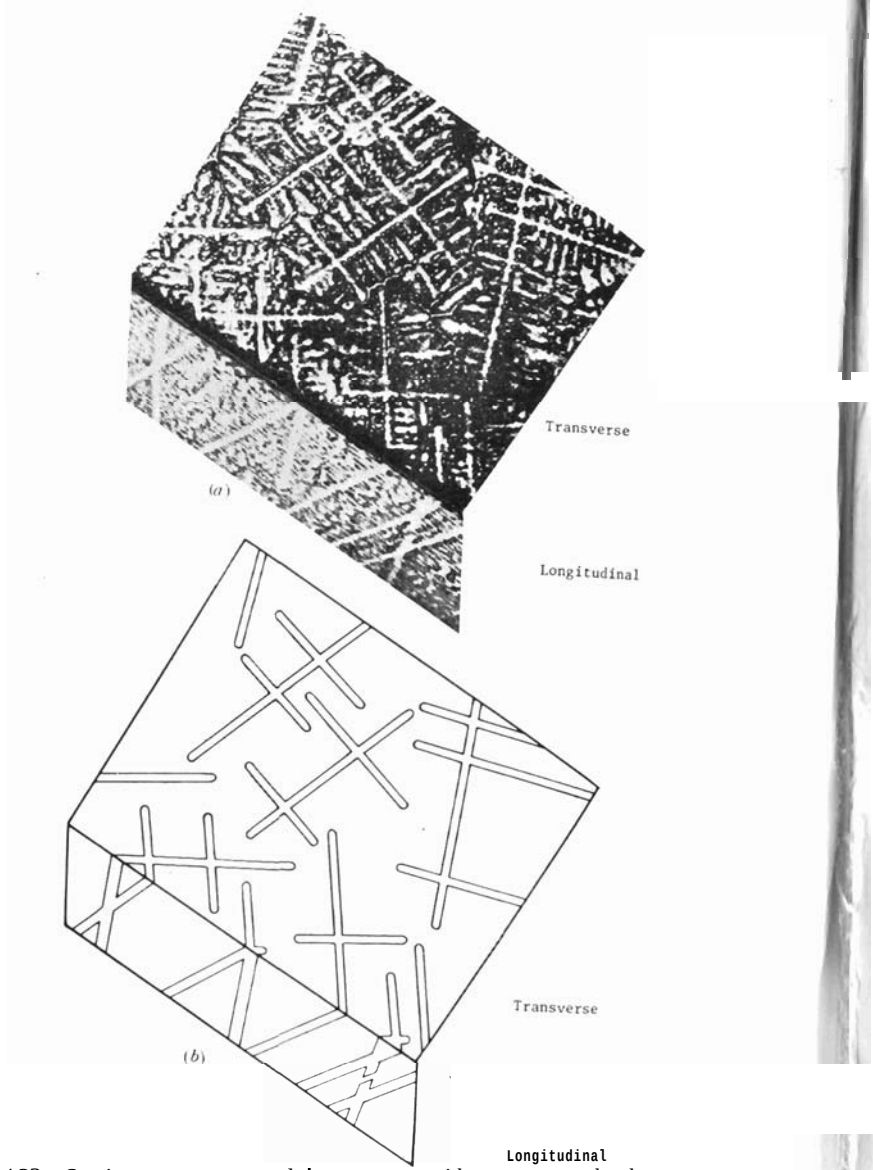

Fig. 4.23 *Sections transverse and longitudinal with respect to the heat flow direction in unidirectionally solidified aluminium–4·5% copper alloy: (a) orthogonal photomicrograph: (b) schematic drawing showing primary dendrite plates (Bower* et al.[25]).

REFERENCES

1. Tiller, W. A., Rutter, J. W., Jackson, K. A. and Chalmers, B. (1953). *Acta Met.*, **1,** 428.
2. Weinberg, F. and Chalmers, B. (1951). *Can.* **J.** *Phys.*, **29,** 382.
3. Jackson, K. A. (1962). *Phil. Mag.*, **7,** 1117.
4. Young, F. W. and Savage, J. R. (1964). **J.** *Appl. Pliys.*, **35,** 1917.
5. Teghtsoonian, E. and Chalmers, B. (1951). *Can.* **J.** *Phys.*, **29,** 270.
6. Doherty, P. E. and Chalmers, B. (1962). *Trans. Met. Soc. AIME*, **224,** 1124.
7. Jaffrey, D. and Chadwick, G. A. (1968). *Phil. Mag.*, **18,** 573.
8. Pfann, W. G. (1952). *Trans. AIME*, **194,** 747.
9. Burton, J. A., Primm, R. C. and Slichter, W. P. (1953). **J.** *Chem. Phys.*, **21,** 1987.
10. Pfann, W. G. (1966). *Zone Melting*, Second Edition, John Wiley, New York.
11. Schildknecht, H. (1966). *Zone Melting*, Academic Press, New York.
12. Chalmers, B. (1964). *Principles of Solidification*, John Wiley, New York, Chapter 5.
13. Tiller, W. A. and Rutter, J. W. (1956). *Can.* **J.** *Pliys.*, **34,** 96.
14. Davies, G. J. (1968). *The Solidification of Metals*, ISI Publication, 110, p. 66.
15. Jackson, K. A. and Hunt, J. D. (1965). *Acta Met.*, **13,** *1212.*
16. Mullins, W. W. and Sekerka, R. F. (1964). **J.** *Appl. Phys.*, **35,** 444.
17. Jackson, K. A., Uhlmann, D. R. and Hunt, J. D. (1967). **J.** *Crystal Growth*, **1,** 1.
18. Glicksman, M. E. and Vold, C. L. (1968). *The Solidification of Metals*, ISI Publication 110, p. 37.
19. Hellawell, A. and Herbert, P. M. (1962). *Proc. Roy. Soc.*, **A269,** 560.
20. Michael, A. B. and Bever, M. B. (1950). *Trans. AIME*, **188,** 47.
21. Alexander, B. H. and Rhines, F. N. (1950). *Trans. AIME*, **188,** 1267.
22. Horwath, J. A. and Mondolfo, L. F. (1962). *Acta. Met.*, **10,** 1037.
23. Morris, L. R. and Winegard, W. C. (1967). **J.** *Crystal Growth, 1,* 245.
24. Sekerka, R. F. (1968). **J.** *Crystal Growth*, **3, 4,** 71.
25. Bowers, T. F., Brody, H. D. and Flemings, M. C. (1966). *Trans. Met. Soc. AIME*, **236,** 624.
26. Kattamis, T. Z. and Flemings, M. C. (1967). *Trans. Met. Soc. AIME*, **239,** 992.
27. Kattamis, T. Z., Coughlin, J. C. and Flemings, M. C. (1967). *Trans. Met. Soc. AIME*, **239,** 1504.
28. Bell, J. A. and Winegard, W. C. (1963–64). **J.** *Inst. Met.*, **92,** 357.
29. Weinberg, F. and Chalmers, B. (1952). *Can.* **J.** *Phys.*, **30,** 488.
30. Nutting, J. and Baker, R. G. (1965). *The Microstructure of Metals*, Inst. of Metals, London, p. 9.

CHAPTER 5

Solidification of Multiphase Metals and Alloys

In the previous chapter the solidification of single-phase metals and alloys was considered with regard to both the constitutional and structural effects which occurred. In this chapter more complex alloys are treated in which two or more phases are present. Eutectics, peritectics and monotectics are considered first. Particles in melts and gases in melts are dealt with subsequently.

5.1 EUTECTICS

5.1.1 Binary eutectics

A typical binary eutectic phase diagram, that for the system lead–tin, is given in Fig. 5.1. Considering the alloy of eutectic composition, the two component phases solidify simultaneously to give a structure consisting of an intimate mixture of these phases. Several different classifications for eutectic structures have been proposed,[1–4] but there is not general agreement. The classification due to Hunt and Jackson[4] has distinct advantages and is based on the a-factor (see eqn. 3.2) characteristics of the component phases. Thus, the different structures are divided into three groups, (i) rough–rough, (ii) rough–faceted and (iii) faceted–faceted, where the descriptions rough and faceted are as given in Section 3.1. Figure 5.2 shows examples of each of these groups for organic eutectics. Most metallic eutectics fall into group (i) and during growth there is coupling between the phases. In coupled growth the two phases grow immediately adjacent to each other with solute movement between the liquid regions in front of each phase. The growth mode shows some mutual dependence. The normal morphologies are lamellar or rod-like (Fig. 5.3). In the presence of impurities, cellular growth occurs and a structure of eutectic colonies results[6] (Fig. 5.4). In lamellar

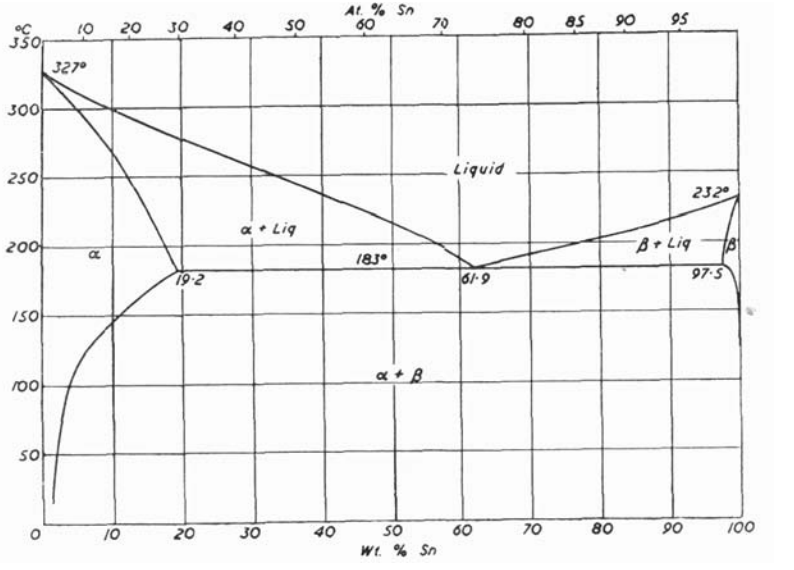

Fig. 5.1 The eutectic system lead–tin.

eutectics the interlamellar spacing, λ, is related to the growth rate, R, by

$$\lambda \propto \frac{1}{R^{\frac{1}{2}}} \tag{5.1}$$

a relation predicted theoretically[7,8] and confirmed experimentally.[9,10] This provides one means of control of the eutectic structure.

For non-eutectic compositions the eutectic reaction is preceded by primary-phase dendritic growth. The resulting structure consists of dendrites in a eutectic matrix (Fig. 5.5).

With group (ii) eutectics the growth process is still coupled with the faceted phase dominant. The resultant structures are less regular. As can be seen in Fig. 5.2(b) the faceted phase is surrounded by the other phase except at the tips of the growing spikes. The important metallurgical systems of aluminium–silicon and iron–graphite are of this type, as has been shown by Day and Hellawell.[11,12] Figure 5.6 shows the aluminium–silicon system. These two systems are both able to be structurally modified by the addition of small quantities (~0.01%) of sodium and cerium or magnesium respectively. Eutectic modification is considered further in Section 5.1.3.

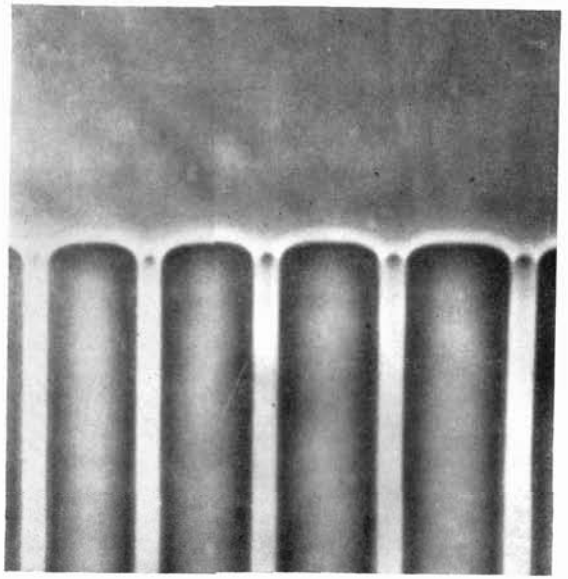

Fig. 5.2 *(a)*

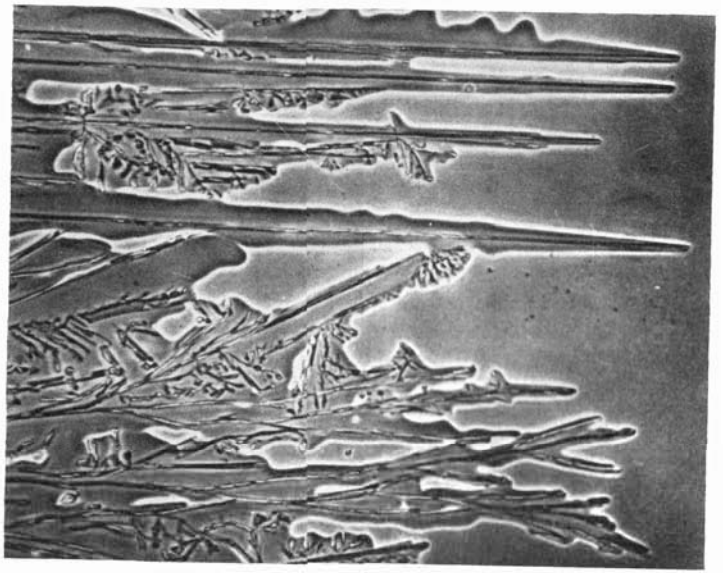

Fig. 5.2 *(b)*

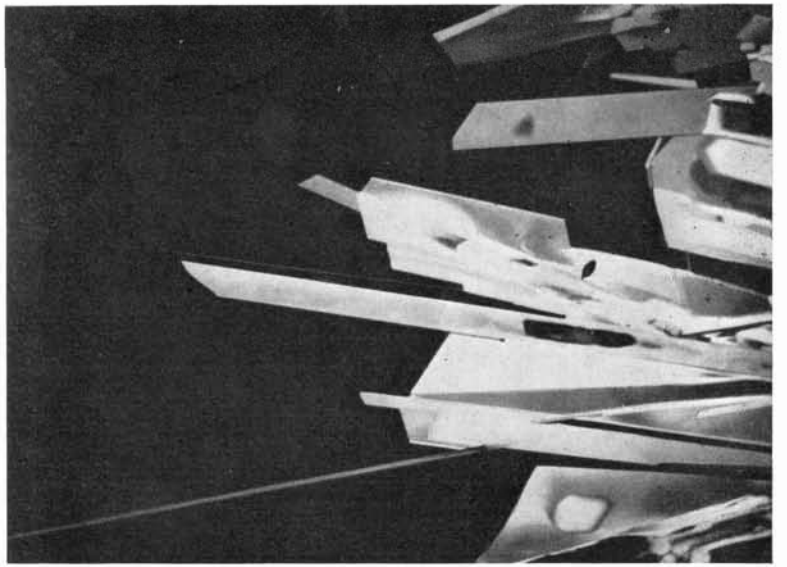

(c)

Fig. 5.2 *(a) A lamellar* ***eutectic*** *structure in the carbon tetrabromide–hexachlorethane system. Both phases normally* ***have*** *rough interfaces (a < 2). (b) An irregular* ***eutectic*** *structure in the succinonitrile (rough, a < 2)–borne01 (faceted, α > 2) system. (c) Complex eutectic structure in the azobenzene–benzil system. Both phases normally haae faceted interfaces (Hunt and* ***Jackson***[4]*). No coupled growth takes place.*

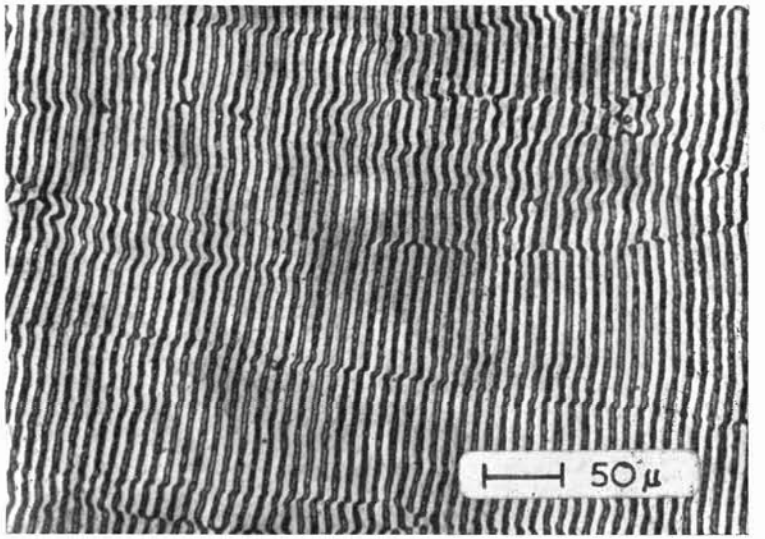

Fig. 5.3 *(a)*

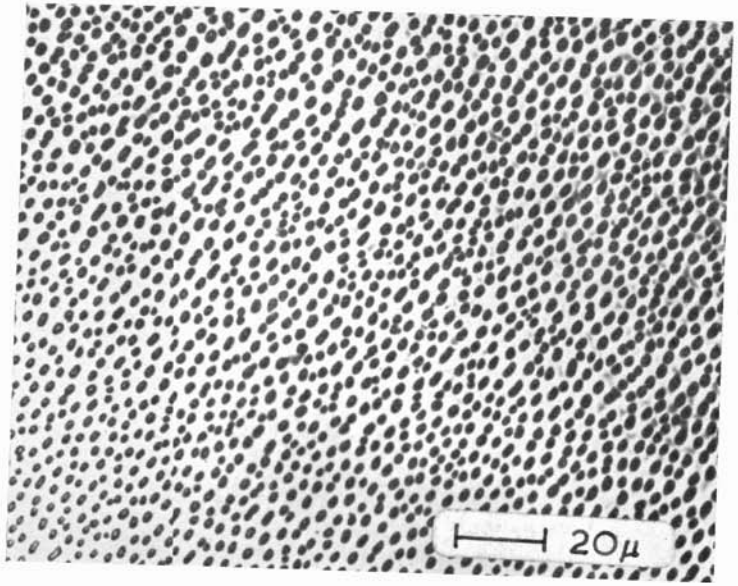

Fig. 5.3 (*b*)(*i*)

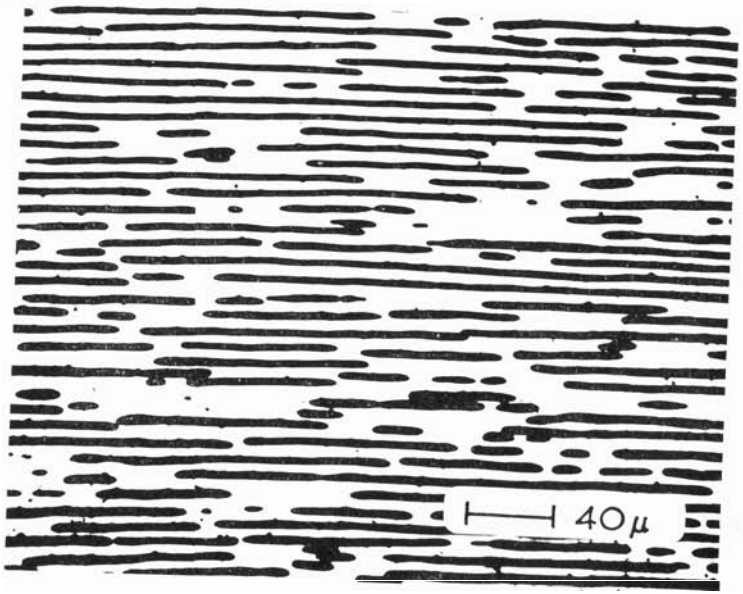

(*b*)(*ii*)

Fig. 5.3 (a) Lamellar eutectic in the lead–tin system. (b) Rod-like eutectic in the aluminium–Al_3Ni system: (i) transverse section, (ii) longitudinal section.

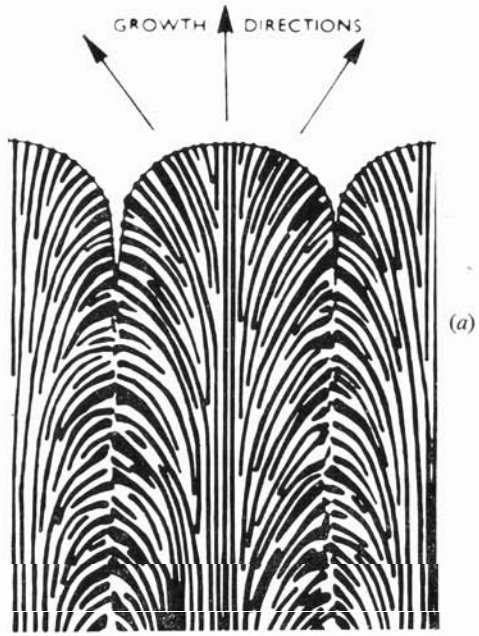

(*a*)

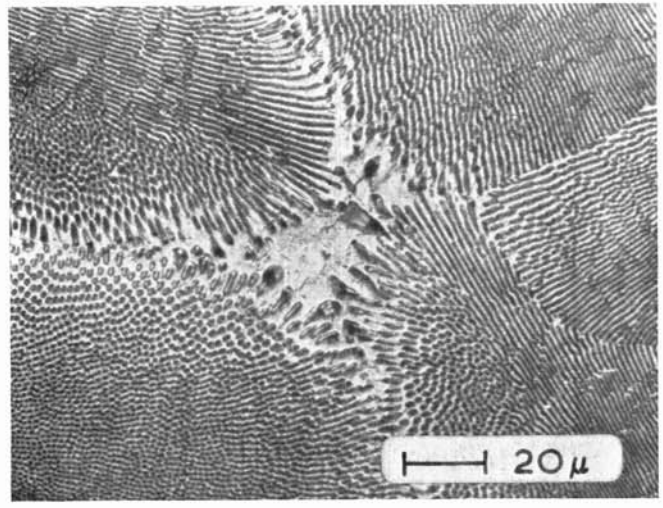

(*b*)

Fig. 5.4 (a) Schematic representation of the growth front of a lamellar eutectic growing with a curved cellular interface. Rods form at the cell boundaries (Hunt and Chilton[5]). (b) Cross section through an impure lead–cadmium alloy showing the eutectic colony structure (Chadwick[6]).

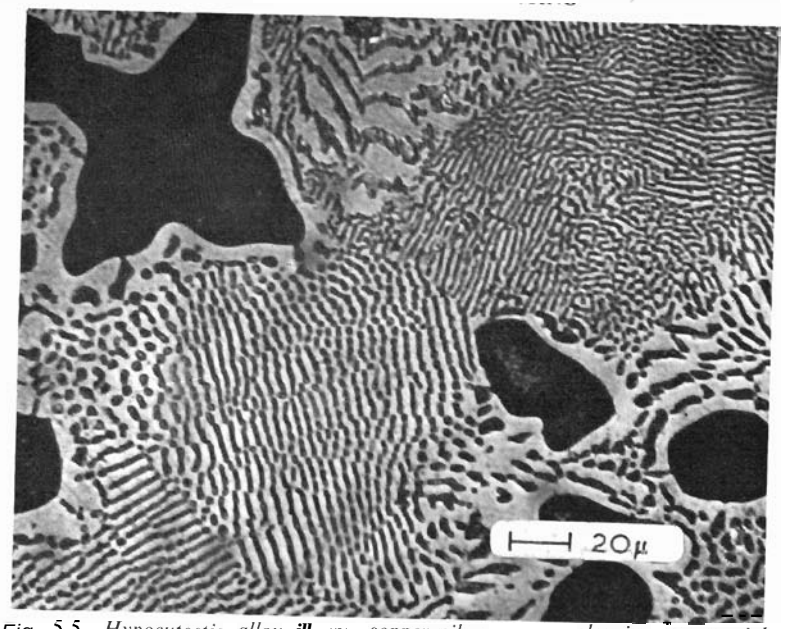

Fig. 5.5 *Hypoeutectic alloy in the copper–silver system showing copper-rich dendrites in a matrix of eutectic colonies.*

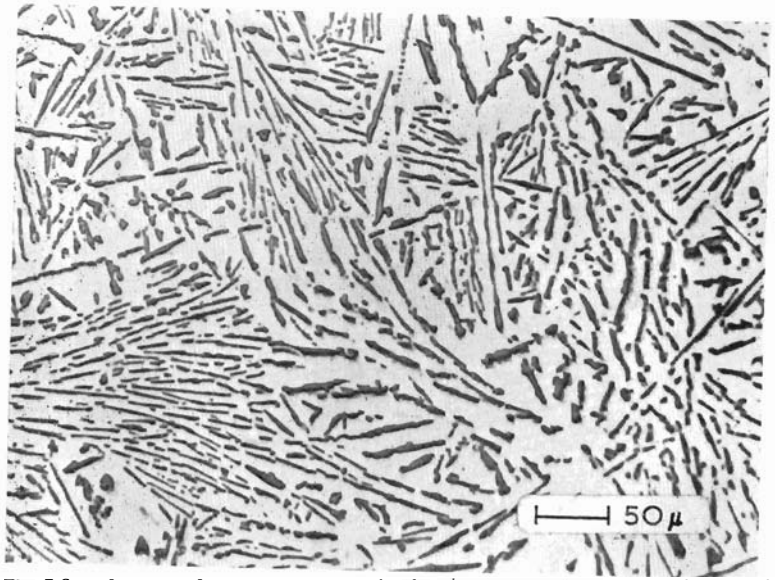

Fig. 5.6 ***The normal eutectic structure in the aluminium–silicon system*** *(Day and Hellawell[11]).*

Where both eutectic components are faceted the growth is no longer coupled and the resulting structure is a random mixture of the two phases ***(see*** Fig. 5.2c). This type of structure is uncommon in metallic systems, but is expected for non-metallic systems where the α-factors of components should be large. This is not always the case, however, since as shown by Hellawell and co-workers[13] inorganic eutectics, ***e.g.*** LiF–NaF, can grow with group (i) structures.

A number of approximate and less appropriate theories of lamellar growth have been proposed ***(see,*** for instance, Tiller[7] and Hunt and Jackson[5]) and these have been reviewed by Hunt.[14] Satisfactory predictions have been made of the interface shape.

Another aspect of binary eutectic solidification which is of importance is the lamellar–rod transition, particularly in view of the consideration given to the use of eutectics for high-strength composites.[15,16] For alloys of eutectic composition the tendency is to form rods when one phase has a low volume fraction relative to the other, and lamellae when the phase proportions are more nearly equal. It is generally accepted that this is controlled by interphase energy considerations,[5] although under some conditions the normal solidification variables (growth rate, temperature gradient at the solid–liquid interface) can influence morphology.[13] The preference for a given habit as determined by simple geometric considerations is shown in Fig. 5.7.

The surface area associated with a fibrous system ***(S,)*** is very sensitive to the volume proportions, rising from zero to a maximum value of -0.8, when the rods would tend to make contact. On the other hand, the surface area of a lamellar array ($S_{,,}$)is independent of volume fraction since it is independent of lamellar thickness. If the interphase energies were the same for lamellae and rods we would only expect the lamellar arrangement at volume fractions greater than about 0.3. However, the lamellar habit is observed to persist to lower volume fractions and this has been attributed to the existence of preferred interphase habit planes with lower surface energies.[13]

Clearly, the anisotropy of surface energy in crystals limits the extent to which the simple geometric model can be used. Nevertheless, in the absence of more detailed information it provides a useful indication of preferred behaviour. Thus, we can see that the rod-like arrangement is not expected at volume fractions greater than about 0·3.

In an attempt to overcome this restriction, Mollard and Flemings,[17,18] following observations by Hunt and Jackson,[4] solidified alloys of non-eutectic composition in a controlled way so as to retain the coupled eutectic-type growth. They were able to

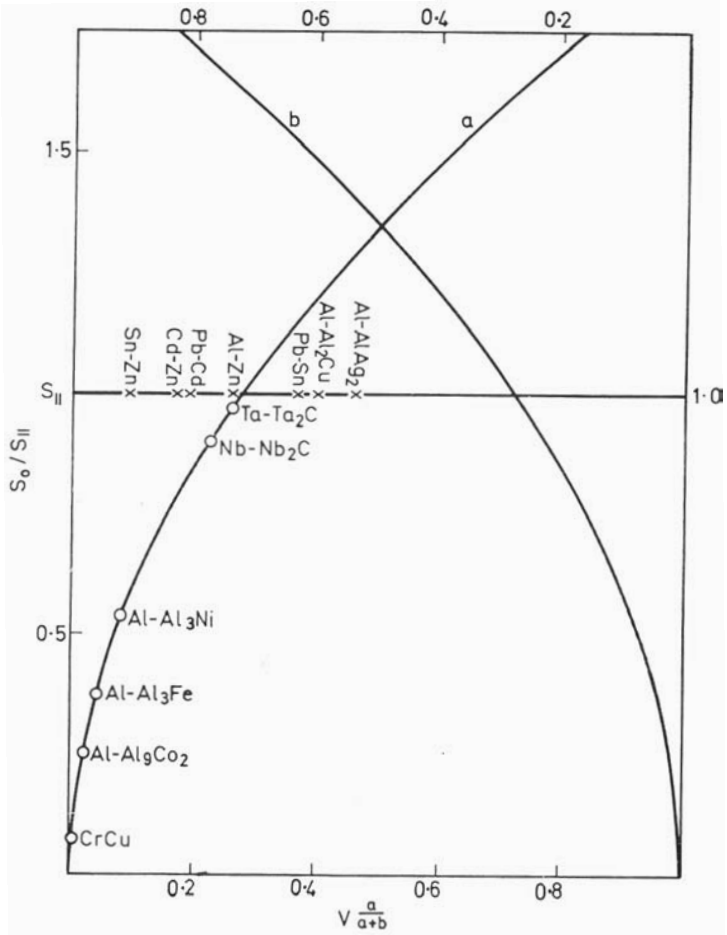

***Fig.* 5.7** *The relative surface areas for lamellar eutectic arrangements,* S_{II}, *compared with those of fibres,* **So,** *or vice versa, as functions of the volume proportions: (a) is the volume fraction of the minor constituent; (h) is the volume fraction of the major constituent. Eutectic alloys having the lamellar habit are marked X and those with a fibrous habit are marked O (Hellawell*[15]*).*

produce eutectic structures with different volume proportions of the component phases, but observed that normally lamellar structures remained lamellar until the volume fraction was very markedly reduced. Thus, as yet it has not proven possible to obtain aligned rod-like eutectics with high volume fractions. However, a more detailed examination of the influence of trace impurities would seem

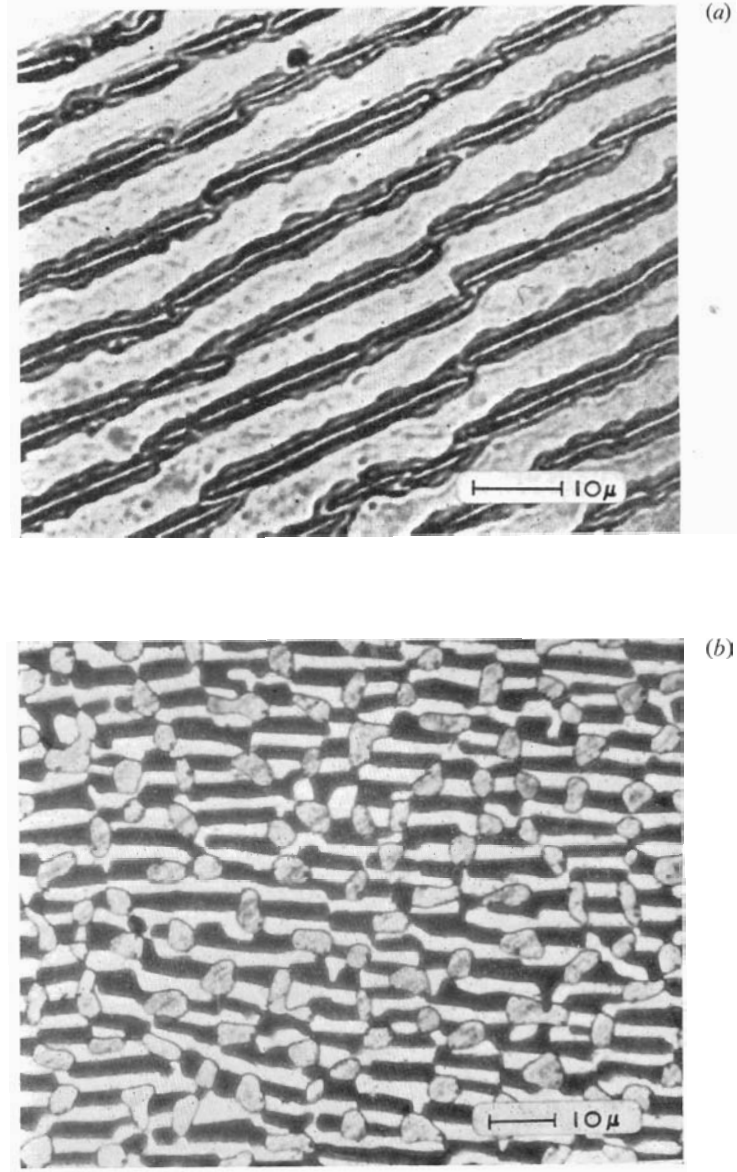

Fig. **5.8** *(a) A triple lamellar ternary eutectic in the system cadmium* (α)–*tin* (β)–*lead* (γ). *The lamellar arrangement is* $\alpha\gamma\beta\gamma\alpha\gamma$ *(Kerr et* **al.**[20]*). (b) The complex ternary eutectic in the aluminium–copper–magnesium system. The lamellar phases are aluminium and* $CuAl_2$ *and the fibrous phase is Mg-rich (Cooksey and Hellawell*[21]*).*

essential[19] provided, of course, the transition can be effected without extensive colony formation. Theories of the lamellar–rod transition and of the extent of the eutectic range have also been discussed by Hunt.[14]

5.1.2 Ternary eutectics

Ternary eutectic structures have not attracted a great deal of attention, although some data are available.[20,21] Microstructures have been reported which have complex lamellar or combined lamellar–rod-like morphologies. Examples of these are shown in Fig. 5.8.

5.1.3 Modification of eutectics

As described above, structural modification is produced in the systems aluminium–silicon and iron–carbon by the addition of sodium and magnesium or cerium, respectively. After modification the structure of Fig. 5.6 appears as shown in Fig. 5.9. Two points should be noted: (i) the modified structure has significantly improved mechanical properties, especially toughness, and (ii) the growth process is affected in such a way that primary dendritic growth occurs in what is nominally an alloy of eutectic composition. These

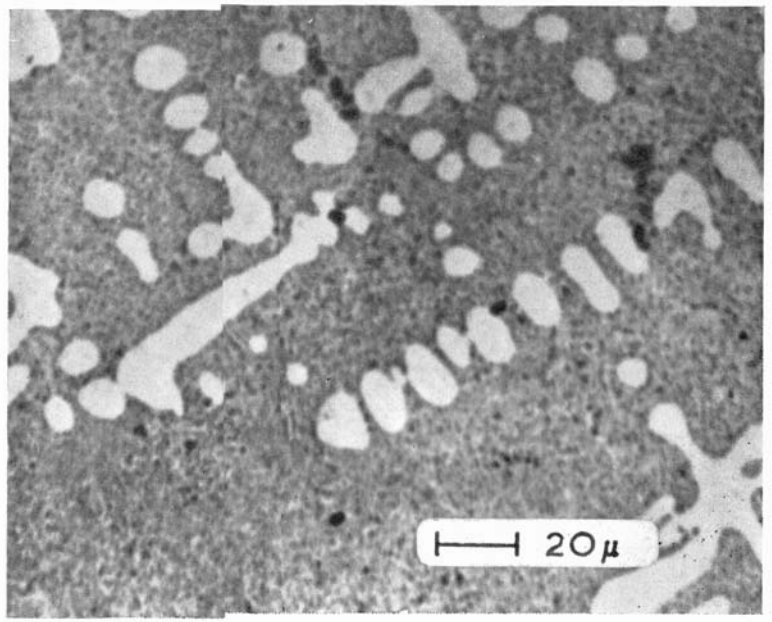

Fig. 5.9 Sodium-modified aluminium–silicon eutectic alloy.

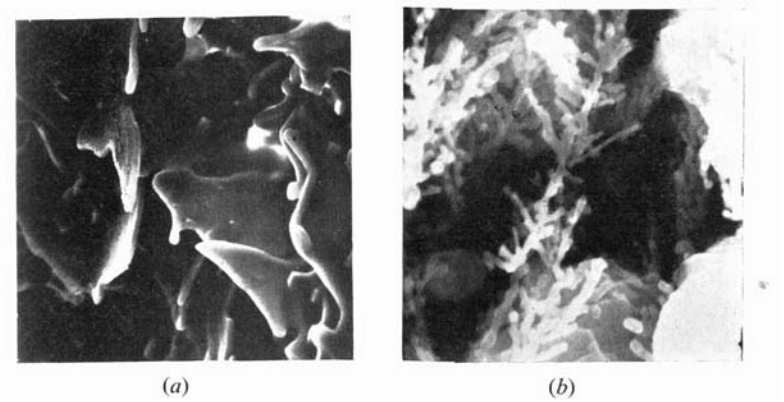

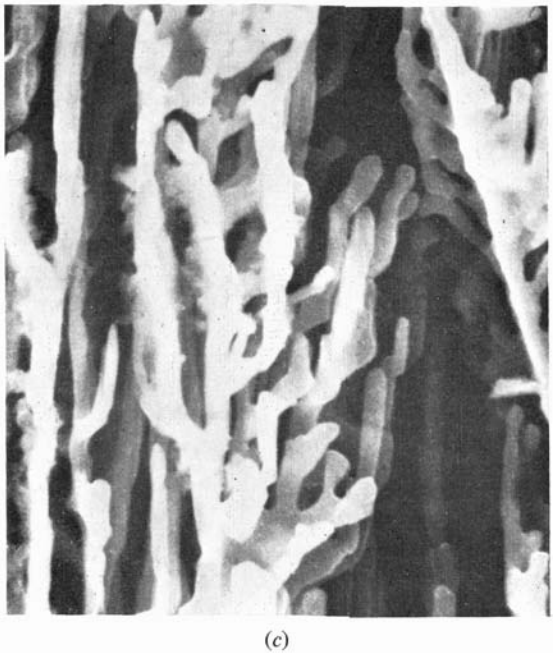

Fig. 5.10 Scanning electron micrographs of aluminium–silicon alloys after heavy etching of the aluminium matrix: (a) coarse silicon structure of unmodified slow-cooled alloy (cf. Fig. 5.6); (b) filamentary silicon in a quenched alloy (growth-rate modified); (c) filamentary silicon in sodium-modified alloy (cf. Fig. 5.9) (Day and Hellawell[11]).

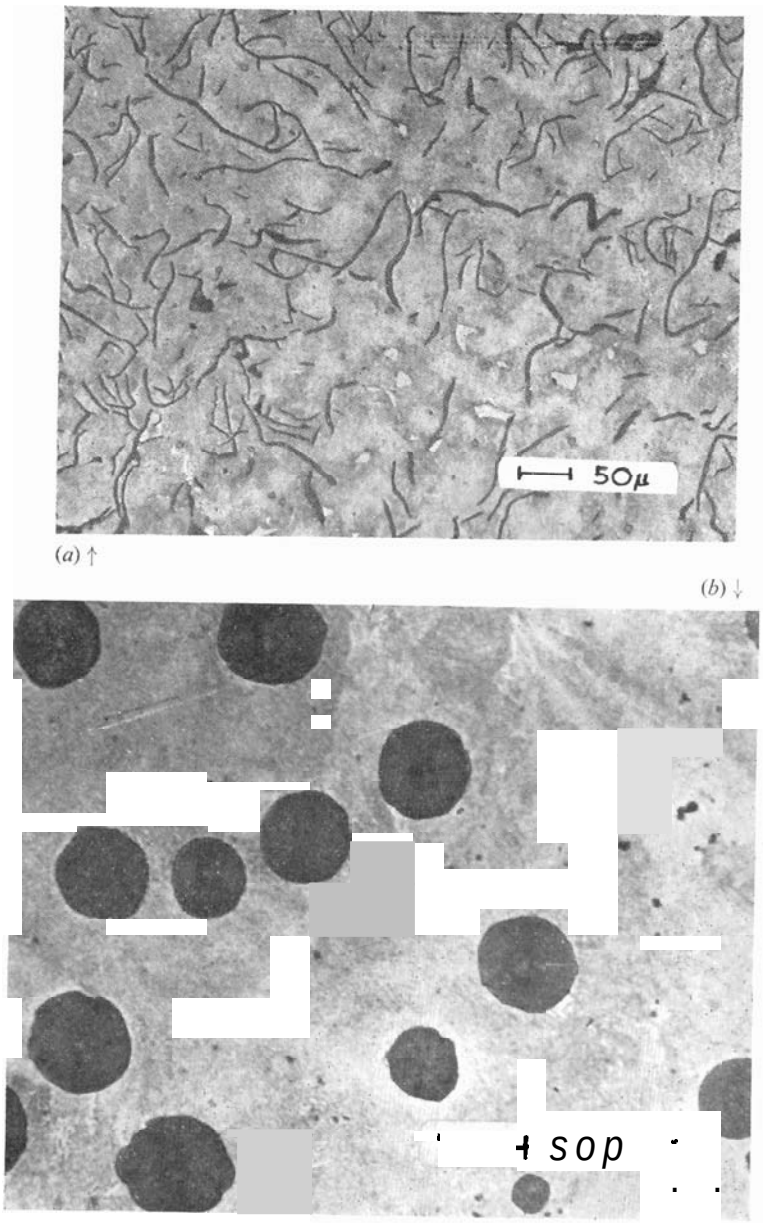

Fig. 5.11 *(a) Normal as-cast grey cast iron showing flake graphite. (b) Modified spheroidal graphite cast iron.*

are both examples of important structural modifications in the development of microstructure.

The recent work of Day[22] has confirmed that this modified structure is the result of a change in the mode of growth and not the result of a change in nucleation behaviour as was earlier proposed.[23,24] The coarse silicon structure of slow-cooled alloys is altered if rapid growth rates are used. A similar effect is produced by adding a modifier (sodium) to the slow-cooled alloy. These are illustrated in Fig. 5.10. The silicon morphology is basically the same in *both* the growth rate-modified ***and*** the additive-modified alloys.

The modification that occurs in the iron–carbon system is even more striking, as shown in Fig. 5.11. Here the normal structure of grey cast iron, graphite flakes in a pearlitic matrix, is altered to graphite spheroids in a pearlitic matrix. In this case also there is a dramatic increase in mechanical properties, particularly toughness. The bulk of the evidence[25] indicates that the spherulites separate directly from the melt without the simultaneous formation of any other solid. Solidification appears to proceed by the growth of the spherulite surrounded by an envelope of austenite, although this hypothesis has been questioned.[26] The reasons for the change in graphite morphology on the addition of magnesium are far from clear, although it has been established[27] that the additive influences the growth of the graphite rather than affecting the nucleation behaviour.

5.1.4 Other eutectic systems

There are a number of other aspects of eutectic solidification, particularly the divorced eutectics,[28] and the pseudo-binary eutectics[29] which occur in multicomponent systems. These are both very specialised topics and will not be dealt with further here.

5.2 PERITECTICS

Figure 5.12 gives the phase diagram for the almost ideal peritectic system, silver–platinum. As discussed by Uhlmann and Chadwick[30] in the first detailed study of peritectic reactions, for virtually all compositions except those near the limits of the system, the microstructure after casting will consist of cored dendrites of one phase surrounded by the second phase. Thus with reference to Fig. 5.12 we would expect this structure for compositions from 30 to 90 wt % platinum. Furthermore, the peritectic reaction should seldom proceed to completion. When the primary phase has cooled to the peritectic

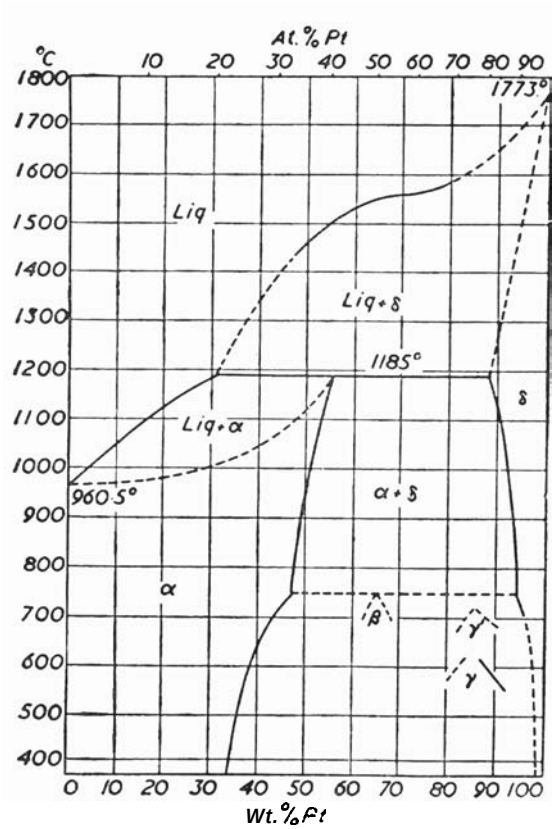

Fig. 5.12 ***The peritectic system silver–platinum.***

temperature (1185°C in Fig. 5.13) it should react with the liquid to form the second component phase. In practice it becomes quickly encapsulated by the second phase and the reaction is stifled by the need for diffusion through this solid layer. This behaviour has been confirmed by Sartell and Mack.[31]

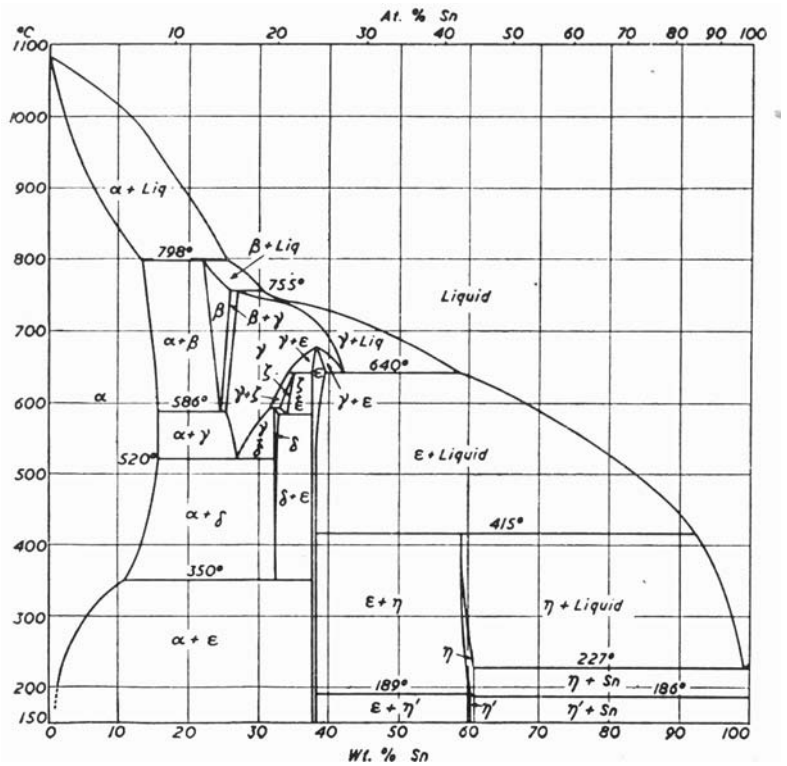

Fig. 5.13 ***The copper–tin phase diagram.***

In those cases where successive peritectic reactions occur, ***e.g.*** tin-rich copper–tin alloys (see Fig. 5.13), considerable deviations from equilibrium result. For instance, if an alloy of nominal composition 80 wt % tin was solidified under equilibrium conditions, the resulting structure would consist of approximately equal proportions of the primary η–Cu_6Sn_5 phase and eutectic. When cast normally, however,

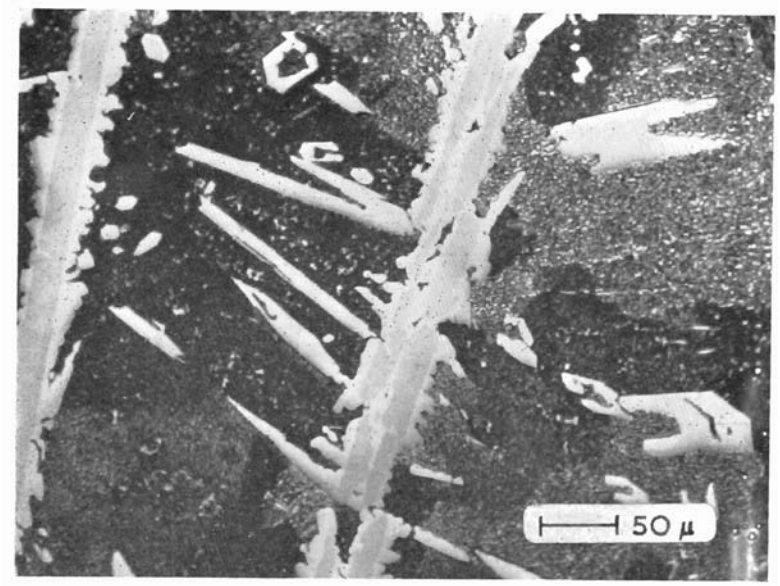

Fig. 5.14 As-cast copper–80 *wt* % *tin. The intermetallic phases are* ε–Cu_3Sn (dark) *in* η–Cu_6Sn_5 (white) *in* a *tin-rich eutectic matrix* (*black*).

it consists of the ε–Cu_3Sn phase enclosed in η–Cu_6Sn_5 in a matrix of eutectic. This is shown in Fig. 5.14.

On the whole, data for metallic systems are limited and there are essentially no data available for non-metallic systems.

5.3 MONOTECTICS

Monotectic reactions in which a liquid phase decomposes to form a solid and another liquid phase (Fig. 5.15) have also received little attention. The experimental work of Delves[32] and the theoretical treatment of Chadwick[33] showed that either regular rod-like structures or macroscopic phase separation should occur, depending on the various interphase surface energies. Subsequently Livingston and Cline,[34] working with copper–lead alloys, established that the growth conditions also had a marked influence on the nature of the transformation structure. Their results are summarised in Fig. 5.16. It would be valuable if these studies could be extended to other suitable systems.

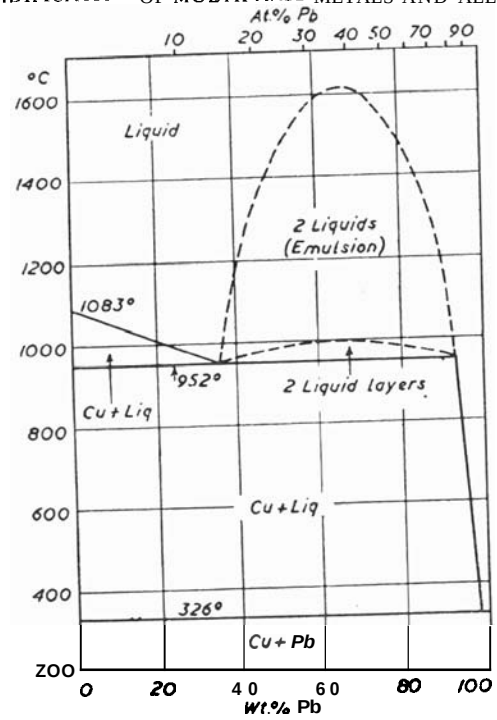

Fig. **5.15** *The copper–lead phase* diagram showing *the monotectic reaction* $L_1 \rightarrow a + L_2$.

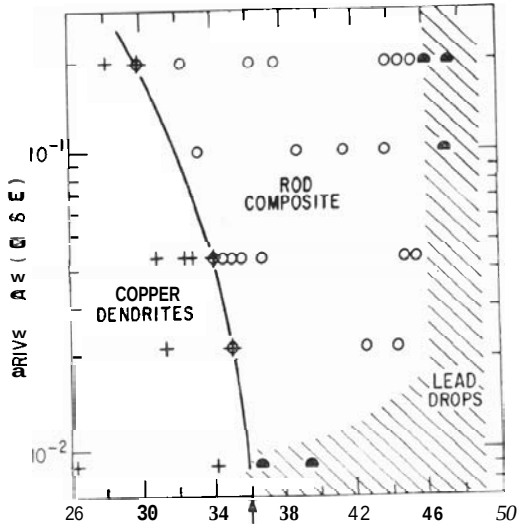

Fig. **5.16** (*a*)

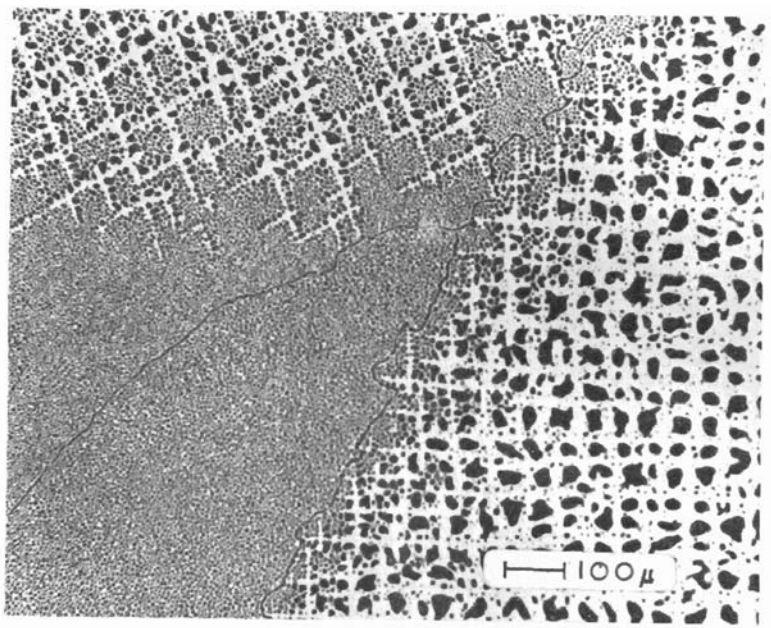

(b)

Fig. 5.16 (a) Composition–velocity plot showing regions over which different microstructure types were observed. (b) Transverse section of transition regions showing composite and dendritic structures: copper—light phase, lend—clark phase. The characteristic alignment of the dendritic structure resulting from the crystallography of dendritic growth is clear (Livingston and Cline[34]).

5.4 PARTICLES AND INCLUSIONS IN MELTS

Foreign particles which do not dissolve in either the liquid or the solid are often present during solidification. These insoluble particles are usually classified as *exogeneous* if they come from external sources (*e.g.* mould and ladle materials, dross) or *endogeneous* if they arise from reactions within the solidifying metal. The interaction between solid particles suspended in the liquid and the solid–liquid interface has been studied comprehensively by Uhlmann *et al.*[35] Using transparent materials, direct observations of particle–interface behaviour were made. For each system it was found that there was a critical growth rate below which the particles were 'pushed' by the interface and above which they were trapped in the solid. Figure 5.17 shows the pile-up of zinc particles at a solid–liquid thymol interface at low growth rate. The rate-controlling step was determined to be

the rate of diffusion of liquid to the growing solid behind the particle. A sufficient flux of liquid is needed to continuously replenish the solidifying material immediately behind the particle and thus keep the particle ahead of the interface. In the main, the critical growth

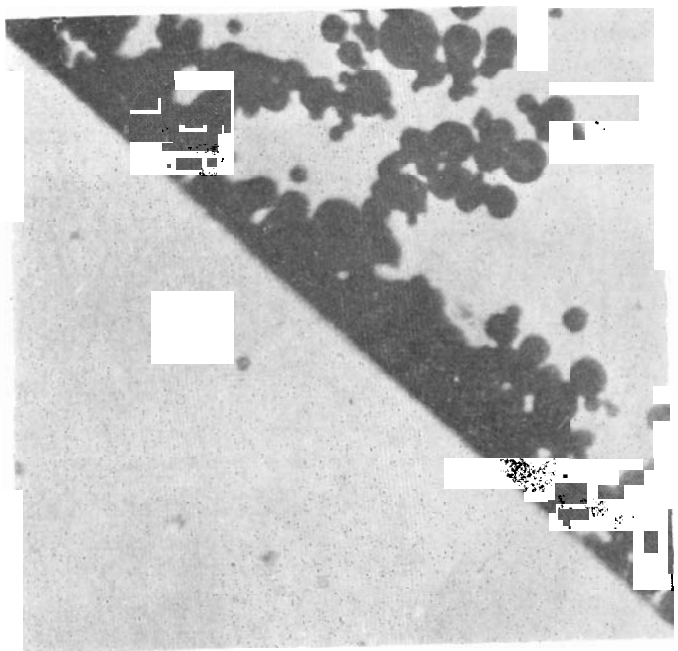

Fig. 5.17 Pile-up of particles at a solid–liquid interface at low growtl rate in the system thymol–zinc (Uhlmann et al.[35]).

rates were all low ($\sim 10^{-3}$ cm sec^{-1}). It is thus expected that entrapment will occur in most practical cases. Towards the end of a solidification process, however, as the growth rates slow down, it is possible for particles to be swept together to produce quite deleterious accumulations of inclusions.

It is also possible for the solid inclusions to act as sites for heterogeneous nucleation (*see* Section 2.3) and it is recognised that they have an important role in ingot solidification.[36–38] To a large extent the segregation patterns observed in ingots (*see* Section 7.3) are influenced by the presence of inclusions.

In some cases the particles appear to have become grown-in because they have been trapped in isolated regions of liquid by the growth of dendrite branches. The constraints imposed on particle

movement by the existence of a solid network in the liquid make predictions of particle distributions very difficult.

5.5 GASES IN MELTS

Apart from the possibility of gases being trapped inadvertently during casting, considerable difficulties can result from the marked differences in the solubility of gases in liquid and solid metals. An example of this is shown in Fig. 5.18. Examination of this figure indicates that

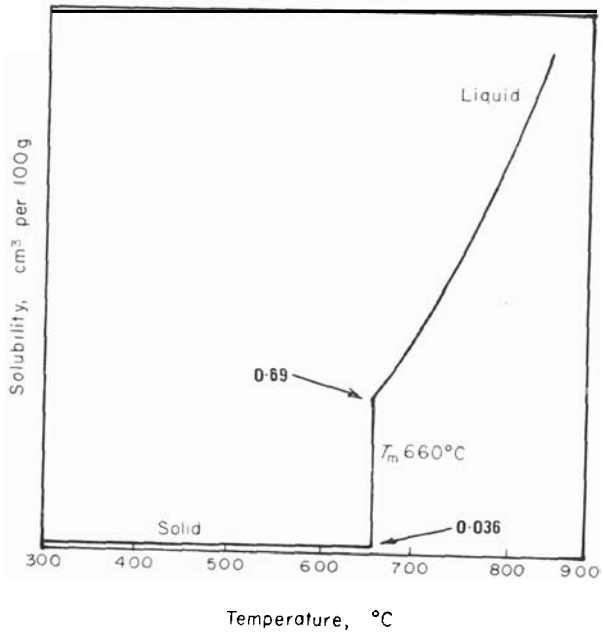

Fig. 5.18 ***Solubility of*** *hydrogen in aluminium* (*data from Ransley and Neufeld*[39]).

the distribution coefficient is effectively $\sim 0{\cdot}05$. As shown in Section 4.3, the corresponding build-up in concentration at the interface ($\propto 1/k_0$) could lead to supersaturations of -20 times the saturated value. Under these conditions it is expected that the gas will come out of solution and appear as bubbles of one form or another.

It is recognised[40,41] that the nucleation of gas bubbles should be difficult, but as pointed out by Campbell[41] shrinkage may make an important contribution to pore nucleation, as may the presence of certain inclusions. In all cases, because of the local supersaturation

the advancing solid–liquid interface should be the preferred site. After nucleation the bubble can behave in a number of different ways:[40]

(i) it can float away, collecting gas in the process, and escape from the liquid at a free surface,
(ii) it can move with the interface, growing at the same time to become entrapped in due course,
(iii) it can become incorporated into the interface to grow as an elongated blowhole,
(iv) it can be rapidly overgrown by the interface and become entrapped.

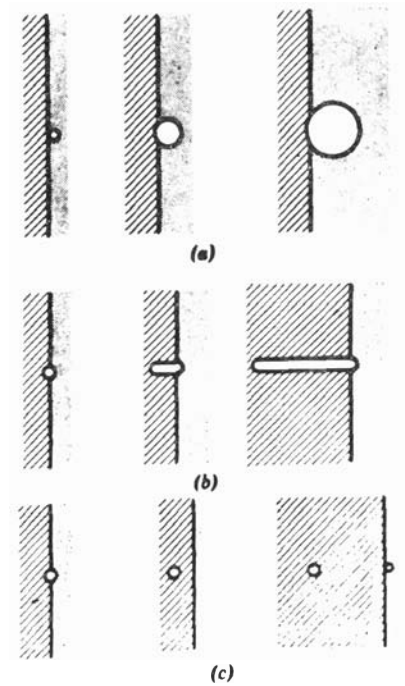

Fig. 5.19 *Effect* ***of growth rate on the interaction*** *between a bubble* ***and the*** *solid–liquid* ***interface: (a) slow growth rates—type (ii) behaviour, pushing;*** (*b*) *intermediate growth* ***rates—type (iii) behaviour, formation of elongated blowholes; (c) fast growth*** *rates—type* ***(iv) behaviour,*** *entrapment* (*Chalmers*[40]).

The occurrence of the latter three types of behaviour is determined by the growth rate and they are illustrated schematically in Fig. 5.19. Woodruff[42] has shown a good example of the formation of an elongated blowhole in an analogue system (Fig. 5.20).

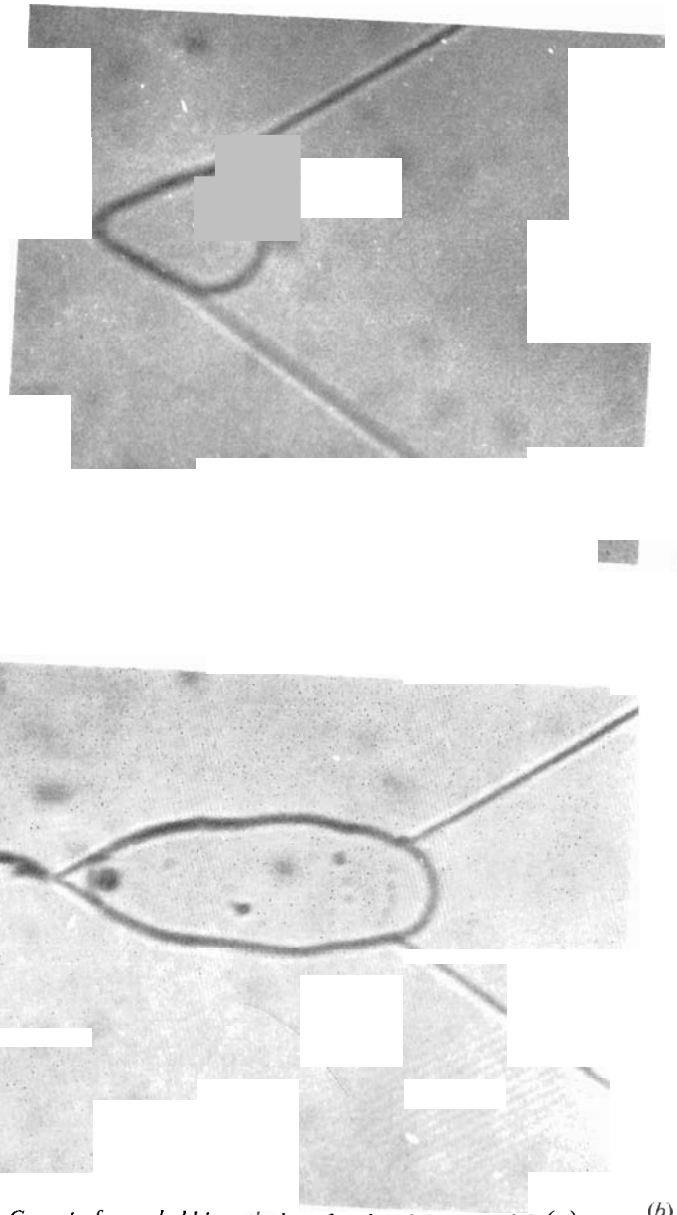

Fig. 5.20 *Growth of a gas bubble at the interface in solidifying salol: (a) nucleation and incorporation into the interface; (b) formation of the elongated blowhole (Woodruff*[42]*).*

There are few reports of investigations dealing with the factors influencing the number, form and distribution of pores in solidified metals. McNair[43] and Jordan *et al.*,[44] for instance, give some data on the effects of gas content, ingot size and solidification conditions on porosity. It is to be hoped that more fundamental work of this type will be carried out. In the meantime it should be noted that effective empirical methods have been developed for the *control* of porosity in ingots and castings *(see* Section 9.1).

REFERENCES

1. Chadwick, G. A. (1963). *Prog. Mat. Sci.,* **12,** 97.
2. Bell, J. A. E. and Winegard, W. C. (1965). J. *Inst. Met.,* **93,** 457.
3. Rumball, W. M. and Kondic, V. (1966). *Trans. Met. Soc. AIME,* **236,** 586.
4. Hunt, J. D. and Jackson, K. A. (1966). *Trans. Met. Soc. AIME,* **236,** 843.
5. Hunt, J. D. and Chilton, J. P. (1962–63). *J. Inst. Met.,* **91,** 338.
6. Chadwick, G. A. (1962–63). J. *Inst. Met.,* **91,** 169.
7. Tiller, W. A. (1958). *Liquid Metals and Solidification,* ASM, Cleveland, p. 276.
8. Jackson, K. A. and Hunt, J. D. (1966). *Trans. Met. Soc. AIME,* **236,** 1129.
9. Chadwick, G. A. (1963–64). J. *Inst. Met.,* **92,** 18.
10. Moore, A. and Elliott, R. (1968). *The Solidification of Metals,* ISI Publication 110, p. 167.
11. Day, M. G. and Hellawell, A. (1968). *Proc. Roy. Soc.,* **A305,** 473.
12. Day, M. G. (1969). J. *Metals,* **21**(4), 31.
13. Cooksey, D. J. S., Munson, D., Wilkinson, M. P. and Hellawell, A. (1964). *Phil. Mag.,* **10,** 745.
14. Hunt, J. D. (1968). J. *Crystal Growth, 3–4,* 82.
15. Hellawell, A. (1967). *Met. and Materials,* **1,** 361.
16. Davies, G. J. (1971). *Strengthening Methods in Crystals* (Ed. by A. Kelly and R. B. Nicholson), Applied Science, Barking, p. 485.
17. Mollard, F. R. and Flemings, M. C. (1967). *Trans. Met. Soc. AIME,* **239,** 1526.
18. Mollard, F. R. and Flemings, M. C. (1967). *Trans. Met. Soc. AIME,* **239,** 1534.
19. Chadwick, G. A. (1968). *The Solidification of Metals,* ISI Publication 110, p. 138.
20. Kerr, H. W., Plumtree, A. and Winegard, W. C. (1964–65). J. *Inst. Met.,* **93,** 63.
21. Cooksey, D. J. S. and Hellawell, A. (1967). J. *Inst. Met.,* **95,** 183.
22. Day, M. G. (1970). J. *Inst. Met.,* **98,** 57.
23. Plumb, R. C. and Lewis, J. E. (1957–58). J. *Inst. Met.,* **86,** 393.
24. Kim, C. B. and Heine, R. W. (1963–64). J. *hzst. Met.,* **92,** 367.

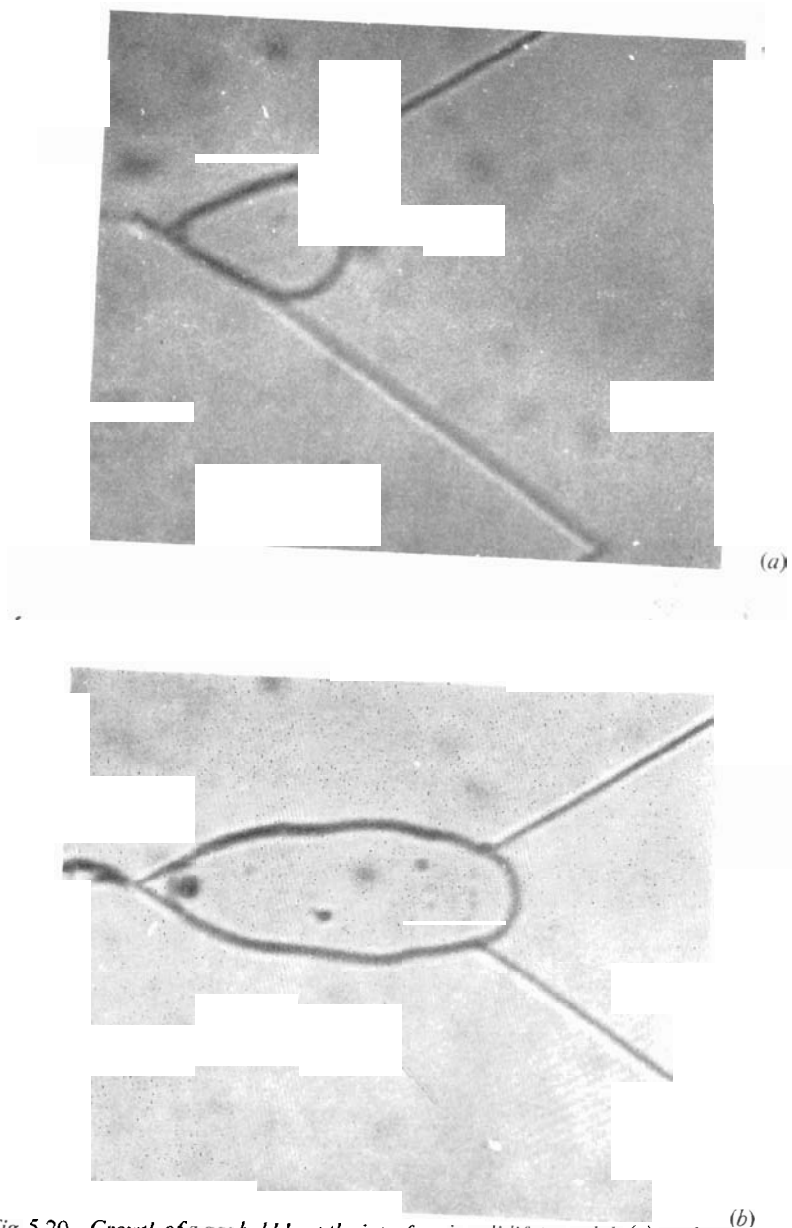

Fig. 5.20 *Growth of a gas bubble at the interface in solidifying salol: (a) nucleation and incorporation into the interface; (b) formation of the elongated blowhole (Woodruff[42]).*

There are few reports of investigations dealing with the factors influencing the number, form and distribution of pores in solidified metals. McNair[43] and Jordan *et al.*,[44] for instance, give some data on the effects of gas content, ingot size and solidification conditions on porosity. It is to be hoped that more fundamental work of this type will be carried out. In the meantime it should be noted that effective empirical methods have been developed for the *control* of porosity in ingots and castings *(see* Section 9.1).

REFERENCES

1. Chadwick, G. A. (1963). *Prog. Mat. Sci.*, **12,** 97.
2. Bell, J. A. E. and Winegard, W. C. (1965). **J.** *Inst. Met.*. **93,** 457.
3. Rumball, W. M. and Kondic, V. (1966). *Trans. Mel. Soc. AIME,* **236,** 586.
4. Hunt. J. D. and Jackson. K. A. (1966). *Trans. Met. Soc. AIME,* **236,** 843.
5. Hunt, J. D. and Chilton, J. P. (1962–63). **J.** *Inst. Met.,* **91,** 338.
6. Chadwick, G. A. (1962–63). **J.** *Inst. Met.,* **91,** 169.
7. Tiller, W. A. (1958). *Liquid Metals and Solidification,* ASM, Cleveland, p. 276.
8. Jackson, K. A. and Hunt, J. D. (1966). *Trans. Met. Soc. AIME,* **236,** 1129.
9. Chadwick, G. A. (1963–64). **J.** *Inst. Met.,* **92,** 18.
10. Moore, A. and Elliott, R. (1968). *The Solidification of Metals,* ISI Publication 110, p. 167.
11. Day, M. G. and Hellawell, A. (1968). *Proc. Roy. Soc.,* **A305,** 473.
12. Day, M. G. (1969). **J.** *Metals,* **21**(4), 31.
13. Cooksey, D. J. S., Munson, D., Wilkinson, M. P. and Hellawell, A. (1964). *Phil. Mag.,* **10,** 745.
14. Hunt, J. D. (1968). *J. Crystal Growth,* **3–4,** 82.
15. Hellawell, A. (1967). *Met. and Materials,* **1,** 361.
16. Davies, G. J. (1971). *Strengthening Methods in Crystals* (Ed. by A. Kelly and R. B. Nicholson), Applied Science, Barking, p. 485.
17. Mollard, F. R. and Flemings, M. C. (1967). *Trans. Met. Soc. AIME,* **239,** 1526.
18. Mollard, F. R. and Flemings, M. C. (1967). *Trans. Met. Soc. AIME,* **239,** 1534.
19. Chadwick, G. A. (1968). *The Solidification of Metals,* ISI Publication 110, p. 138.
20. Kerr. H. W.. Plumtree. A. and Winegard, W. C. (1964–65). **J.** *Inst. Met.,* **93,** *63.*
21. Cooksey, D. J. S. and Hellawell, A. (1967). **J.** *Inst. Met.,* **95,** 183.
22. Day, M. G. (1970). **J.** *Inst. Met.,* **98,** 57.
23. Plumb, R. C. and Lewis, J. E. (1957–58). **J.** *Inst. Met.,* **86,** 393.
24. Kim, C. B. and Heine, R. W. (1963–64). **J.** *Inst. Met.,* **92,** 367.

25. Morrogh, H. G. (1968). *The Solidification of Metals.* ISI Publication 110, p. 238.
26. Jolley, G. (1968). *The Solidification of Metals,* ISI Publication 110, p. 242.
27. Hunter, M. J. and Chadwick, G. A. (1972). **J.** *Iron Steel Inst.,* 210, 117.
28. Collins, W. T. Jr and Mondolfo, L. F. (1965). *Trans. Met. Soc. AIME,* **233.** 1671.
29. Bates, H. E., Wald, F. and Weinstein, M. (1969). **J.** *Mat. Sci., 4,* 25.
30. Uhlmann, D. R. and Chadwick, G. A. (1961). *Acta Met.,* **9,** 835.
31. Sartell, J. A. and Mack, D. J. (1964–65). *J. Inst. Met.,* **93,** 19.
32. Delves, R. T. (1965). *Brit.* **J.** *Appl. Phys.,* **16,** 343.
33. Chadwick, G. A. (1965). *Brit.* **J.** *Appl. Phys.,* **16,** 1095.
34. Livingston, J. D. and Cline, H. E. (1969). *Trans. Met. Soc. AIME,* 245, 351.
35. Uhlmann, D. R., Chalmers, B. and Jackson, K. A. (1964). **J.** *Appl. Phys., 35,* 2986.
36. salmon–COXP. H. and Charles, J. A. (1963). *J. Iron Steel Inst.,* **201,** 863.
37. Charles, J. A. (1968). *The Solidification of Metals,* IS1 Publication 110, p. 309.
38. Blank, J. R. and Pickering, F. B. (1968). *The Solidification of Metals,* ISI Publication 110, p. 370.
39. Ransley, C. E. and Neufeld, H. (1948). *J. Inst. Met.,* 74, 599.
40. Chalmers, B. (1964). *Principles of Solidification,* John Wiley, New York, p. 189 *et seq.*
41. Campbell, J. (1968). *The Solidification of Metals,* ISI Publication 110, p. 18.
42. woodruff, D. P. (1969). *Metals and Materials,* **3,** 171.
43. McNair, P. M. (1948). **J.** *Iron Steel Inst.,* **160.** 151
44. Jordan, M. F., Denyer, G. D. and Turner, A. N. (1962–63). *J. Inst. Met.,* **91,** 48.

CHAPTER 6

The Structure of Castings

The structure of a casting is of great importance since many materials properties, especially mechanical properties, depend on grain shape and grain size. In addition, segregation resulting from the various modes of redistribution of solute can have marked effects. In this chapter we will examine the nature of the macroscopic cast structure and discuss the underlying reasons for the development of the different types of structure. This leads to the consideration of the control of the cast structure, since this is one of the most useful techniques available to the metallurgist or materials scientist concerned with the development of microstructure with the specific intention of improving properties. This is important if the material is to be used in the as-cast form or if it is to be worked to a final shape. In Chapter 7 we will consider segregation.

6.1 MACROSTRUCTURE

In most as-cast polycrystalline solids three distinct zones with different grain structures can be identified (Fig. 6.1), namely:

(i) the chill zone—a boundary layer, adjacent to the mould wall, of small equiaxed crystals with random orientations;

(ii) the columnar zone—a band of elongated crystals aligned parallel to the directions of heat flow;

(iii) the equiaxed zone—a central region of uniform crystals. The properties of this central region are comparatively isotropic provided the grain size is small. The grain size in the equiaxed zone is, however, normally larger than that of the chill zone.

Probably the most important factor in determining subsequent properties is the relative proportions of the columnar and equiaxed zones. The chill zone is normally only a small number of grains thick and has a very limited influence.

If the object of the control of grain structure is to obtain isotropy, a fine-grained equiaxed structure is required. This is brought about by encouraging those conditions which lead to the breakdown of columnar growth and the formation of the equiaxed zone. Understanding of the factors responsible for the formation of the equiaxed

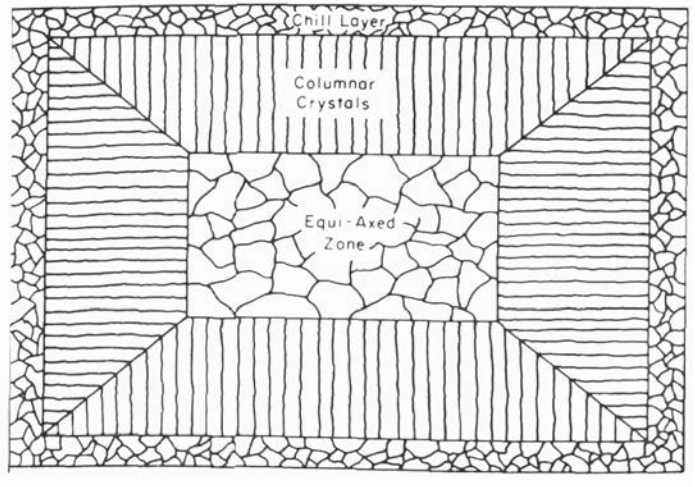

Fig. 6.1 Transverse section of an as-cast structure showing the chill zone, columnar zone and equiaxed zone (Walker[6]).

zone has significantly increased in recent years. On the other hand, if anisotropic properties are required, the columnar zone will need to predominate. The relative proportions of the different zones can be controlled by altering the casting variables, *e.g.* the alloy composition, the pouring temperature, the rate of cooling, etc., and an ingot can vary from being fully columnar to being fully equiaxed (Fig. 6.2). This is considered in detail in subsequent sections.

The grain boundaries form by the impingement of the growing grains and the effects of the boundaries derive both from crystallographic sources and particularly because of the accumulation of soluble and insoluble impurities that can occur. Thus the effects of these grain boundaries depend both on the change in orientation at the boundary and on the special properties of the boundaries themselves. So far as fracture is concerned they can form easy paths for crack propagation, especially in the presence of solute segregation.[1,2] If the equiaxed zone is absent, accumulation of soluble and insoluble impurities in the regions where the columnar structures impinge

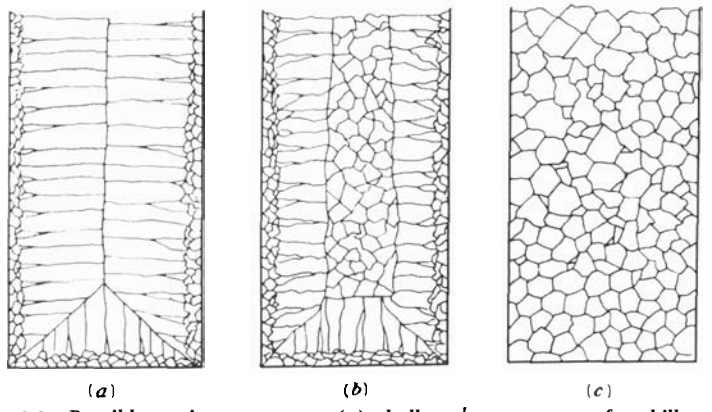

Fig. 6.2 Possible casting structures: (a) wholly columnar except for chill zone; (b) partially columnar, partially equiaxed; (c) wholly equiaxed (Heine et al.[3]).

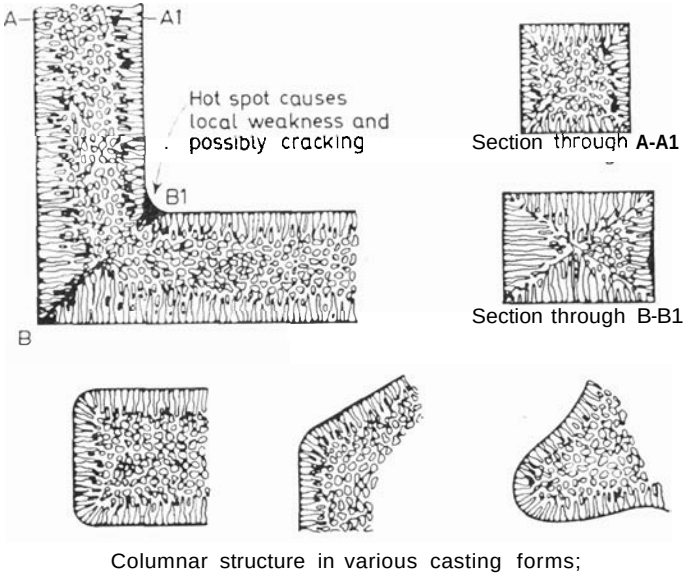

Fig. 6.3 Planes of weakness caused by unfavourable shape effects (Heine et al.[3]).

can have disastrous results; for example, this is commonly the case in fusion welds.

In castings, the consequences of grain impingement are particularly bad at sharp corners, in rectangular sections and at perpendicular surface junctions, as shown in Fig. 6.3. These can usually be corrected by suitable design procedures. We are going to be concerned with control by manipulation of the casting procedures. Before doing so, it should be noted that if the ingot structure is going to be subjected to ***extensive*** working in the solid state, the final grain structure will be dictated by solid state changes. Nevertheless, careful control in the initial stage can have beneficial results particularly as far as the attainment of homogeneity is concerned. For instance, Antes ***et*** *al.*[4] have shown that a controlled fine-grained cast structure facilitates homogenisation. This is an important ancillary function attainable by the control of grain size and shape.

6.2 THE CHILL ZONE

The chill crystals nucleate on or near the mould wall. Observations of undercoolings make it clear that they are the result of heterogeneous nucleation. The formation of the chill zone was initially explained[5–7] in terms of the copious nucleation considered to occur in the *thermally* undercooling region adjacent to the mould wall. The extent of nucleation was largely determined by the thermal conditions at the mould wall, but also by the efficiency of the mould wall as a substrate for heterogeneous nucleation and by the existence of effective nucleants in the chilled liauid laver. The existence of localised constitutional supercooling can also play a p'art.[7] Overall, the numbers of crystals in the chill zone depend on the superheat of the liquid, the temperature of the mould, the thermal properties of the metal and the mould, as well as on the nucleation potency of the mould wall or of particles in the liquid. In extreme cases it would be possible for chill crystals formed initially to subsequently remelt.

This ***nucleation*** theory has been modified[8] to allow for crystal multiplication by the fragmentation of the initial nuclei. Crystal multiplication by the remelting of dendritc arms resulting from growth fluctuations (produced, for instance, by convection) was observed by Jackson ***et*** *al.*[9] This is shown in Fig. 6.4 and was used as a basis for a theory of equiaxed zone development ***(see*** Section 6.5). Biloni[10] has established that both mechanisms are operable in the generation of the chill zone, with their relative importance depending on the casting conditions. The crystals in the chill zone are normally equiaxed and of random orientation.

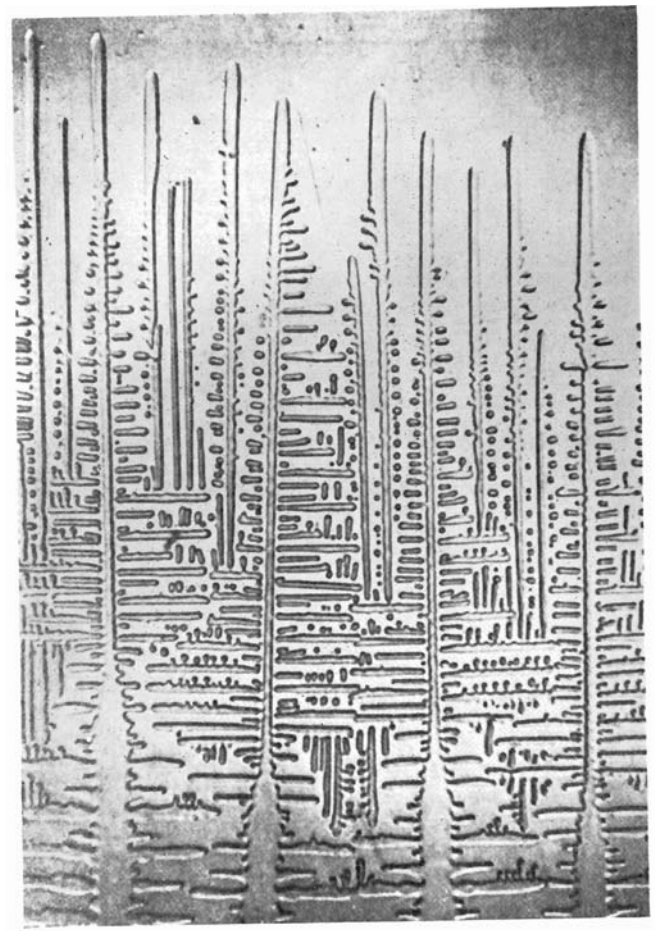

Fig. 6.4 *Dendrite* **structure in carbon** *tetrabromide with salol added, after* **a growth rate fluctuation. The** *detachment* **by melting of** *dendrite* **arms can** *be clearly seen* (*Jackson* **et al.**[9]).

6.3 THE COLUMNAR ZONE

The columnar crystals develop predominantly from the chill zone and show a strong preferred crystallographic orientation which corresponds with the preferred crystallographic directions of dendritic growth.[11,12] Some few grains appear in the columnar zone which do not originate in the chill zone.[10,12] The substructure in the columnar zone can show all stages of development through planar to

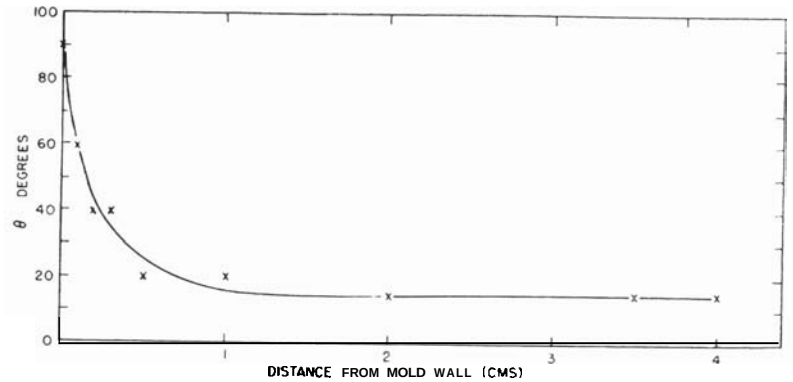

Fig. 6.5 *Change in preferred orientation with distance from the mould wall for an aluminium–2% silver alloy poured at the liquidus temperature: θ is the spread in orientation (Walton and Chalmers[11]).*

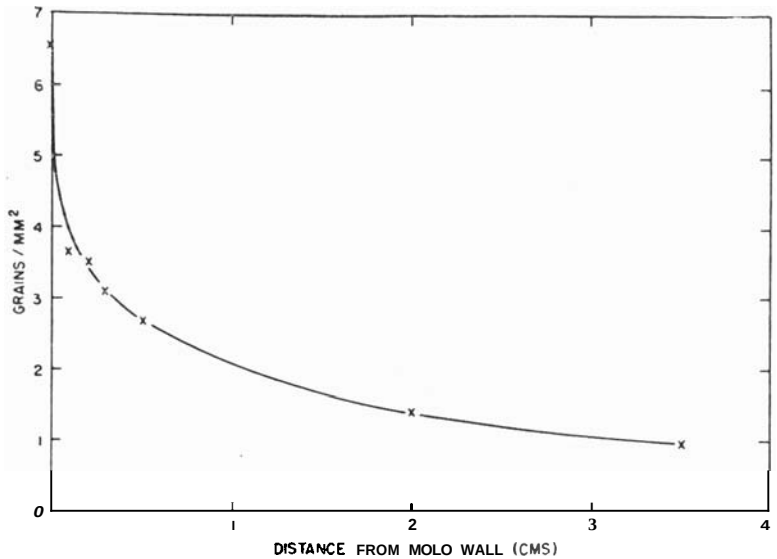

Fig. 6.6 *Increase in grain size with distance from the mould wall for the alloy of Fig. 6.5 (Walton and Chalmers[11]).*

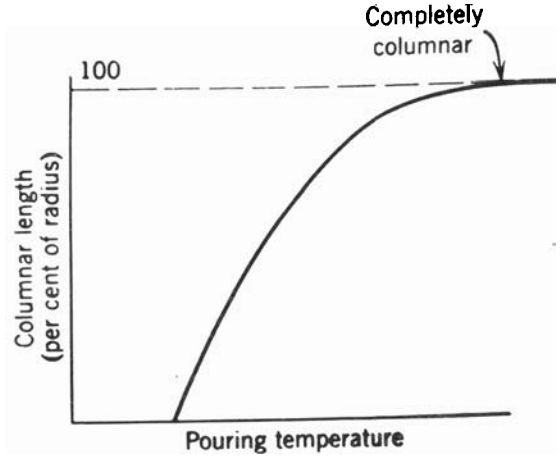

Fig. 6.7 *Variation of the length of the columnar zone with pouring temperature (Chalmers[7]).*

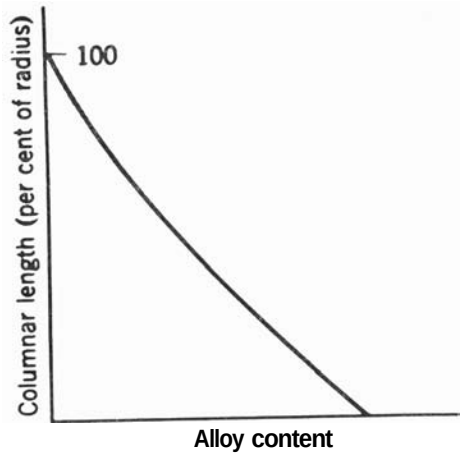

Fig. 6.8 *Variation of the length of the columnar zone with the alloy content for constant pouring temperature (Chalmers[7]).*

cellular and to cellular dendritic.[10] The axes of the columnar crystals are normally parallel to the heat flow direction. There is competitive growth between the crystals growing from the chill zone such that those with the steepest thermal gradient parallel to the preferred growth direction (the dendrite arm axis direction) grow

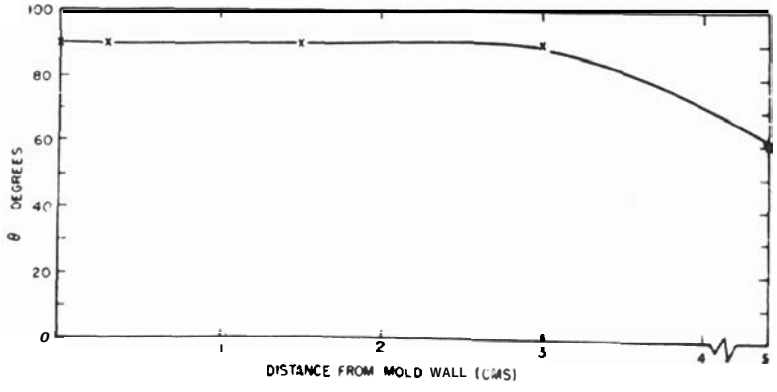

***Fig.* 6.9** *Change in* **preferred** *orientation* **with** *distance* **from the** *mould* **wall** *for* **pure aluminium:** *θ* **is the spread** *in orientation* (*Walton and Chalmers*[11]).

more rapidly than their less favourably oriented neighbours. They expand and overwhelm their neighbours to dominate the growth process. This is clearly illustrated by the observation that the spread in orientation decreases as the columnar zone extends (Fig. 6.5), while at the same time the average grain size increases (Fig. 6.6).

For a given alloy the extent of the columnar region increases as the pouring temperature increases (Fig. 6.7). For given pouring conditions the extent of the columnar region decreases as the alloy content increases (Fig. 6.8). With pure metals the as-cast structure is normally fully columnar and there is little development of preferred orientation (Fig. 6.9). For pure metals it appears that the growth front is essentially planar and dendritic growth does not occur to a significant degree. This would account for the absence of preferred orientation. Furthermore, the persistence of the columnar crystals would seem to be a consequence of an *inability* to produce equiaxed crystals. In the presence of profuse nucleation in the chill zone, or if crystals are produced at the free surface,[12] some equiaxed crystals should be present.

Explanations of the extent and nature of the columnar zone begin, as described above, with the development from the chill crystals. The main controlling factor is the ***appearance*** of the equiaxed zone.

The evidence is that the columnar crystals will persist provided conditions are not favourable for the formation of equiaxed crystals. Because of this, control over the columnar growth is normally exerted by inducing the formation of equiaxed crystals. It is this control which is foremost in the control of the overall cast structure.

6.4 THE EQUIAXED ZONE

The crystals in the equiaxed zone usually have a grain size larger than that of the chill zone and their orientation is effectively random. As shown in Figs. 6.7 and 6.8, the formation of an extensive equiaxed

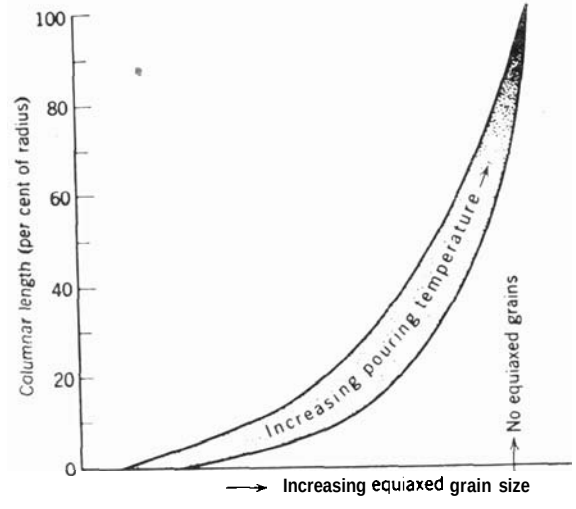

Fig.* 6.10** ***Correlation between columnar length, equiaxed grain size and pouring temperature (Chalmers [14]).

zone is favoured by pouring with low superheat and by higher alloy contents. As the pouring temperature increases the tendency to form equiaxed grains decreases, but on the other hand the equiaxed grains that occur do so with increasing grain size (Fig. 6.10). It is important to recognise that there is a significant size effect influencing the development of the equiaxed zone.[23] For instance, the relationships between the columnar zone length and the degree of superheat and the equiaxed grain size and the degree of superheat are only valid for small ingots.

Studies of metal analogue systems[9,15] show quite clearly that the 'nuclei' of the equiaxed crystals arise from a number of sources:

(a) by apparently isolated nucleation events;
(b) from the growing columnar zone; and
(c) from events occurring at the free surface.

For instance, Fig. 6.11 shows a sequence from the solidification of a NH_4Cl–water ingot which contains evidence of these different processes. The relative importance of the different processes has been the subject of considerable controversy and is discussed in the next section.

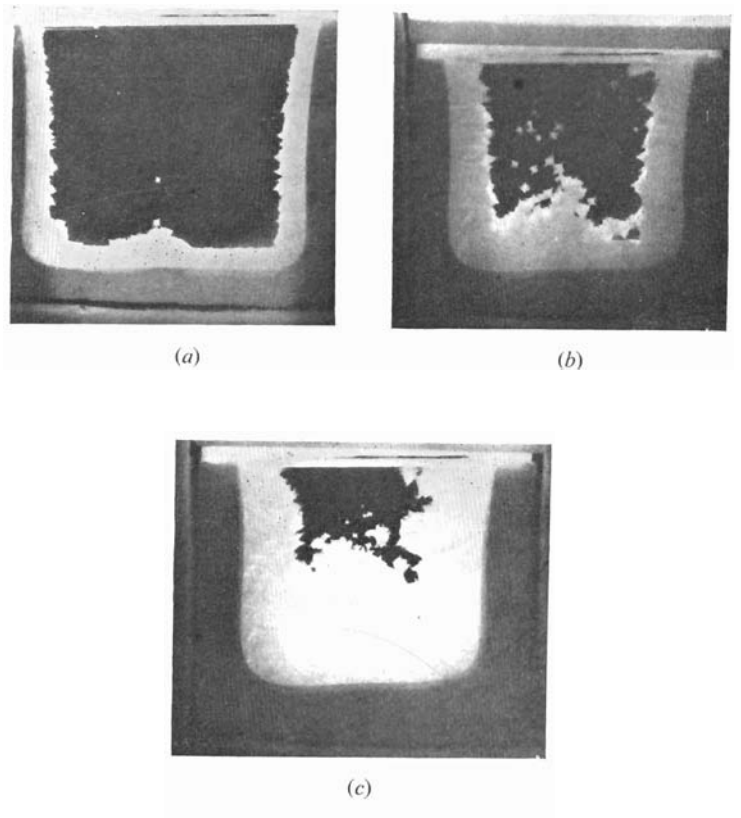

Fig. 6.11 *Successive stages in* ***the*** *solidification of an* NH_4Cl*-water ingot,* ***saturated at*** 50°C, *poured at* 75°C: ***(a)*** *1 minute after* ***pouring;*** *(h)* ***2 minutes after pouring; (c)*** $2\frac{1}{2}$ *minutes after pouring* (*Jackson* ***et*** al.[9]).

6.5 THEORIES OF THE DEVELOPMENT OF THE EQUIAXED ZONE

Four major theories have been proposed, three of which are generally agreed to be of importance.

(i) Winegard and Chalmers[16] proposed that the equiaxed zone formed after some initial columnar growth when constitutional supercooling ahead of the growing crystals became sufficient to induce heterogeneous nucleation. The subsequent growth of these crystals blocked off the columnar zone and the remaining liquid was then considered to solidify in the equiaxed form. This theory has now been discarded for several reasons. Experiment showed that the proposed conditions were at variance with experimental evidence of the thermal history of solidifying melts.[14,17] Furthermore, it was difficult to explain how the development of the required undercooling could be delayed until extensive columnar growth had occurred.[14] Finally, observations[18,19] of equiaxed zone formation in melts free from heterogeneous nucleants were not compatible with the requirement of nucleation ahead of the growing columnar front. All subsequent theories do not rely upon the need for *nucleation* ahead of the growth front, but propose different methods for independently producing the nuclei of the equiaxed grains.

(ii) Chalmers,'[4] recognising the inadequacies of this earlier theory, proposed what became known as the 'big bang' mechanism. This required that the nuclei for both the columnar and the equiaxed crystals were formed during the initial chill near the mould wall. These nuclei then either grew as columnar crystals or drifted into the central zone to become equiaxed crystals. It is interesting to note that a similar proposal had been made many years earlier.[20] The columnar-to-equiaxed transition resulted from the obstruction of columnar growth by the network barrier of equiaxed dendrites.

There is considerable evidence[21–24] in support of this mechanism, particularly for melts cast from near the liquidus temperature. The experiments of Walker[18,19] make it clear, however, that some other mechanisms must also be occurring.

(iii) Another mechanism of significance is that in which crystal multiplication occurs[9] by the melting off of the arms of growing columnar dendrites ***(see*** Fig. 6.4). During dendritic growth a solute-rich layer builds up around the growing dendrite tip. Any side branches must grow through this layer and this leads to the formation of a neck of lower melting point material[9] and this, in addition to the local curvature,[25] will favour remelting of the neck in the presence of thermal fluctuations. These thermal fluctuations are attributed to

natural convection. Certainly it is well established that large temperature fluctuations can occur during growth[26,27] and that conditions that favour convection also favour the development of the equiaxed zone.[21,28] What is more, it has been shown[21,23] that suppression of convection leads to suppression of equiaxed growth. More recently the direct observations[29,30] of dendrite remelting in metals provide further confirmatory evidence of the part played by dendrite remelting in forming an equiaxed zone.

(iv) Southin[13] (following Rosenhain[31]) proposed that the nuclei for the equiaxed crystals formed at the free surface of the ingot and showered down into the liquid ahead of the columnar zone, growing as they descended. The nuclei may simply be considered as free surface dendrites which detach arid sink under their own weight or, alternatively, dendrite remelting (see iii above) may play a contributory part. In either case subsequent work has confirmed[32,33] that the surface does generate crystals in the equiaxed region.

In the light of the above it can only be concluded that all three of the mechanisms described in (ii), (iii) arid (iv) are operative during the solidification of ingots and castings. The relative contributions will depend on the actual conditions existing during solidification. Nevertheless, recognising the importance of the three mechanisms enables the development of methods for controlling the grain structure. Before considering the different methods it is only fair to point out that many of these were worked out empirically before there was any agreed understanding of the mechanisms of formation of the equiaxed zone.

6.6 CONTROL OF GRAIN STRUCTURE IN CAST METALS

For all but a few very specialised applications, e.g. magnet alloys,[33] single crystal turbine blades,[34,35] fine-grained equiaxed structures are required in castings and ingots. These structures are isotropic and their properties are markedly superior. To develop these structures requires the suppression of columnar growth and this can be achieved by encouraging conditions favourable to the formation of the equiaxed nuclei. A necessary prerequisite is the establishment of a crystal network to act as an effective barrier to further columnar growth. Two main approaches have been adopted, namely,

(a) the control of nucleation by control of the casting conditions or by the use of inoculants (see Section 2.3.2), and

(b) the use of physical methods, e.g. stirring, ultrasonic vibration, to induce dynamic grain refinement.

6.6.1 Control of nucleation behaviour

The simplest approach for a given alloy is to cast from near the liquidus temperature so as to promote copious heterogeneous nucleation in the initially chilled liquid (see Figs. 8.7 and 6.10). This has disadvantages with complex castings, where there will be a wide range of thermal conditions and where fluidity requirements often make it necessary to cast with a comparatively high degree of superheat. It is also a rather haphazard process since without the deliberate introduction of nucleating agents the nucleation process depends on the chance existence of suitable heterogeneous nucleants. For this reason it is usual to make additions of inoculants prior to casting. As discussed in Section 2.3.2, both structural and chemical factors play an important part in determining the nucleating effectiveness of an inoculant. In the final analysis empirical methods are needed and these have led to a wide range of inoculants becoming available. Empirical methods have also been used to develop 'growth restrictors' which reduce the rate of growth of the first nuclei to form and thus promote the formation of larger numbers of nuclei.[40]

Detailed information concerning specific materials can be obtained from the many papers on the use of inoculants, e.g. aluminium alloys,[36–38] magnesium alloys,[28,37,39] steels,[40] or from recent reviews,[41,42] A summary is given in Table 6.1. The effectiveness of inoculants can be quite striking, as shown in Figs. 6.12 and 6.13.

TABLE 6.1

SOME GRAIN REFINING NUCLEANTS[a]

Metal or alloy	*Grain refiner*	*Comments*
Magnesium and Mg–Zr alloys	Zirconium added as alloy or salts	Zr or Zr-enriched Mg peritectic nuclei
Magnesium–aluminium	Carbon, for example as hexachlorethane	Al_4C_3 or $AlNAl_4C_3$ nuclei
Magnesium–aluminium	Superheating	In presence of C, Al_4C_3 and/or Al–Mn nuclei
Magnesium–aluminium–manganese	$FeCl_3$	Fe–Al–Mn or Al_4C_3 nuclei
Mg Zn	$FeCl_3$ or Zn–Fe	Fe compound nuclei
Mg Zn	NH_3	Nucleated by H_2 (?)
Al alloys	Ti as reducible halide salts or as Al–Ti hardener	TiC nucleus or peritectic $TiAl_3$
Al alloys	Ti + B as reducible halide salts or as Al–Ti–B hardener	TiB_2 nuclei, more resistant to melt history

TABLE 6.1—*continued*

Metal or alloy	*Grain refiner*	*Comments*
Al alloys	Boron as reducible halide salts or Al–B	AlB_2 nuclei
Al alloys	Niobium	
Cu alloys	Fe metal or alloy	Fe-rich peritectic nuclei
Bronzes	Transition nitrides and borides or FeB	
Cu–Al_2Cu eutectic	Titanium	Nucleates primary Al
Cu–7%Al	Mo, Nb, W, V	
Cu–9%Al	Bi	
Low alloy steel	Titanium	
Low alloy steel	Transition elements and carbides	
Silicon steel	TiB_2	Dissolves and precipitates TiN or TiC
Low alloy steel	Fe powder	Introduction of micro-chilling particles
Austenitic steel	$CaCN_2$, nitrided Cr and other metallic powders	In presence of increased nitrogen
Tin alloys	Germanium or indium	
Lead alloys	S	
Lead alloys	Se, Te	
Type metal	As, Te	
Monel	Lithium	
Al–Si hypereutectic	Phosphorus as Cu–P, $PNCl_2$ or proprietary inoculant	Refines primary Si
Fe–C (graphite)	Carbon	Refines eutectic, probably through nucleating graphite
Fe–C–Si (graphite)		
Grey cast iron		
Grey cast iron	Si alloys containing aluminium, alkaline earths and/or rare earths	Refines eutectic, may nucleate through precipitation of carbides or graphite

[a] Data from Hughes.[42]

The addition of an inoculant will only be effective provided it remains uniformly distributed through the melt and does not become contaminated or melt. The growth of the nucleus also requires that some supercooling exists in the liquid. This will usually be constitutional supercooling, although at the beginning of the solidification

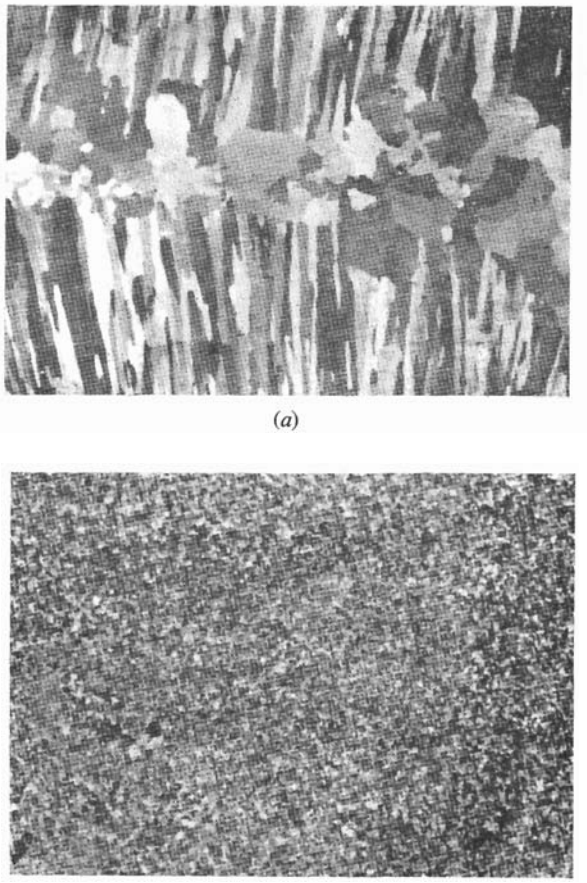

(*a*)

(*b*)

Fig. 6.12 (a) Normal coarse-grabled cast *structure* in 18% chromium–12% nickel steel; (*b*) same steel as (a) refined by *inoculation* (Hall and *Jackson*[40]).

process some thermal undercooling may occur. As shown in Section 4.4, constitutional supercooling is favoured by low temperature gradients in the liquid, high rates of growth and, for k, < 1, low distribution coefficients. To ensure efficient use of inoculants the solidification process should be controlled to achieve these conditions.

One other approach to the introduction of heterogeneous nucleants is the use of mould In this procedure the mould walls are treated with a wash containing the nucleating agent; this ensures that all parts of the casting have access to the nucleant.

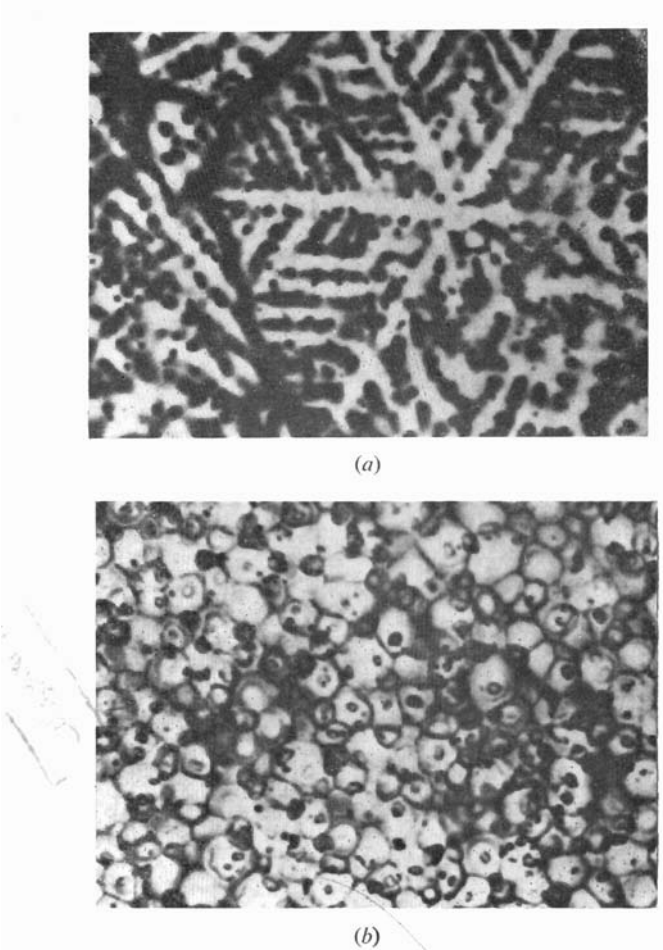

Fig. 6.13 ***(a) A*** *magnesium–zinc dendritic alloy specimen; dendrite* ***arm*** *spacing* ***40 p. (h) Magnesium–zinc*** *with* ***zirconium*** *grain refinement. Non-dendritic* ***alloy*** *specimen; grain size* ***75*** *μ (Flemings*[28]*).*

6.6.2 Dynamic grain refinement

Various methods have been used to produce dynamic fragmentation of the growing dendrites, and thus to promote equiaxed growth. All involve some degree of physical disturbance and differ only in the way this disturbance is produced. Mechanical stirring (vibration, oscillation and rotation,[46–52] enhanced natural convection,[47,50] magnetic and electromagnetic stirring,[52–58] sonic and ultrasonic vibrations[59–62] ***(see also*** Chalmers[63]) and agitation with gas bubbles[62] have all been used effectively to produce dynamic grain refinement. In all cases the principal mechanism for producing the nuclei for the equiaxed grains is dendrite remelting[9] ***(see*** Section 6.5), although dendrite mechanical deformation or fracture can occur to some degree. The effect of the physical disturbance is to produce

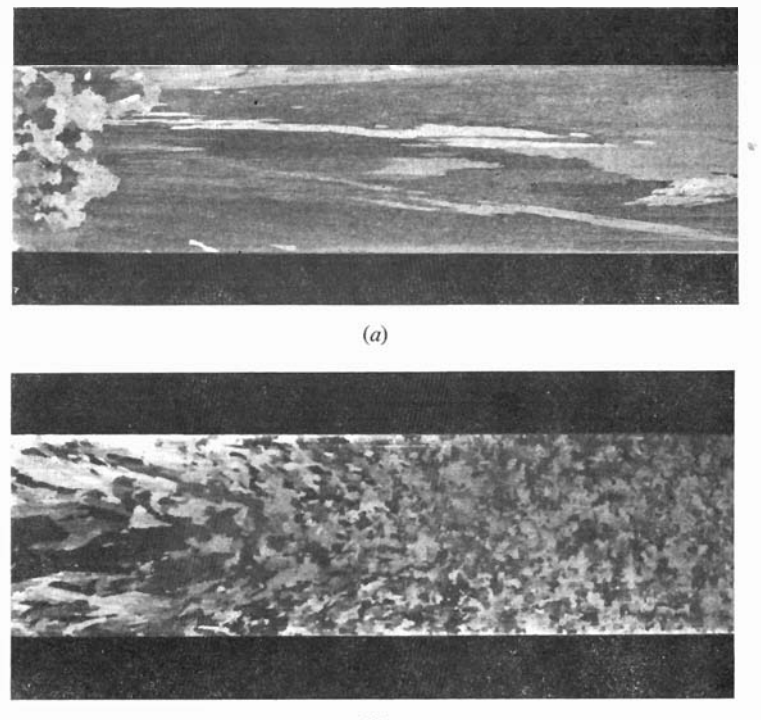

Fig. ***6.14*** *Macrostructures* ***of aluminium4 wt*** *%* ***copper solidified: (a) without stirring; and*** *(b)* ***after*** *stirring (Wojciechowski* ***and*** *Chalmers*[51]*).*

localised thermal fluctuations as the liquid metal flows backwards and forwards around the growing dendrites. It is these forced thermal fluctuations that produce the conditions conducive to dendrite remelting.

A major advantage of dynamic grain refinement is that it can (in one or other of its various forms) be applied to quite complex castings provided, of course, disruption of the mould is not produced.

Figures 6.14 and 6.15 show examples of grain refinement by mechanical stirring and ultrasonic vibration, respectively. The refining action that is achieved in each case is plainly evident.

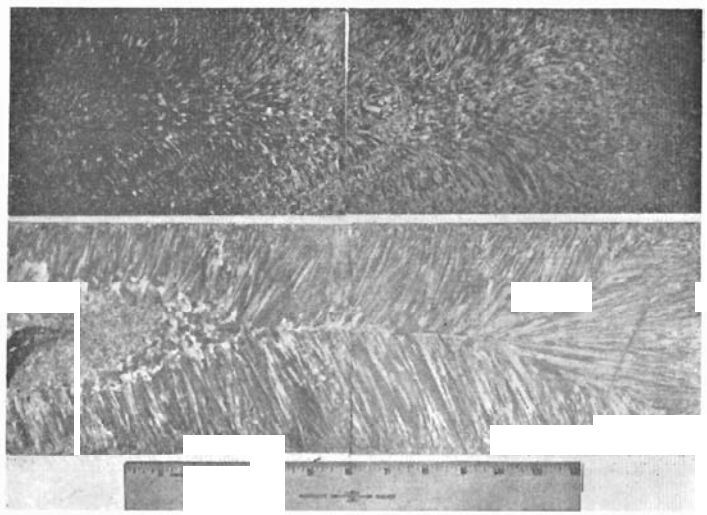

Fig. 6.15 *Macrostructure of stainless steel ingots, left—cast without ultrasonic vibration, right—cast with ultrasonic vibration (Lane et al.*[60]).

6.7 MACROSTRUCTURE OF FUSION WELDS

The mechanisms involved in the solidification of fusion welds are basically the same as those of normal castings. The main differences are,

(i) that the solidification rates are high, and

(ii) the temperature gradients in the liquid are steep. The temperatures in the centre of the weld pool are significantly higher than the melting temperature.

There is no equivalent of the chill zone in a fusion weld macrostructure because the partially melted grains at the molten zone boundary act as the sites which initiate columnar growth. This occurs as soon as the heat source moves away, and does not require a nucleation event. The grains grow in a columnar form and usually extend to the centre line (Fig. 6.16). The normal range of growth structures ranging from cellular through cellular–dendritic is observed,[64,65] as is some free dendritic growth. Although there is a great deal of turbulence in the weld pool,[66] and thus conditions favourable for dynamic grain refinement, an equiaxed zone is not normally observed. As discussed in a previous section, for an equiaxed zone to form, dendrite fragments (formed by remelting or fracture)

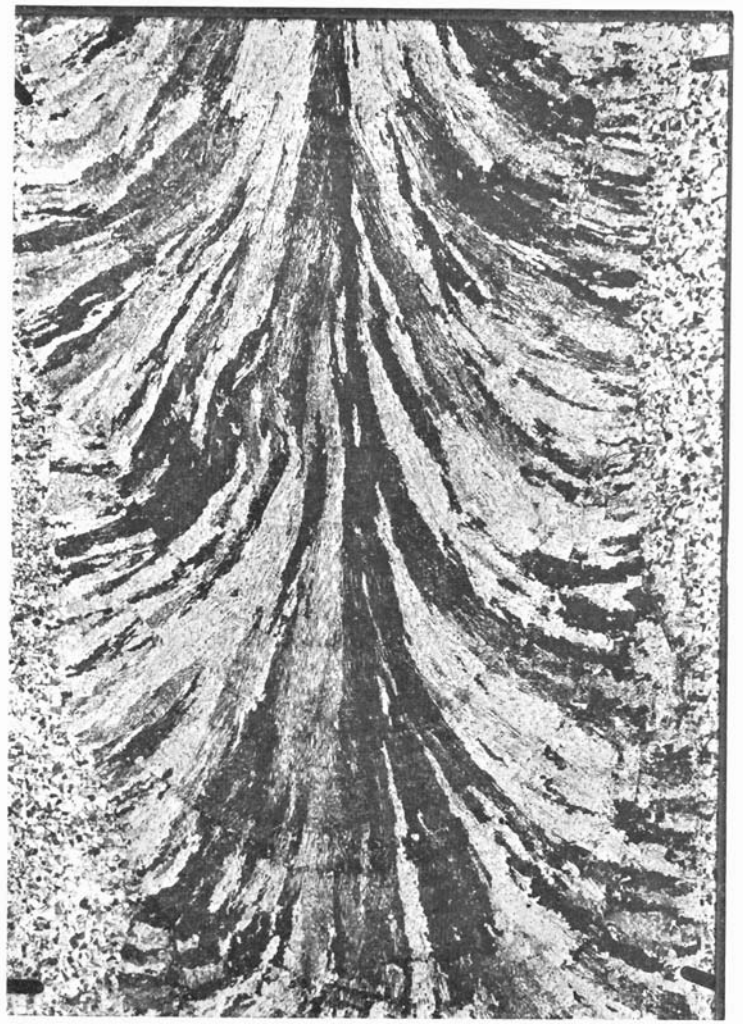

Fig.6.16 Columnar solidification pattern of a srrbmerged-arcweld bead (Garland[73]).

must survive without melting, in the liquid away from the interface. The very high temperatures at the weld pool centre make survival difficult.

The methods available for the control of cast structures ***(see*** Section 6.6) can be applied to fusion welds, but there are practical difficulties. Magnetic stirring,[67,68] ultrasonic vibration[69,70] and

nucleant inoculation[71,72] have all been used with some success. Stimulation of surface nucleation with gas jets, and arc vibration, have also been used effectively[73] to produce equiaxed structures.

REFERENCES

1. Gifkins, R. C. (1961). J. *Aust. Inst. Metals,* **6,** 227.
2. McLean, D. (1962). *Mechanical Properties of Metals,* John Wiley, New York, p. 251.
3. Heine, R. W., Loper, C. R. Jr and Rosenthal, P. C. (1967). *Principles of Metal Casting,* McGraw-Hill, New York, p. 694.
4. Antes, H. W., Lipson, S. and Rosenthal, H. (1967). *Trans. Met. Soc. AIME,* **239,** 1634.
5. Henzel, F. R. (1937). *Trans. AIME,* **124,** 300,
6. Walker, J. L. (1958). *Liquid Metals and Solidification,* ASM, Cleveland, p. 319.
7. Chalmers, B. (1964). *Principles of Solidification,* John Wiley, New York, p. 259 *et seq.*
8. Bowers, T. F. and Flemings, M. C. (1967). *Trans. Met. Soc. AIME,* **239,** 216.
9. Jackson, K. A., Hunt, J. D., Uhlmann, D. R. and Seward, T. P. III (1966). *Trans. Met. Soc. AIME,* **236,** 149.
10. Biloni, H. (1968). *The Solidification of Metals,* ISI Publication 110, p. 74.
11. Walton, D, and Chalmers, B. (1959). *Trans. Met. Soc. AIME,* **215,** 447.
12. Herbert, P. M. and Hellawell, A. (1962). *Proc. Roy. Soc.,* **A269,** 560.
13. Southin, R. T. (1967). *Trans. Met. Soc. AIME,* **239,** 220.
14. Chalmers, B. (1963). *J. Aust. Inst. Metals,* **8,** 255.
15. Ohno, A. (1968). *The Solidification of Metals,* ISI Publication 110, p. 349.
16. Winegard, W. C. and Chalmers, B. (1953). *Trans. ASM,* 46, 1214.
17. Hogan, L. M. and Southin, R. T. (1968). *Cast Metals Res.,* **4,** 1.
18. Walker, J. L. (1961). *Physical Chemistry of Process Metallurgy* (Ed. by G. R. St. Pierre), Interscience, New York. Vol. II, p. 845.
19. Tarshis, L. A., Walker, J. L. and Rutter, J. W. (1971). *Met. Trans.,* **2,** 2589.
20. Gender, R. (1926). *J. Inst. Metals,* **35,** 259.
21. Cole, G. S. and Bolling, G. F, (1965). *Trans. Met. Soc. AIME,* **233,** 1568.
22. Biloni, H. and Chalmers, B. (1968). J. *Mat. Sci.,* **3,** 139.
23. Morando, R., Biloni, H., Cole, G. S. and Bolling, G. F. (1970). *Met. Trans.,* **1,** 1407.
24. Spittle, J. A., Dellamore, G. W. and Smith, R. W. (1968). *The Solidification of Metals,* ISI publication 110, p. 318.
25. Coughlin, J., Kattamis, T. Z. and Flemings, M. C. (1967). *Trans. Met. Soc. AIME,* **239,** 1504.

26. Cole, G. S. and Winegard, W. C. (1964–65). J. *Inst. Metals,* **93,** 153.
27. Cole, G. S. (1967). *Trans. Met. Soc. AIME,* **239,** 1287.
28. Flemings, M. C. (1968). *The Solidification of Metals,* ISI Publication 110, p. 277.
29. Schaeffer, R. J. and Glicksman, M. E. (1967). *Trans. Met. Soc. AIME,* **239,257.**
30. Glicksman, M. E. and Schaeffer, R. J. (1968). *The Solidification of Metals,* ISI Publication 110, p. 43.
31. Rosenhain, W. (1926). *J. Inst. Metals,* **35,** 282.
32. Weinberg, F. and Buhr, R. K. (1968). *The Solidification of Metals,* ISI Publication 110, p. 295.
33. Makino, N. and Kimura, Y. (1965). *J. Appl. Phys.,* **36,** 1185.
34. Ver Synder, F. L. and Piearcey, B. J. (1966). *SAE Joirrnal,* **74**(8), 36.
35. Piearcey, B. J., Kear, B. H. and Smashey, R. W. (1967). *Trans. ASM,* **60,** 634.
36. Cibula, A. (1949). J. *Inst. Metals,* **76,** 321.
37. Glasson, E. L. and Emley, E. F. (1968). *The Solidification of Metals,* ISI Publication 110, p. 1.
38. Cole, G. S., Casey, K. W. and Bolling, G. F. (1970). *Met. Trans.,* **1,** 1413.
39. Kattamis, T. Z., Holmberg, U. T. and Flemings, M. C. (1967). J. *Inst. Metals,* **95,** 343.
40. Hall, H. T. and Jackson, W. J. (1968). *The Solidification of Metals,* ISI Publication 110, p. 313.
41. Cibula, A. (1969). *Grain Control,* Inst. of Metals, London, p. 22.
42. Hughes, I. C. H. (1971). *Progress in Cast Metals,* Inst. Metallurgists, London, p. 1.
43. Reynolds, J. A. and Tottle, C. R. (1951). *J. Inst. Metals,* **80,** 93.
44. Bryant. M. D. and Moore, A. (1971). *Brit. Foundryman,* **64,** 215.
45. Clifford, M. J. (1961). *BCIRA Journal,* **9,** 377.
46. Richards, R. S. and Rostoker, W. (1956). *Trans. ASM,* **48,** 884.
47. Roth, W. and Schippers, M. (1956). Z. *Metal ke,* **47,** 78.
48. Kondic, V. (1958). *Acta Met.,* **6,** 660.
49. Southin, R. T. (1966). *J. Inst. Met.,* **94,** 401.
50. Cole, G. S. and Bolling, G. F. (1967). *Trans. Met. Soc. AIME, 239,* 1824.
51. Wojciechowski, S. and Chalmers, B. (1968). *Trans. Met. Soc. AIME,* **242,** 690.
52. Cole, G. S. and Bolling, G. F. (1968). *The Solidification of Metals,* ISI Publication 110, p. 323.
53. Crossley, F. A., Fisher, R. D. and Metcalfe, A. G. (1961). *Trans. Met. Soc. AIME,* **221.** 419.
54. Langenberg, F. C., Pestel, G. and Honeycutt, C. R. (1961). *Trans. Met. Soc. AIME,* 221, 993.
55. Johnston, W. C., Kotler, G. R. and Tiller, W. A. (1963). *Trans. Met. Soc. AIME,* **227,** 890.
56. Johnston, W. C., Kotler, G. R., O'Hara, S., Ashcom, H. V. and Tiller, W. A. (1965). *Trans. Met. Soc. AIME,* **233,** 1856.

57. Uhlmann, *D. R.*, Seward, T. P. III and Chalmers, B. *(1966). Trans. Met. Soc. AIME,* **236,** *527.*
58. Cole, *G.* S. and Bolling, G. F. *(1966). Trans. Met. Soc. AIME,* **236,** 1366.
59. Freedman, A. *H.* and Wallace, J. F. *(1957). Trans. AFS,* **65,** *578.*
60. Lane, *D. H.,* Cunningham, J. W. and Tiller, W. A. *(1960). Trans. Met. Soc. AIME,* **218,** *985.*
61. Frawley, *J. J.* and Childs, W. J. (1968). *Trans. Met. Soc. AIME,* **242,** *256.*
62. Southin, *R.* T. *(1968). The Solidification of Metals,* ISI Publication *110,* p. *305.*
63. Chalmers, B. *(1965). Liquids: Structure, Properties, Solid Interactions,* (Ed. by T. J. Hughel) Elsevier, Amsterdam, p. *308.*
64. Calvo, F. A., Bentley, K. P. and Baker, R. G. *(1960). Acta Met.,* **8,** *898.*
65. Savage, W. *F.,* Lundin, C. D. and Hrubec, R. J. *(1968). Welding J., 47, 420s.*
66. Woods, *R.* A. and Milner, D. R. *(1971). Welding J.,* 50, *164s.*
67. Erokhin, A. A. and Silin, L. L. *(1960). Welding Production,* **7,** *4.*
68. Matveev, *Y. M. (1968). Welding Production,* **15,** *30.*
69. Brown, D. C., Crossley, F. A., Kudy, J. F. and Schwartzbert, H. *(1962). Welding J.,* **41,** *241.*
70. Capchenko, M. *N. (1970). Automatic Welding,* **23,** *36.*
71. Alov, A. A. and Bobrov, G. V. *(1959). Welding Production, 6,* 1.
72. Movchan, *B.* A. and Kushnirenko, B. N. *(1960). Automatic Welding,* **13,** *89.*
73. Garland, *J.* G. *(1972).* Ph.D. Thesis, University of Cambridge.

CHAPTER **7**

Segregation

Segregation results from the various ways in which the solute elements can become redistributed within the solidified structure. The different types of segregation are usually classified as ***micro-***

TABLE *7.1*

TYPES OF SEGREGATION

Microsegregation (short range)	*Macrosegregation (long range)*
Cellular	(a) Occurring prior to solidification
Dendritic	gravity
Grain-boundary	Ludwig–Soret
	(b) Occurring during solidification
	normal
	inverse
	freckle
	banding

segregation or ***macrosegregation.*** Microsegregation is a short-range phenomenon and extends over distances of the order of the grain size or less. In the case of cellular or dendritic segregation, the compositional differences may be confined to distances of a few microns. When the compositional differences show long-range variation, for instance between the outside and inside of an ingot, this is considered as macrosegregation. It is normally considered to occur over distances of greater than a few grain diameters. The different types of segregation are classified in Table 7.1. We will first consider microsegregation and then macrosegregation.

Some aspects of the different segregation phenomena were considered in Chapter 4. For completeness, some repetition is necessary.

To a large extent the compositional variations that occur adjacent to the solid–liquid interface during solidification determine the nature and extent of segregation. For macrosegregation the longer range flow of unsolidified liquid is of great importance. Both these aspects will be examined.

Finally, some consideration will be given to the segregation patterns of a very characteristic type that appear in cast ingots.

7.1 MICROSEGREGATION

7.1.1 Cellular segregation

As discussed in Section 4.5, a cellular substructure (see Fig. 4.17) develops in single-phase alloys during the initial stages of growth

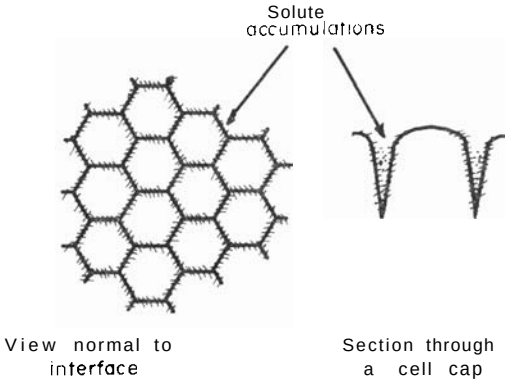

Fig. 7.1 *Schematic representation of solute distribution during cellular* **solidification.**

with low degrees of constitutional supercooling. As the interface advances, the liquid adjacent to the interface is richer in solute for values of k_0 (the distribution coefficient) less than 1 and is depleted in solute for $k_0 > 1$. This was illustrated in Figs. 4.7 and 4.8. Once the rounded cell projection is stabilised, solute will be rejected ($k_0 < 1$) from the sides of the projection as well as from the top. Since the projection rejects solute laterally, an accumulation of solute will occur in the cell boundaries. The most severe segregation will be expected at the junction points (nodes) in the hexagonal array. The situation is then as shown in Fig. 7.1. For $k_0 > 1$, the cell boundary regions are depleted of solute. The variation in solute concentration from the cell centre to the cell boundaries is known as 'cellular segregation'. It extends over distances of the order of the cell size, ***i.e.*** approximately 5×10^{-3} cm.

Cellular segregation has been studied qualitatively by a number of workers[1-6] and the segregation behaviour described above has been confirmed. Quantitative studies[3,5] utilising combined metallography and microprobe analysis showed that the solute concentrations at cell boundary nodes could be up to two orders of magnitude greater than the bulk average concentration. Nevertheless, because of the short range of the compositional variations, homogenisation can be carried out without difficulty. To some extent diffusion during cooling of the solid will reduce the degree of cellular segregation. For a cell size of $\sim 5 \times 10^{-3}$ cm, and assuming the solid state diffusion coefficient to be $\sim 10^{-8}$ cm^2 sec^{-1}, annealing times of the order of an hour should be sufficient to eliminate cellular segregation.

There is no acceptable theory for quantifying cellular segregation and it has been pointed out[2] that considerable difficulties must be overcome before such a theory can be proposed. Recently, a model has been proposed[7] for the solute distribution during solidification with a two-dimensional elongated cell structure (see Fig. 4.19c), which was found to be in good agreement with experimental data.

7.1.2 Dendritic segregation

The microsegregation that results from solute redistribution during dendritic solidification leads to *coring*, i.e. a variation in the solute concentration between the centre and the outside of a dendrite arm (see Fig. 4.20). In extreme cases the accumulation of solute between the growing dendrite arms can lead to the formation of second phases in the interdendritic region in amounts significantly greater than those predicted from the equilibrium diagram.

Figure 7.2 shows the solute distributions expected in a solid bar frozen from the liquid under different conditions of solute mixing in the liquid. The thickening of a dendrite arm can be considered, in the simplest sense, as the progressive unidirectional solidification of an assembly of miniature bars. The solute variation from centre to outside of the dendrite arm should then follow one of the profiles shown in Fig. 7.2, depending on the mixing conditions in the liquid. Evidence has been given that diffusion-limited solute mixing is observed in some cases[8] while more complete mixing occurs in others.[9-11] It is most probable that conditions vary widely and that these two cases are limits which can be operable at different stages of the solidification process.

Figure 7.3 shows the complex nature of the concentration profiles in a columnar dendrite as determined by electron probe microanalysis. These clearly reflect the anisotropic morphology of the dendrite growth. The profiles agree with earlier results obtained using autoradiography[12,13] and with subsequent studies[14,15] using a

combination of techniques. Microsegregation is more severe across and between primary dendrite arms than secondary dendrite arms. The relative severity of segregation (the ratio of maximum to minimum solute content) is greatest at low alloy contents, even though there is no fundamental difference in the mode of solidification. Both columnar and equiaxed dendrites exhibit essentially the same microsegregation features.[9]

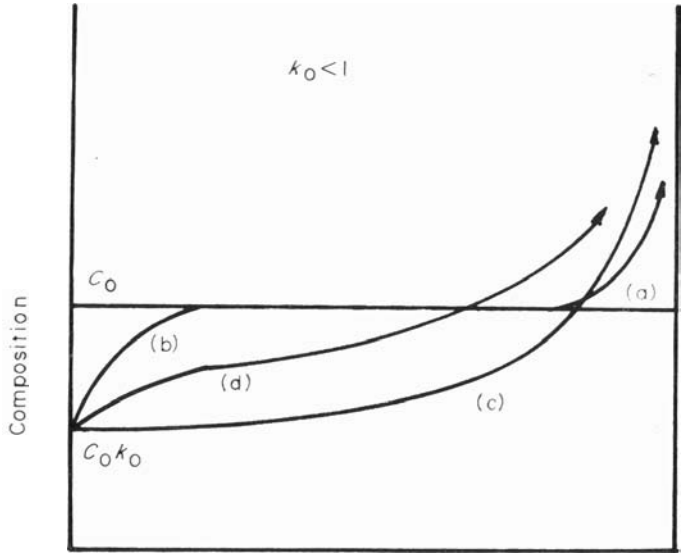

Fig. 7.2 Solute distributions in a solid bar frozen from liquid of initial concentration, C_0, for (a) equilibrium freezing; (b) solute mixing in the liquid by diffusion only; (c) complete solute mixing in the liquid: (d) partial solute mixing in the liquid. ($k_0 < 1$).

The dendrite arm spacing defines the range of dendritic microsegregation. Measurements of the dendrite arm spacing as a function of the solidification conditions'[6–18] have been rationalised'[1] to show that it is the 'local solidification time' which has the important influence. The local solidification time is defined[11] as the time at a given location in a casting or ingot between initiation and completion (or near completion) of solidification. It is inversely proportional to the average cooling rate at that location. Furthermore, the dendrite arm spacing is not simply determined by the initial growth behaviour, but subsequent coarsening effects, wherein small dendrite arms disappear and large dendrite arms grow larger, are important.[19]

This leads to the dendrite arm spacing varying inversely with the cooling rate to a power of between one-third and one-half.

The greater the dendrite arm spacing the more difficult is homogenisation by subsequent heat treatment. For a given alloy heat treated at a fixed temperature, the homogenisation time is proportional to the square of the dendrite arm spacing. For coarse dendrite

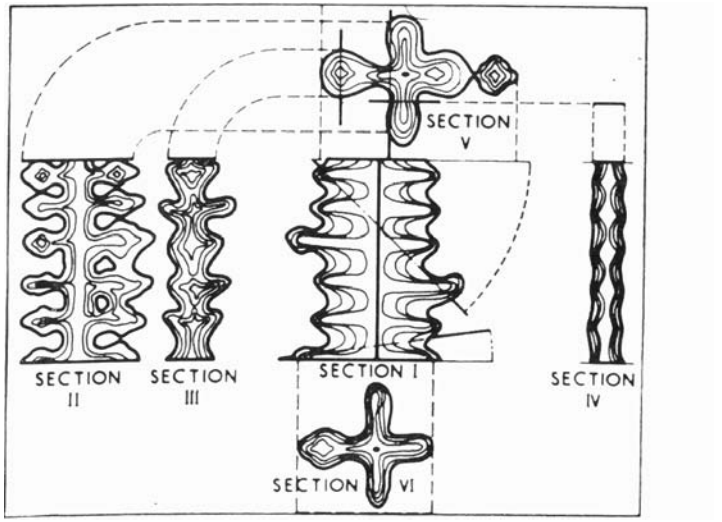

Fig. 7.3 Isoconcentration surfaces in a columnar dendrite grown in a low-alloy steel melt (Kattamis and Flemings[9]).

arm spacings ($\sim 10^{-2}$ cm) in steels, heat treatment of ~300 hours at 1200°C is needed (in the absence of simultaneous working) to produce any appreciable reduction in dendritic microsegregation. Simultaneous working improves the position only marginally. Refining the dendrite arm spacing by increasing the cooling rate can therefore have extremely beneficial effects.

Complete elimination of dendritic microsegregation leads to enhanced mechanical properties.[20–22] This is particularly difficult if second-phase particles are formed.[22] For instance, Turkdogan and Grange[23] observed second-phase sulphide inclusions to form in the solute-rich interdendritic regions in steel towards the last stage of freezing. These inclusions were extremely stable, inhibited grain refinement and together with the solute microsegregation were considered to be responsible for subsequent banding of the wrought steel. The importance of dendritic microsegregation on the occurrence of banding or fibering had been previously discussed by

Flemings.[24] The control of homogenisation behaviour through the control of dendrite arm spacing is undoubtedly going to become increasingly important.

7.1.3 Grain-boundary segregation

Grain-boundary segregation during solidification arises from two sources. First, if the grain boundary lies parallel to the growth direction, surface energy requirements give rise to a grain-boundary groove (see Fig. 7.4 and also Fig. 3.2a), where the boundary meets

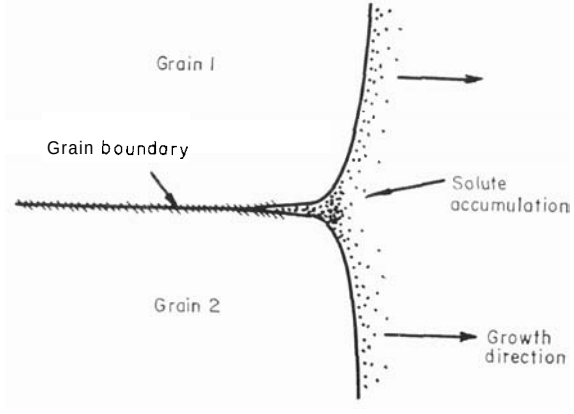

Fig. 7.4 Schematic representation of a section through a grain-boundary groove.

the interface. The groove is typically about 10^{-3} cm deep.[25,26] In the presence of constitutional supercooling, conditions are energetically favourable[27] for significant segregation to the grain-boundary groove. Certainly the experimental evidence shows that solute segregation to this type of boundary is marked for growth with a cellular interface.[3-5] When dendritic growth occurs, the situation is more complex and movements of liquid in the interdendritic spaces have a predominant effect. This is discussed in Section 7.2.

The second type of grain-boundary segregation results from the impingement of two interfaces moving with a growth component normal to each other (Fig. 7.5). For growth of macroscopically planar boundaries (cells may exist without affecting the situation) in a solidifying alloy there are solute pile-ups ($k_0 < 1$) which converge to produce a region of extremely high solute concentration. The impingement boundary receives, in effect, two terminal solute transients (see Fig. 7.2). This type of segregation should properly be considered as a form of macrosegregation.

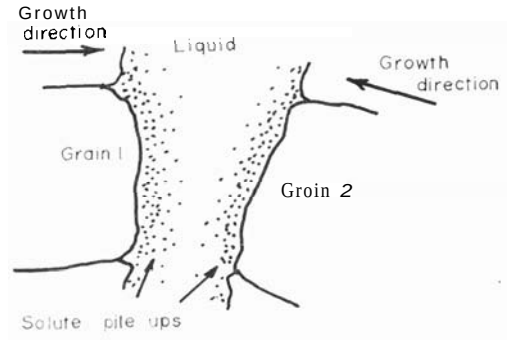

Fig. 7.5 *Formation of a grain boundary by impingement (schematic).*

7.2 MACROSEGREGATION

Long-range segregation can result either from changes that occur in the liquid before the solidification front has proceeded very far or as the result of fluid motion in the mushy zone behind the solidification front.

7.2.1 Gravity segregation

Gravity segregation normally occurs during the early stages of solidification, before, or just after, the initial growth nuclei have formed. It is the result of density differences which lead to differential movements within the liquid. In the simplest case, if liquid alloys are made up from atomic species of very different densities, ***e.g.*** copper (density 8.24 gm cm^{-3})–lead (density 10.04 gm cm^{-3}) alloys, it is commonly observed that the liquid becomes richer at the top in the lower density species, being correspondingly depleted at the bottom, and vice versa. **A** very goodexample of this type of behaviour was given by Dismukes and Ekstrom,[28] who found that during the zone levelling of germanium–silicon alloys the germanium content was several percent greater at the bottom of a horizontal ingot than at the top (liquid germanium is significantly more dense than liquid silicon). The position is particularly bad if the liquid phase shows a miscibility gap (see, for instance, Fig. 5.15) when layering can be produced by density differences.

Gravity segregation in polyphase systems is of even greater importance. If free dendrites form, their density relative to that of the unsolidified liquid will primarily determine the way in which they move. This can best be illustrated by considering the case of the tin-base bearing metals containing copper and antimony. During

the solidification of these alloys two primary intermetallic phases are formed, cuboids of SbSn (density less than the liquid) and needles of Cu_6Sn_5 (density greater than the liquid). In isolation, the SbSn cuboids will float to the surface while, correspondingly, the Cu_6Sn_5 needles will sink.[29] Together they form an entangled network and remain unsegregated. This form of behaviour has been widely reported in bearing alloys.[30,31]

In a similar way, since there is usually a contraction in volume on solidification, free primary dendrites tend to sink and this can give rise to segregation effects (*see* Section 7.3).

The sink rate is controlled (in the absence of convection) by a form of Stokes equation which states that, for a spherical body of radius r in a liquid of viscosity η, the sink velocity is given by

$$V = \frac{2gr^2(\rho - \sigma)}{9\eta}$$

where p and a are the densities of the solid and liquid respectively. The sink velocities are not expected to be high and there is some evidence[33] that thermal convective stirring (*see* Cole and Winegard[32]) can overcome significant density differences. Clearly, the existence of pronounced free or forced convective stirring will cause unpredictable distributions of freely floating phases.

7.2.2 The Ludwig–Soret effect

This is a very minor, but nonetheless interesting, form of behaviour wherein apparently homogeneous liquid of uniform composition held in a temperature gradient becomes non-uniform in composition.[34] For example, with lead–tin, copper–tin and zinc–tin alloys held in a temperature gradient it was found[31] that the tin always migrated to the higher temperature end. Quite large concentration differences could be produced in this way, *e.g.* for a **36%** lead in tin alloy the excess lead content at the cooler end was 5·28%. Again convection must cause a significant divergence from ideal behaviour.

7.2.3 Normal segregation

This type of segregation is usually associated with the movement of a planar or almost planar interface through the liquid and is considered in terms of the solute distributions parallel to the growth direction. Average concentrations are used to describe normal segregation and microsegregation effects are ignored. The solute distributions for $k_0 < 1$ are expected to conform broadly to one or other of the types shown in Fig. **7.2** and this has been confirmed experimentally.[13,36]

Figure **7.6** shows normal segregation in tin–silver alloy bars

solidified at various rates. It should be noted that this form of solute distribution is only expected if the interface has not degenerated to a very complex dendritic form, thus only at *low* overall solute concentrations. Then an overall solute distribution in a columnar ingot

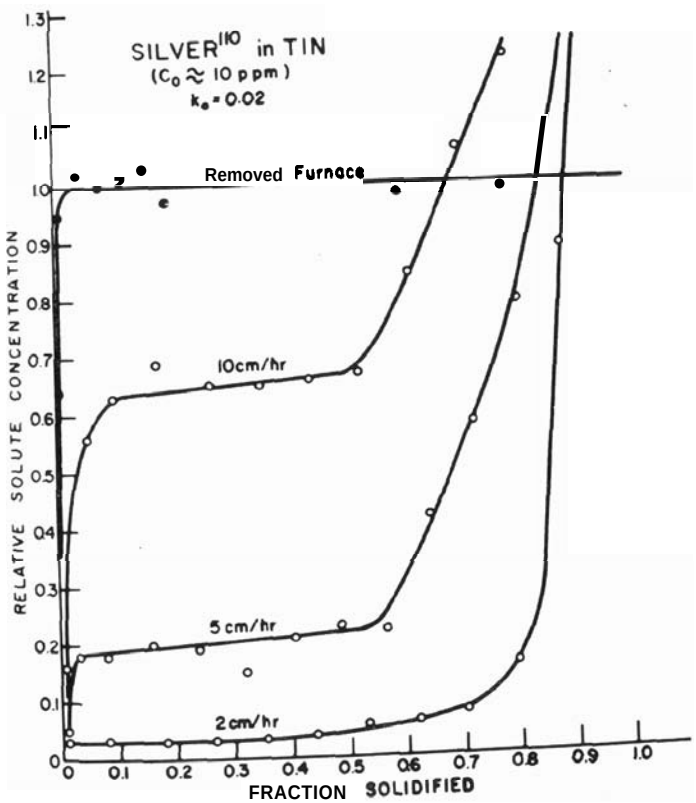

Fig. 7.6 The relative solute concentration of silver in tin plotted as a function of the fraction solidified for a rod progressively solidified from one end at the rates indicated (Weinberg[13]).

might be as shown in Fig. **7.7.** The relationship between the predicted solute distribution and the distributions of Fig. **7.2** is obvious.

At high solute concentrations a well-developed dendrite structure occurs (*see* Section 4.5) and under these conditions fluid flow between the dendrites becomes dominant. Normal segregation is no longer expected.

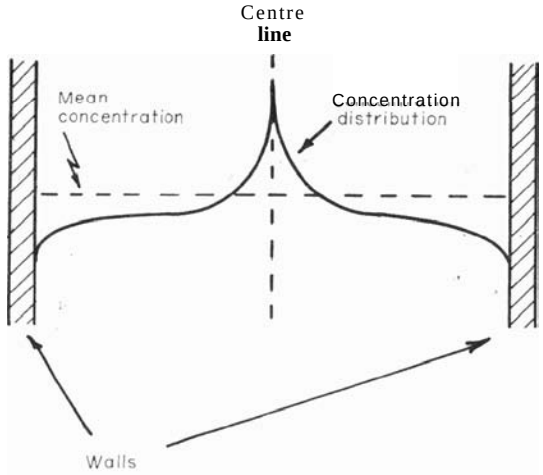

Fig. 7.7 ***Normal*** *segregation in a columnar ingot solidified with an almost planar interface (schematic).*

7.2.4 Inverse segregation

If we consider the solidification of an ingot of an alloy with $k_0 < 1$, as outlined above, we would expect the last liquid to solidify to be solute rich. If, however, there is pronounced dendritic growth, solute concentrations build up between the dendrites and there is fluid flow in the interdendritic spaces to compensate for the volume changes accompanying solidification. For most metals there is a contraction on solidification and thus the flow takes place in a direction opposite to the growth direction. As a result, solute-rich liquid is fed down the channels between the dendrites to give abnormally high solute concentrations at the outer regions of the ingot. The condition where the solute distribution is opposite to that expected for normal segregation is known as *inverse* segregation.

The existence of a network of interdendritic channels has been clearly demonstrated[37–39] and the way in which the last low melting point liquid to solidify ($k_0 < 1$) flows is evident by the ease with which tin *sweat* and *phosphide sweat* can occur. In these extreme cases of inverse segregation the interdendritic liquid actually bursts through the surface of the cast metal to form exudations (*see* Fig. 7.8). It has been shown by Youdelis[40] that this is mainly a result of loss of good thermal contact between the mould wall and the cast metal.

Following the complete qualitative description of inverse segregation by Adams,[41] a number of workers[42–44] have presented theories that account quantitatively for the solute flow and show how the

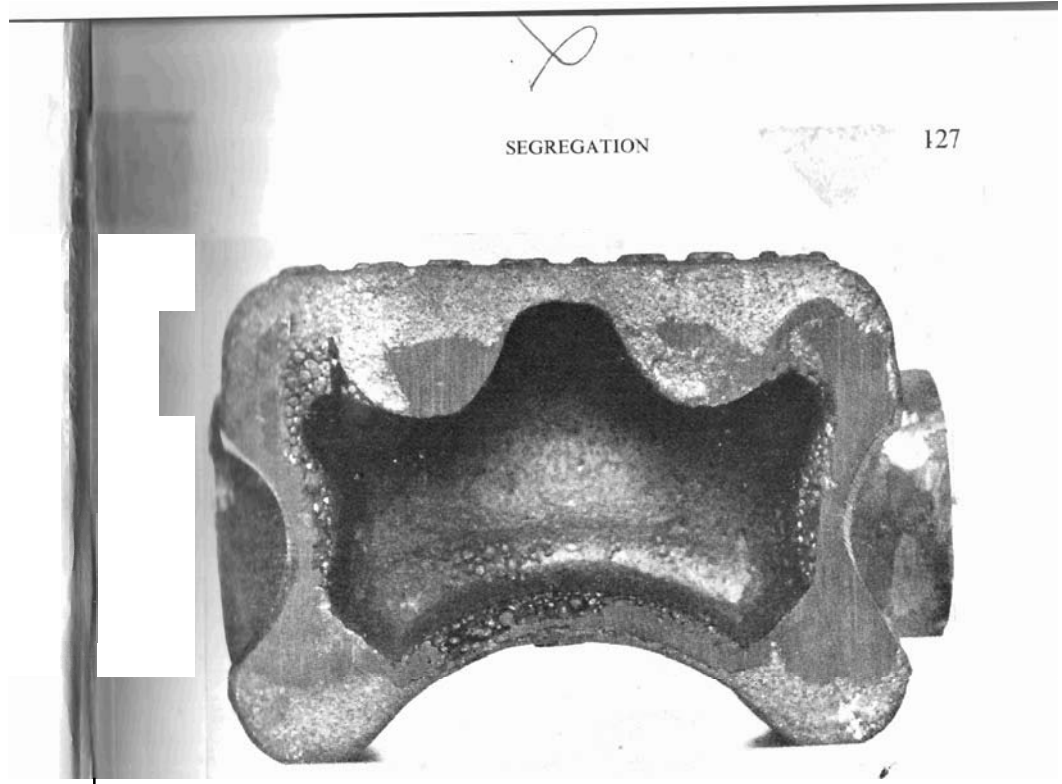

Fig. 7.8 ***Phosphide eutectic sweat appearing as rounded exudations on the surface of a grey-iron casting.***

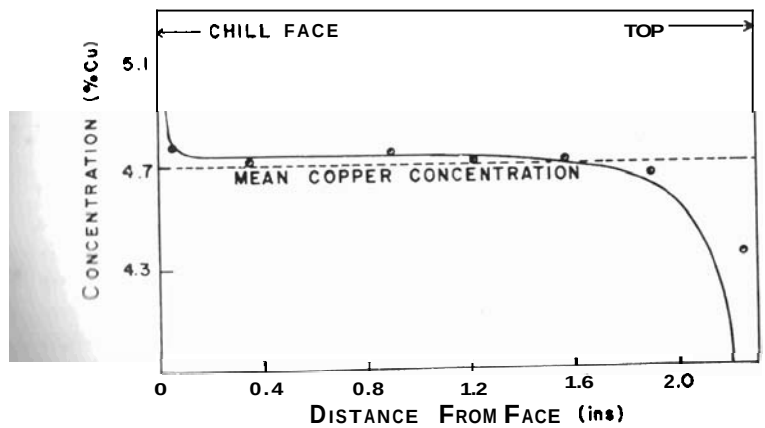

Fig *7.9 (a)*

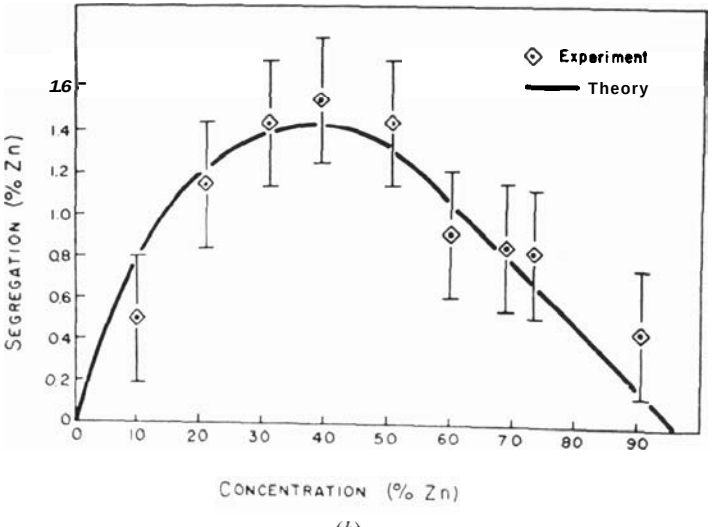

(*b*)

Fig. 7.9 ***(a)*** *Experimental and theoretical concentration distributions* **for** *inverse* ***segregation in an aluminium–4.7*** *%* ***copper*** *alloy* **(Kirkaldy** *and Youdelis*[43]**).** ***(b)*** ***Experimental*** *and theoretical determinations* **of** *the* ***maximum inverse segregation*** **in** *aluminium–zinc ingots* **(Youdelis** *and Cotton*[44]**).**

unexpected solute distribution could be established. These theories were able to predict both the maximum segregation and the concentration distribution, as shown in Fig. 7.9.

Two other observations which support the general acceptance that the mechanism of inverse segregation is one of volume contraction on solidification followed by interdendritic flow of enriched residual liquid to the contracted regions are,

(i) no inverse segregation occurs in alloys which expand on freezing,[41] and

(ii) the amount of inverse segregation increases with time as solidification progresses,[45] and thus as the amount of contraction-stimulated flow increases.

7.2.5 **Freckle**

Freckles are chains of equiaxed grains which appear on the surface of some cast metals (see Fig. 7.10) and are regions enriched in all but the inversely segregated solute.[46] It has been shown that these are the result of fast flowing liquid jets in the partly solidified zone which are driven by density inversions produced by thermal and

solute transport effects.[47,48] The importance of these thermosolutal channelling effects has only recently been recognised and it seems that they also play an important part in influencing the overall segregation patterns in ingot structures.[48,49] This is discussed further in the next section.

Fig. ***7.10*** ***A freckle line on the surface of a nickel-base superalloy casting*** *(Giamei and Kear*[46]**).**

7.2.6 **Banding**

This form of segregation appears as a change in composition and structure in a band parallel to the solid–liquid interface.[50,51] The band is produced by growth fluctuations which are the result of thermal or mechanical disturbances. For instance, in the presence of a solute layer adjacent to the interface, if there is a growth rate fluctuation then changes in the solute boundary layer give rise to compositional variations in the solid **(see** Section 4.3.4, especially Fig. 4.14). At the same time changes in the interface structure can occur, such as a coarsening of the cellular-dendritic structure. Banding is very common in fusion welds because of the periodicity of the heat input[52] and is apparent as both substructural bands and surface rippling. Figure 7.11 shows structural banding in an aluminium alloy fusion weld.

A special form of banding segregation, known as 'microbanding' because of the scale, appears in centrifugal castings[53] (see Section 8.9) and has been attributed to perturbations arising from both pouring variations and mechanical vibrations.

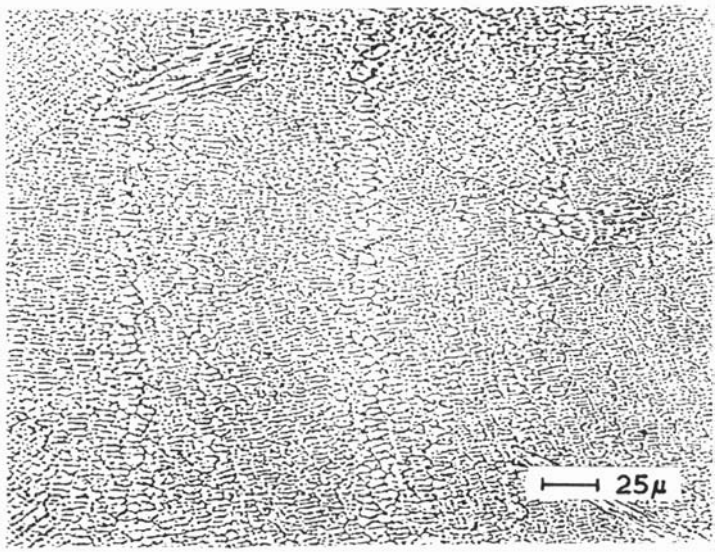

Fig. 7.11 *Structural banding in an aluminium-alloy fusion weld (Garland and Davies[52]).*

7.3 SEGREGATION PATTERNS IN INGOTS

Superimposed on the cast structures of ingots discussed in the previous chapter are macroscopic segregation patterns which for ingots show both horizontal and vertical variations. The most characteristic of these is the segregation pattern of sulphur in cast killed-steel ingots. This is shown in Fig. 7.12. In this illustration the regions of positive (concentration greater than average) and negative (concentration less than average) segregation are as indicated.

The region of high purity material at the bottom of the ingot has been attributed to the gravity segregation of primary dendrites formed by dendrite remelting in the columnar zone[54] or by nucleation on inclusions,[55,56] and also to constrained convective fluid flow.[48] Model studies[54,57] lend considerable support to the gravity segregation mechanism.

The regions of positive segregation have two characteristic forms. The outer bands are referred to as A-segregates and are arranged as rope-like stringers of segregation located on the surface of cones with their bases at the base of the ingot. They occur predominantly in a zone near and almost parallel to the end of the columnar zone.

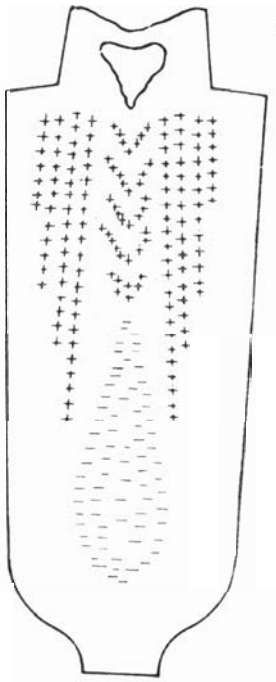

Fig. 7.12 ***Typical segregation pattern for sulphur in a killed-steel ingot.***

Inner bands of V-segregates also occur which consist of fairly uniform segregate distributions on the surfaces of cones with their points downwards. These occur at the ingot centre in the equiaxed zone.

The A-segregates seem to be the result of channelled flow in the interdendritic regions of the columnar zone,[48,49] whereas the V-segregates, which appear late in the solidification process, are apparently a consequence of the general settling of crystals in the equiaxed zone.[49,58] In either event, it is clear that interdendritic flow plays a most important part in determining the overall macrosegregation patterns in solidifying ingots.[48,59–61]

REFERENCES

1. Rutter, J. W. and Chalmers, B. (1953). *Can. J. Phys., 31,* 15.
2. Kramer, J. J., Bolling, G. F. and Tiller, W. A. (1963). *Trans. Met. Soc. AIME, 227,* 374.
3. Biloni, H. and Bolling, G. F. (1963). *Trans. Met. Soc. AIME, 227,* 1351.
4. Biloni, H., Bolling, G. F. and Cole, G. S. (1965). *Trans. Met. Soc. AIME, 233,* 251.
5. Biloni, H., Bolling, G. F. and Domian, H. A. (1965). *Trans. Met. Soc. AIME, 233,* 1926.
6. Biloni, H., Bolling, G. F. and Cole, G. S. (1966). *Trans. Met. Soc. AIME, 236,930.*
7. Donaghey, L. F. and Tiller, W. A. (1968). *The Solidification of Metals,* ISI Publication 110, p. 87.
8. Doherty, R. D. and Melford, D. A. (1966). *J. Iron Steel Inst., 204,* 1131.
9. Kattamis, T. Z. and Flemings, M. C. (1965). *Trans. Met. Soc. AIME, 233,* 992.
10. Brody, H. D. and Flemings, M. C. (1966). *Trans. Met. Soc. AIME, 236,* 615.
11. Bowers, T. F., Brody, H. D. and Flemings, M. C. (1966). *Trans. Met. Soc. AIME, 236,* 624.
12. Crussard, C., Kohn, A., de Beaulieu, C. and Philibert, J. (1959). *Rev. Met., 56,* 395.
13. Weinberg, F. (1961). *Trans. Met. Soc. AIME, 221,* 844.
14. Weinberg, F. and Buhr, R. K. (1968). *The Solidification of Metals,* ISI Publication 110, p. 295.
15. Thresh, H., Bergeron, M., Weinberg, F. and Buhr, R. K. (1968). *Trans. Met. Soc. AIME, 242,* 853.
16. Michael, A. B. and Bever, M. B. (1954). *Tram. AIME, 200,* 47.
17. Brown, P. A. and Adams, C. M. (1961). *Trans. AFS, 69,* 879.
18. Horwath, J. A. and Mondolfo, C. F. (1962). *Acta Met., 10,* 1037.
19. Kattamis, T. Z., Coughlin, J. C. and Flemings, M. C. (1967). *Trans. Met. Soc. AIME, 239,* 1504.
20. Jatczak, C. F., Girardi, D. J. and Rowland, E. S. (1956). *Trans. ASM, 48,* 279.
21. Quigley, F. C. and Ahearn, P. J. (1964). *Trans. AFS, 72,* 813.
22. Antes, H., Lipson, S. and Rosenthal, H. (1967). *Trans. Met. Soc. AIME, 239,* 1634.
23. Turkdogan, E. T. and Grange, R. A. (1970). *J. Iron Steel Inst.,* **208,** 482.
24. Flemings, M. C. (1968). *The Solidification of Metals,* IS1 Publication 110, p. 277.
25. Bolling, G. F. and Tiller, W. A. (1960). *J. Appl. Phys., 31,* 1345.
26. Bolling, G. F. and Tiller, W. A. (1960). *J. Appl. Phys., 31,* 2040.
27. Tiller, W. A. (1962). *J. Appl. Phys., 33,* 3106.
28. Dismukes, J. P. and Ekstrom, L. (1965). *Trans. Met. Soc. AIME,* **233,** 672.

29. Ellwood, E. C. (1960). *Tin and its Alloys* (Ed. by E. S. Hedges), Arnold, London, p. 248.
30. Watson, J. H. (1932). *J. Inst. Metals, 29,* 347.
31. Harding, J. V. and Pell-Wallpole, W. T. (1948–49). *J. Inst. Metals,* **75,** 115.
32. Cole, G. S. and Winegard, W. C. (1964–65). *J. Inst. Metals, 93,* 153.
33. Davies, G. J. (1964–65). *J. Inst. Metals, 93,* 197.
34. Jost, W. (1960). *Diffusion in Solids, Liquids, Gases,* Academic Press, New York, p. 521.
35. Ballay, M. (1928). *Rev. Metal, 25,* 427 and 509.
36. Weinberg, F. and McLaren, E. H. (1963). *Trans. Met, Soc. AIME, 227,* 112.
37. Williams, W. M. and Smith, C. S. (1952). *J. Metals, 5,* 9.
38. Emley, E. F. (1958). *British Foundryman, 51,* 501.
39. Nicholas, K. E. L. (1960). *BCIRA Journal, 8,* 29.
40. Youdelis, W. V. (1968). *The Solidification of Metals,* ISI Publication 110, p. 112.
41. Adams, D. E. (1948). *J. Inst. Metals, 75,* 809.
42. Scheil, E. (1947). *Metallforsschung, 2,* 69.
43. Kirkaldy, J. S. and Youdelis, W. V. (1958). *Trans. Met. Soc. AIME, 212,* 833.
44. Youdelis, W. V. and Cotton, D. R. (1960). *Trans. Met. Soc. AIME, 218,* 628.
45. Fricke, W. G. (1969). *Trans. Met. Soc. AIME, 245,* 1126.
40. Giamei, A. F. and Kear, B. H. (1970). *Met. Trans.,* **1,** 2185.
47. Copley, S. M., Giamei, A. F., Johnson, S. M. and Hornbecker, M. F. (1970). *Met. Trans., 1,* 2193.
48. Mehrabian, R., Keane, M. and Flemings, M. C. (1970). *Met. Trans.,* 1, 1209.
40. McDonald, R. J. and Hunt, J. D. (1969). *Trans. Met. Soc. AIME, 245,* 1893.
50. Winegard, W. C., Majka, S., Thall, B. M. and Chalmers, B. (1957). *Can. J. Chem., 29,* 320.
51. Stewart, M. T., Thomas, R., Wauchope, K., Winegard, W. C. and Chalmers, B. (1951). *Phys. Rev., 83,* 657.
52. Garland, J. G. and Davies, G. J. (1970). *Metal Constr. and Brit. Weld. J., 2,* 171.
53. Howson, H. O. (1968). *The Solidification of Metals,* ISI Publication 110, p. 334.
54. Jackson, K. A., Hunt, J. D., Uhlmann, D. R. and Seward, T. P. III (1966). *Trans. Met. Soc. AIME, 236,* 149.
55. Salmon-Cox, P. H. and Charles, J. A. (1963). *J. Iron Steel Inst., 201,* 863.
56. Salmon-Cox, P. H. and Charles, J. A. (1965). *J. Iron Steel Inst.,* **203,** 493.
57. Ohno, A. (1968). *The Solidification of Metals,* ISI Publication 110, p. 349.
58. Kohn, A. (1968). *The Solidification of Metals,* ISI Publication 110, p. 156.

59. Flemings, M. C. and Nereo, G. E. (1967). *Trans. Met.* Soc. ***AIME,*** 239, 1449.
60. Flemings, M. C., Mehrabian, R. and Nereo, G. E. (1968). *Trans.* Met. ***Soc. AIME, 242, 41.***
61. Flemings, M. C. and Nereo, G. E. (1968). *Trans.* Mef. Soc. ***AIME,*** **242, 50.**

CHAPTER 8

Casting Processes and Procedures

In the preceding chapters we have been mainly concerned with fundamental aspects of the solidification process. In this and the following chapter some consideration will be given to the practical side of casting. Within the present framework it is not possible to give exhaustive details of all casting technology. Instead, the basic steps involved in making castings will be discussed and the principal casting processes will be described. Finally, some comparisons will be made between the different processes and an assessment of the relative advantages and disadvantages will be given.

For full technological details of all aspects of casting, and in particular for information on the casting of specific metals and alloys, standard reference works[1-3] should be consulted.

8.1 BASIC ASPECTS AND TERMINOLOGY

The basis of all casting processes is the feeding of molten metal into a cavity of the required shape in a mould, followed by cooling to produce a solid object. The various processes differ principally in the way in which the mould is formed. In some cases, *e.g.* sand moulding, a mould is made up for each cast and subsequently broken up to remove the casting. In other cases, ***e.g.*** die casting, a permanent mould is used repeatedly for a succession of casts and the casting is removed after each cast without damage to the mould. In both cases provision must be made for the molten metal to flow into all parts of the system and to remain there until solidification is complete.

The basic steps and the terminology can best be illustrated by considering the casting of a simple object in a sand mould. First, a *pattern* of the object to be cast is needed. This can be manufactured from wood or metal or other materials; the mould is made by packing sand around the pattern, the whole being contained in a moulding box (or flask). Usually the mould is in two parts, an upper part

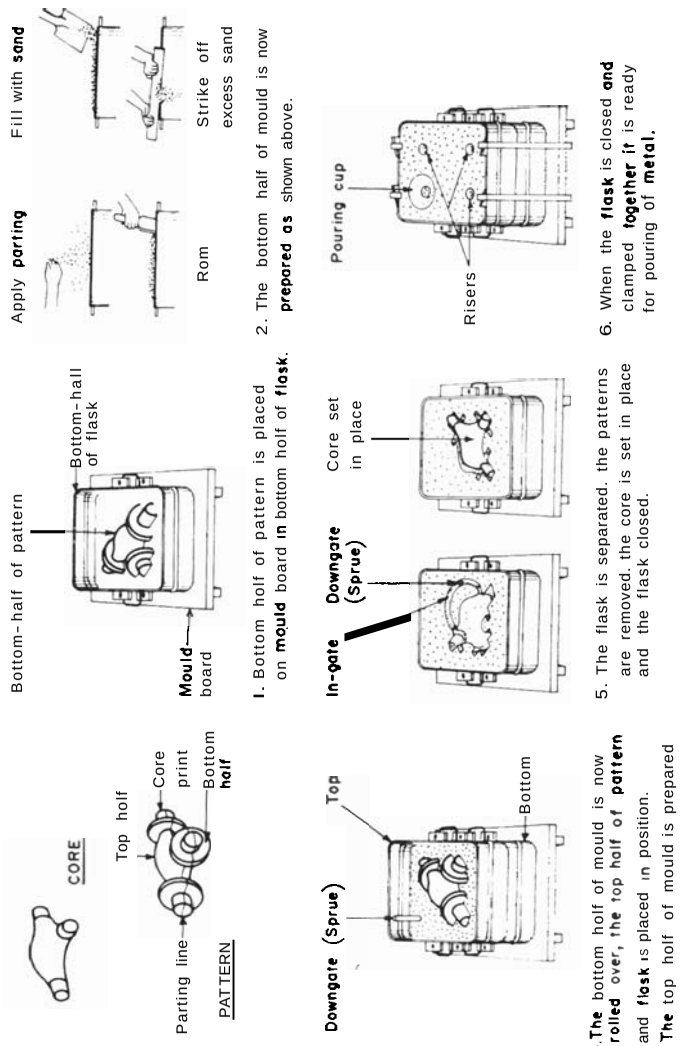

Fig. 8.1 *Steps in making a simple mould by hand (from Ref. 2, p. 64).*

...the *cope* and a lower part known as the *drag*. During the ...ing process the surface of the pattern is treated to facilitate ...emoval after moulding. If the casting is to be hollow, separate ...oldings (known as *cores*) are made and placed inside the cavity left by the patter... The space between the mould-cavity and the ...re then becomes the casting.

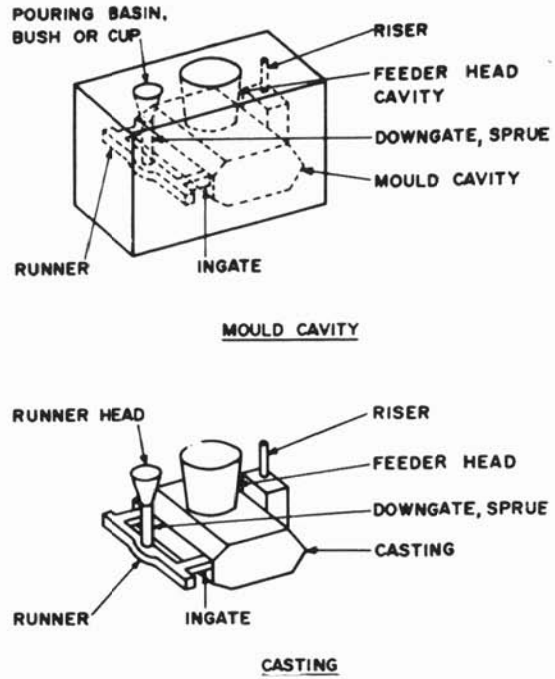

Fig. 8.2 *The terminology of gating systems (from Ref.* 2, *p.* 70).

Provision is made for the feeding of the casting by forming a *gating* system in the mould. At the same time an enlarged opening (a *pouring cup*) is made to enable easy pouring, and channels are cut to allow metal to flow out of the mould cavity after filling it, thus maintaining a metallostatic head during solidification; these channels are known as *risers*.

The metal is run from the pouring cup down a *downgate* (or sprue), through *runners* (or crossgates) and into the mould cavity through *ingates*. These steps are illustrated in Fig. 8.1, which shows a simple moulding process. Figure 8.2 shows diagrammatically the terminology of the gating system.

After solidification is complete the rough casting is removed from the mould, any cores are knocked out and the feeders and risers are cut off. Loose sand, etc. is removed and the casting is then ready for any machining operations. The preparation of the rough casting for machining is known as ***fettling.***

For the permanent mould processes, metal moulds are used; these are formed complete with the requisite running and rising system. The difficulties involved in the production of metal moulds are largely responsible for the high costs of the permanent mould processes.

During the solidification process, control of the direction of movement of the solid–liquid growth front can be achieved by the control of heat flow in the mould. Solidification can be initiated by the use of ***chills;*** these are metal inserts which conduct heat away more rapidly than the mould material. On the other hand, by using insulating materials or exothermic compounds, heat flow conditions can be controlled to delay freezing in a particular part of the mould.

8.2 SAND CASTING

The elements of the sand casting process have already been described ***(see*** Fig. 8.1).

8.2.1 Moulding sands

The major constituent of modern moulding sands is silica. This is obtained from naturally occurring sand deposits which are usually relatively uniform in size and rounded in shape (Fig. 8.3a), or by crushing rock or sandstone which gives angular particles of disproportionate sizes (Fig. 8.3b). The physical properties of the sands are more important than their chemical properties. Uniform grain distributions of rounded particles are preferred. Recent practice has involved the use of finer sand grades since these produce moulds with a high resistance to penetration or erosion by the molten metal.

The silica content is usually greater than 90%, with the remainder comprised of clay binders (montmorillonite or bentonite, kaolinite and illite) with about 2% moisture. In some cases additions are used to give the sand some special property. For instance, cellulose materials are frequently added in amounts of up to 2% as a buffer to improve collapsibility and thus to reduce the incidence of hot tearing ***(see*** Section 9.3).

For special applications, ***e.g.*** in the production of heavy steel castings, non-siliceous sands such as zircon or olivine are employed.

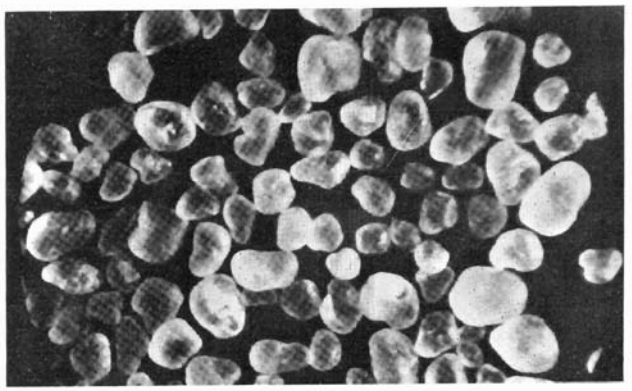

(*a*)

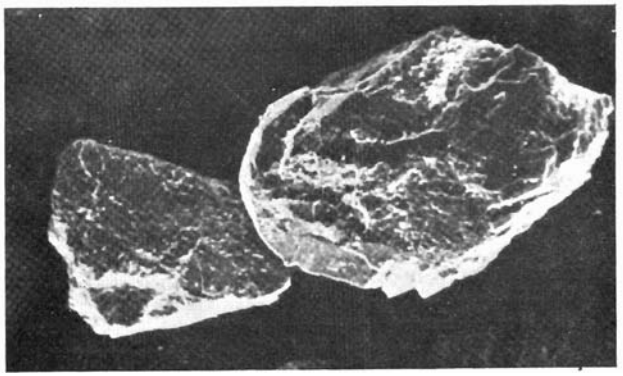

(*b*)

Fig. **8.3** ***(a) Naturally occurring silica sand (x 16). (b) Sand obtained from crushed rock (x 200) (from Ref.*** 2, *p.* **36).**

8.2.2 Core sands

Core sands are basically the same as moulding sands except that oil and cereal are added to give a stronger bond. Typically, a core sand will contain ~1% linseed oil and ~2% starch. The clay content must be kept as low as possible since it interferes with the bonding. reaction. After moulding, the cores are baked at temperatures of the order of 200°C to produce bonding.

8.2.3 Moulding procedures

The simplest and oldest method of forming the mould is ramming by hand. This is still common practice with large moulds or when

sample castings are being produced. For larger scale production, automatic or semi-automatic procedures are adopted. In these, a split pattern mounted on a pattern plate is used so that the cope and the drag can be moulded independently. The moulding machines in general use produce compaction by repeated jolting (Fig. 8.4a) or by a combination of jolting and squeezing (Fig. 8.4b); the former

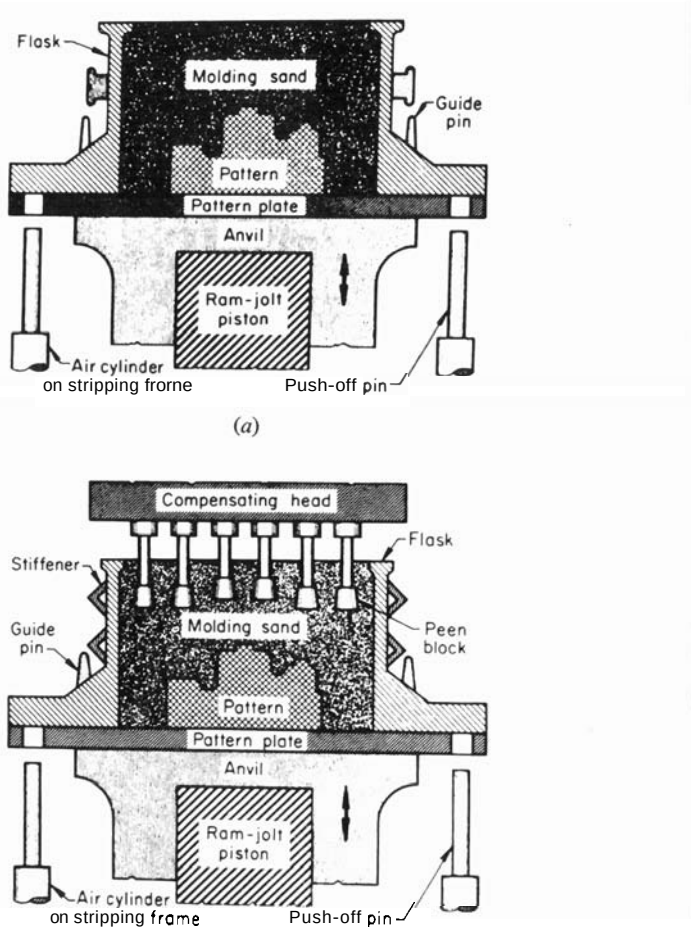

Fig. 8.4 The essential features of: (a) a jolt-type moulding machine. The jolting action is produced by lifting the anvil and allowing it to fall back against a stop; (b) a jolt–squeeze moulding machine. After compaction by jolting, pressure is applied to the peen blocks (from Ref. 1, p. 164).

produces a less uniform and less dense mould than the latter. Jolt–squeeze machines are necessary for making large moulds and when high rates of production are required.

8.2.4 Advantages and disadvantages

The basic sand casting process has many advantages. It has great flexibility as a process, is simple, economical and can be used to produce castings of a wide range of sizes from a few ounces up to several tons. There is little wastage of material since the sand can be reconditioned for reuse.

On the other hand, sand casting cannot be employed for thin sections or intricate shapes, and the dimensional accuracy and surface finish is usually poor. In many cases, and particularly with very large castings, erosion of the mould face by the molten metal causes serious difficulties. To overcome these the majority of developments in sand casting have been aimed at increasing mould and core rigidity.

8.3 DEVELOPMENTS IN SAND CASTING

8.3.1 Cement–sand moulding

In this process[4] Portland cement (approximately 10%) is mixed with sand with an increased moisture content (up to about 5%). This mixture is used to form the surfaces in contact with the pattern or pattern plate and is backed by previously used sand. After moulding, the boxes are left for one to two days to harden. This produces a mould face with very good mechanical strength.

8.3.2 The CO_2/sodium silicate process

This involves the mixing of clay-free siliceous sand with up to 5% sodium silicate, and the use of the mixture to form moulds and cores which are hardened by carbon dioxide (CO_2) gas.[5–7] The bonding process is not a simple chemical reaction involving the formation of sodium carbonate and silica gel, but is a combination of three processes:

(i) the precipitation of silica gel;

(ii) an alteration of the Na_2O to SiO_2 ratio in the silicate, producing setting; and

(iii) the drying of the unaltered silicate. The loss of water causes a large change in viscosity and a consequent hardening.

The complex interaction between these different processes makes the hardening reaction dependent on the gassing time and the silicate composition. Care must be taken to avoid over reaction, which leads to a deterioration in strength.

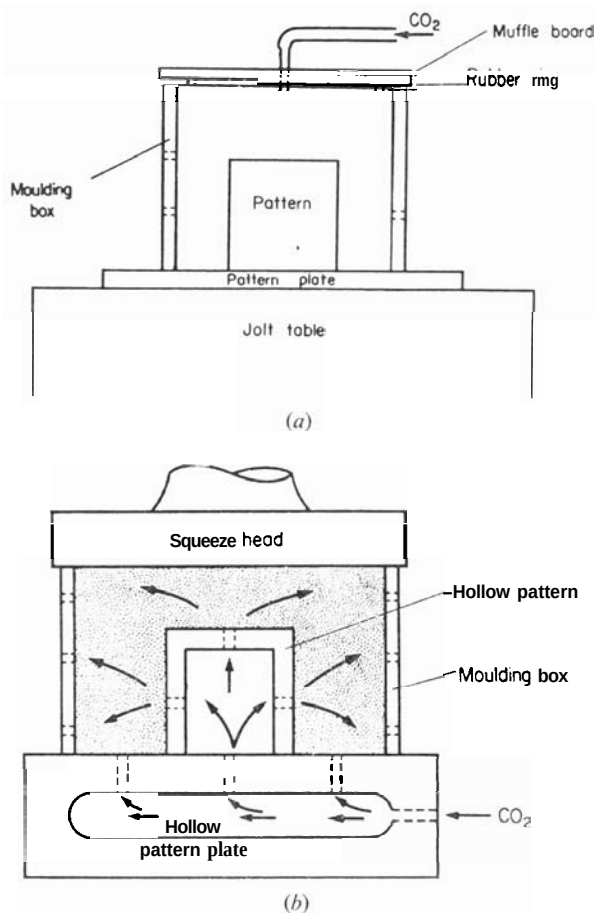

Fig. 8.5 ***(a) Carbon*** *dioxide gassing* ***of a*** *mould using a sealed muffle* ***board.*** *(b)* ***Carbon dioxide*** *gassing* ***of*** *a mould through a hollow pattern plate (Sarkar[7]).*

Several techniques have been developed for gassing and although it is possible to gas simple moulds after stripping, most procedures are aimed at gassing *in-situ* immediately after moulding and before stripping. This strengthens the mould, thus reducing the probability of damage during stripping. After stripping, the hardened mould

can be conveyed directly to the pouring station. Figures 8.5(a) and (b) show two of the many methods for CO, gassing. The first simply exposes the back of the mould to the gas and depends for its effectiveness on the permeation of the gas through the compacted sand. The second uses a hollow pattern and pattern plate and thus guarantees effective hardening of the mould face.

R.3.3 Self-setting sand processes

In these processes a reactive binder and some form of catalyst are mixed with the sand prior to moulding. The hardening reaction takes place without further treatment, the mould developing strength over a period of time. One consequence of this is that the mixing and moulding processes must be carried out within a limited period before any hardening occurs. This requirement has led to the development of continuous mixers which can feed directly to the moulding box. Several different combinations of binder and catalyst have been developed, for instance,

(i) the self-setting silicate process,' in which hardeners such as ferro-silicon or dicalcium silicate are incorporated into the sand–silicate mix,

(ii) the furan-resin process,[9] in which polymerisation of the resin is catalysed with phosphoric or toluene sulphonic acid to give a strongly bonded sand,

(iii) cold-setting oil systems, in which the binder is a modified linseed oil with a metallic drying agent (cobalt naphthanate). An isocyanate hardener is added to this mixture; the hardener controls the setting time and bench life.

Each of these processes has had wide application in mould and core production as alternatives to the cement–sand and conventional carbon dioxide processes. Another alternative is the thermosetting resin process known as 'shell moulding'. Because of its importance it is properly considered in the next section.

8.4 SHELL MOULDING

In shell moulding, the moulding sand is coated with a synthetic resin binder (phenolformaldehyde, urea formaldehyde, alkyd or polyester resin) and brought into contact with a heated pattern plate; the resin then thermosets to give a strong, rigid shell, which is stripped from the plate and forms the basis for the shell mould. Two shells are normally clamped together to make the mould. The shells may be

made rigid enough to be self supporting or they may be supported by some form of backing in a mould box.

Figure 8.6 shows the essential steps in making a shell mould and Fig. 8.7 provides a typical example of such a mould. After an initial thermosetting period while in contact with the pattern plate, the

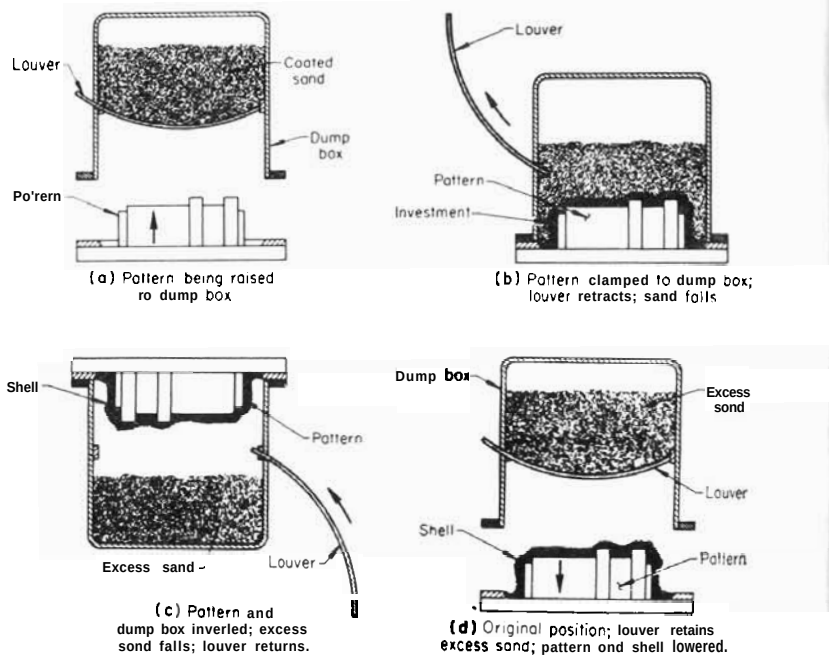

Fig. 8.6 Steps in the production of a shell mould using a louvre-type dump box (*from* ***Ref. 1, p.*** 188).

excess sand is removed as shown. A further hot curing treatment is often carried out before stripping; this ensures that the degree of setting is the same throughout the shell, thus minimising warping. This is particularly important if the shells are to be used unsupported since joint-to-joint contact is only effective if the surfaces are flat. Even then it is normal practice to glue the two halves of the shell mould together.

The shell moulding process readily lends itself to automation and produces castings with an extremely good surface finish and good detail definition. The economics of shell moulding vary considerably

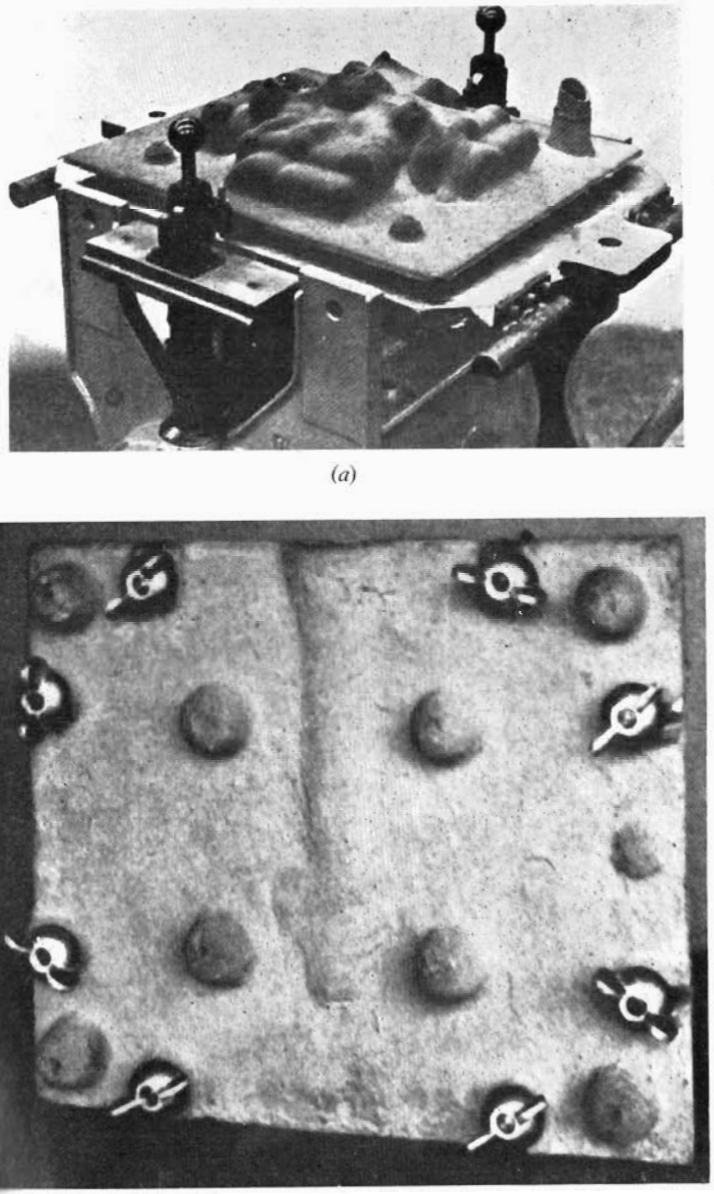

(*a*)

(*b*)

Fig. H.7 Shell moulding: ***(a) shell being stripped from the pattern plate on the*** *moulding machine;* ***(b) shells clamped together wady for casting*** (*Weaver*[9]).

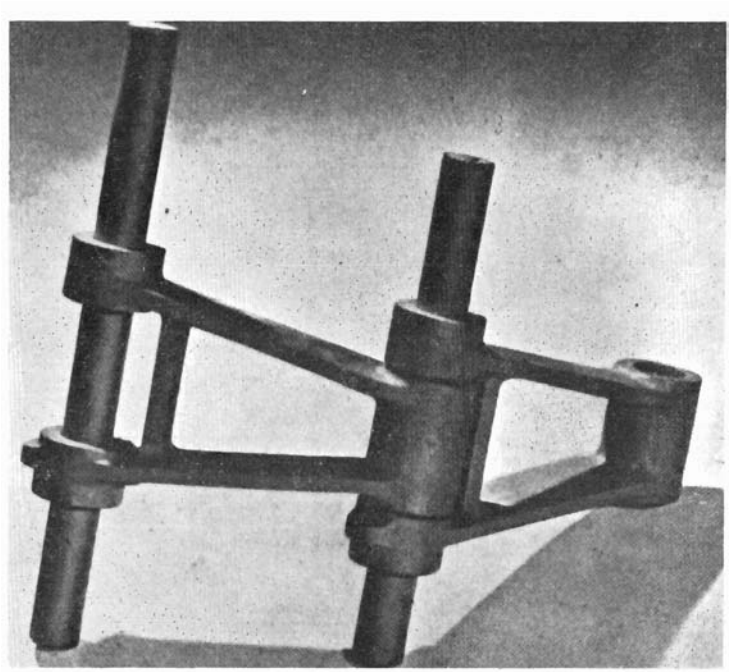

Fig. 8.8 *Heat-resisting steel links produced by casting in a shell mould* (*Osborn* et al.[10]).

with the type of casting being produced and finds its best application in medium-size batch production. Figure 8.8 shows a pair of furnace links cast in heat-resisting steel in a shell mould.

8.5 PLASTER CASTING

Plaster casting uses gypsum (calcium sulphate) slurries to form the mould. The mixture is cast onto the pattern plate in a mould flask or into a core box and allowed to set. It is then oven-heated to dry the plaster and remove both free and chemically combined water. This produces moulds and cores with very smooth surfaces and high dimensional accuracy. These are reflected in the quality of the castings produced by the process. The moulds have low heat capacity and therefore cooling rates are slow; this facilitates feeding but slows down production time. The overall lengthiness of the processing procedures makes plaster casting an expensive process, and thus

the teridency is only to use it when acceptable results cannot be obtained by simpler processes such as conventional sand casting.

8.6 INVESTMENT CASTING

The investment casting, or 'lost wax', process is a very ancient one which has become of increasing importance as the demand for complex close-tolerance products has increased. The initial step

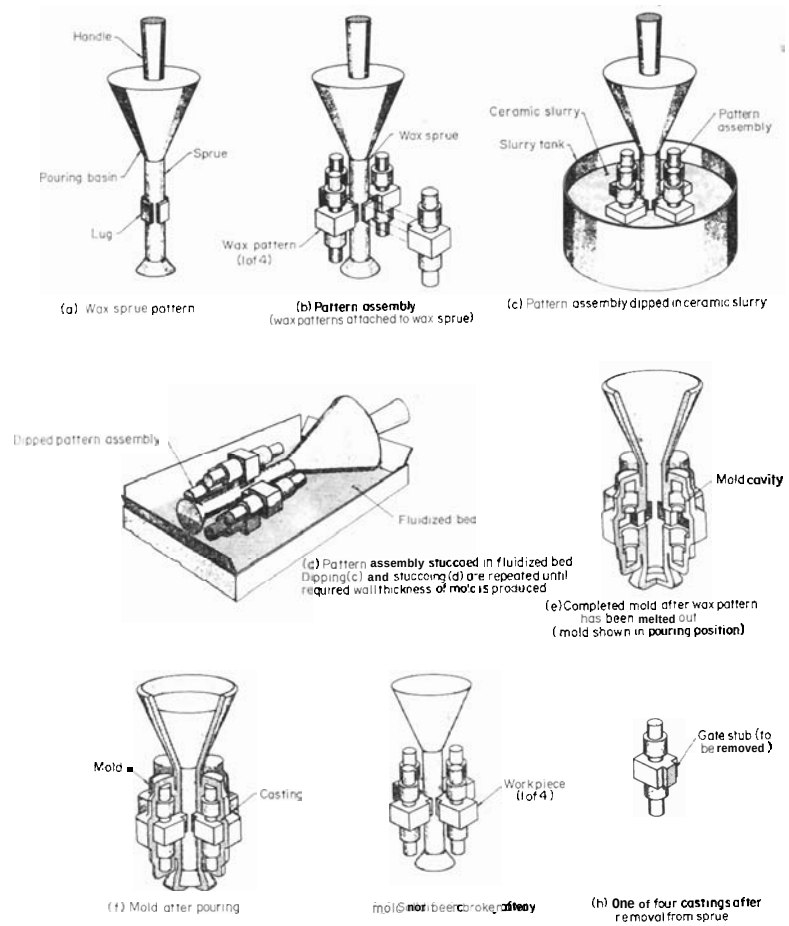

Fig. 8.9 *Steps in the production of a ceramic shell investment casting* (*from Ref.* 1, *p.* 238).

requires the production of an expendable pattern in wax or plastic; this is then coated (invested) in a suitable refractory coating, dried and then fired. During the firing process the refractory becomes strongly bonded and the wax investment is melted out. Plastic investments, usually polystyrene, are burned out without leaving a residue. The metal is then cast into the resulting hollow mould.

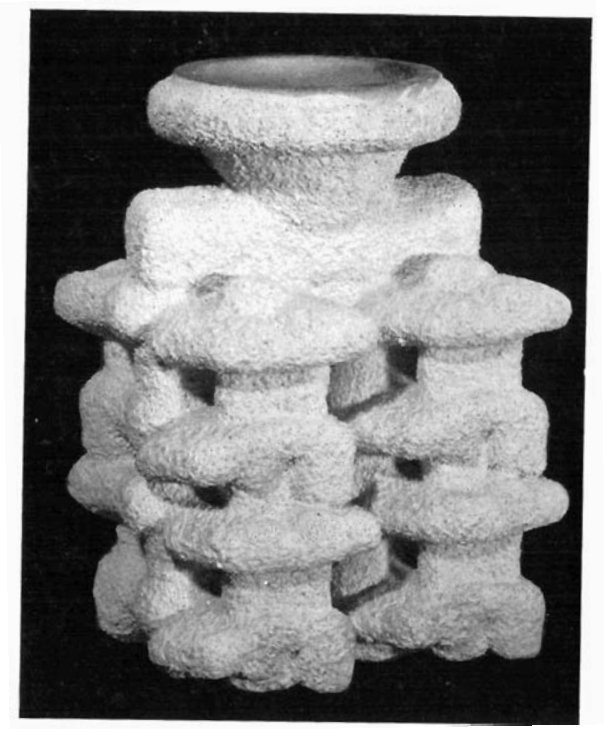

Fig. 8.10 *A typical ceramic shell investment casting mould.*

The pattern is made by pouring or injecting wax into a metal mould. In some cases a simple pattern may be produced in one step with an integral gating system, while in other cases complex patterns may be assembled from a number of separate components prepared individually. In the ceramic shell process, after the wax pattern is formed it is dip-coated with a primary slurry coat of very fine particles to give a smooth surface; it is then stuccoed with coarser refractory and dried. These steps are repeated until the required mould thickness is achieved. The primary and secondary dip-coats contain binders such as ethyl silicate, and the refractories are principally zircon, sillimanite

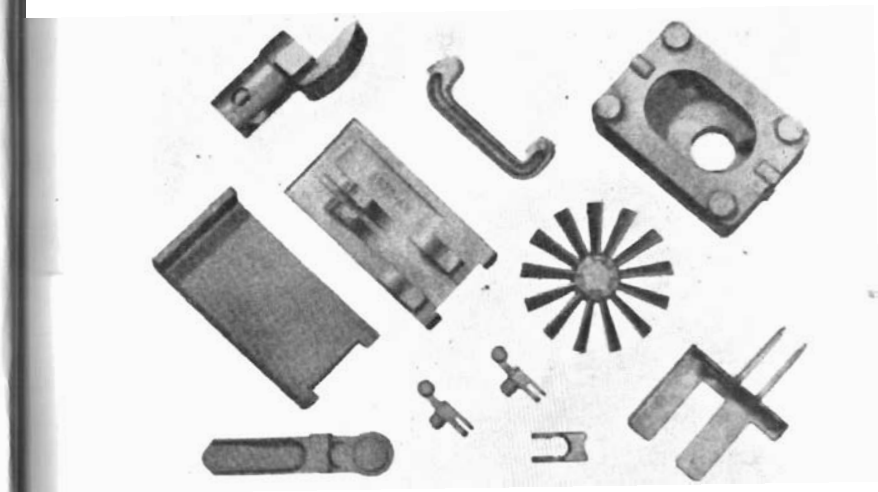

Fig. 8.11 ***Some investment-cast components*** *in martensitic stainless steel* (*Hocking*[11]).

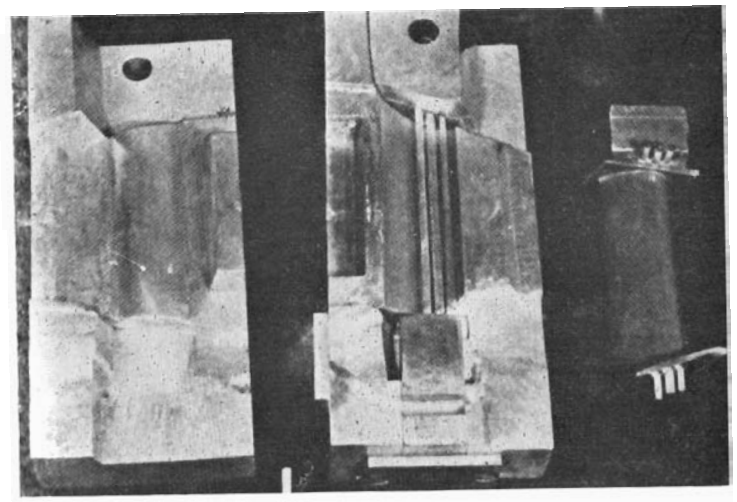

Fig. X.12 ***Silica-tube*** *method* ***of coreing a wax pattern*** *for* ***investment casting*** (*Tedds*[12]).

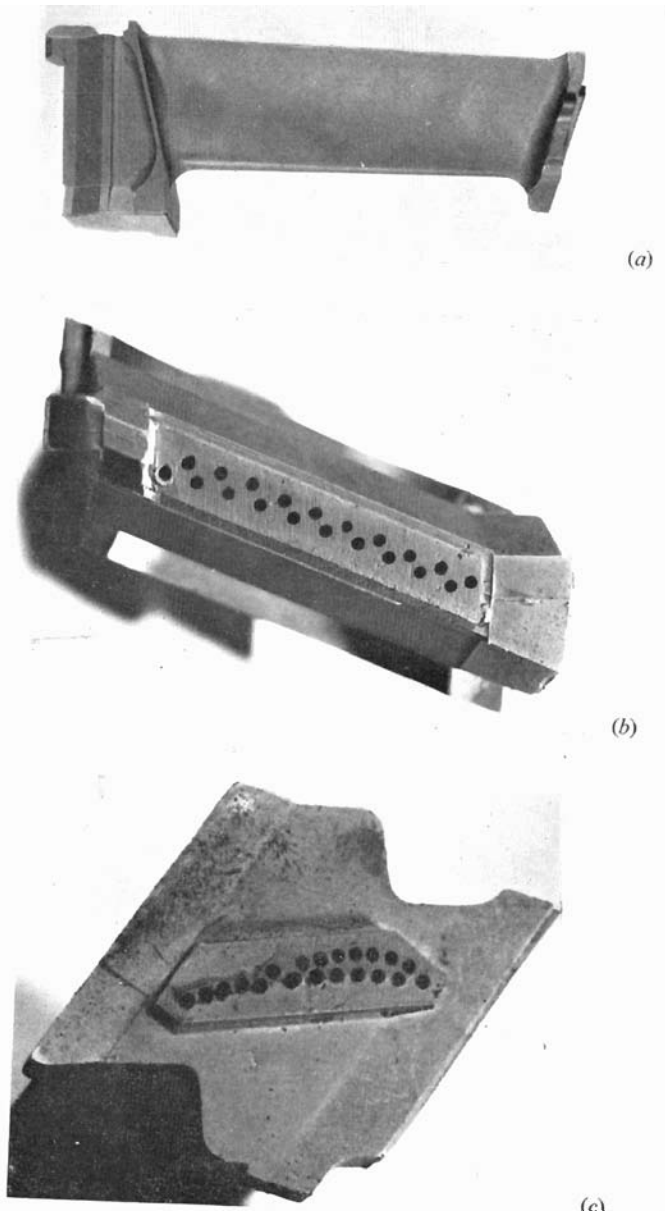

Fig. 8.13 *A turbine blade* **produced by** *investment* **casting: (a) finished blade; (b) cooling passage** *layout* **at root end; (c) cooling passage** *layout* **at** *tip end.*

and aluminosilicate. The stuccoing process is carried out by 'raining' or by immersion in a fluidised bed. It is common practice to use a combination of these ***i.e.*** raining for the initial coat and fluidising for subsequent coats. This is illustrated in Fig. 8.9, which also shows the subsequent steps in the process.

An alternative process, the 'block mould process', requires the pattern to be coated with the primary investment, to be placed in a moulding flask and to have the secondary investment poured around it to form a monolithic mould.

The ceramic shell process is widely employed for producing large castings in steel, nickel and other high melting point materials. The, block mould process is mainly used for light alloys and in the production of small and medium-size castings.

Figure 8.10 shows a ceramic shell ready for casting and typical products produced by investment casting are shown in Fig. 8.11.

It is of interest to note that modern practice frequently involves the use of soluble cores to produce complex, hollow, investment-cast objects. This was originally achieved by having complex die assemblies for forming the wax pattern or by making the wax pattern in parts and joining them together. Now, preformed cores, e.g. in water-soluble polyethylene glycol, are fitted into coreprints in the wax-injection die and surrounded by wax. When the wax is melted out the core is left in to be incorporated into the casting. Figure 8.12 shows an example of the production of a gas-turbine blade pattern with silica tubes as cores. After casting the silica is dissolved out (in hydrofluoric acid), leaving hollow passages for blade cooling. The ends of a modern blade with a complex array of cooling passages are shown in Fig. 8.13. The different layouts at either end are a consequence of the requirement that the cooling passages follow the twist in the blade profile. Silica tubes were used to shape the cooling passages and it is difficult to see how such a configuration could be produced without the use of the cored investment casting process.

8.7 PERMANENT MOULD CASTING (GRAVITY DIE CASTING)

In permanent mould casting (frequently referred to as 'gravity die casting') the parts of the mould (the cope and the drag) are made from metal. Where holes or recesses are required, loose metal cores are used, although in some cases it is necessary to employ sand or soluble cores. This is avoided if possible because the core material can get between the faces of the metal mould and hinder efficient working. The molten metal is poured into the mould in a conventional

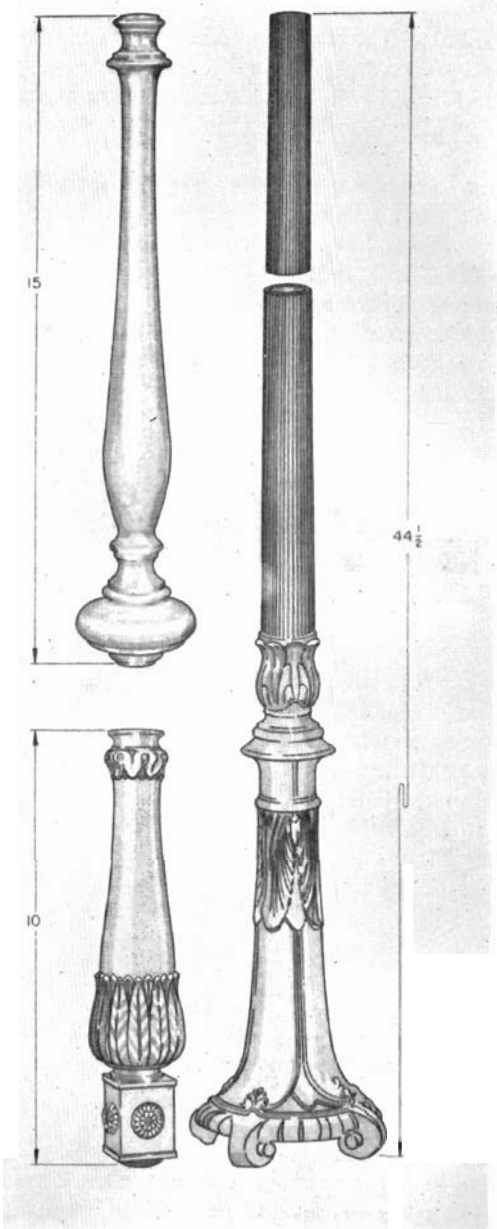

Fig. **8.14** *Lamp bases cast by slush casting. The* $44\frac{1}{2}$*-in high floor lamp column at the right is about the maximum size commercially producable by the slush casting process (from* ***Ref.*** *1, p.* **334).**

manner and allowed to fill the cavity under the influence of gravity. The process is particularly suitable for the high-volume production of small, *simple* castings without complex undercuts or intricate coring. Good surface finish and high definition of detail are achieved with permanent moulds.

8.7.1 Slush casting

This is a variation on the permanent mould process wherein hollow objects are produced without the use of cores. This is achieved by pouring the molten metal into the mould, allowing it to cool for a predetermined time (during which a solid skin is formed) and then inverting the mould to pour out the unsolidified liquid. The thickness of the skin is determined by the casting temperature and cooling time. The exterior surface finish of such a casting is good, but the inner surface is rough. Slush casting is not widely employed, although some cheap, simple objects, ***e.g.*** lamp bases (Fig. 8.14), are still produced by this technique.

8.8 PRESSURE DIE CASTING

Pressure die casting differs from permanent mould casting in that a positive pressure is maintained on the metal in the mould during solidification. Metal moulds are used and the liquid metal is usually forced into the mould under pressure. For high pressure work (using pressures of up to thousands of pounds per square inch) two processes are commonly used. In *hot-cllamber* die casting a reservoir of molten metal is maintained in a holding furnace which forms part

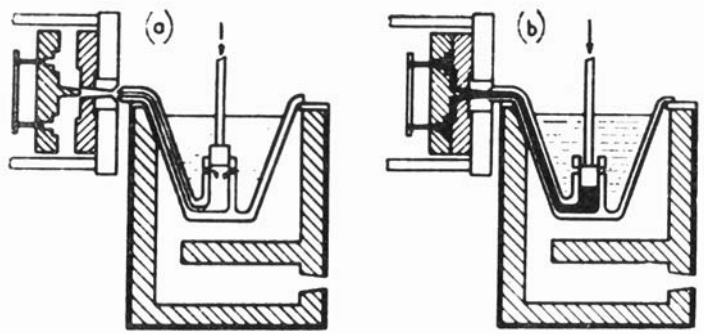

Fig. X.15 *A piston-operated hot-chamber die casting* ***machine*** *(goose neck machine): (a) mould open* ***prior*** *to metal injection; (b) piston operated to inject metal into the mould (Sharp*[13]*).*

of the machine. The pumping system is immersed in the molten metal and the pump forces it into the mould cavity (Fig. 8.15). Use of the hot-chamber process is restricted to the lower melting point metals, principally zinc-based alloys injected at temperatures of around 400°C.

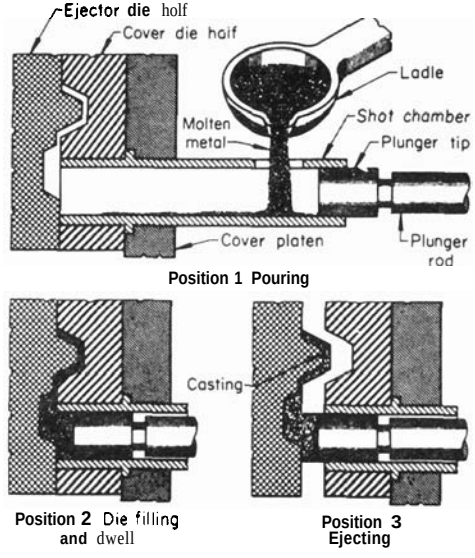

Fig. 8.16 *Operating cycle of a horizontal cold-chamber die casting machine (from Ref. 1, p. 286).*

For higher melting point alloys, ***e.g.*** aluminium-based alloys injected at temperatures above 500°C, ***cold-chamber*** die casting is employed. Here a transfer chamber adjacent to the mould is charged with molten metal, which is then forced into the die. Both vertical and horizontal machines are available. An example of the horizontal cold-chamber process is shown in Fig. 8.16.

Whereas hot-chamber machines use pressures of 300–4000 lb/in^{-2}, considerably higher pressures in the range 4000–15 000 lb in^{-2} are employed with cold-chamber machines.

Recently, a *low-pressure* die casting process using pressures of only a few pounds per square inch has been developed, primarily for use with aluminium alloys. This has an airtight furnace chamber with the mould mounted above it. Gas is admitted to the chamber and used to force the molten metal in a crucible up a feed tube into the mould cavity. This has the advantage of very fine control. It is, however, essentially a variant on gravity die casting.

The balance between the different processes is determined firstly by the material being cast. Hot-chamber die casting is used for the zinc alloys, cold-chamber and low-pressure die casting being employed for aluminium alloys and to some extent for magnesium and copper-base alloys. The larger and heavier the object to be cast the more the low-pressure process is favoured. Greater production requirements and more intricate sectional requirements tilt the balance in favour of the cold-chamber process. This latter process has the important advantage that the pressure can be maintained during solidification to produce high-density castings of very high precision. Examples from the wide range of products produced by die casting are shown in Fig. 8.17.

8.9 CENTRIFUGAL CASTING

Centrifugal casting involves the solidification of metal in a rotating mould. The majority of castings are produced in horizontal moulds

Fig *8.17 (a)*

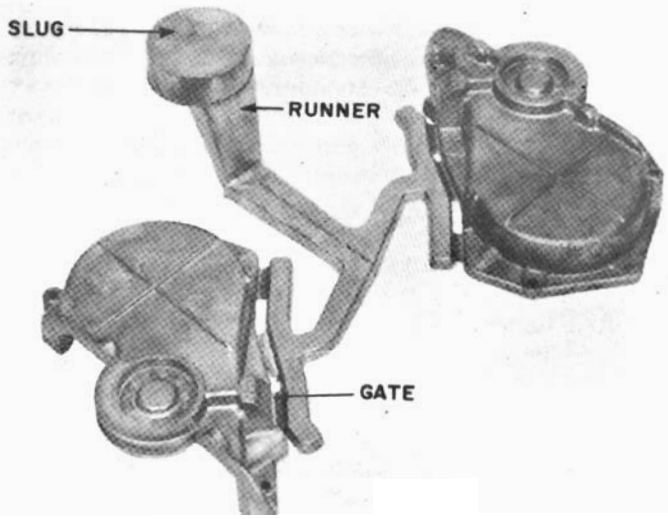

Fig 8.17 *(b)*

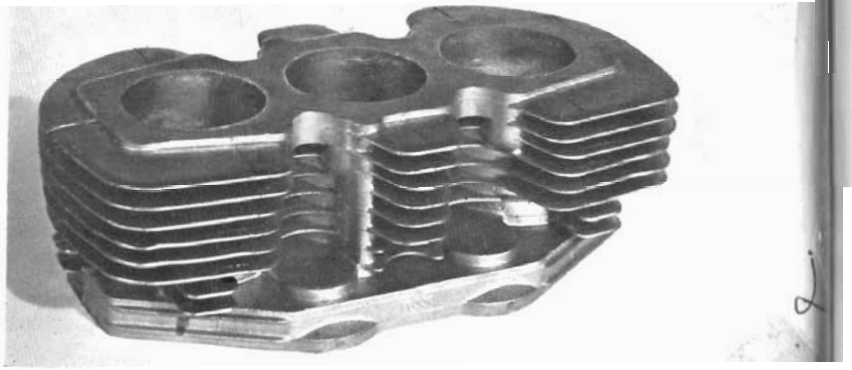

Fig 8.17 *(c)*

Fig. 8.17 *Typical die castings:* ***(a) hot-chamber zinc*** *alloy die castings (from Ref.* 2, *p.* 177); ***(b) cold-chamber aluminium alloy*** *die castings* ***of*** *an automobile part, shown with slug and* ***runner attached*** *(from Ref.* 2, *p.* 100); *(c) low-pressure aluminium alloy* ***casting of a cylinder*** *head (from Ref.* 2, *p.* 166).

rotated about their longitudinal axis. Molten metal is fed into the mould through a spout and flows to cover the inner surface of the mould. In the widely-used De Levaud process the pouring spout is traversed parallel to the axis of rotation and the thickness of the casting is determined by the rate of feeding. The metal mould, usually

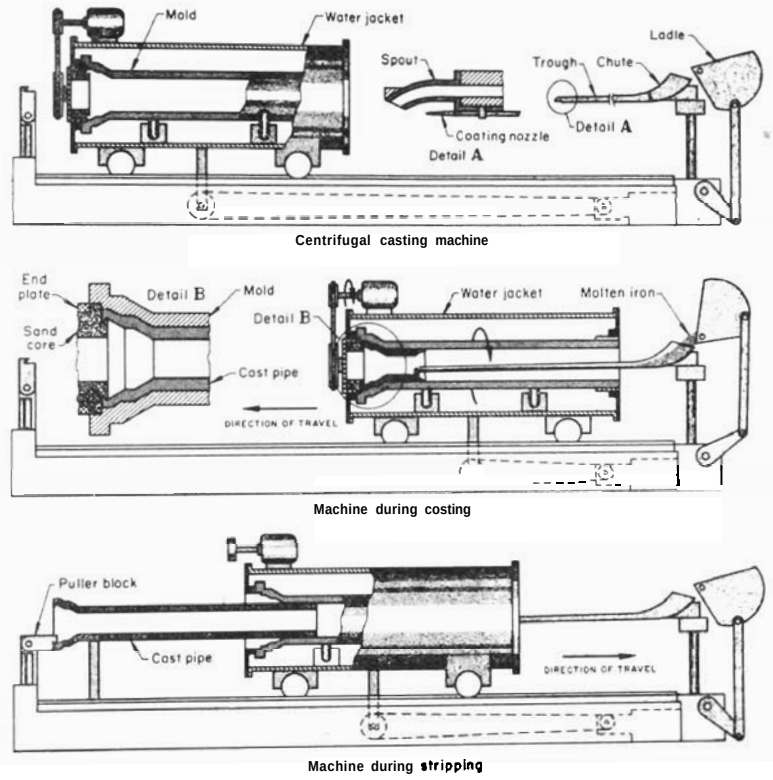

Fig.* 8.18** *Centrifugal casting* ***of an iron pipe *(from Ref.* 1, *p.* 267).

water cooled, is coated with a refractory mould dressing both to prolong life and to enable easy removal of the casting from the mould. The process is illustrated in Fig. 8.18, which shows the casting of a pipe. The inner surface of the pipe is unconstrained and is usually rough. However, this is not necessarily a disadvantage, particularly if some form of protective coating is to be applied later to the inner surface.

In some applications a conventional mould is used, and during or after pouring the mould is rotated about a vertical axis to promote

feeding. This is known as 'semi-centrifugal casting'. Centrifuged castings are produced when an assembly of small irregularly shaped castings is placed symmetrically in a cluster around a central sprue and the whole is rotated at relatively high speeds during casting. In both these cases the final shape of the cast product is determined by the shape of the mould cavity.

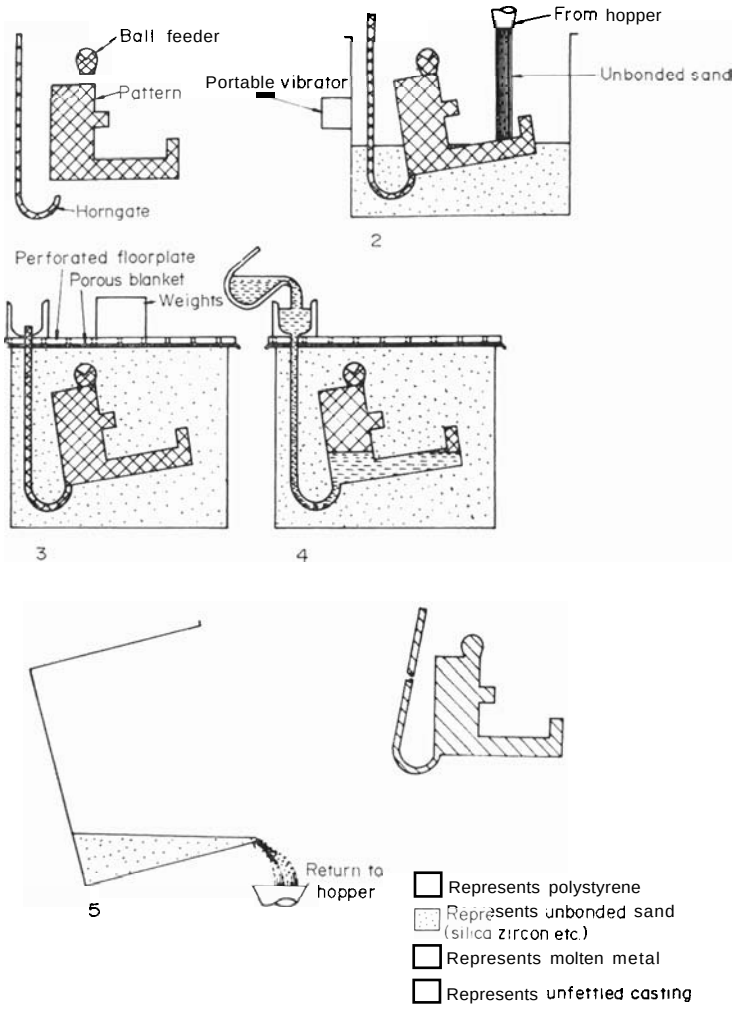

Fig. 8.19 Schematic diagram of the moulding and casting stages in the full-mould process (Butler[14]).

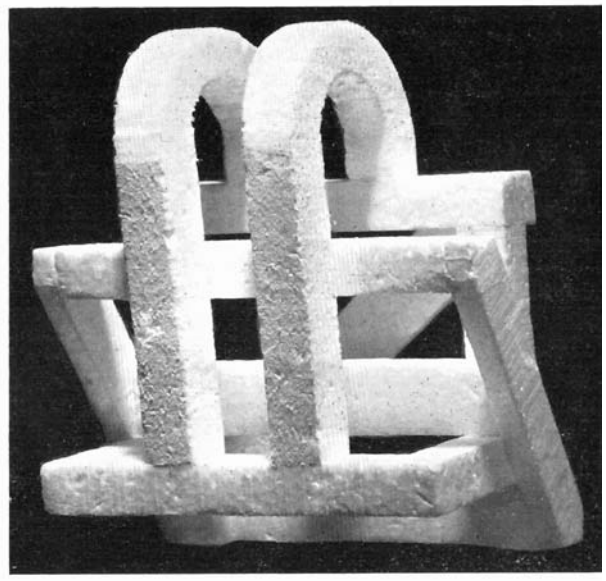

(*a*)

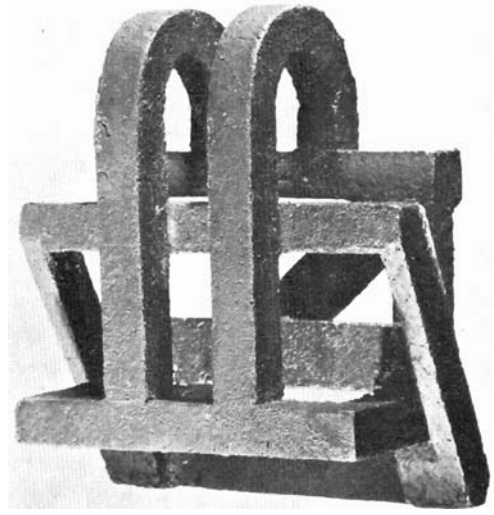

(*b*)

Fig. 8.20 ***A complex-shaped full-mould casting which would haae been extremely difficult to mould by conventional 'empty' mould methods: (a) polystyrene pattern; (b) finished grey cast iron casting (Butler[14]).***

8.10 FULL-MOULD CASTING

The full-mould, or cavityless, casting process is a recent development, the basic concept of which is very simple. The pattern is made from a suitable combustible or vaporisable material, usually expanded polystyrene, and the mould is formed around it. The pattern is not removed and the molten metal is poured into the full mould, progressively decomposing it as filling proceeds until the whole of the mould is filled with metal. The sequence is shown in Fig. 8.19. It is similar to the investment casting process in that the pattern is destroyed as part of the process. However, master moulds can be used to mass produce patterns (including cores, runners and risers) by conventional polystyrene-forming procedures. The full-mould process can be employed to produce very complex castings, such as that shown in Fig. 8.20.

8.11 CONTINUOUS CASTING

This is not a process used to produce a range of objects in the same way as the processes considered previously. Rather, it is a means of

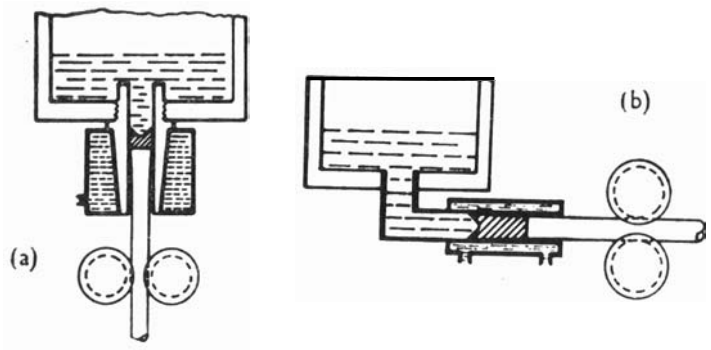

Fig. 8.21 Continuous casting with stationary moulds: (a) vertical; (b) horizontal (Morton[15]).

making a continuous cast strand for subsequent working. The majority of wrought metal begins by being cast as an ingot in a permanent mould; the ingot is then worked to the required shape. To overcome the need for extensive working in the earlier stages, continuous casting was devised as a means of producing a cast form nearer in size to that of the ingot after the initial working stages. This was achieved by casting the liquid metal from a tundish into a mould

without a base and drawing the cast strand out through the mould aperture. For the non-ferrous metals, both stationary and moving moulds have been used with the casting moving vertically or horizontally. Figure 8.21 shows the basic configurations for vertical and horizontal casting with a stationary mould. The use of moving wall moulds, ***e.g.*** as in the Hazelett machine for strip casting (Fig. 8.22),

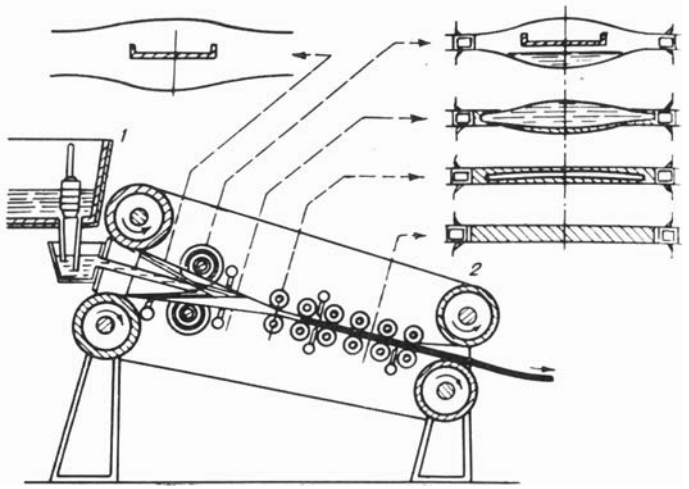

Fig. 8.22 The Hazelett process for continuous casting of strip: (1) machine; (2) cross sections.

has the advantage of eliminating friction between the casting and the mould. For high melting temperature metals, such as steels, reciprocating moulds are employed.[15] In all cases the control of both the cast structure and segregation is difficult.

8.12 EVALUATION OF THE DIFFERENT CASTING PROCEDURES

The comparison and evaluation of the different casting procedures described in the previous sections is important if the most economic method is to be adopted in a given situation. Unequivocal evaluation is not possible because of the many variables involved. The most economic choice of any process for the production of a particular casting will depend on the alloy being cast, the size and complexity of the casting, the quantity required, the tolerances specified and the surface finish required. Not all these factors will be of equal economic

importance, and in any particular situation it is possible that one factor will have a decisive influence.

The most important material factor influencing the choice of a casting procedure is the melting temperature. Processes using refractory materials for moulds (***e.g.*** sand casting, investment casting) can be used for a virtually unlimited range of alloys. On the other hand, those that require a permanent metal mould or die must usually be used with the lower melting point alloys, ***e.g.*** aluminium-, magnesium-, zinc- and copper-based alloys. This limitation is necessary to ensure an acceptable die life.

Casting processes are extremely flexible with regard to size and weight, and castings with weights from less than a gramme to thousands of kilogrammes are in normal production. The largest castings invariably use the simple sand-casting process or one of its variants, ***e.g.*** the CO_2/silicate process, full-mould casting. Smaller castings are best produced by die casting or investment casting, depending on the alloy being cast.

The ability of casting processes to reproduce complex three-dimensional shapes in a simple operation is of fundamental importance. The most complex shapes require the use of expendable patterns such as those used in investment casting or full-mould casting. The high costs involved in the manufacture of metal dies, together with the requirement that the casting can be easily removed, place restrictions on the complexity of objects which can be produced by permanent mould processes. Nevertheless, with modern die-making techniques very complex castings are regularly produced.

One of the important factors is the minimum section thickness a process can produce. This is a function of both the mould surface finish and the method of introducing the molten alloy, as well as being dependent on the limitations involved in forming the mould cavity. The processes most capable of producing thin sections are those where the molten metal is forced into the mould, ***e.g.*** pressure die casting, or those where very thin intricate sections can be moulded, ***e.g.*** investment casting. In the latter case, some form of pressure is needed to ensure complete filling of the mould. Semi-centrifugal methods or the use of high metallostatic heads are normally necessary.

Casting precision (dimensional accuracy, surface finish) varies greatly from process to process. Those using permanent metal moulds tend to give the greatest dimensional accuracy and the best surface finish. With refractory moulds these factors depend on the rigidity of the mould and the size of the refractory used. Processes using fine refractories and rigid moulds, ***e.g.*** investment casting, are the more accurate; conventional sand moulding processes are much less satisfactory.

TABLE 8.1

PROCESS CAPABILITIES FOR THE MAIN CASTING TECHNIQUES[a]

Process	*Material*	*Normal technical weight limit (kg)*	*Thinnest section (mm)*	*Surface finish (μm) centre line average*	*Dimensional tolerance on a dimension of x mm*
Sand moulding	Steel	0·1 – 200 000	6	8	0·005 *x* to 0·030 *x*
	Iron	0·03 – 50 000	3·5	8	
	Aluminium	0·03 – 100	3	4	
Shell moulding	Steel	0·05 – 120	3·5	6	0·010 *x* to 0·025 *x*
	Iron	0·03 – 50	3	6	
	Aluminium	0·03 – 15	1·5	2·5	
Plaster casting	Aluminium	0·1 – 50	1·5	1	0·005 *x*
Investment casting	Steel	0·005 – 25	1	1	0·003 *x* to 0·005 *x*
	Aluminium	0·002 – 10	0·8	1	
Permanent mould casting	Iron	0·1 – 10	5	2	0·010 *x* to 0·025 *x*
	Aluminium	0·1 – 50	3	2	
Die casting	Aluminium	0·015 – 25	0·8	1	0·0015 *x*
	Zinc	0·05 – 50	0·8	1	

[a] Data from Short,[16] Alexander and Brewer[17] and Reynolds.[18]

Table 8.1 summarises the process capabilities for the main casting techniques, giving information for different alloys.

The costing of the different casting processes can be broken down into three sub-divisions, *i.e.* equipment, labour and materials. To these should be added the finish machining costs since these are largely determined by the precision with which the casting is produced. High precision processes have low finishing costs and vice versa. Quantitative assessment is not practicable since detailed costing practice varies from organisation to organisation. However, the qualitative assessment given in Table 8.2 will enable some

TABLE 8.2

AN ASSESSMENT OF THE LEVEL OF COSTS OF THE MAIN CASTING TECHNIQUES[a]

Process	*Equipment cost*	*Labour cost*	*Finishing cost*
Sand moulding	Low	Low–medium	High
Shell moulding	Medium	Medium	Medium
Plaster casting	Low	Medium	Low
Investment casting	Medium	High	Low
Permanent mould casting	High	Medium	Low
Die casting	High	Low	Low

[a] **Data** from **Alexander** and Brewer[17] and Reynolds.[18]

comparisons to be made. The equipment cost reflects the requirements for complex machines and dies, and is particularly high in those cases (die casting) where the die life is limited.

To make a detailed assessment for a specific situation requires more data than can reasonably be presented here. Details of costing procedures are available in the literature, e.g. Reynolds,[18] and this and the technological data available in summary texts and journals should be referred to in given circumstances. A bibliography of appropriate reference works is given in Appendix 3.

REFERENCES

1. *Metals Handbook, Forging and Casting* (1970). Vol. 5, 8th Edition, ASM, Cleveland, pp. 149–448.
2. *Castings* (1971). (Ed. by J. D. Beadle), Macmillan, London.
3. Heine, R. W., Loper, C. R. Jr. and Rosenthal, P. C. (1967). *Principles of Metal Casting*, McGraw-Hill, New York.

4. McIntyre, J. B. (1952). *Foundry*, **80**(12) 90.
5. Taylor, D. A. (1960). *BCIRA Journal*, 8, 112.
6. Petrzela, L. and Gajdusek, J. (1962). *Modern Castings*, **41**(2), 67.
7. Sarkar, A. D. (1964). *Foundry Core and Mould Making by the Carbon Dioxide Process*, Pergamon, Oxford.
8. Nicholas, K. E. L., Donald, W. and Conacher, D. M. (1969). *Brit. Foundryman*, 62, 309.
9. Weaver, T. H. (1957). *Brit. Foundryman*, 50, 421.
10. Osborn, J. H., Marsden, T. A. and Horton, R. F. (1958). *British Foundryman*, 51, 64.
11. Hocking, L. N. (1959). *British Foundryman*, 52, 395.
12. Tedds, D. F. B. (1959). *British Foundryman*, 52, 13.
13. Sharp, H. J. (1959). *British Foundryman*, 52, 368.
14. Butler, R. D. (1964). *British Foundryman*, 57, 265.
15. Morton, J. S. (1964). *Met. Reviews*, **9**, 121.
16. Short, A. (1961). *British Foundryman*. 54, 400.
17. Alexander, J. M. and Brewer, R. C. (1963). *Manufacturing Properties of Materials*, Van Nostrand, London, p. 135.
18. Reynolds, J. A. (1971). *Progress in Cast Metals*, Institute of Metallurgists, London, p. 4.1.

CHAPTER *9*

Defects in Casting

The production of sound castings is of great economic importance. It is an essential step to be able to recognise the different kinds of defects that can arise in casting processes, and when they occur to define the steps necessary to eliminate them from subsequent castings. Design and practice are of importance in influencing the incidence of casting defects. Often errors in design can be overcome by the adoption of procedures involving careful control of the cast metal and of the casting procedure. In many cases, in order to facilitate production it is of greater practical and economic merit to modify the design of an object to be cast.

In this chapter we will mainly be concerned with the major defects that are observed. Comprehensive details of casting defects, of the causes and of remedies can be found in the special publications of the Institute of British Foundrymen,† and the American Foundrymen's Society.' Far too often the remedy lies in an improvement in casting practice. Nevertheless, a clear understanding of casting defects is necessary for those involved in the practical aspects of solidification.

9.1 BLOWHOLES

These are round or elongated cavities, usually with smooth walls, found on or under the surface of castings. They can arise from a number of causes:

(i) Because of the entrapment of air during the pouring of metal into the mouth (Fig. 9.1).

(ii) By the generation of gas by reaction of the molten metal with the mould or core materials. In some cases steam can be

† The illustrations in this chapter are largely drawn from Ref. 1, the ***Atlas of Defects*** in ***Castings***, published ***by*** the Institute of British Foundrymen. Their co-operation is gladly acknowledged.

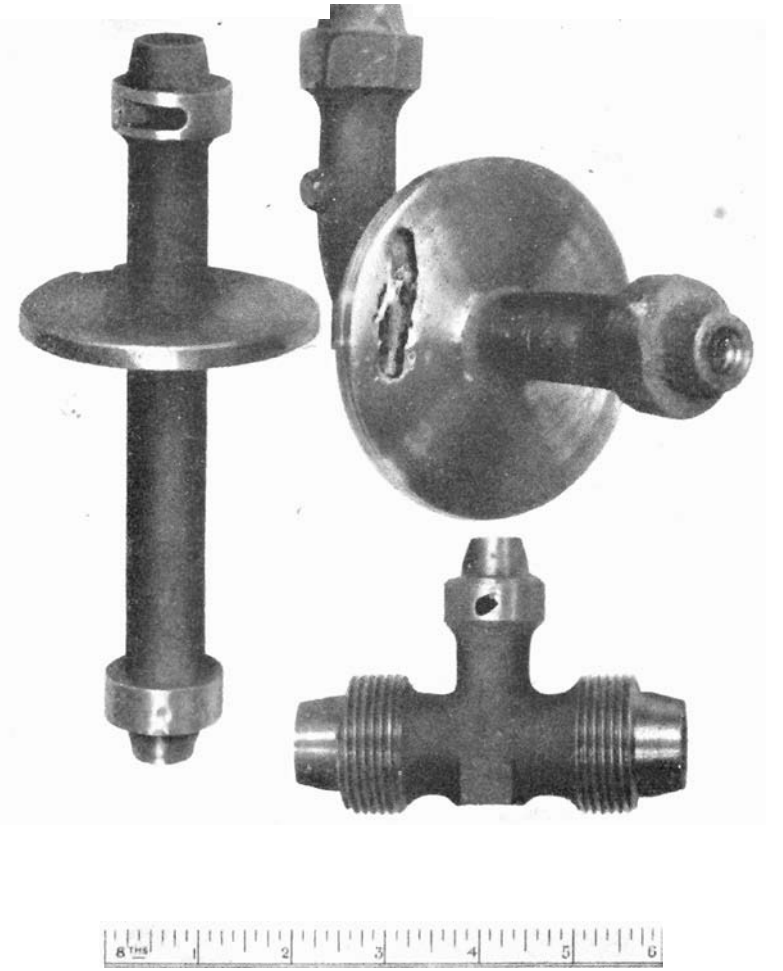

Fig. 9.1 ***A blowhole in the surface of a small gunmetal pipe connection caused by entrapped air. The object was cast in green sand.***

evolved from moisture in the moulding sand. This can give rise to localised patches of cavities of considerable size on the surface (Fig. 9.2) which are often coloured with oxidation tints, or to sub-surface cavities (Fig. 9.3). In other cases fumes are generated when the molten metal comes into contact with

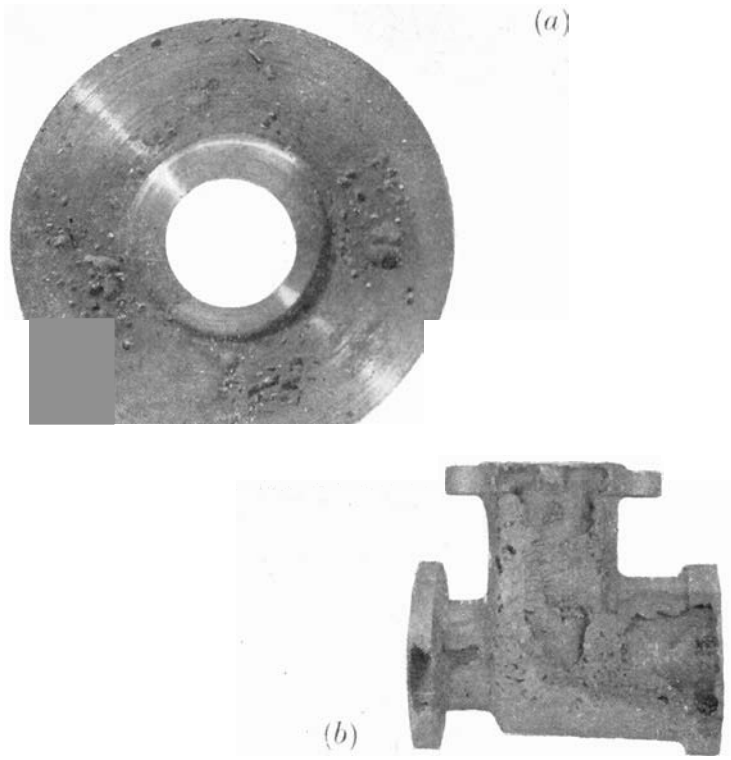

Fig. 9.2 Surface blowholes on (a) a gunmetal flange connection and (b) a grey-iron valve-body casting. In each case the cause was excessive moisture in the moulding sand.

the oil-binder of the core (Fig. 9.4). With investment castings, incomplete removal of residues from the wax pattern can cause trouble (Fig. 9.5).

(iii) As the result of chemical reactions taking place in the molten metal during cooling and solidification. Among the best-known

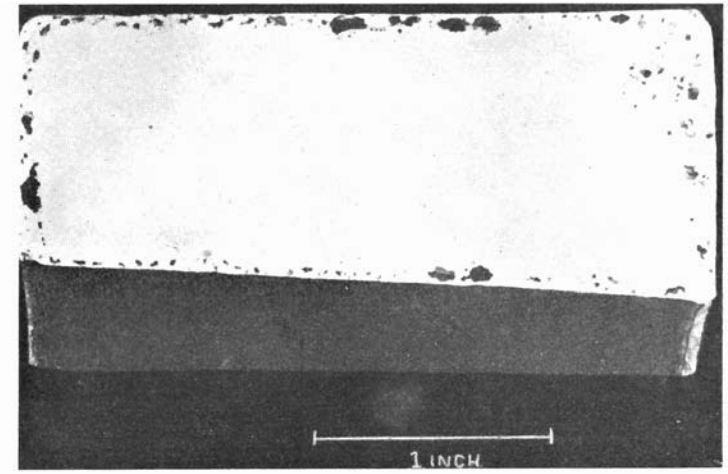

Fig. 9.3 Cross section of a cast gunmetal ring showing sub-surface pores produced by reaction of the molten metal with wet sand.

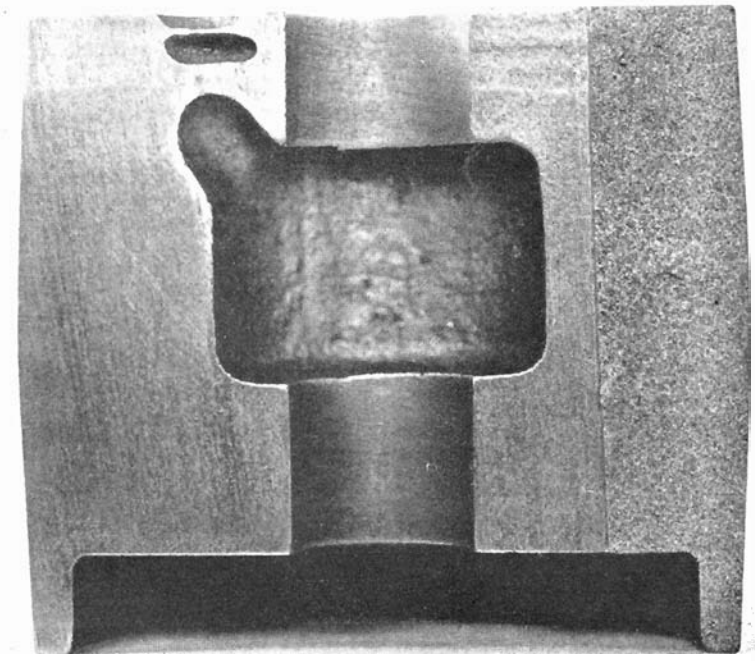

Fig. 9.4 Large blowholes produced in a grey-iron pulley wheel casting by gas evolved from a core.

Fig. 9.5 *Localised areas of cavities in an investment casting. These result from incomplete removal of wax pattern residues and entrapped* **air.**

examples are the blowholes produced in cast steel ingots (Fig. 9.6) by the evolution of carbon monoxide according to the reaction

$$FeO + C \rightarrow Fe + CO$$

Interactions between slags and molten metals can also cause defects which are frequently observed on or near the surface (Fig. 9.7).

(iv) By the evolution of gas during the solidification process. These cavities can be small, when they are known as 'pinholes' (Fig. 9.8), or of quite large size (Fig. 9.9).

Most of the remedies for eliminating blowholes of types (i) and (ii) involve changes in the practice. Care during pouring or the provision of extra venting will remove entrapped air, and careful drying of

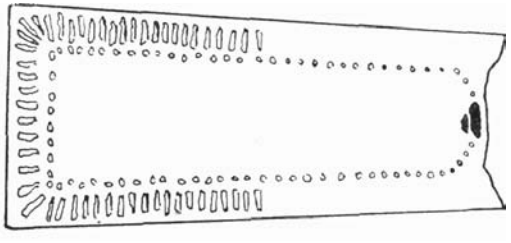

Fig. 9.6 ***Cross section of a rimmed steel ingot showing carbon monoxide blowholes (schematic).***

materials prior to casting eliminates moisture, thus avoiding the evolution of steam. In the same way, careful preparation and baking of cores will produce improved results.

Where the cause is chemical reaction, care is only sometimes effective. It is usually necessary to introduce additions into the metal

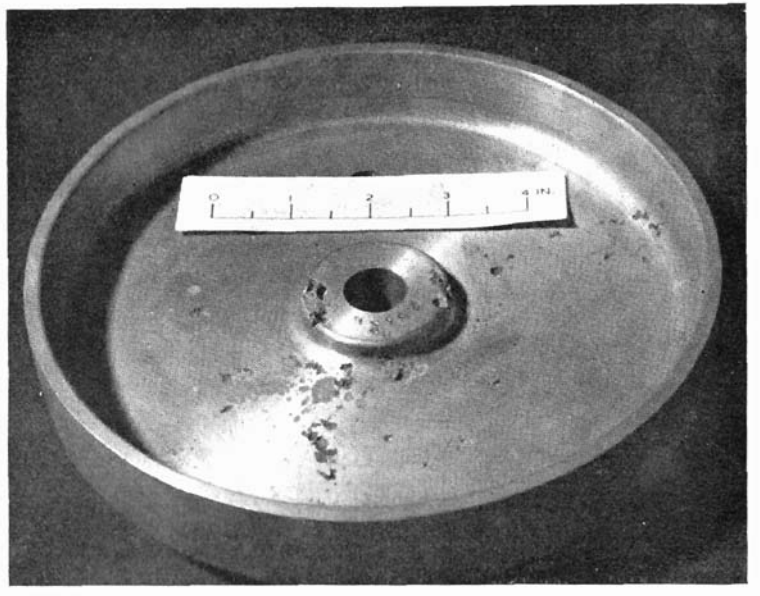

Fig. 9.7 *Blowholes produced by reaction between the* **molten metal** *and entrapped* **slag.** *These* **generally** *have discoloured surfaces and* **are associated** *with slag inclusions*

to remove the reactants before gas is evolved. For example, aluminium is used to 'kill' steel by deoxidising the molten metal and preventing the reaction which produces carbon monoxide.

The evolution of dissolved gases can only be prevented by taking steps to eliminate the gas before the molten metal is introduced into the mould. This can be done by degassing, ***i.e.*** bubbling an inert gas such as nitrogen or argon through the molten metal in the ladle, or by adding chemicals which evolve a non-soluble gas which bubbles through the melt, ***e.g.*** the use of hexachloroethane tablets to degas aluminium. The effectiveness of these scavenging degassing procedures depends on the evolution of dissolved gas into the bubbles of inert gas and the subsequent expulsion into the atmosphere.

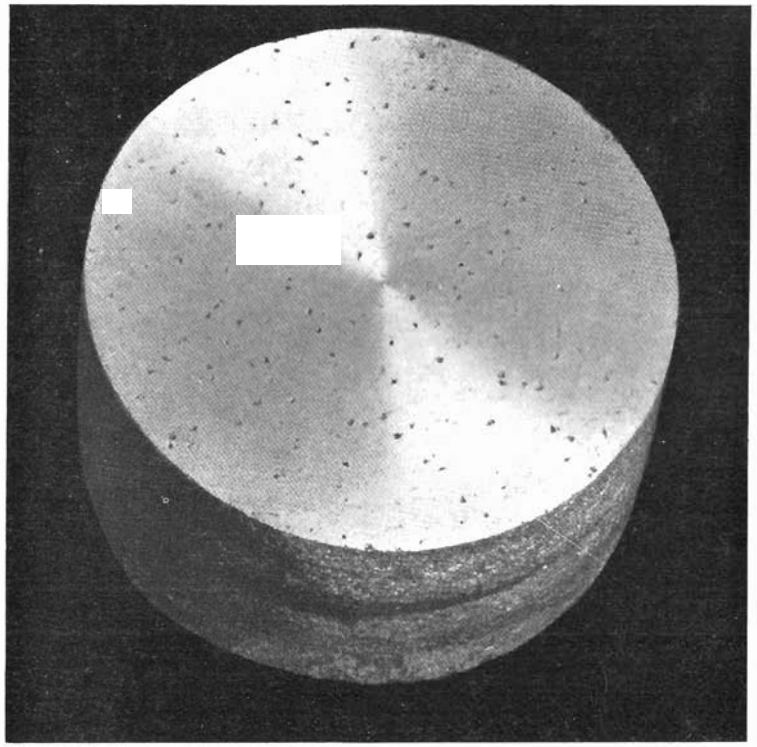

Fig. 9.8 Pinhole cavities in a sand-cast aluminium alloy, the result of hydrogen evolution on cooling.

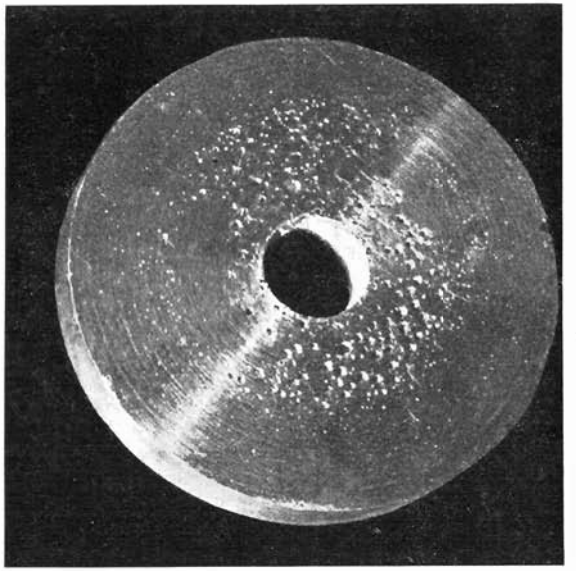

Fig. 9.9 Large gas holes in a 10% tin–bronze sand casting.

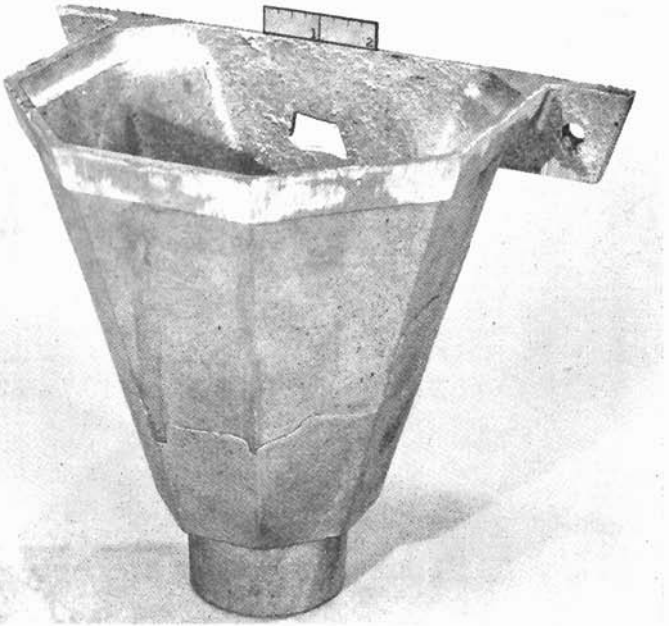

Fig. 9.10 A cold shut or cold trap on the surface of an aluminium alloy sand casting.

9.2 COLD SHUTS

A 'cold shut' is produced when two streams of metal flowing from different regions in the casting meet without union. The shuts appear as apparent cracks or wrinkles in the surface, together with oxide

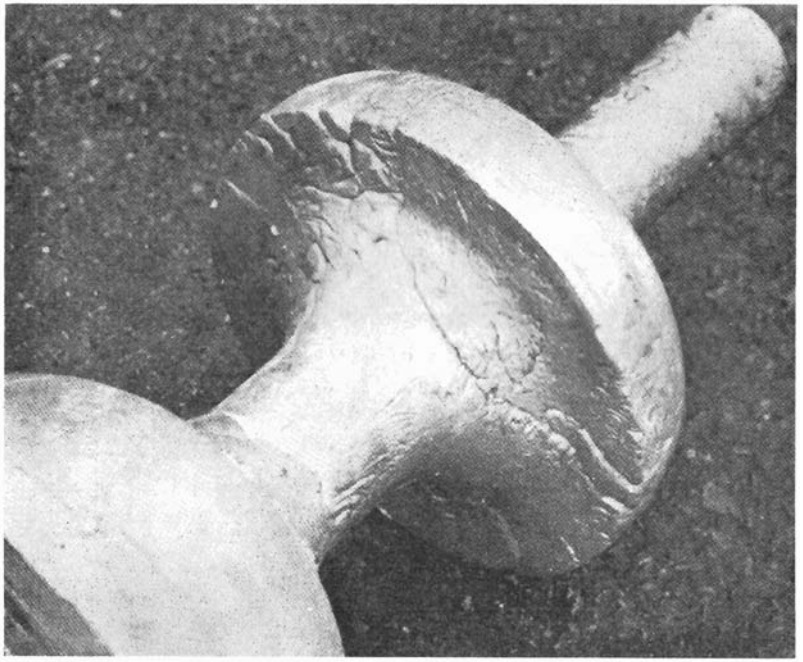

Fig. 9.11 Cold shuts in an alloy steel casting.

films (Figs. 9.10 and 9.11). This defect is usually the result of insufficient fluidity in the metal or the use of unsatisfactory methods of running and gating. Interrupted pouring can also give rise to cold shut formation.

The remedy is to increase fluidity either by raising the pouring temperature or by preheating the mould. Relocation of runners and ingates can often be equally effective.

9.3 CONTRACTION CRACKS

These are irregularly shaped cracks formed when the metal pulls itself apart while cooling in the mould or after removal from the

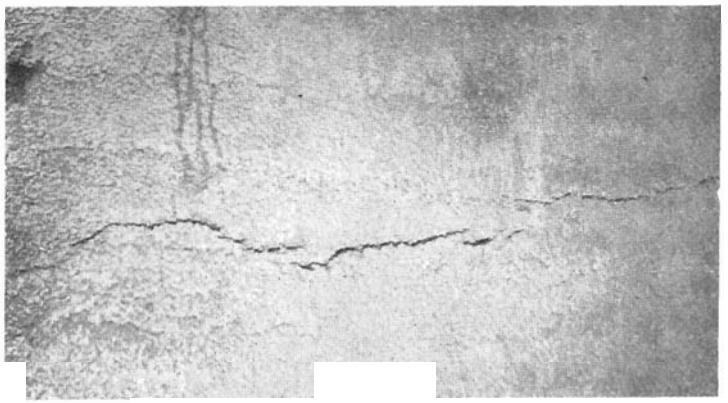

Fig. 9.12 A hot tear in a steel casting.

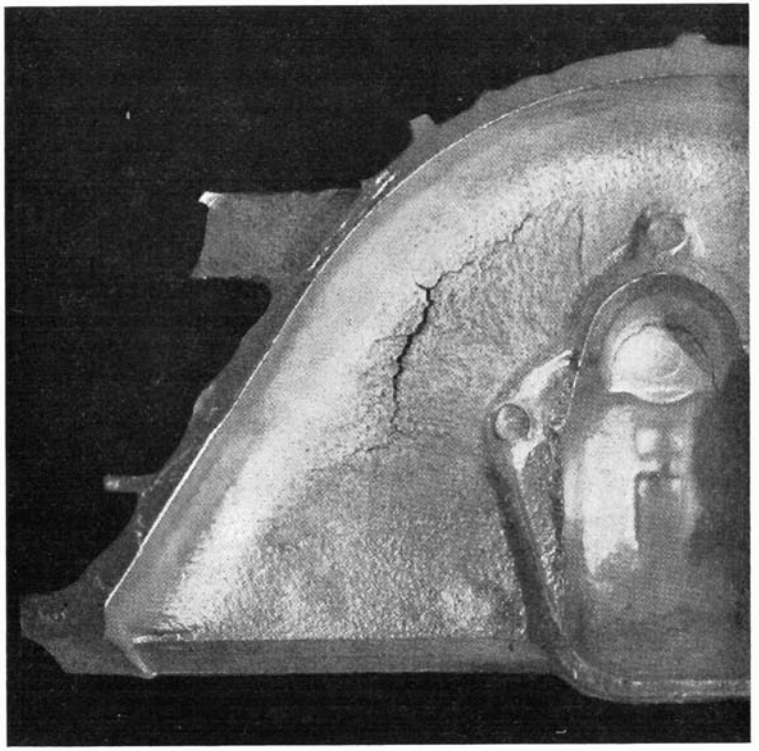

Fig. 9.13 A contraction crack formed in an aluminium alloy die casting during cooling in the mould after solidification was complete.

mould. When the crack appears during the last stages of solidification it is known as a 'hot tear' or a 'pull' (Fig. **9.12).** In this case the crack faces are usually heavily oxidised. Hot tearing is most common in metals and alloys that have a wide freezing range, for then isolated regions of liquid become subjected to thermal stresses during cooling and fracture results.

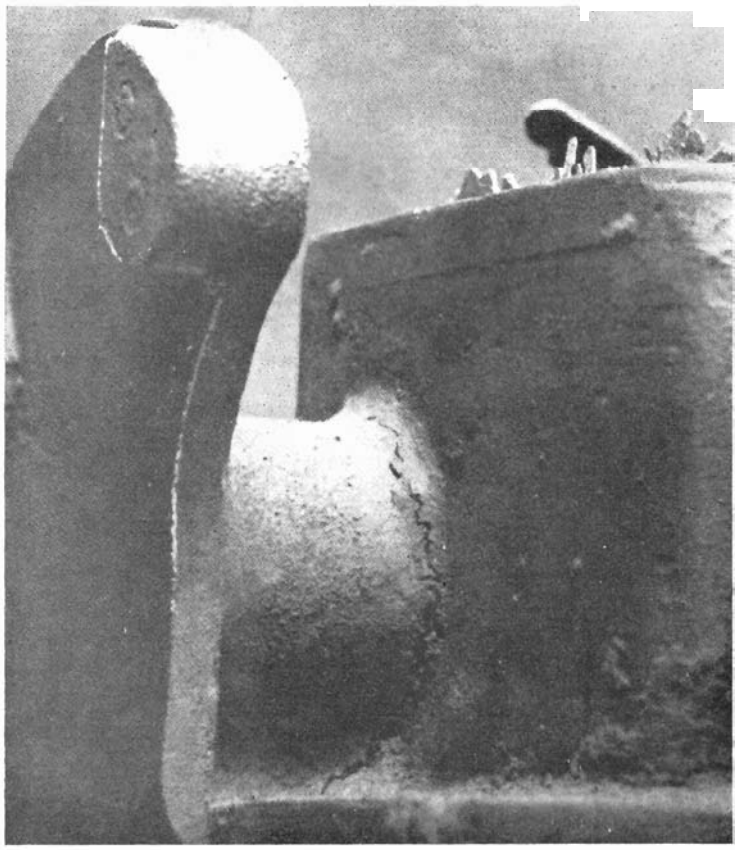

Fig. 9.14 *A contraction crack in the fillet of a small gunmetal sand casting.*

In other cases contraction cracks arise during the period when the metal is solid but still at a temperature where the mechanical strength is low (Fig. 9.13).

Contraction cracks and hot tears result from the hindered contraction of the casting; this gives rise to complex internal stresses.

I ... al hot spots or high thermal gradients contribute to these high tresses, particularly if the mould or core is rigid enough to restrict ... lative movement of the different parts of the casting.

Several steps are necessary if this type of defect is to be avoided. I irst, the cores and mould should be made more collapsible, for instan... by incorporation of elastically soft material, ***e.g.*** cellulose, into the mould material or by minimising the compaction during moulding. In addition, alterations in design to avoid ***abrupt*** changes in ... tion may be necessary. Hot spots can be eliminated, and thermal ... ontrolled, by modification of the gating system or by the ... chills.

It should be noted that contraction cracks often have an external appearance very similar to a shrinkage cavity **(see** Section **9.6).** They can be differentiated from the latter because there is no cavity or porous area beneath the surface. Furthermore, contraction cracks are normally located in positions clearly related to the geometry of the casting and to the restriction of free contraction by parts of the mould. A good example of this is shown in Fig. **9.14,** where cracking has occurred in the fillet region between two parts of the casting.

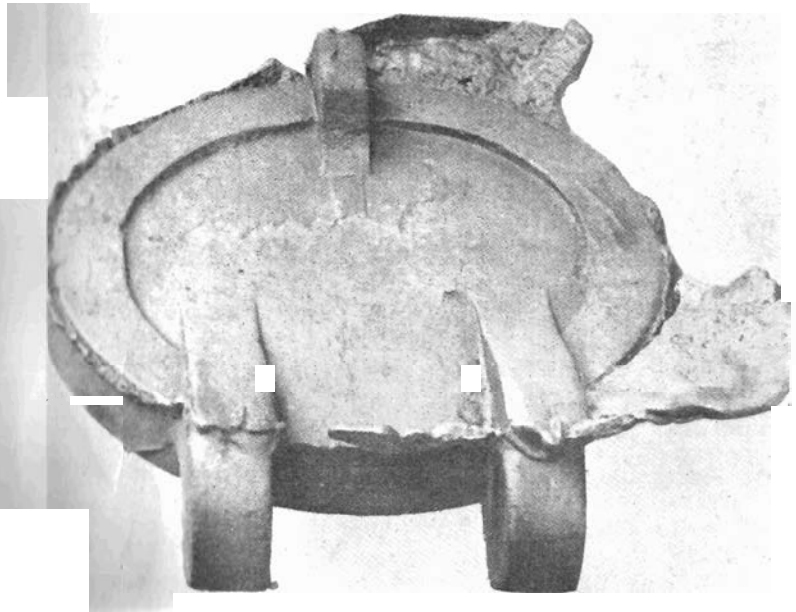

... 15 Excessive flash or fin ***along the parting line of a grey-iron casting.***

9.4 FLASH

The development of 'flash' (or 'fin') involves the formation of a run of metal around the parting line of the mould caused by the flow of liquid metal into the space between the halves of the mould. This

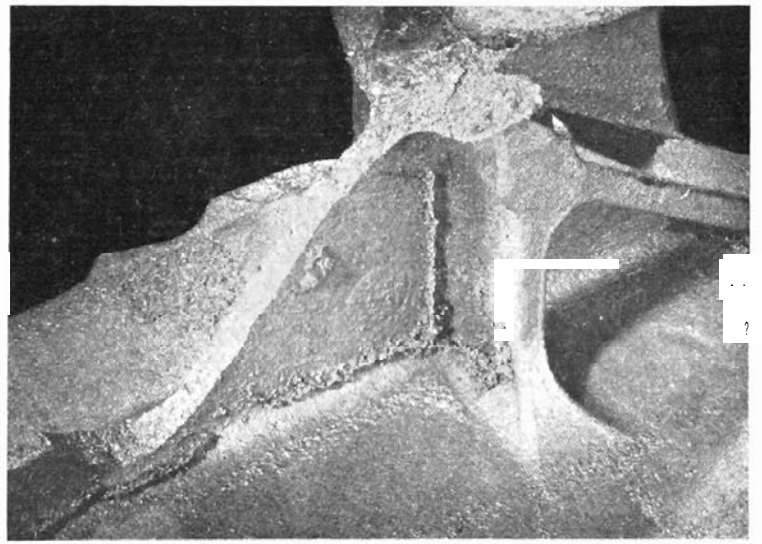

Fig. 9.16 Veining caused by the penetration of cast high-duty iron into cracks in an oil-bonded core.

defect is known as 'veining' when liquid metal penetrates into cracks in the mould or core. Examples of these are shown in Fig. 9.15 and 9.16.

Rigid clamping of the mould boxes and hardening of the mould and core faces will usually overcome this type of defect. In some instances a lowering of the pouring temperature is necessary since the appearance of finning or veining is accentuated by the high fluidity of liquid metals cast with high degrees of superheat.

If the two parts of the mould are displaced relative to each other, this produces a different but associated defect known as a 'crossjoint' (Fig. 9.17). Here the remedy is obvious.

9.5 OXIDE AND DROSS INCLUSIONS

These result from the entrapment of surface oxide or other foreign matter during pouring. Often they are not immediately apparent and

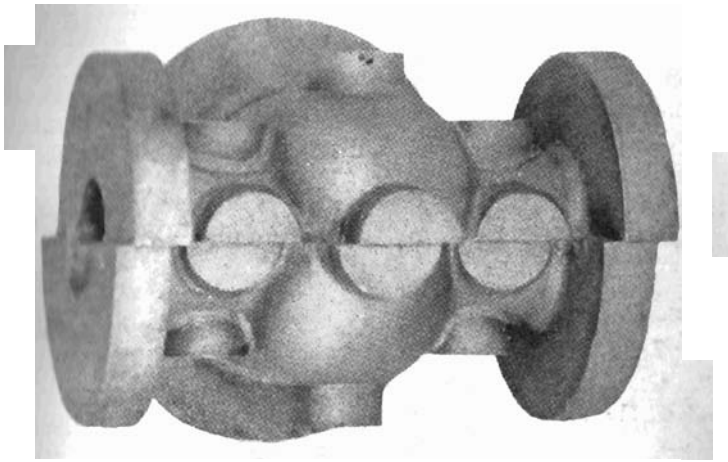

Fig. 9.17 A crossjoint in a large grey-iron valve body casting produced by mismatch of the top and bottom parts of the mould.

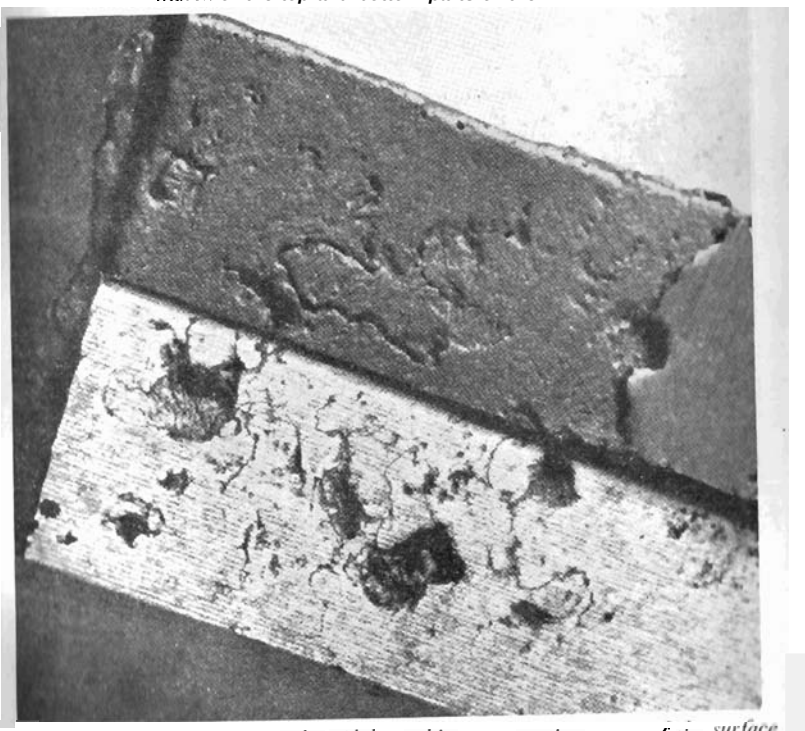

Fig. 9.18 Inclusions in an spheroidal graphite iron casting. Part of the surface has been machined away to show the nature of the defect more clearly.

can only be clearly seen after machining of the casting surface (Fig. 9.18). These defects invariably result from poor casting practice. Insufficient skimming before pouring, the use of dirty ladles and turbulence due to improper grating methods can all contribute. Redesign of the feed system and attention to care and cleanliness are needed to avoid these inclusions.

9.6 SHRINKAGE CAVITIES

As described in Chapter 1, the majority of metals show a significant increase in volume on melting *(see* Table 1.1). This change in volume

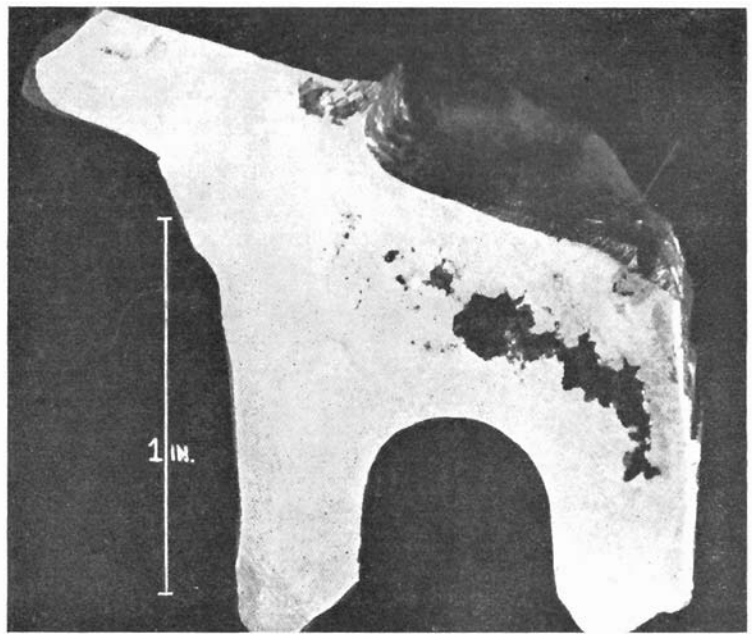

Fig. 9.19 ***A*** *large shrinkage cavity in the interior of an aluminium–bronze sand casting.*

manifests itself as shrinkage during the reverse transformation from liquid to solid. If insufficient attention is given to ensuring that all parts of the casting are supplied with liquid metal throughout the whole of the solidification process, areas of liquid can become isolated. The shrinkage then appears as a cavity of irregular shape.

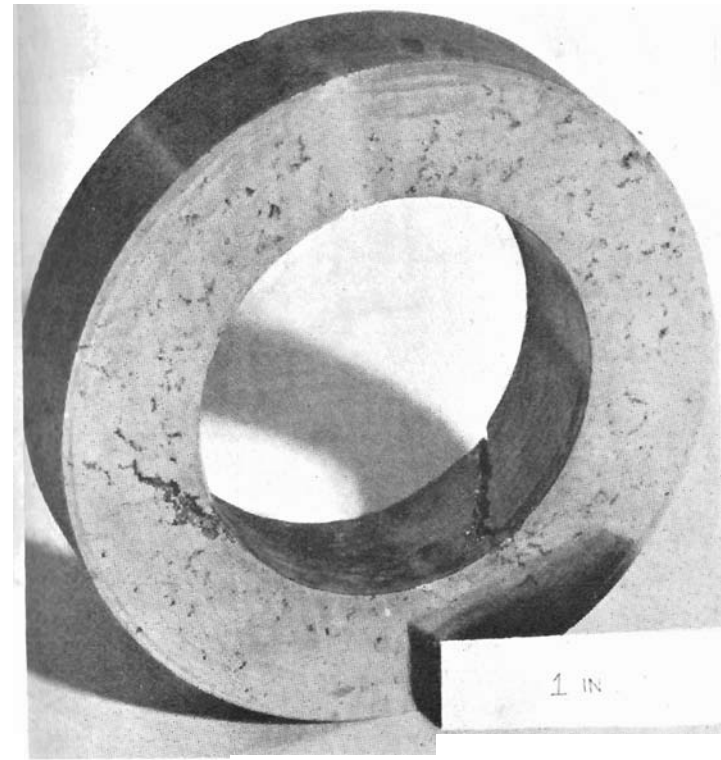

Fig. 0.20 ***Dispersed shrinkage cavities in a section of a sand-cast tin–bronze. A surface hot fear can also be seen.***

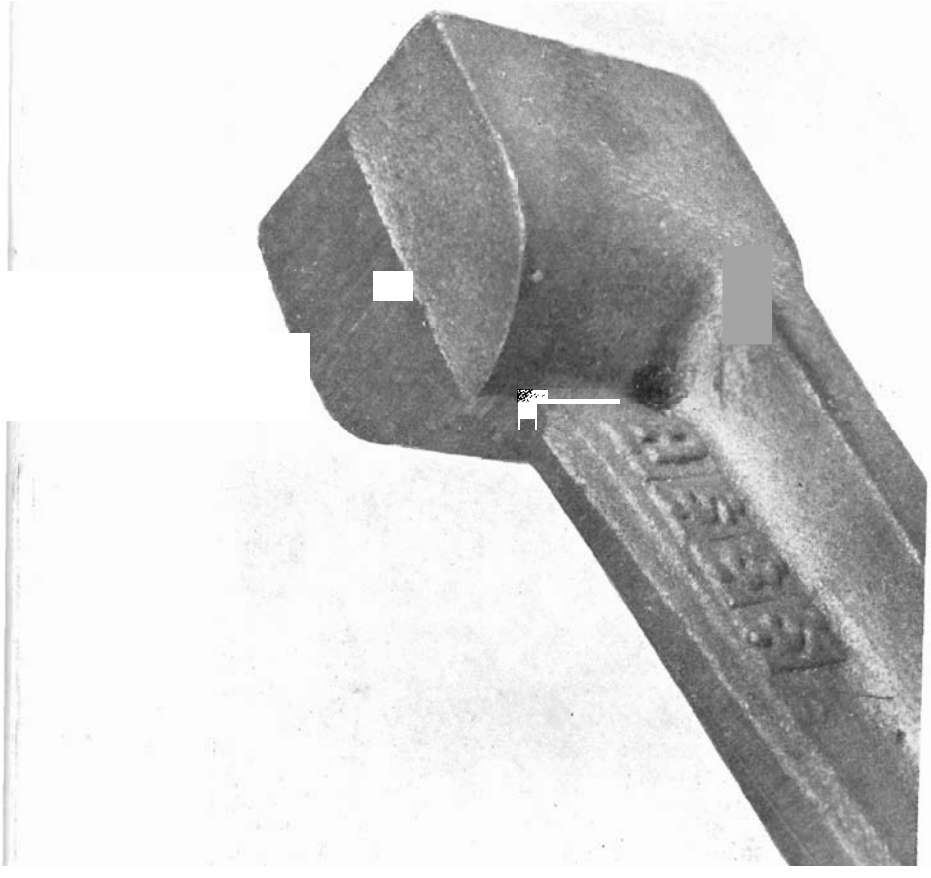

Fig. 9.21 Surface shrinkage in a grey-iron casting.

these cavities are frequently widely dispersed and located below the surface, and thus difficult to detect. Examples are shown in Figs. 9.19 and 9.20. If the shrinkage occurs near the surface, the cavities can be detected because of the presence of small depressions in the surface of the casting (Fig. 9.21). A similar case to this latter form is

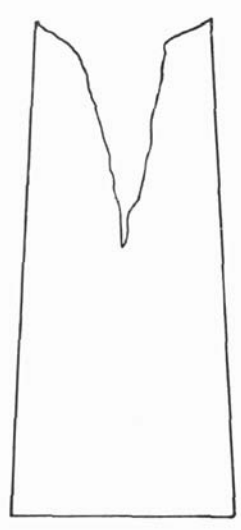

Fig. 9.22 Cross section of a killed steel ingot showing pipe development (schematic). The piped region must be cut off before working, thus giving a low useful metal yield.

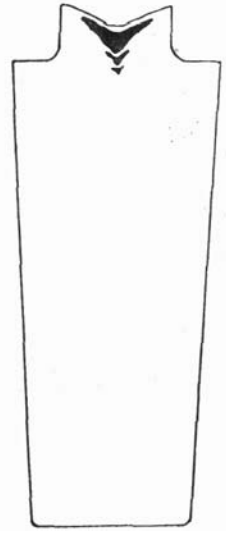

Fig. 9.23 Cross section of a killed steel ingot cast into a mould with a refractory hot top (schematic). Shrinkage is confined to the top of the ingot and yield is increased.

the large conical depression observed in the top of some ingots, and known as *pipe* (Fig. 9.22).

The major cause is the failure to obtain directional solidification towards desired heat centres such as risers or ingates. If the location of these feed points is bad, then shrinkage is much more likely. Relocation of feeding can help considerably. The use of higher pouring temperatures is also normally an advantage. Often proprietary methods involving exothermic heating in the mould cavity can be used to encourage directional solidification. When these are used with judicious location of refractory inserts and chills to promote transfer to the mould, shrinkage defects can largely be

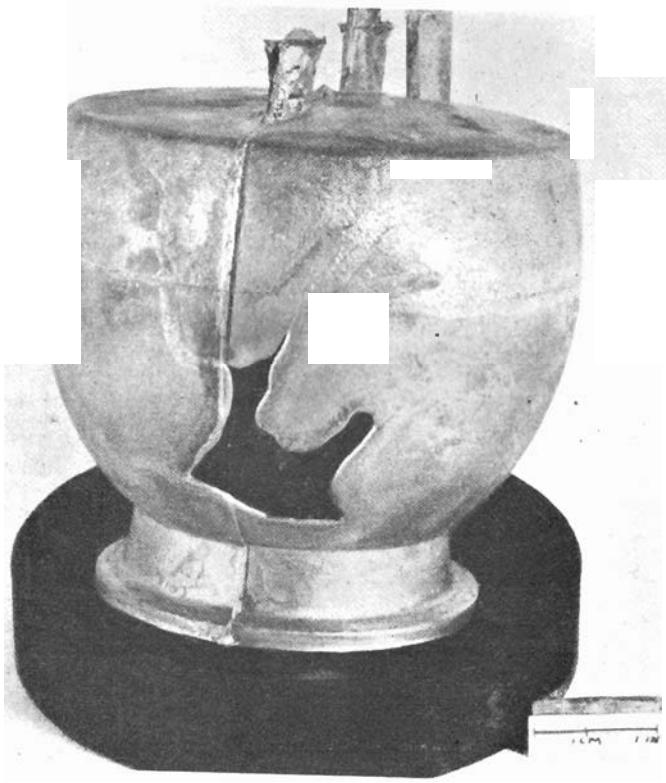

Fig. 9.24 *A misrun in* ***a brass*** *gravity die casting.*

some. With ingots, the use of refractory hot-tops will increase [illegible] (Fig. 9.23).

9.7 MISRUNS

An exaggerated form of shut is the 'misrun' ***(see*** Figs. 9.24 and 9.25). These are produced when the liquid metal fails to fill the mould either because of low fluidity or if the methods of running are

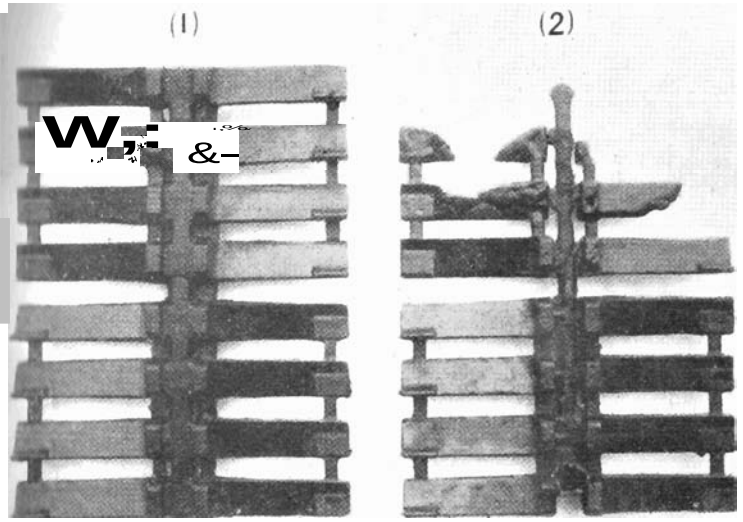

Fig. 0.25 ***A striking example of a misrun*** *which* ***resulted*** *in* ***an incompletely filled*** *mould* ***(a*** *'short run'). **Both a complete*** (1) ***and a misrun casting (2) are shown.***

unsatisfactory. They are evident as smooth irregular-shaped holes, with rounded edges, through the casting wall. Poor venting of moulds and cores can have a contributory effect. Raising the pouring temperature and reconsidering the position, size and number of ingates and vents will usually eliminate this defect.

9.8 SUMMARY

The sections preceding this summary describe the major defects that occur in castings. These are summarised in Table 9.1. Details of

TABLE 9.1

SUMMARY OF CASTING DEFECTS GIVING CAUSES AND REMEDIES

Defect	*Cause*	*Foundry remedy*	*Design remedy*
Blowholes	Occlusion of gases	(i) Increased venting (ii) Elimination of materials that can react to produce gas (iii) Degassing	Avoid feed systems which have high flow velocities
Cold shuts	Non-union of metal streams	(i) Raise pouring temperature (ii) Preheat mould	Relocate runners and ingates
Contraction cracks	Tearing of the metal under thermal stress	(i) Use collapsible moulds (ii) Control of thermal gradients with chills	Avoid abrupt changes in section
Flash	Flow into the mould join	(i) Lower pouring temperature (ii) Increase mould box clamping	
Oxide and dross inclusions	Entrapment of foreign matter	(i) Increase care and cleanliness during pouring	
Shrinkage cavities	Lack of sufficient feed metal	(i) Promote directional solidification by control of heat flow (ii) Raise pouring temperature	Relocate risers and ingates
Misruns	Low metal fluidity	(i) Raise pouring temperature	Reconsider position, size and number of ingates and vents

less common defects can be found in the references to this
apter.

REFERENCES

1. *Atlas of Defects in Castings* (1961). The Institute of British Foundrymen London, 2nd Edition.
2. *Analysis of Casting Defects* (1947). American Foundrymen's Society Des Plaines, Illinois.

APPENDIX 1

The Relationship Between the Interfacial Energies and the Contact Angle in Heterogeneous Nucleation

In Chapter 2 it was given that under stable conditions the contact angle, θ (see Fig. A1.I), was related to the surface energies of the liquid–crystal interface, γ_{LC}, the crystal–substrate interface, γ_{CS}, and the liquid–substrate interface, γ_{LS}, by

$$\cos\theta = \frac{\gamma_{LS} - \gamma_{CS}}{\gamma_{LC}}$$

A superficial examination of Fig. A1.1 might suggest that this relation is an obvious consequence of the force balance. This appendix

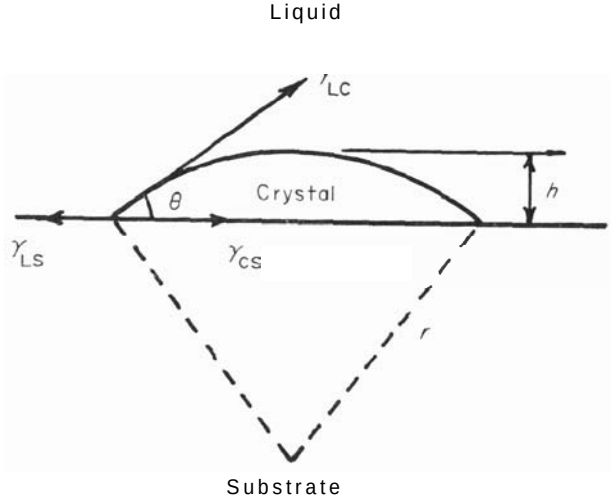

Fig.* A1.1** ***Spherical cap of solid formed on aplanar substrate.

gives a rigorous proof based on a method of virtual displacements. The proof depends on the assumption that the condition for stability is that the total surface energy should remain unchanged for a virtual displacement at constant volume.

Considering a spherical cap of radius r (Fig. A1.1), the area of the cap in contact with the surface is

$$A_1 = \pi r^2 \sin^2\theta \qquad \textbf{(A1.1)}$$

The area of the cap in contact with the liquid is

$$A_2 = 2\pi r^2(1 - \cos\theta) \qquad \text{(A1.2)}$$

Total excess surface energy introduced into the system by the formation of the spherical cap equals

$$A_1(\gamma_{CS} - \gamma_{LS}) + A_2 \cdot \gamma_{LC}$$

For a small displacement the assumption above means that

$$dA_1(\gamma_{CS} - \gamma_{LS}) + dA_2 \cdot \gamma_{LC} = 0$$

that is

$$\frac{\gamma_{LS} - \gamma_{CS}}{\gamma_{LC}} = \frac{dA_2}{dA_1}$$

Differentiating eqns. (A1.1) and (A1.2) and substituting gives, after simplification,

$$\frac{\gamma_{LS} - \gamma_{CS}}{\gamma_{LC}} = \frac{r \cdot \sin\theta + 2(1 - \cos\theta)(dr/d\theta)}{r \cdot \sin\theta\cos\theta + \sin^2\theta(dr/d\theta)} \qquad \text{(A1.3)}$$

The volume of a spherical cap is

$$V = \tfrac{1}{3}\pi r^3(2 - 3\cos\theta + \cos^3\theta)$$

For constant volume, $dV = 0$. Thus

$$\frac{dr}{d\theta} = \frac{r \cdot \sin\theta(1 + \cos\theta)}{(1 - \cos\theta)(2 + \cos\theta)}$$

Substituting this in eqn. (A1.3) leadsto

$$\frac{\gamma_{LS} - \gamma_{CS}}{\gamma_{LC}} = \cos\theta$$

APPENDIX 2

The Solute Distribution in a Bar Solidified under Conditions of Complete Mixing in the Liquid

In Chapter 4 it was stated that the solute profile in a bar solidified directionally with complete solute mixing in the liquid was given by

$$C_s = C_0 k_0 (1 - x)^{k_0 - 1}$$

where C, is the solute concentration in the bar at a point where a fraction x of the bar has solidified, C, is the initial solute concentration and k_0 is the equilibrium distribution coefficient. This equation has been derived in various forms by a number of workers.[1-3] The treatment given here is that of Pfann.

Let x be the fraction of the original volume (assumed as unity) that has solidified, w the weight of solute remaining in the liquid and w_0 the total amount of solute before solidification commenced. If C is the solute concentration in the liquid after the fraction x has solidified, by definition

$$C^* = Ck_0 \qquad \text{(A2.1)}$$

Now

$$C = \frac{w}{1 - x} \qquad \text{(A2.2)}$$

where the solute concentration is expressed in units of solute per unit volume of liquid.

If at this stage an additional fraction dx solidifies, the concentration in this frozen layer is

$$C_s = -\frac{dw}{dx}$$

where dw is the amount of solute entrapped. But from eqns. (A2.1) and (A2.2),

$$C_s = \frac{k_0 w}{1 - x}$$

Therefore

$$-\frac{dw}{w} = \frac{k_0 \cdot dx}{1 - x}$$

Integrating these relations from the beginning of the process to the point where a fraction x is solid,

$$\int_{o}^{w} -\frac{dw}{w} = \int_{0}^{x} \frac{k_0 \cdot dx}{1 - x}$$

gives

$$w = w_0 (1 - x)^{k_0}$$

From this

$$C_s = -\frac{dw}{dx} = w_0 k_0 (1 - x)^{k_0 - 1}$$

and since unit volume was assumed

$$C_0 = w_0$$

Thus

$$C_s = C_0 k_0 (1 - x)^{k_0 - 1}$$

REFERENCES

1. Scheuer, E. (1931). *Z. Metallke,* ***23,*** 237.
2. Hayes, A. and Chipman, J. (1939). ***Trans. AIME,*** 135, 85.
3. Pfann, W. G. (1952). ***Trans. AIME, 194, 747.***

APPENDIX 3

Selected Bibliography

The literature on solidification and casting is large and diverse. It embraces a spectruni from the very fundamental physics of liquid metals through to the detailed technology of foundry practice. At the end of each chapter appropriate references have been given. In this appendix, however, summary information is given of the more general sources for obtaining data on both the fundamental and technological aspects of solidification and casting. The hooks and journals listed are recommended as providing a base for searching for specific information.

GENERALREFERENCES

The Solidification of Metals, Iron and Steel Institute Publication 110 (1968).

This conference volume is a valuable contemporary assessment of all aspects of solidification, primarily fundamental, but with a strong technical flavour.

Metals Abstracts, published jointly by the American Society for Metals and the Institute of Metals.

Sections 1.2, 3.1 and 5.1 contain the main fundamental and technological references. There is an excellent subject index which is a considerable aid to information retrieval.

MORE TECHNOLOGICAL SOURCES

Books

Metals Handbook: Vol. 5—Forging and Casting, American Society for Metals, Cleveland (1970).

Castings (Ed. by J. D. Beadle), Macmillan, London (1971)

Principles of Metal Casting, R. W. Heine, C. R. Lopcr, Jr. and P. C. Rosenthal, McGraw-Hill, New York (1967).

Progress in Cast Metals, Institution of Metallurgists, London (1971).

Journals

The British Foundryman (Journal of the Institute of British Foundrymen).

Transactions of the American Foundrpen's Society.

Modern Castings.

British Cast Iron Research Association Journal.

MORE FUNDAMENTAL SOURCES

Books

Principles of Solidification, B. Chalmers, John Wiley, New York (1964).

The Art and Science of Growing Crystals (Ed. by J. J. Gilman), John Wiley, New York (1963).

Liquids: Structure, Properties, Solid Interactions (Ed. by T. J. Hughel), Elsevier, Amsterdam (1965).

Crystal Growth (Ed. by H. S. Pieser), Pergamon, Oxford (1967).

Journals

Journal of Crystal Growth.

Transactions of the Metallurgical Society of AIME (now *Metallurgical Transactions).*

Journal of the Institute of Metals.

Journal of the Iron and Steel Institute.

Author Index

Page numbers are given in bold type when they refer to a list of references.

Subject Index

Acknowledgements

I would like to express my thanks to the following for granting permission for the use of figures and tables from copyrighted publications:

American Institute of Physics
American Society for Metals
Butterworths Scientific Publications
The Institute of British Foundrymen
The Institute of Metals
The Institution of Metallurgists
The Iron and Steel Institute
John Wiley and Sons Inc.
McGraw-Hill Publishing Company
The Macmillan Press Limited
North Holland Publishing Company
Pergamon Press
The Royal Society

Particular sources are acknowledged in the captions to figures and tables.

volume of the component atoms or molecules and a/V^2 is a term which allows for interactions between these components. In this case the basic many-body problem of an aggregate of components was also overcome by considering it as a single-body problem with summation over a number of apparently identical components.

The understanding of the solid state, on the other hand, was beset with difficulties until early in the twentieth century, when diffraction procedures clearly established the structure of crystalline solids as one in which atoms or groups of atoms are arranged in regular geometrical patterns in space. Here it was clear that interactions between individual atoms had necessarily to be taken into account, but since the relative atomic positions were defined? the interactions of an atom with its neighbours could be estimated. The overall properties of the assembly could then he determined by summation over the total of atoms. Here again the many-body problem was overcome by considering it as a sum of single-body problems.

The study of liquids encountered difficulty because it was essentially a true many-body problem. Interactions bctwccn neighbouring components needed to be taken into account, but the relative atomic positions were not well defined. In general the environment of any individual atom was more unlike than like that of another. The principal approaches to the study of liquids came from two directions. Liquids were considered as either dense gases or rather disordered solids. More recently a geometrical concept in which the liquid is considered as a 'heap' of atoms or molecules has been the subject of study.

Before turning our attention to an examination of these different theories it is useful to consider the experimental facts which these theories must account for as far as possible.

1.1 EXPERIMENTAL CONSIDERATIONS

1.1.1 The change in volume on melting

Table 1.1 lists a number of common metals togcthcr with their crystal structure, melting point and change in volume on melting. It can be seen that in most cases there is an expansion of from 3 to 5% except for a small number of metals with rather open structures in which there is a small contraction on melting.

† The atomic position can be simply considered as the mean position of the atomic centre. In practice this is only true on average since the atom is normally undergoing thermal vibrations. For a rigorous treatment it may be necessary to 'stop' the atoms by assuming the solid is at 0°K.

TABLE 1.1

THE CHANGE IN VOLUME ON MELTING OF SOME COMMON METALS[a]

Metal	*Crystal structure*	*Melting point* (°C)	*Change in volume on melting* (%)
Aluminium	f.c.c.	660	+6.0
Gold	f.c.c.	1063	+5.1
Zinc	h.c.p.	420	+4·2
Copper	f.c.c.	1 083	+4·15
Magnesium	h.c.p.	650	+4·1
Cadmium	h.c.p.	321	+4.0
Iron	b.c.c./f.c.c.	1 537	+3.0
Tin	tetr.	232	+2.3
Antimony	rhombohedral	631	−0.95
Gallium	f.c. orthorhombic	30	−3.2
Bismuth	rhombohedral	271	−3.35
Germanium	dia. cubic	937	−5.0

[a] Data from Schneider and Heymer.[1]

TABLE 1.2

LATENT HEATS OF MELTING AND VAPORISATION OF SOME COMMON METALS[a]

Metal	*Crystal structure*	*Melting point* (°C)	*Latent heat*[b] *of melting* (L_m)	*Boiling point* (°C)	*Latent heat*[b] *of vaporisation* (L_b)	$\frac{L_b}{L_m}$
Aluminium	f.c.c.	660	2·5	2 480	69·6	27·8
Gold	f.c.c.	1 063	3·06	2 950	81·8	26·7
Copper	f.c.c.	1 083	3·11	2 575	72·8	23·4
Iron	f.c.c./b.c.c.	1 536	3.63	3 070	81·3	22·4
Zinc	h.c.p.	420	1·72	907	27·5	16·0
Cadmium	h.c.p.	321	1·53	765	23·8	15·6
Magnesium	h.c.p.	650	2·08	1 103	32·0	15·4

[a] Data from Smithells.[2]
[b] Latent heats in kcal mol^{-1}.

CHAPTER 2

Nucleation

Nucleation may be defined as the formation of a new phase in a distinct region separated from the surroundings by a discrete boundary. During solidification, solid nuclei form in the liquid and subsequently grow until the whole of the volume is solid. We are concerned with a change from one position of stable or metastable equilibrium to another in response to a driving force. The existence of a driving force, namely a decrease in the free energy of the system, indicates that the transformation is favourable. This driving force is a necessary but not sufficient requirement. Whether or not the transformation takes place is determined by kinetic factors. First, we must ask can the transformation begin? This is a problem of nucleation and is dealt with in this chapter. Second, we must ascertain that after nucleation the transformation can continue. This involves the study of growth and is considered in Chapter 3. Before we can examine the different processes of nucleation we must examine the nature of the driving force.

2.1 THERMODYNAMIC ASPECTS

When considering the development of microstructure we are concerned with heterogeneous equilibrium, i.e. equilibrium involving more than one phase. The free energy, G, of a component phase is defined by

$$G = H - TS \tag{2.1}$$

where H is the enthalpy, T the absolute temperature and S the entropy. For most metallurgical systems, pressure can be considered to be constant, so that

$$\left(\frac{\partial G}{\partial T}\right)_{p=\text{constant}} = -S$$

Thus the free energy decreases with increasing temperature.

The variation of the free energies of the different pure metal phases is shown schematically in Fig. 2.1. The change in free energy on transformation at constant temperature from one phase to another is given by

$$AG = AH - TAS$$

At equilibrium between two phases,

$$AG = 0$$

and this defines the equilibrium melting point, T_m, and boiling point, T_b. At other temperatures, the equilibrium phase is that which has

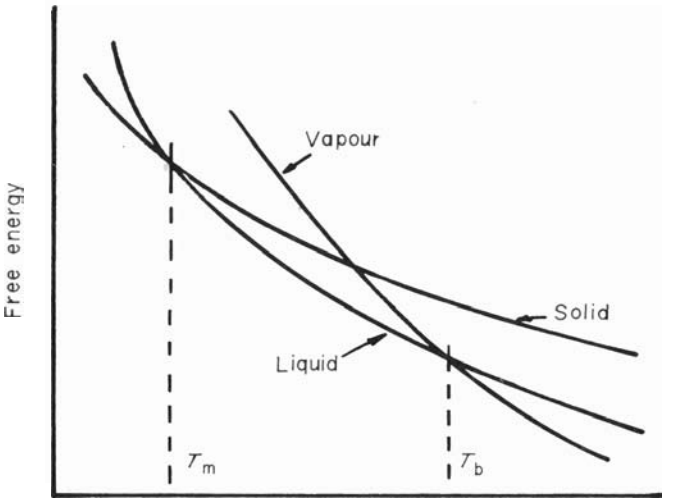

Fig. 2.1 The variation in free energy of metallic phases with temperature (schematic).

the minimum free energy; AG, the difference between the free energies, provides the driving force for transformation.

With simple binary alloys the free energy can vary with composition in several ways, as shown in Fig. 2.2. The free energy curves for the component phases move relatively as the temperature changes. For a particular composition the equilibrium phase or phases at a given temperature are those which give the minimum overall free energy at that temperature.† The difference between the free energies

† A full description of the free-energy composition diagram and its relation to the equilibrium phase diagram can be found in the books by Cottrell[1] and Darken and Gurry.[2]

of the component phases before and after transformation is the driving force.

In many cases the final equilibrium state is not reached and the system rests in a state of metastable equilibrium.

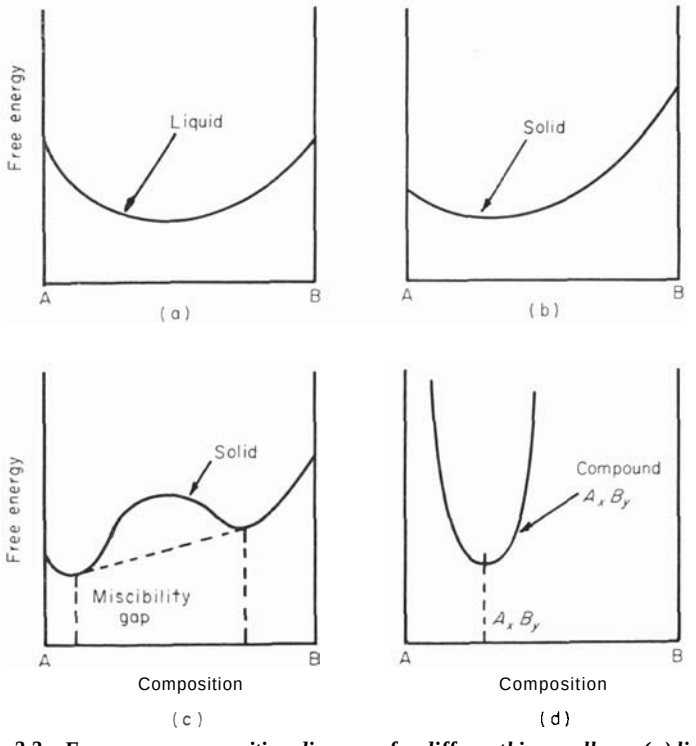

Fig. 2.2 Free-energy composition diagrams for different binary alloys: (a) liquid; (b) solid; (c) solid with a miscibility gap; and (d) an intermetallic compound.

For the transformation from liquid to solid the volume free energy chance AG, is

$$\mathbf{AG_v} = G_{\mathrm{L}} - G_{\mathrm{S}}$$

where G, and G, are the free energies of the liquid and solid respectively. From eqn. (2.1)

$$\Delta G_{\mathrm{v}} = (H_{\mathrm{L}} - H_{\mathrm{S}}) - T(S_{\mathrm{L}} - S_{\mathrm{S}})$$

If we assume that the temperature dependence of the changes of enthalpy and entropy are small, then

$$H_{\mathrm{L}} - H_{\mathrm{S}} = \mathbf{L_m}$$

where I,,,,is the latent heat of melting. At the equilibrium melting point, since ΔG is zero, the entropy of melting is given by

$$S_{\mathrm{L}} - S_{\mathrm{S}} = \frac{L_{\mathrm{m}}}{T_{\mathrm{m}}}$$

Thus

$$\mathbf{AG_v} = L_{\mathrm{m}} \frac{\Delta T}{T_{\mathrm{m}}} - \frac{L_{\mathrm{m}} \cdot \Delta T}{T_{\mathrm{m}}} \qquad (2.2)$$

In this equation A T is the temperature interval between the equilibrium melting point and the temperature of transformation and is known as the supercooling.

2.2 HOMOGENEOUS NUCLEATION

2.2.1 Energetics of nucleation

The classical theory of nucleation was developed by Volmer and Weber,[3] and Becker and Doring[4] for the condensation of a pure vapour to form a liquid. The subsequent theory[5,6] for the liquid–solid transformation was based on this earlier work. The theory considered homogeneous nucleation, *i.e.* the formation of one phase by the aggregation of components of another phase without change of composition and without being influenced by impurities or external surfaces. Impurity particles and external surfaces are taken into account in heterogeneous nucleation theory (Section 2.3). Modifications to the classical theory are necessary to allow for the effects of compositional changes.

Consider the free energy changes which occur if a spherical embryo of solid is formed within a uniform liquid. First, there will be a change in free energy associated with the difference in volume free energy of the atoms in the solid and the liquid.† Second, there will be a term introduced because a number of the atoms occur in the transition region between liquid and solid. These atoms will be in a high energy state and are the origin of the surface free energy of the embryo.

† **One of the inherent difficulties of nucleation theory is associated with the use of macroscopic thermodynamic properties, *e.g.* volume free energy and surface energy, in microscopic situations. This is unavoidable but does not normally introduce serious numerical error.**

For a spherical embryo of radius r, the overall change in free energy, ΔG, is given by

$$\Delta G = 4\pi r^2 \gamma_{LC} + (\tfrac{4}{3})\pi r^3 \cdot \Delta G_v \qquad (2.3)$$

where γ_{LC} is the surface free energy (erg cm^{-2}). As above, ΔG_v is the volume free energy change (erg cm^{-3}). Above the melting point,

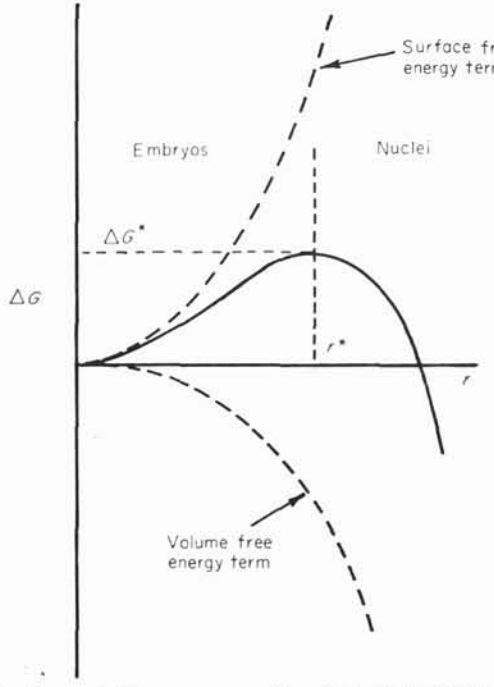

Fig. 2.3 The change in free energy resulting from the formation of a spherical embryo of solid in the liquid.

ΔG_v is positive and below it ΔG_v is negative. The variation of the different free energy terms below T_m and the overall change in free energy are shown in Fig. 2.3. Any embryos which form above T_m will rapidly disperse. On the other hand, below T_m, provided the embryo reaches a critical size with radius r^*, at which $(\partial(\Delta G)/\partial r) = 0$, it is equally probable that it will disperse or that it will grow as a stable nucleus. To form this critical nucleus a random fluctuation producing a localised energy change ΔG^* is required. Differentiating eqn. (2.3) and allowing for the sign of ΔG_v we find

$$r^* = \frac{2\gamma_{LC}}{\Delta G_v}$$

This is the critical nucleus size. Substituting from Eqn. (2.2) gives

$$r^* = \frac{2\gamma_{LC} \cdot T_m}{L_m \cdot \Delta T} \qquad (2.4)$$

The localised energy change, ΔG^*, can then be determined by introducing r^* into eqn. (2.3):

$$\Delta G^* = \frac{16\pi \gamma_{LC}^3 \cdot T_m^2}{3(L_m \cdot \Delta T)^2} \qquad (2.5)$$

ΔG^* is often referred to as 'the work of nucleation'. Since ΔG_v increases approximately linearly as the temperature falls, the critical radius decreases rapidly as does the work of nucleation (Fig. 2.4).

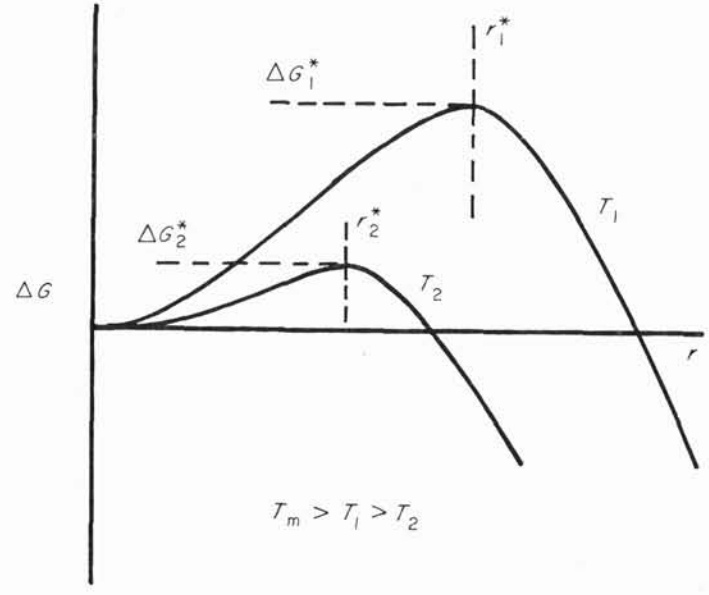

Fig. 2.4 The effect of decreasing temperature on the critical radius for nucleation and on the work of nucleation.

2.2.2 Rate of nucleation

The theory for the rate of nucleation also follows from that derived for vapours. Becker[7] originally proposed that the nucleation rate, I, in condensed systems, such as are involved in the liquid–solid transformation, was determined by an expression of the type

$$I = K \exp(-(\Delta G^* + \Delta G_A)/kT)$$

in the liquid will play an important part.? There is at present no theoretical treatment for this problem. However, experimental observations[10] on copper–nickel alloys showed that the undercooling required for homogeneous nucleation was —0.2 of the liquidus temperature.

The form of the nucleation rate equation is such that at very large undercoolings there should be a decrease in the rate of nucleation resulting from a decreased mobility of atoms. We might thus expect the curve of Fig. 2.5 to tend towards a maximum as indicated. For most metallic systems, however, it is not possible to cool through the range of temperature at which copious nucleation occurs at a rate fast enough to suppress nucleation. Quench rates of the order of 10^6 °C sec–' have been used unsuccessfully with melts of pure liquid metals. In binary alloy systems where redistribution of solute must occur as part of the nucleation process, some aniorphous solids have been produced using rapid quenching techniques.[11–13]

The occurrence of amorphous phases results from the combined influence of two exponential factors, one related to the transfer of

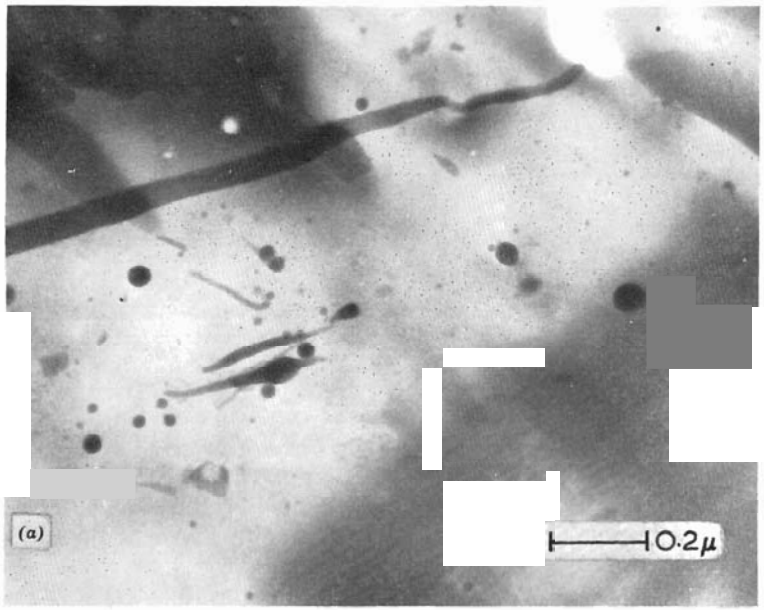

Fig. 2.6 (*a*)

† **There is some evidence that in special cases the** *earliest* **stages of nucleation and growth take place without solute** redistribution.[35]

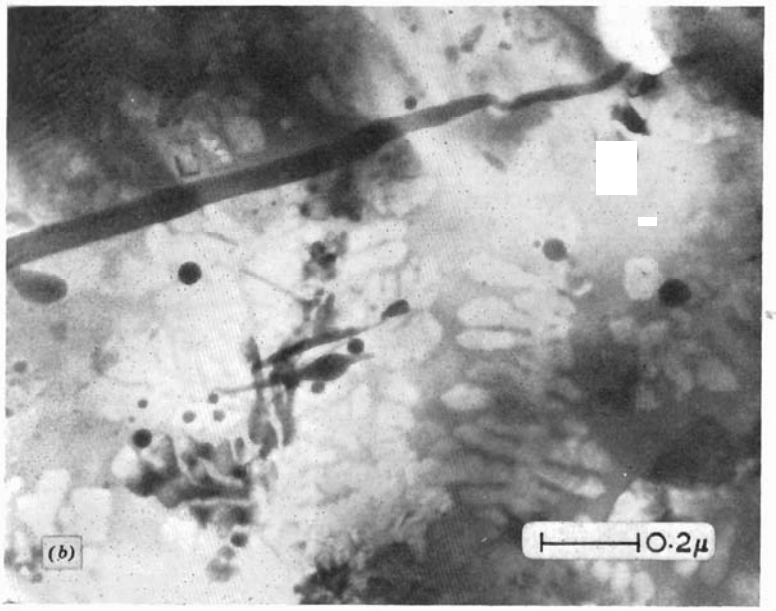

Fig. 2.6 The electron microstructure of splat-cooled tellurium–15 at. 90 germanium in (a) the amorphous state arid (b) after heating. The growth of dendrites can be seen clearly in the latter micrograph (Willens[13]).

atoms from the liquid to the solid and the other associated with bulk diffusion in the liquid. On reheating, transformation to the crystalline state occurs quite rapidly, as shown in Fig. 2.6.

It should be noted that the treatment given assumed a spherical nucleus. Simple modifications result from considering nuclei of other shapes. One of the more realistic shapes may be that described by Chalmers[14] in which it was proposed that the nucleus was bounded by planes of high atomic density (Fig. 2.7).

Before considering heterogeneous nucleation it is interesting to question how the liquid structure affects homogeneous nucleation. This has been considered by Walton.[15] The structure of the liquid influences the nucleation rate firstly through ΔG^*, since this term contains the volume free energy change **AG,**. If clustering occurs in the liquid this will aid nucleation. Oriani and Sundquist[16] have estimated that for most metals supercoolings of more than 10°C will be sufficient to promote embryo formation as the liquid structure orders. The structure of the liquid also has a direct effect on **AG,,** the diffusion term, and on the liquid–crystal interfacial energy, γ_{LC}.

shape together with segregation effects occurring during casting can have a significant influence on the physical, mechanical and chemical properties of the cast product. Most commonly, control is exerted by the use of nucleating agents (inoculants). The nature of heterogeneous nucleation and its relation to inoculant effectiveness has been reviewed by Chadwick.[24] As described above, the nucleation potency is strongly dependent on the contact angle (Fig. 2.8). For

TABLE 2.2

COMPOUNDS USED TO STUDY THE HETEROGENEOUS NUCLEATION OF ALUMINIUM FROM ITS MELT[a]

Compound	*Crystal structure*	δ *for close-packed planes*	*Nucleating effect*
VC	Cubic	0·014	Strong
TiC	Cubic	0·060	Strong
TiB_2	Hexagonal	0·048	Strong
AlB_2	Hexagonal	0·038	Strong
ZrC	Cubic	0·145	Strong
NbC	Cubic	0·086	Strong
W_2C	Hexagonal	0·035	Strong
Cr_3C_2	Complex		Weak or nil
Mn_3C	Complex		Weak or nil
Fe_3C	Complex		Weak or nil

[a] Data from Chadwick.[24]

easy nucleation, low contact angles are required and evidence[19,25] supports the view that when the chemical parameters (bond type and bond strength) of the crystal and the substrate are similar the lattice mismatch between crystal and substrate is important. The lattice mismatch is defined as

$$\delta = \frac{Aa}{a}$$

where a is lattice parameter of the crystal being nucleated and Aa is the difference in the lattice parameters of crystal and substrate. Table 2.2 gives data for the heterogeneous nucleation of aluminium from its melt. It is apparent from this table that the chemical parameters have a greater effect than originally anticipated.[19] Nevertheless, despite the fundamental difficulties, efficient inoculants have been determined for most metals, for the most part by processes of trial and error. The results of Cibula,[25] Reynolds and Tottle[26] and Hall and Jackson[27] (see Fig. 2.10) are good examples of the practical development of effective inoculation procedures.

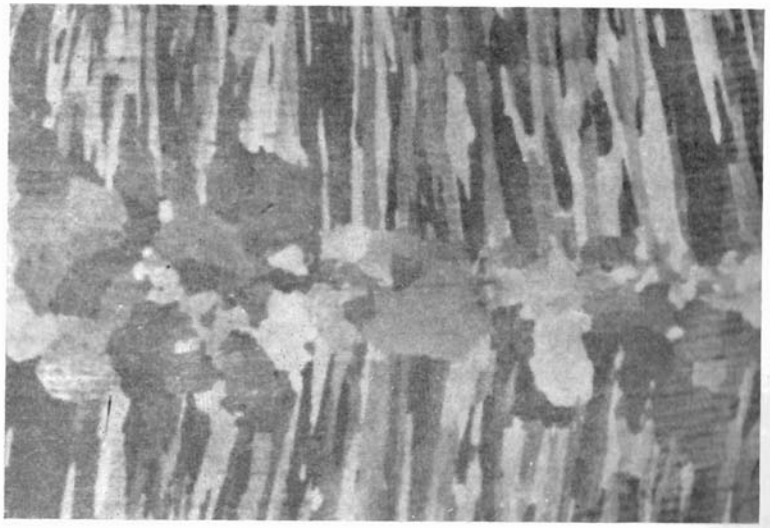

(*a*)

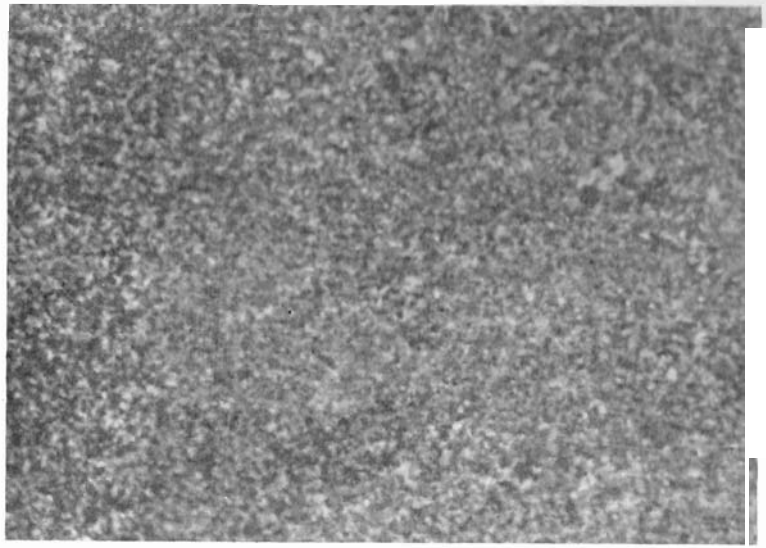

(*b*)

Fig. **2.10** (*a*) **Normal coarse-grained** *structure in* **18%** *chromium–12%* **nickel** *steel.* (*b*) *Same* **steel as (a) refined** *by inoculation* **(Hall** *and Jackson*[27]).

2.4 DYNAMIC NUCLEATION

So far we have considered nucleation in an essentially static situation. Only temperature and the potency of nucleating substrates have been considered as having any effect. It is possible to induce nucleation by subjecting the liquid metal to dynamic stimuli. Two distinct forms can be identified:

(i) an initial nucleation phenomenon induced mechanically, and
(ii) a grain-refining action which is a consequence of crystal multiplication, and is not a nucleation event in the normal sense.

The latter form is usually the result of fragmentation of existing solid. It is an important means of exerting control over the grain structure and we will examine this in some detail in Chapter 6.

There are few reliable data concerning true dynamic nucleation [(i) above]. Walker,[28] Stuhr[29] and Frawley and Childs[30] have all shown how mechanical vibrations can cause nucleation to occur at lower supercoolings than normally required. It was proposed by Chalmers[31] that cavitation followed by internal evaporation was responsible. This was disproved, however, by Hickling.[32] The most feasible hypothesis is that of Vonnegut,[33] who argued that the positive pressure wave generated by the collapse of an internal cavity in the liquid could be large enough to raise the melting point for metals which contract on freezing by an amount sufficient to increase the effective supercooling of the melt and thus to produce nucleation. Nucleation in systems which expand on freezing would be affected similarly by the rarefaction following the initial pressure pulse. The hypothesis has some support from both calculation[30] and experiment.[34]

REFERENCES

1. Cottrell, A. H. (1955). ***Theoretical Structural Metallurgy,*** Arnold, London, p. 139 ***et seq.***
2. Darken, L. S. and Gurry, R. W. (1953). ***Physical Chemistry of Metals,*** McGraw-Hill, New York, p. 326 ***et seq.***
3. Volmer, M. and Weber, A. (1926). ***Z. Phys. Chem.,*** **119,** 227.
4. Becker, R. and Döring, W. (1935). ***Ann. Phys.,*** **24,** 719.
5. Turnbull, D. and Fisher, J. C. (1949). ***J. Chem. Phys.,*** **17,** 71.
6. Holloman, J. H. and Turnbull, D. (1953). ***Progress. Met. Physics,*** **4,** 333.
7. Becker, R. (1938). *Ann. Phys.,* **32,** 128.
8. Turnbull, D.' 1950). ***J. Metals,*** **188,** 1144.

9. Turnbull, D. (1950). ***J. Appl. Phys.,*** 21, 1022.
10. Tarshis, L. A., Walker, J. L. and Rutter, J. W. (1971). ***Met. Trans.,*** **2,** 2589.
11. Duwez, P., Willens, R. H. and Klements, W., Jr. (1960). ***J. Appl. Phys.,*** **31,** 1136.
12. Duwez, P. and Willens, R. H. (1963). ***Trans. Met. Soc. AIME,*** **227,** 362.
13. Willens, R. H. (1962). J. ***Appl. Phys.,*** **33,** 3269.
14. Chalmers, B. (1959). *Physical Metallurgy,* John Wiley, New York, p. 246.
15. Walton, A. G. (1969). *Nucleation* (Ed. by A. C. Zettlemoyer), Dekker, New York, p. 225.
16. Oriani, R. A. and Sundquist, B. E. (1962). ***J. Chem. Phys.,*** **36,** 2604.
17. Turnbull, D. (1950). ***J. Chem. Phys.,*** **18.** 198.
18. Volmer, M. (1929). *Z. Electrochem.,* **35,** 555.
19. Turnbull, D. and Vonnegut, B. (1952). *Ind. Eng. Chem.,* **44,** 1292.
20. Sundquist, B. E. and Mondolfo, L. F. (1961). *Trans. Met. Soc. AIME,* **221,** 157.
21. Sundquist, B. E. and Mondolfo, L. F. (1961). ***Trans. Met Soc. AIME,*** **221,** 607.
22. Turnbull, D. (1952). ***J. Chem. Phys.,*** **20,** 411.
23. Mondolfo, L. F. (1965). ***J. Aust. Inst. Met.,*** **10,** 169.
24. Chadwick, G. A. (1969). ***Met. and Materials,*** **3,** 77.
25. Cibula, A. (1949). ***J. Inst. Metals, 76,*** 321.
26. Reynolds, J. A. and Tottle, C. R. (1951). ***J. Inst. Metals,*** **80,** 93.
27. Hall, H. T. and Jackson, W. J. (1968). ***The Solidification of Metals,*** ISI Publication 110, p. 313.
28. Walker, J. L. (1959). ***Physical Chemistry of Process Metallurgy*** (Ed. by G. R. St. Pierre), Interscience, New York, p. 845.
29. Stuhr, D. (1962). M.S. Thesis, Rennselaer Polytechnic Institute, New York.
30. Frawley, J. J. and Childs, W. J. (1968). ***Trans. Met. Soc. AIME,*** **242,** 256.
31. Chalmers, B. (1965). ***Liquids: Structures, Properties, Solid Interactions,*** (Ed. by T. J. Hughel), Elsevier, Amsterdam, p. 308.
32. Hickling, R. (1965). ***Liquids: Structures, Properties, Solid Interactions,*** (Ed. by T. J. Hughel), Elsevier, Amsterdam, p. 324.
33. Vonnegut, B. ***(see*** Turnbull, D.) (1950). ***Thermodytzamics in Physical*** *Metallurgy,* ASM, Cleveland, p. 282.
34. Hunt, J. D. and Jackson, K. A. (1966). ***J. Appl. Phys.,*** **37,** 254.
35. Biloni, H. and Chalmers, B. (1965). ***Trans. Met. Soc. AIME,*** **233,** 373.

or a few unoccupied sites. The first type of interface was classified as 'rough' and the second type of interface as 'smooth' or 'faceted'. Further analysis showed that most metals had a $\lesssim 2$, in which case they were expected to grow with a rough interface whose position was approximately determined by the isotherm fractionally below T_m. Inorganic and organic liquids normally have a $\gtrsim 5$, in which case the growing nucleus rapidly becomes bounded by crystallographic faces. A small group of materials exist, e.g. silicon, bismuth, which occupy the middle ground in that $\alpha = 2$–5 for different faces. In these materials the behaviour is more complex and often a mixed growth form results.[3,4] It must be emphasised that the analysis of Jackson considers the relative free energy change with the fraction of sites occupied on the surface, and thus in essence it does not predict the true minimum energy form of a stationary equilibrated interface. This latter point has been examined by Miller and Chadwick.[5]

Nevertheless, the treatment has been of considerable value in increasing the understanding of the factors influencing the interface form during solidification. The studies of Jackson and Hunt[6] and Jackson *et al.*[4]—in which transparent organic crystals, chosen with a range of α-factors and thus analogous to a range of materials both metallic and non-metallic, were observed during solidification—were largely in agreement with Jackson's original predictions.' Figure 3.2 shows examples of the different types of interface.

There are inadequacies in the theory of Jackson, particularly those associated with kinetic influences and related to details of the crystal structure, *e.g.* the anisotropy of growth.

One approach to the problem of the relation between the interface structure and the growth of the interface was that of Cahn[7] *(see also* Cahn ***et*** *al.*[8]) who considered in detail the 'diffuseness' of the interface, *i.e.* the number of atomic layers comprising the transition from solid to liquid. Cahn concluded that the degree-of diffuseness was dependent on both the material and the driving force for transformation. The driving force is determined by the undercooling at the interface. As a result it was predicted that at low driving forces the interface would be discrete and propagation would take place by the transverse motion of interface steps, while at large driving forces the growth would be normal with the interface diffuse. This theory was examined in detail by Jackson *er al.*,[4] who compared the predictions with experimental data for a considerable range of materials. The examination showed that the evidence did not support the predictions.

Jackson[9] followed up his earlier work with a more general theory of crystal growth which related both structure and growth rate. This led to reasonable predictions for growth rate anisotropy. The theory

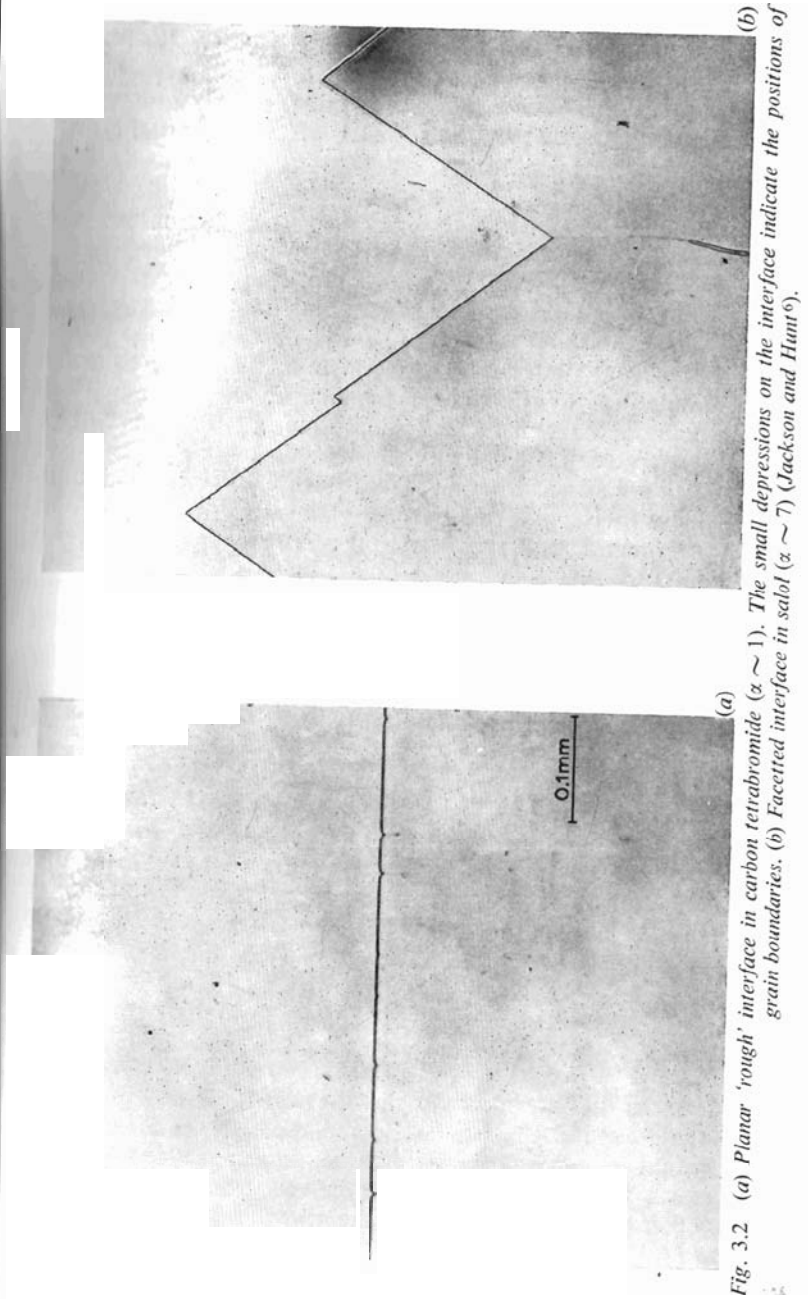

Fig. 3.2 (a) Planar 'rough' interface in carbon tetrabromide (α ~ 1). The small depressions on the interface indicate the positions of grain boundaries. (b) Facetted interface in salol (α ~ 7) (Jackson and Hunt[6]).

predicted interface structures which correlated well with the previous predictions' based on the α-factor (eqn. 3.2). This theory was extended by the development of a fundamental rate equation for crystal growth[10] and this is examined further in the next section. It was, however, unable to explain the anisotropy of crystal growth for processes such as dendritic growth (see Section 4.6).

3.2 GROWTH OF THE INTERFACE

The growth rate of a crystal depends on the difference between the rate at which atoms add themselves to the interface and the rate at which they leave the interface. In the previous section two principal forms of interface were characterised, one atomically rough and non-crystallographic in character and the other smooth and crystallographically faceted. Different mechanisms of interface advance can be attributed to these different interface forms. The normal procedure is to define a mechanism and calculate the mean rate of interface motion as a function of the undercooling AT. Three mechanisms will be considered:

(i) the normal growth mechanism;
(ii) growth by repeated surface nucleation; and
(iii) growth on imperfections.

The latter two mechanisms require the existence of growth steps on the interface.

3.2.1 Normal growth

In normal growth[11] all sites on the interface are considered to be equivalent and the interface advances by the continuous random addition of atoms. The theory was based on earlier work by Wilson[12] and Frenkel[13] and it predicts that the mean growth rate, $\bar{R}$, is proportional to the undercooling, *i.e.*

$$\bar{R} = \mu_1 \cdot \Delta T \qquad (3.3)$$

where p, is a constant.

For normal growth the growth rates can be quite high and the requirement of site equivalence implies the need for a rough interface. This is the growth mechanism considered applicable to most metals. The constant μ_1 can be calculated to be ~ 1 cm sec^{-1} K^{-1}. Thus high growth rates are expected for relatively small undercoolings. On the other hand, it follows that at the growth rates encountered in practice ($\sim 10^{-2}$ cm sec^{-1}, see Table 4.1) the undercoolings are immeasurably small. This makes experimental verification of the

mal growth theory difficult. The rate controlling mechanism is ·ully the rate of removal of latent heat. Since the materials with ıgh interfaces also tend to have low latent heats of melting, the ınal growth rates are comparatively easily sustained.

? Growth by surface nucleation

. ■ . theory[14] (see also Hollomon and Turnbull'[15]) assumes that the tal interface is smooth (faceted) and that growth proceeds by the mogeneous nucleation of new layers in the form of disc nuclei · h prow *laterally* until a complete layer is formed. This is shown

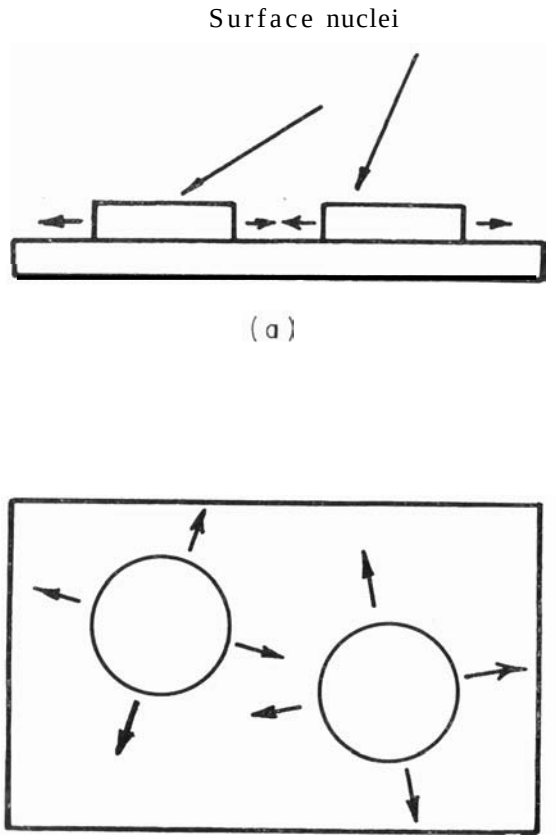

· ı *Schematic view of the formation of disc-shaped nuclei on a crystal* · *(a) view parallel to the surface; and (b) view normal to the surface.*

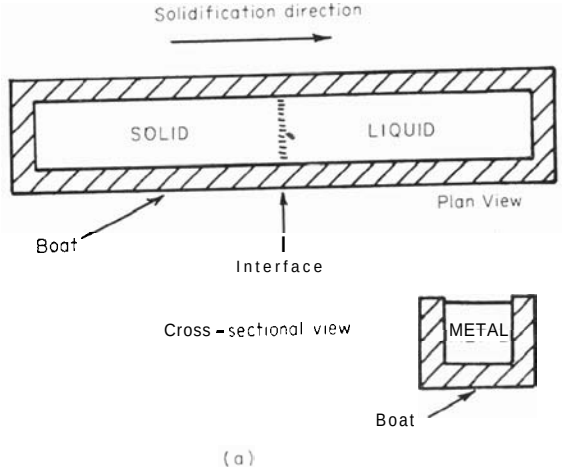

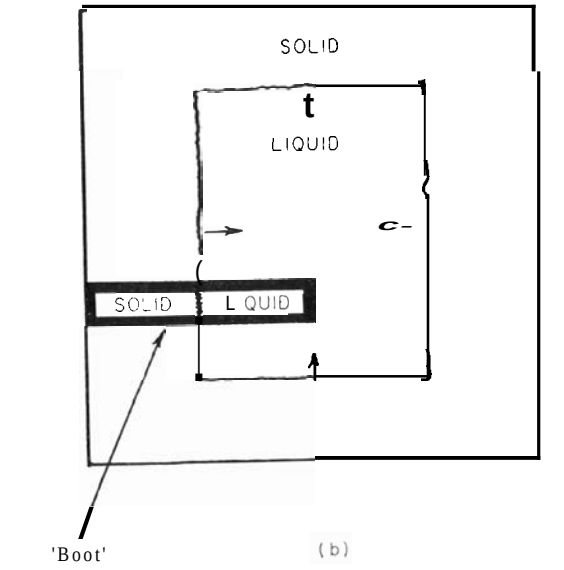

Fig. 4.2 *(a) A casting boat used for controlled directional solidification (schematic). The metal is shown as partially solidified. (b) Schematic view of the cross section of a partially solidified ingot showing how the casting boat can he considered as a section of the ingot.*

If the effect of the solute is to lower the liquidus temperature, then $k_{\mathrm{E}} < 1$ and vice versa.

It is sometimes convenient to define an 'effective' distribution, k_{E}, as

$$k_{\mathrm{E}} = \frac{\text{instantaneous composition of solid formed}}{\text{average composition of the liquid at that time}}$$

This definition is of importance in Section 4.3 when we consider solute redistribution effects during solidification.

(e) The *slope of the liquidus* ***line*** is given the symbol m. In their classical paper on solute redistribution, Tiller ***et*** al.' defined the liquidus slope shown in Fig. 1(a) as ***positive*** m and that shown in Fig. 1(b) as *negative* m. It should be noted that although this is contrary to normal mathematical practice, this convention has been adhered to throughout the literature on solidification and will be followed in this chapter.

(f) The earliest solidification studies of Chalmers and his co-workers involved the ***unidirectional*** *solidification* of metals and alloys under controlled conditions in casting 'boats' of graphite or a similar material. The solidification process in the boat was essentially treated as if it were a section from a larger ingot or casting undergoing solidification, as shown in Fig. 4.2. This approach yielded valuable fundamental data on solidification processes and has been widely adopted since. We will have frequent occasion to refer to this type of unidirectional solidification procedure throughout this chapter.

4.2 PURE METALS

4.2.1 Interface **forms**

The growth of puremetals in a region ofpositive temperature gradient is controlled by the flow of heat away from the interface through the solid. The interface is normally rough and isothermal, being at a temperature below the equilibrium temperature just necessary to provide sufficient kinetic driving force. This kinetic undercooling has been estimated as $\sim 0{\cdot}01^{\circ}\mathrm{K}$. Non-metallic materials of high purity are expected to behave in a similar way within the constraints conferred upon them by the need to fulfil the interface requirements outlined in the previous chapter. The growing interface for both groups of materials should progress in a stable form. Any localised instability formed on the interface would project into a region at a temperature higher than the melting temperature and would rcmelt to restore the isothermal interface. The sequence of events is illustrated schematically in Fig. **4.3.**

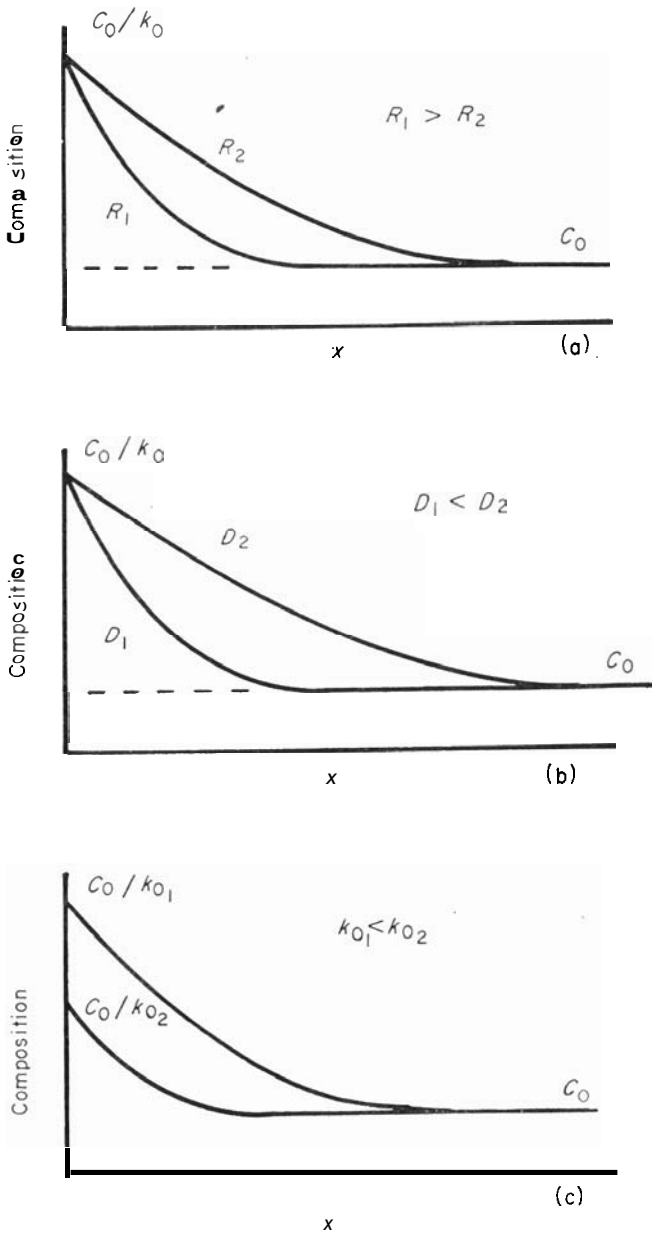

Fig. 4.9 Changes in the solute concentration ahead of a growing interface for changes in the growth parameters: (a) growth rate; (b) diffusivity; (c) distribution coefficient.

For solute concentrations higher than about 0·5% the solute pile-up effects are very marked and the physical nature of the interface alters to a non-planar configuration (this is considered in detail in the next section). Under these conditions, eqn. (4.2). is no longer valid, although it can be used to give some approximate indication

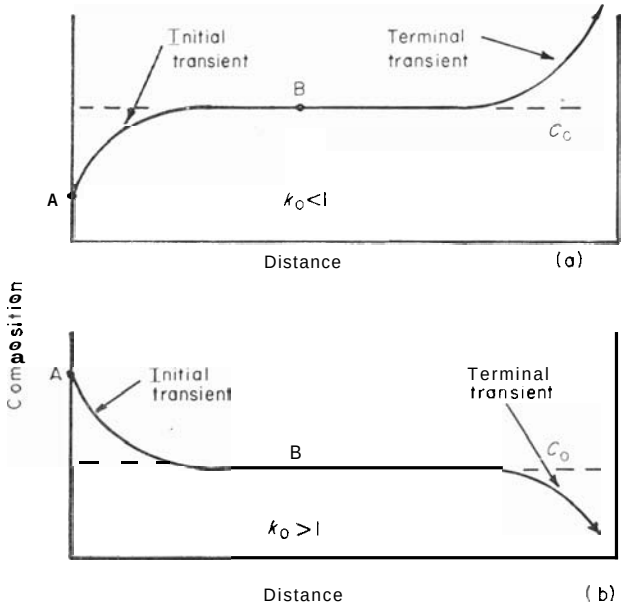

Fig. 4.10 *Concentration–distance profiles* ***for a bar solidified*** *under condition: where solute* ***transport*** *in* ***the liquid is by*** *diffusion* ***only: (a)*** $k_0 < 1$*; (b)* $k_0 > 1$.

of the solute distributiori near the interface. Calculation shows that the solute pile-up would seldom exceed a thickness of 0·1 mm without a significant change in the interface form.

For a case in which eqn. (4.2) holds, if a boat full of liquid of initial composition C, is solidified to a bar under the conditions considered above, the final solute distribution is as shown in Fig. 4.10, making allowance for the initial and terminal transients. At points A and B on these two curves the compositions of the solid formed instantaneously are C_0k_0 and C_0, respectively. The average composition (ignoring the small *overall* average increase resulting from the localised interface pile-up) in both cases is C_0. Thus the *effective* ***distribution coefficients*** are k, and 1 for the two cases. The distribution coefficient is therefore seen to vary from the equilibrium value k_0 to the value 1 as the steady-state is approached.

(v) low diffusivity in the liquid;
(vi) very low k_0 for $k_0 < 1$ or very high k_0 for $k_0 > 1$.

In the presence of constitutional supercooling the undercooling is,

$$\Delta T = T_L - T$$

Thus

$$\Delta T = \frac{mC_0(1 - k_0)}{k_0}\left[1 - \exp\left(-\frac{Rx}{D}\right)\right] - Gx \qquad (4.8)$$

This is as shown in Fig. 4.10. The maximum undercooling can be determined from eqn. (4.8) and is,

$$\Delta T_{max} = \frac{mC_0(1 - k_0)}{k_0} - \frac{GD}{R}\left[1 + \ln\frac{(mC_0(1 - k_0)R)}{GDk_0}\right] \qquad (4.9)$$

This maximum undercooling occurs at a point given by

$$x = \frac{D}{R}\log_e\left[\frac{mC_0(1 - k_0)R}{GDk_0}\right] \qquad (4.10)$$

The above treatment assumes that solute mixing in the liquid is the result of diffusion only. It can be modified to allow for partial or complete mixing in the liquid (*see* Chalmers[12]). In these circumstances long-range segregation will still occur.

4.5 STRUCTURAL EFFECTS RESULTING FROM SOLUTE REDISTRIBUTION IN ALLOYS

In the absence of constitutional supercooling, the behaviour during growth is essentially the same as that of pure materials with the exception that long-range segregational effects occur which are associated with the initial and final transients in the solidification process (Fig. 4.13).

The existence of a zone of constitutional supercooling, and thus a negative gradient of free energy, ahead of the interface will make an initially planar interface unstable to perturbations in shape. At low degrees of supercooling a cellular interface develops (Fig. 4.17) from the planar interface after first becoming pock-marked and then showing elongated cells. The breakdown from the planar to the cellular form can be shown experimentally to be governed by eqn. (4.7).[13,14] As the degree of supercooling increases the cell caps becomes extended and eventually branch to form cellular dendrites

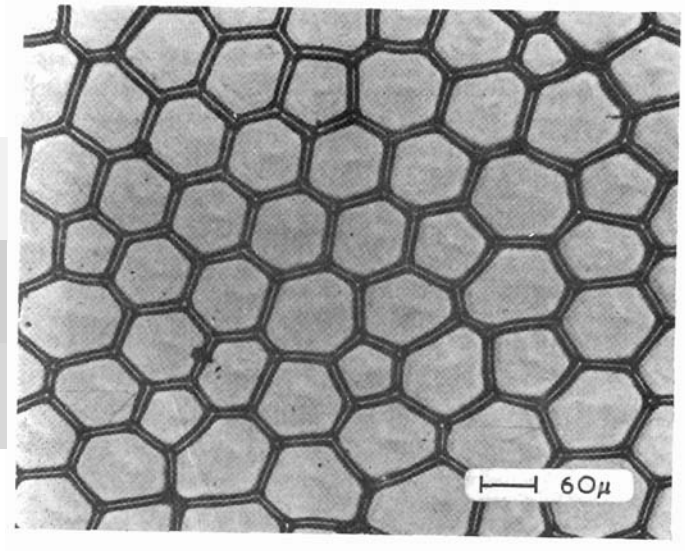

(*a*)

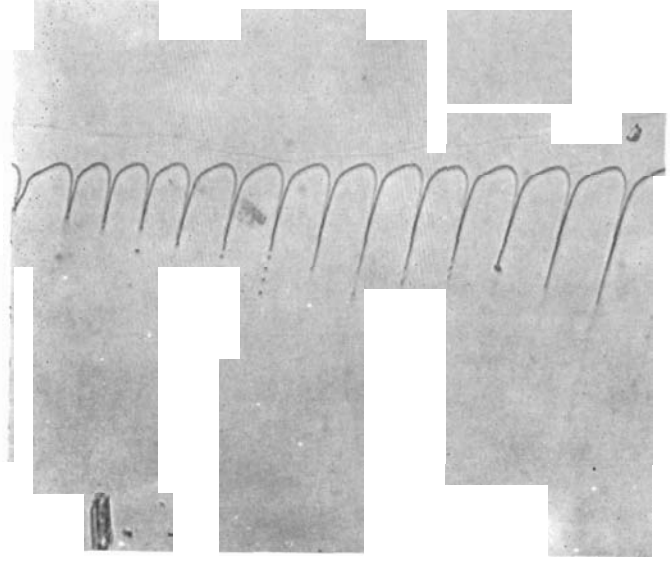

(*b*)

Fig. 4.17 *The cellular interface structure: (a) normal view of a decanted interface; and (b) view of growing interface in impure carbon tetrabromide (Jackson and Hunt*[15]*).*

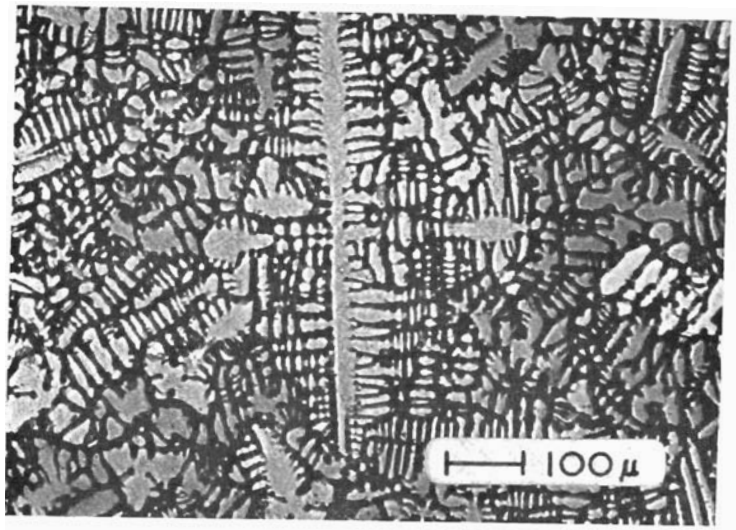

(*a*)

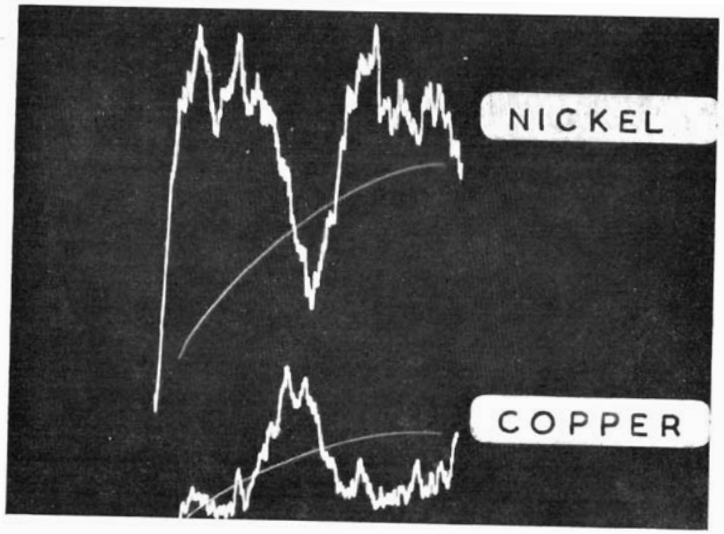

(*b*)

Fig. 4.20 *Coring in chill-cast cupronickel* ($k_0 < 1$)*: (a) as-cast structure; and (b) electron-beam microanalyser trace across the boundary between two dendrite arms. The qualitative nature of the segregation is apparent as a maximum and a minimum in the copper and nickel respectively.*

(Fig. 4.18). There is no clear criterion for the transition from cells to cellular dendrites.[14] The overall transition sequence is as shown in Fig. 4.19. In the case of both cells and cellular dendrites, microsegregation occurs. The intercellular regions are rich in solute for $k_0 < 1$ and depleted of solute for $k_0 > 1$. Under these conditions, long-range segregation effects similar to those shown in Fig. 4.13 are also bound to occur.

On a macroscopic scale this mean that a dendrite will show a variation in composition from inside to out, *i.e.* the phenomenon of *coring*. This is illustrated in Fig. 4.20; in this figure the dendritic structure is clearly evident. Although it cannot be resolved, the dendrite arms would undoubtedly show microscopic cellular segregation. Both forms of segregation can be eliminated by a homogenising heat treatment although, of course, macrosegregation effects involve long diffusion distances and thus long heat-treatment times. The effect of homogenisation is shown in Fig. 4.21.

A quite different approach to the problem of interface breakdown is that of Mullins and Sekerka,[16] who considered the stability of the interface in the presence of shape fluctuations. This treatment has some advantages, particularly since it predicts some of the parameters, *e.g.* cell size, which were not treated in the original analysis of constitutional supercooling. The treatment is mathematically complex and details can be obtained from the original paper.

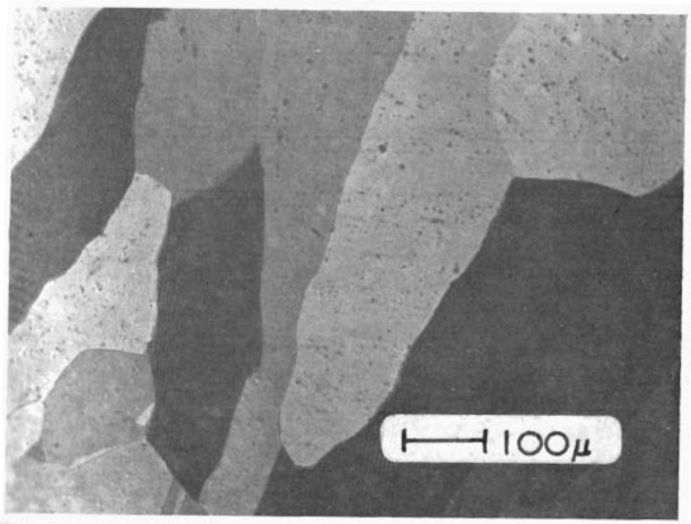

Fig. 4.21 (*a*)

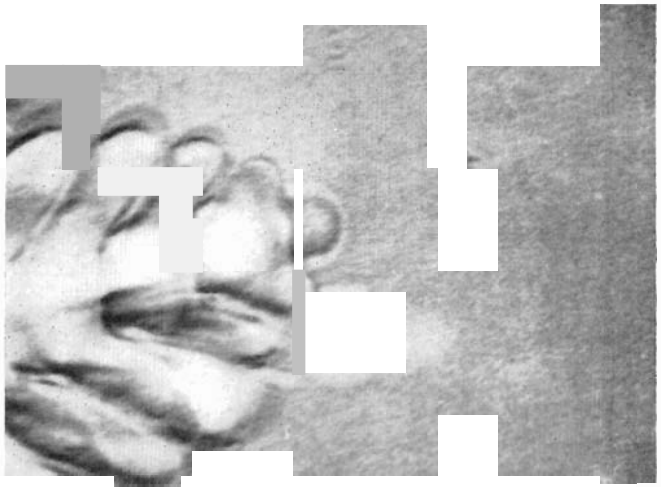

Fig. 4.22 (*a*)

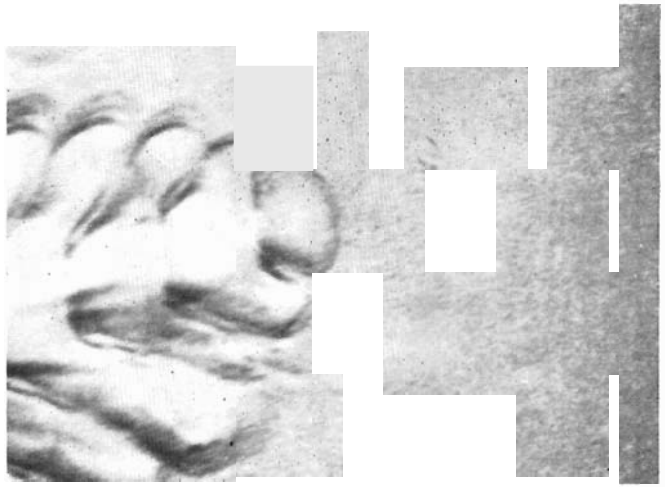

Fig. 4.22 (*b*)

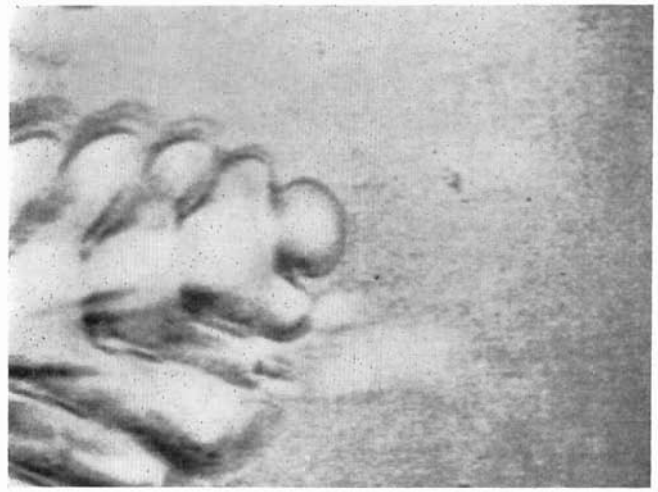

(*c*)

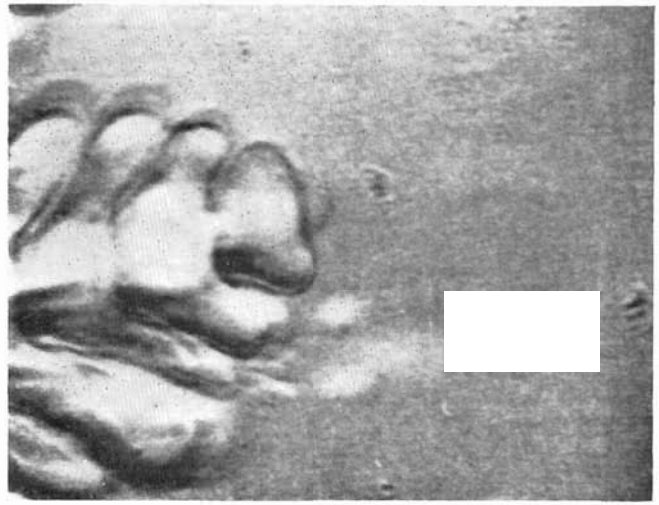

(*d*)

Fig. 4.22 *Tip of a growing dendrite showing progressive steps in tip morphology. The time interval between* (*a*) *and* (*b*) *was* 1·2 *sec; between* (*b*) *and* (*c*) 1·2 *sec; and between* (*c*) *and* (*d*) 2·1 *sec* (*Morris and Winegard*[23]).

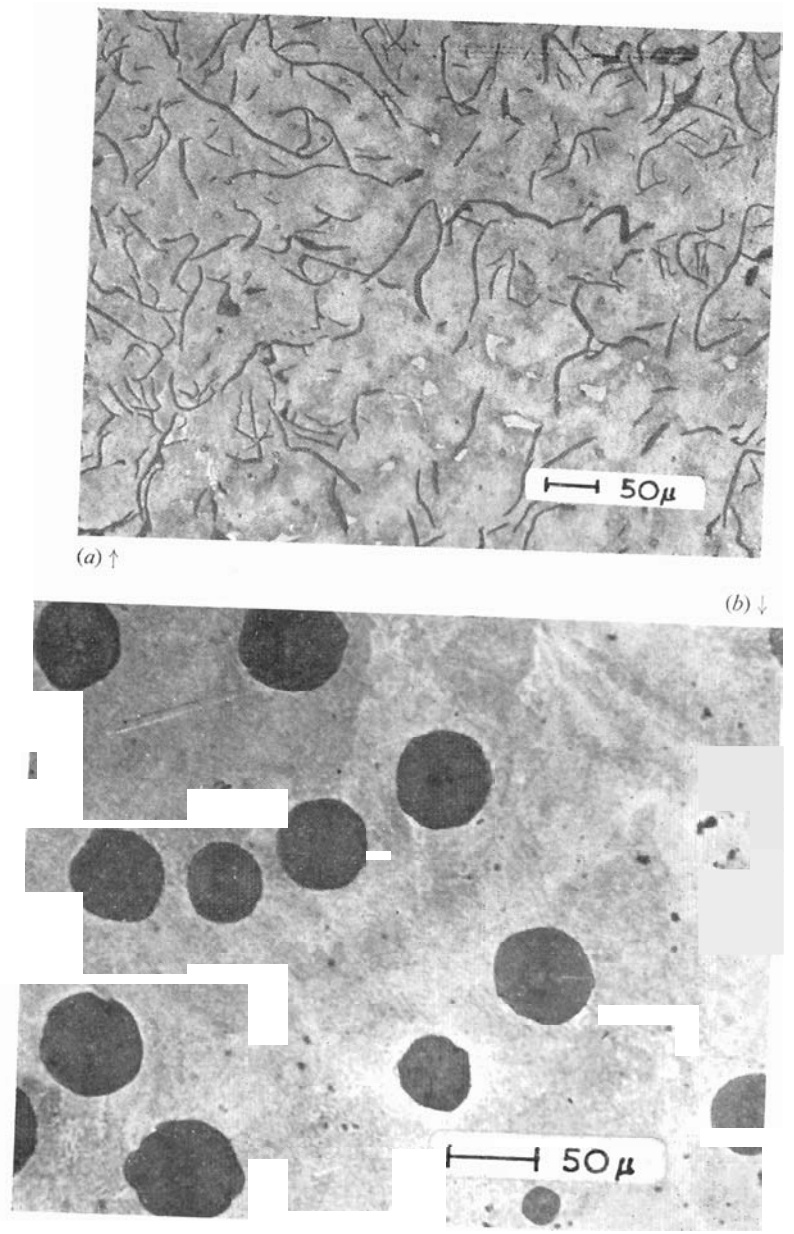

Fig. 5.11 *(a) Normal* **as-cost** *grey cast iron showing flake graphite.* **(b)** *Modified* **spheroidal** *graphite* **cast iron.**

are both examples of important structural modifications in the development of microstructure.

The recent work of Day[22] has confirmed that this modified structure is the result of a change in the mode of growth and not the result of a change in nucleation behaviour as was earlier proposed.[23,24] The coarse silicon structure of slow-cooled alloys is altered if rapid growth rates are used. A similar effect is produced by adding a modifier (sodium) to the slow-cooled alloy. These are illustrated in Fig. 5.10. The silicon morphology is basically the same in *both* the growth rate-modified *and* the additive-modified alloys.

The modification that occurs in the iron–carbon system is even more striking, as shown in Fig. 5.11. Here the normal structure of grey cast iron, graphite flakes in a pearlitic matrix, is altered to graphite spheroids in a pearlitic matrix. In this case also there is a dramatic increase in mechanical properties, particularly toughness. The bulk of the evidence[25] indicates that the spherulites separate directly from the melt without the simultaneous formation of any other solid. Solidification appears to proceed by the growth of the spherulite surrounded by an envelope of austenite, although this hypothesis has been questioned.[26] The reasons for the change in graphite morphology on the addition of magnesium are far from clear, although it has been established[27] that the additive influences the growth of the graphite rather than affecting the nucleation behaviour.

5.1.4 Other eutectic systems

There are a number of other aspects of eutectic solidification, particularly the divorced eutectics,[28] and the pseudo-binary eutectics[29] which occur in multicomponent systems. These are both very specialised topics and will not be dealt with further here.

5.2 PERITECTICS

Figure 5.12 gives the phase diagram for the almost ideal peritectic system, silver–platinum. As discussed by Uhlmann and Chadwick[30] in the first detailed study of peritectic reactions, for virtually all compositions except those near the limits of the system, the microstructure after casting will consist of cored dendrites of one phase surrounded by the second phase. Thus with reference to Fig. 5.12 we would expect this structure for compositions from 30 to 90 wt % platinum. Furthermore, the peritectic reaction should seldom proceed to completion. When the primary phase has cooled to the peritectic

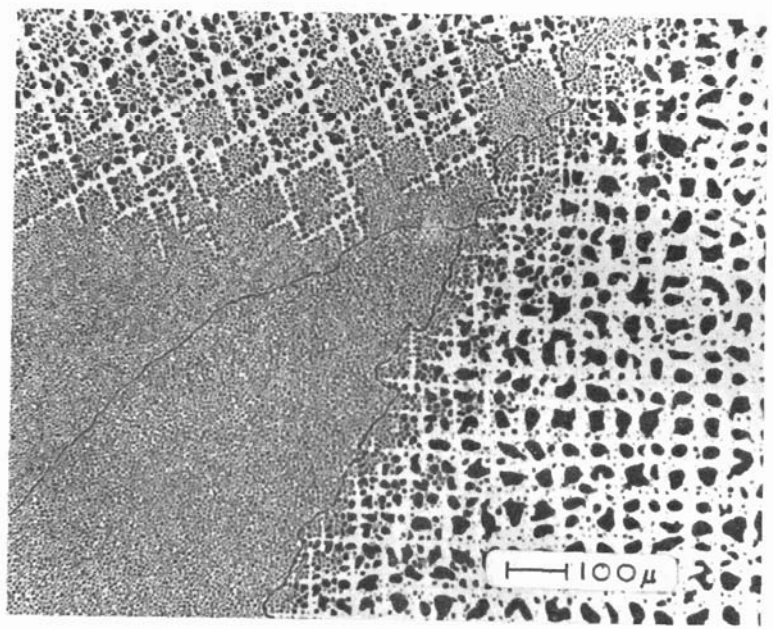

(*b*)

Fig. 5.16 (*a*) *Composition–velocity plot showing regions over which different microstructure types were observed.* (*b*) *Transverse section of transition regions showing composite and dendritic structures: copper—light phase, lead—dark phase. The characteristic alignment of the dendritic structure resulting from the crystallography of dendritic growth is clear* (*Livingston and Cline*[34]).

5.4 PARTICLES AND INCLUSIONS IN MELTS

Foreign particles which do not dissolve in either the liquid or the solid are often present during solidification. These insoluble particles are usually classified as *exogeneous* if they come from external sources (*e.g.* mould and ladle materials, dross) or *endogeneous* if they arise from reactions within the solidifying metal. The interaction between solid particles suspended in the liquid and the solid–liquid interface has been studied comprehensively by Uhlmann *et al.*[35] Using transparent materials, direct observations of particle–interface behaviour were made. For each system it was found that there was a critical growth rate below which the particles were 'pushed' by the interface and above which they were trapped in the solid. Figure 5.17 shows the pile-up of zinc particles at a solid–liquid thymol interface at low growth rate. The rate-controlling step was determined to be

the rate of diffusion of liquid to the growing solid behind the particle. A sufficient flux of liquid is needed to continuously replenish the solidifying material immediately behind the particle and thus keep the particle ahead of the interface. In the main, the critical growth

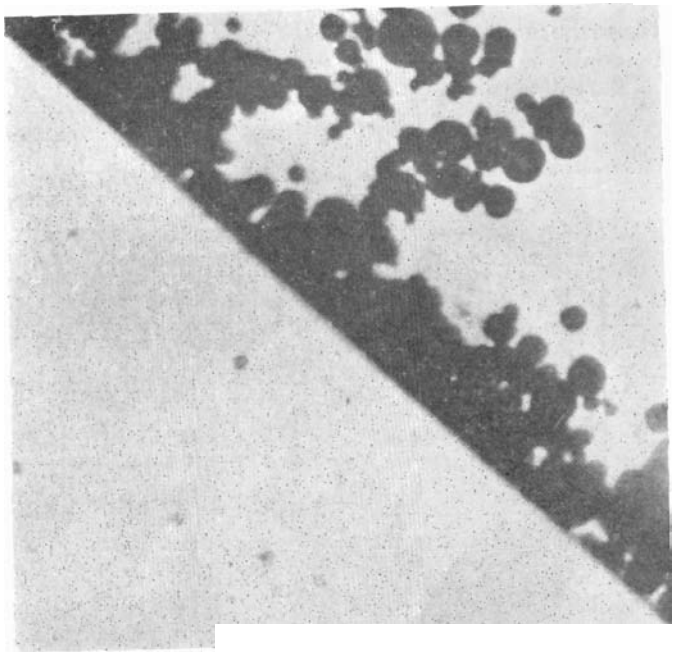

Fig. 5.17 *Pile-up of particles at a solid–liquid interface at low growth rate in the system thymol–zinc* (*Uhlmann et al.*[35]).

rates were all low ($\sim 10^{-3}$ cm sec^{-1}). It is thus expected that entrapment will occur in most practical cases. Towards the end of a solidification process, however, as the growth rates slow down, it is possible for particles to be swept together to produce quite deleterious accumulations of inclusions.

It is also possible for the solid inclusions to act as sites for heterogeneous nucleation (*see* Section 2.3) and it is recognised that they have an important role in ingot solidification.[36–38] To a large extent the segregation patterns observed in ingots (see Section 7.3) are influenced by the presence of inclusions.

In some cases the particles appear to have become grown-in because they have been trapped in isolated regions of liquid by the growth of dendrite branches. The constraints imposed on particle

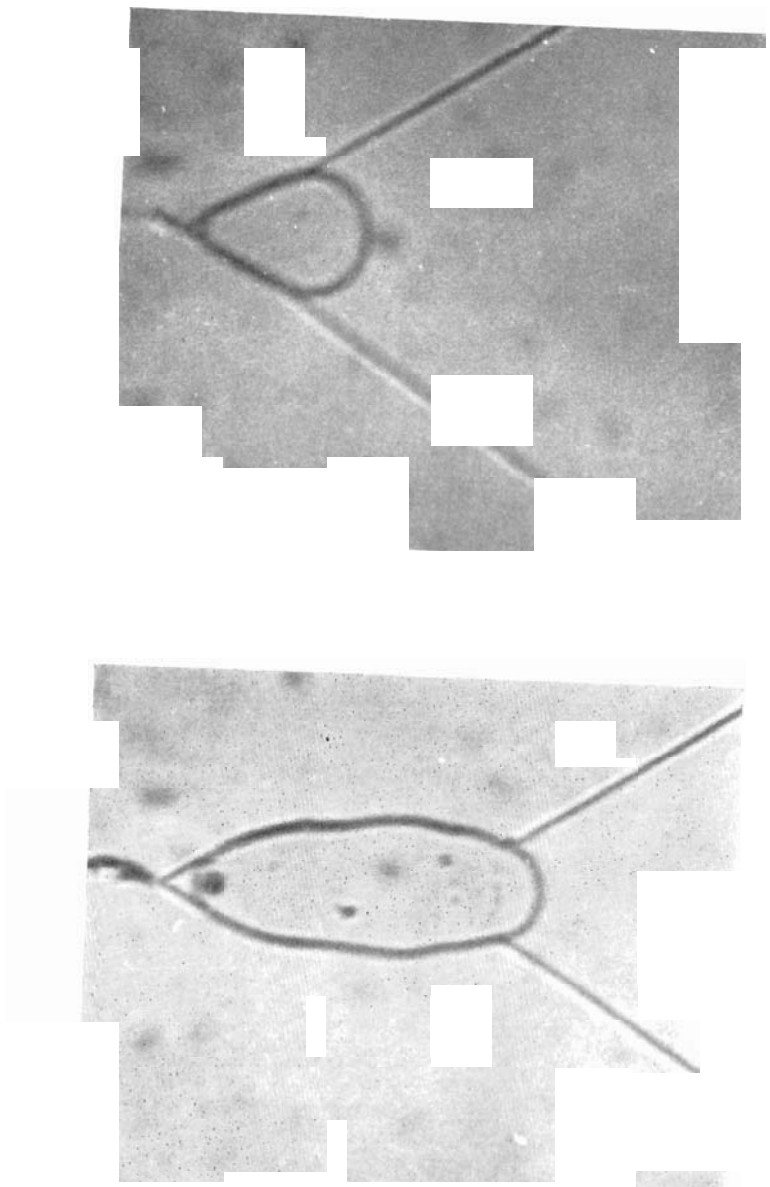

Fig. 5.20 Growth of agar bubble at the interface in solidifying salol: (a) nucleation and incorporation into the interface; (h) formation of the elongated blowhole (Woodruff[42]).

There are few reports of investigations dealing with the factors influencing the number, form and distribution of pores in solidified metals. McNair[43] and Jordan *et al.*,[44] for instance, give some data on the effects of gas content, ingot size and solidification conditions on porosity. It is to be hoped that more fundamental work of this type will be carried out. In the meantime it should be noted that effective empirical methods have been developed for the *control* of porosity in ingots and castings (see Section 9.1).

REFERENCES

1. Chadwick, G. A. (1963). *Prog. Mat. Sci.*, 12, 97.
2. Bell, J. A. E. and Winegard, W. C. (1965). **J.** *Inst. Met.*, 93, 457.
3. Rumball, W. M. and Kondic, V. (1966). *Trans. Met. Soc. AIME*, 236, 586.
4. Hunt, J. D. and Jackson, K. A. (1966). *Trans. Met. Soc. AIME*, 236, 843.
5. Hunt, J. D. and Chilton, J. P. (1962–63). **J.** *Inst. Met.*, 91, 338.
6. Chadwick, G. A. (1962–63). **J.** *Inst. Met.*, 91, 169.
7. Tiller, W. A. (1958). *Liquid Metals and Solidification*, ASM, Cleveland, p. 276.
8. Jackson, K. **A.** and Hunt, J. D. (1966). *Trans. Met. Soc. AIME*, 236, 1129.
9. Chadwick, G. A. (1963–64). **J.** *Inst. Met.*, 92, 18.
10. Moore, A. and Elliott, R. (1968). *The Solidification of Metals*, ISI Publication 110, p. 167.
11. Day, M. G. and Hellawell, *A.* (1968). *Proc. Roy. Soc.*, **A305,** 473.
12. Day, M. G. (1969). **J.** *Metals*, **21**(4), 31.
13. Cooksey, D. J. S., Munson, D., Wilkinson, M. P. and Hellawell, A. (1964). *Phil. Mag.*, 10, 745.
14. Hunt, J. D. (1968). **J.** *Crystal Growth*, 3–4, 82.
15. Hellawell, A. (1967). *Met. and Materials*, **1,** 361.
16. Davies, G. J. (1971). *Strengthening Methods in Crystals* (Ed. by *A.* Kelly and R. B. Nicholson), Applied Science, Barking, p. 485.
17. Mollard, F. R. and Flemings, M. C. (1967). *Trans. Met. Soc. AIME*, 239, 1526.
18. Mollard, F. R. and Flemings, M. C. (1967). *Trans. Met. Soc. AIME*, 239, 1534.
19. Chadwick. G. A. (1968). *The Solidification of Metals*, ISI Publication 110, p. 138.
20. Kerr, H. W., Plumtree, A. and Winegard, W. C. (1964–65). **J.** *Inst. Met.*, 93, 63.
21. Cooksey, D. J. S. and Hellawell, A. (1967). **J.** *Inst. Met.*, 95, 183.
22. Day, M. G. (1970). **J.** *Inst. Met.*, 98, 57.
23. Plumb, R. C. and Lewis, J. E. (1957–58). **J.** *Inst. Met.*, 86, 393.
24. Kim, C. B. and Heine, R. W. (1963–64). **J.** *Inst. Met.*, 92, 367.

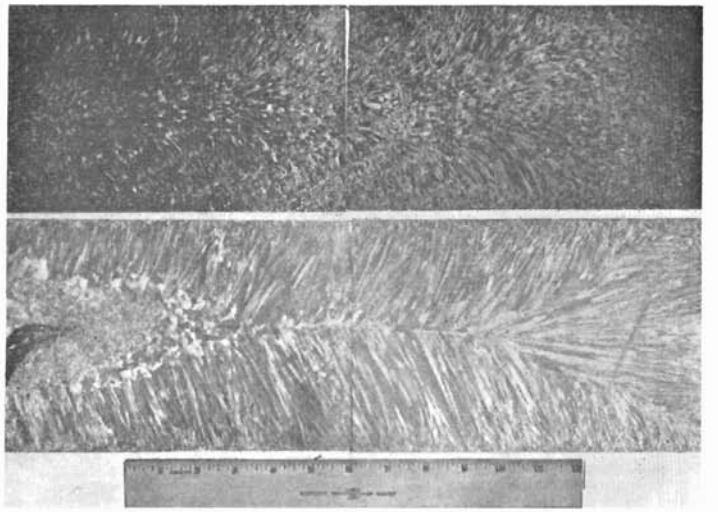

Fig. 6.15 *Macrostructure of stainless steel ingots, left—cast without ultrasonic vibration, right—cast with ultrasonic vibration* (*Lane* et al.[60]).

6.7 MACROSTRUCTURE OF FUSION WELDS

The mechanisms involved in the solidification of fusion welds are basically the same as those of normal castings. The main differences are,

(i) that the solidification rates are high, and

(ii) the temperature gradients in the liquid are steep. The temperatures in the centre of the weld pool are significantly higher than the melting temperature.

There is no equivalent of the chill zone in a fusion weld macrostructure because the partially melted grains at the molten zone boundary act as the sites which initiate columnar growth. This occurs as soon as the heat source moves away, and does not require a nucleation event. The grains grow in a columnar form and usually extend to the centre line (Fig. 6.16). The normal range of growth structures ranging from cellular through cellular–dendritic is observed,[64,65] as is some free dendritic growth. Although there is a great deal of turbulence in the weld pool,[66] and thus conditions favourable for dynamic grain refinement, an equiaxed zone is not normally observed. As discussed in a previous section, for an equiaxed zone to form, dendrite fragments (formed by remelting or fracture)

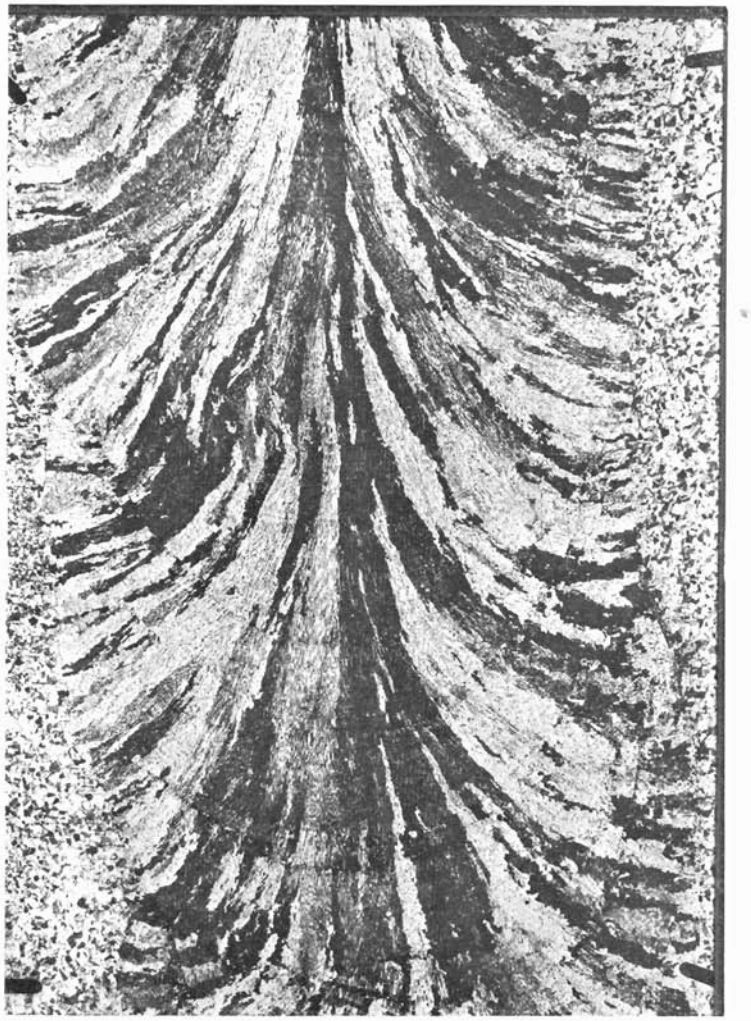

Fig. 6.16 *Columnar solidification pattern of a submerged-arc weld bead* (*Garland*[73]).

must survive without melting, in the liquid away from the interface. The very high temperatures at the weld pool centre make survival difficult.

The methods available for the control of cast structures (*see* Section 6.6) can be applied to fusion welds, but there are practical difficulties. Magnetic stirring,[67,68] ultrasonic vibration[69,70] and

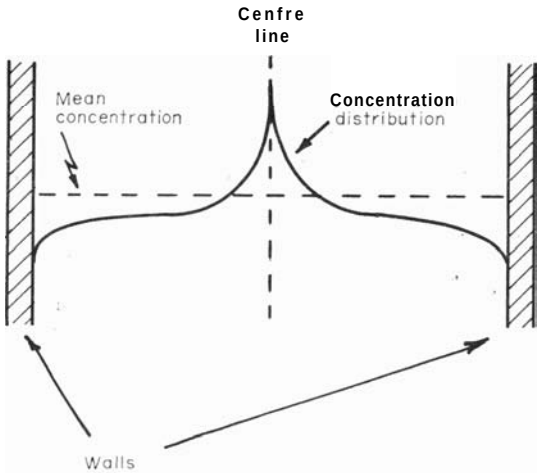

Fig. 7.7 ***Normal*** *segregation in a columnar ingot solidified with an almost planar interface (schematic).*

7.2.4 Inverse segregation

If we consider the solidification of an ingot of an alloy with k, < 1, as outlined above, we would expect the last liquid to solidify to be solute rich. If, however, there is pronounced dendritic growth, solute concentrations build up between the dendrites and there is fluid flow in the interdendritic spaces to compensate for the volume changes accompanying solidification. For most metals there is a contraction on solidification and thus the flow takes place in a direction opposite to the growth direction. As a result, solute-rich liquid is fed down the channels between the dendrites to give abnormally high solute concentrations at the outer regions of the ingot. The condition where the solute distribution is opposite to that expected for normal segregation is known as *inverse* segregation.

The existence of a network of interdendritic channels has been clearly demonstrated[37–39] and the way in which the last low melting point liquid to solidify (k, < 1) flows is evident by the ease with which tin *sweat* and *phosphide sweat* can occur. In these extreme cases of inverse segregation the interdendritic liquid actually bursts through the surface of the cast metal to form exudations (*see* Fig. 7.8). It has been shown by Youdelis[40] that this is mainly a result of loss of good thermal contact between the mould wall and the cast metal.

Following the complete qualitative description of inverse segregation by Adams,[41] a number of workers[42–44] have presented theories that account quantitatively for the solute flow and show how the

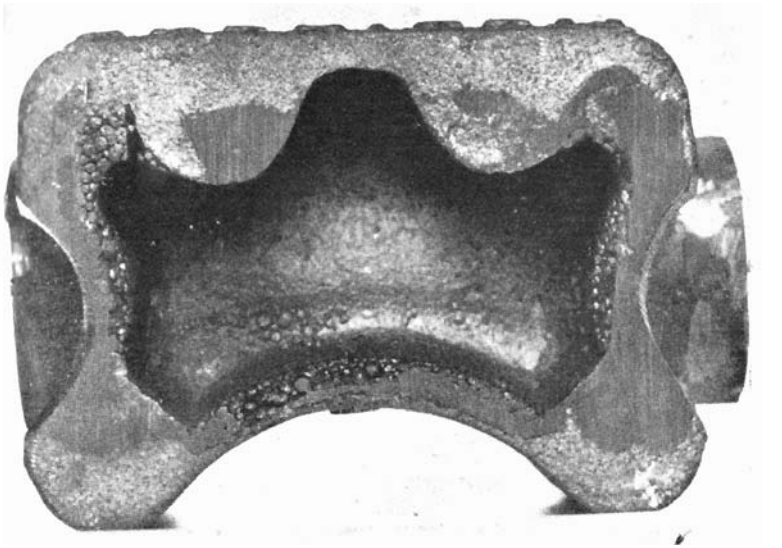

Fig. 7.8 ***Phosphide eutectic sweat appearing as rounded exudations on the surface of a grey-iron casting.***

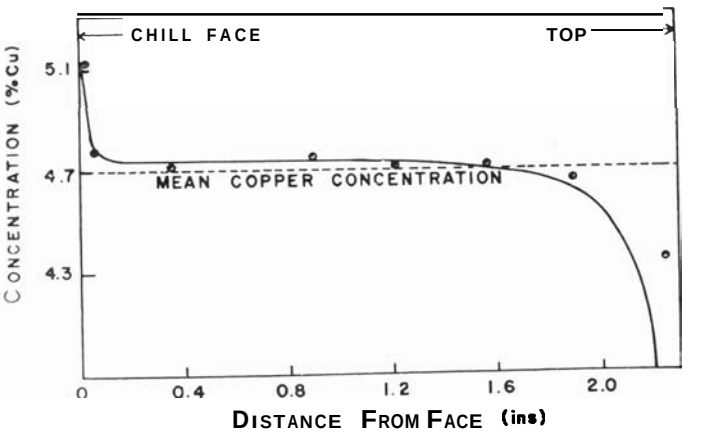

Fig *7.9* ***(a)***

evolved from moisture in the moulding sand. This can give rise to localised patches of cavities of considerable size on the surface (Fig. 9.2) which are often coloured with oxidation tints, or to sub-surface cavities (Fig. 9.3). In other cases fumes are generated when the molten metal comes into contact with

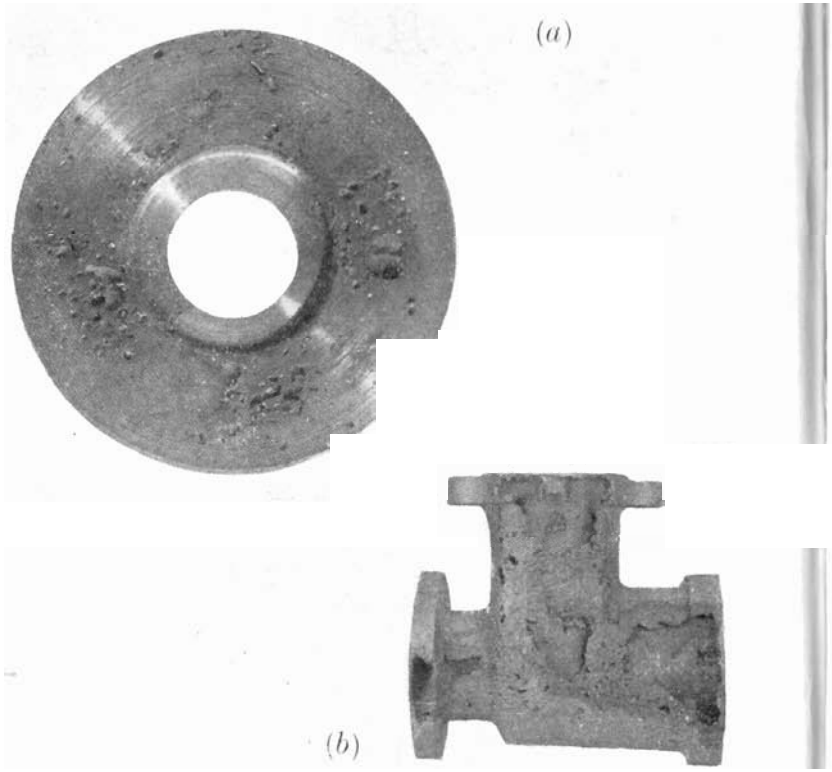

Fig. 9.2 *Surface blowholes on (a) a gunmetal flange connection and (b) a grey-iron valve-body casting. In each case the cause was excessive moisture in the moulding sand.*

the oil-binder of the core (Fig. 9.4). With investment castings, incomplete removal of residues from the wax pattern can cause trouble (Fig. 9.5).

(iii) As the result of chemical reactions taking place in the molten metal during cooling and solidification. Among the best-known

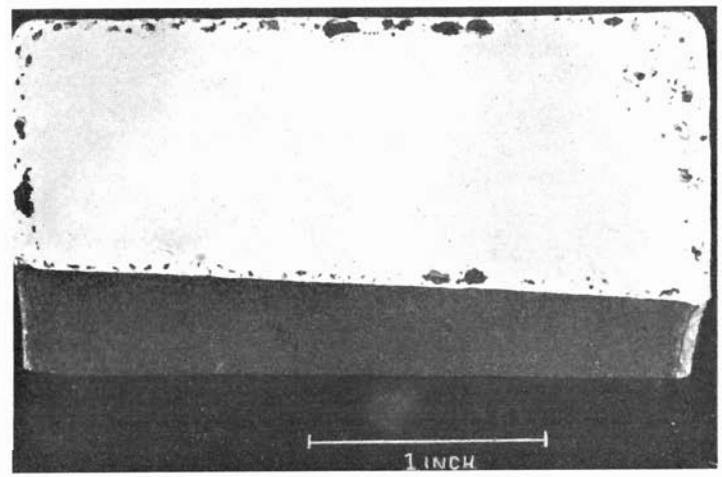

Fig. 9.3 *Cross section of a cast gunmetal ring showing sub-surface pores produced by reaction of the molten metal with wet sand.*

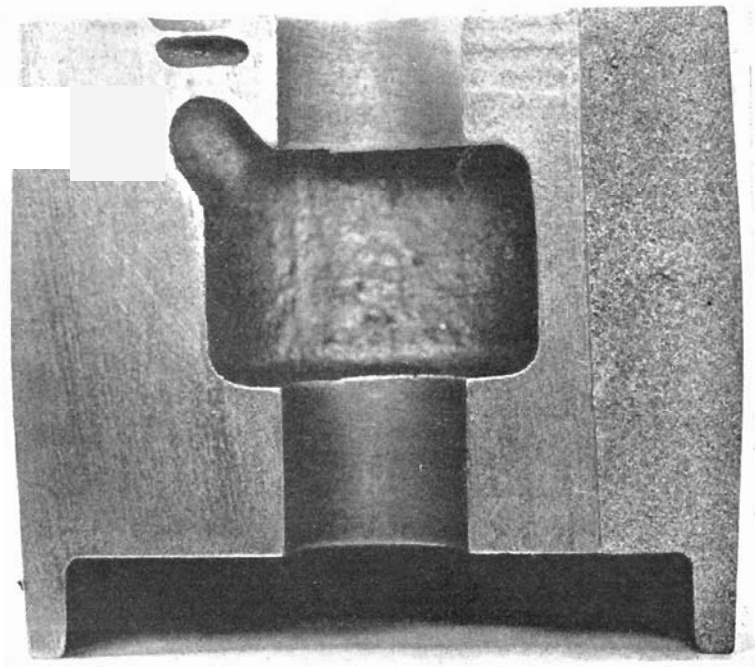

Fig. 9.4 *Large blowholes produced in a grey-iron pulley wheel casting by gas evolved from a core.*

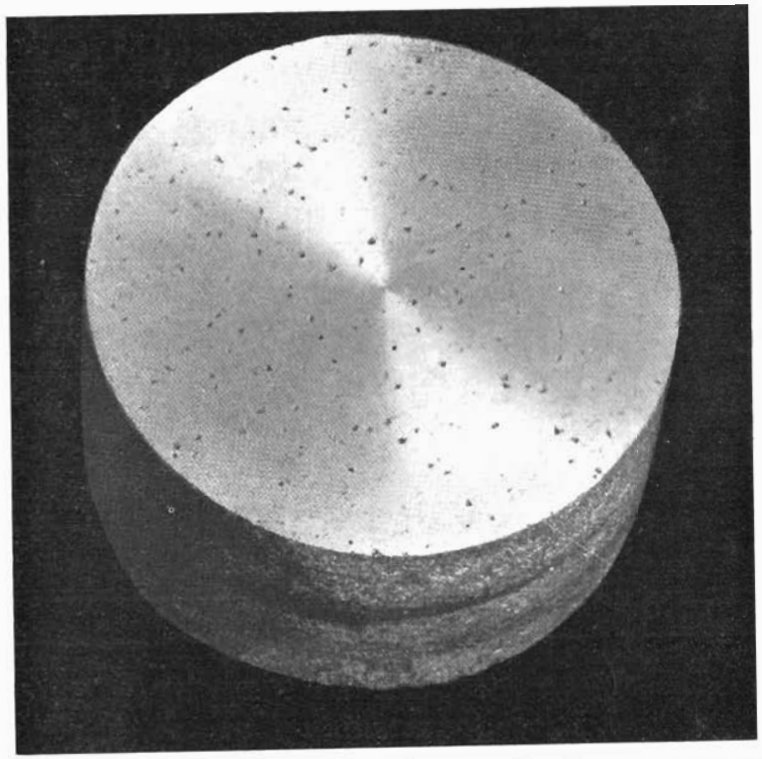

Fig. 9.8 Pinhole cavities in a sand-cast aluminium alloy, the result of hydrogen evolution on cooling.

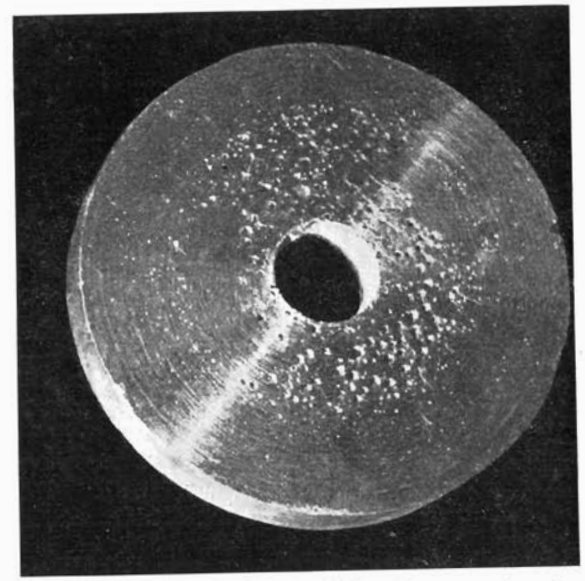

Fig. 9.9 Large gas holes in a 10% tin–bronze sand casting.

Fig. 9.10 A cold shut or cold trap on the surface of an aluminium alloy sand casting.

9.2 COLD SHUTS

A 'cold shut' is produced when two streams of metal flowing from different regions in the casting meet without union. The shuts appear as apparent cracks or wrinkles in the surface, together with oxide

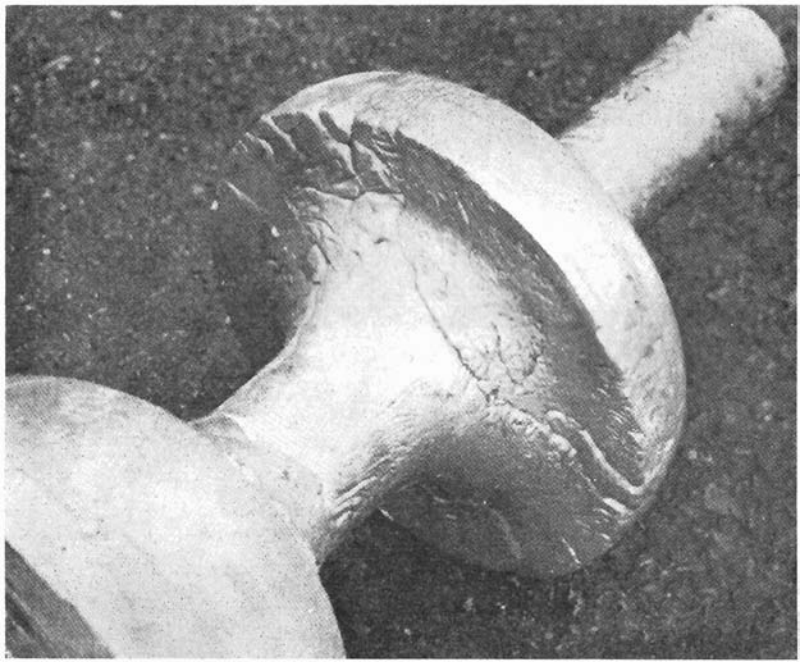

Fig. 9.11 Cold shuts in an alloy steel casting.

films (Figs. 9.10 and 9.11). This defect is usually the result of insufficient fluidity in the metal or the use of unsatisfactory methods of running and gating. Interrupted pouring can also give rise to cold shut formation.

The remedy is to increase fluidity either by raising the pouring temperature or by preheating the mould. Relocation of runners and ingates can often be equally effective.

9.3 CONTRACTION CRACKS

These are irregularly shaped cracks formed when the metal pulls itself apart while cooling in the mould or after removal from the

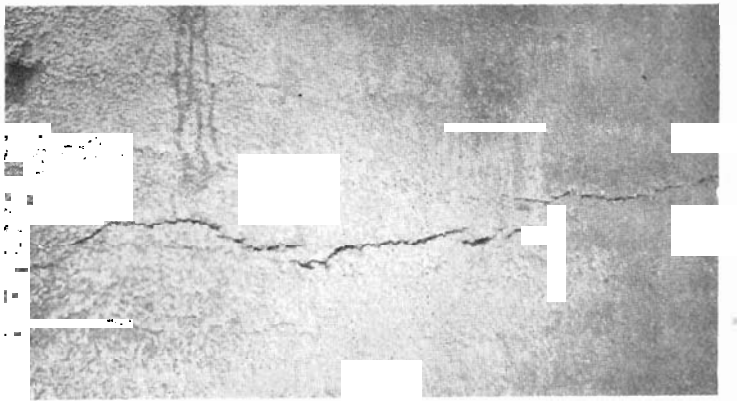

Fig. 9.12 A hot tear in a steel casting.

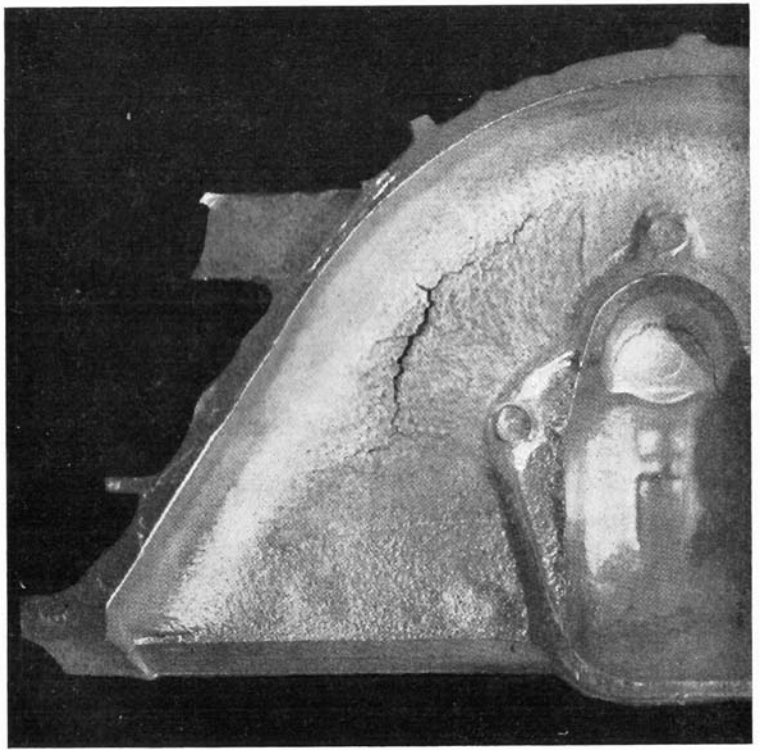

Fig. 9.13 A contraction crack formed in an aluminium alloy die casting during cooling in the mould after solidification was complete.

mould. When the crack appears during the last stages of solidification it is known as a 'hot tear' or a 'pull' (Fig. 9.12). In this case the crack faces are usually heavily oxidised. Hot tearing is most common in metals and alloys that have a wide freezing range, for then isolated regions of liquid become subjected to thermal stresses during cooling and fracture results.

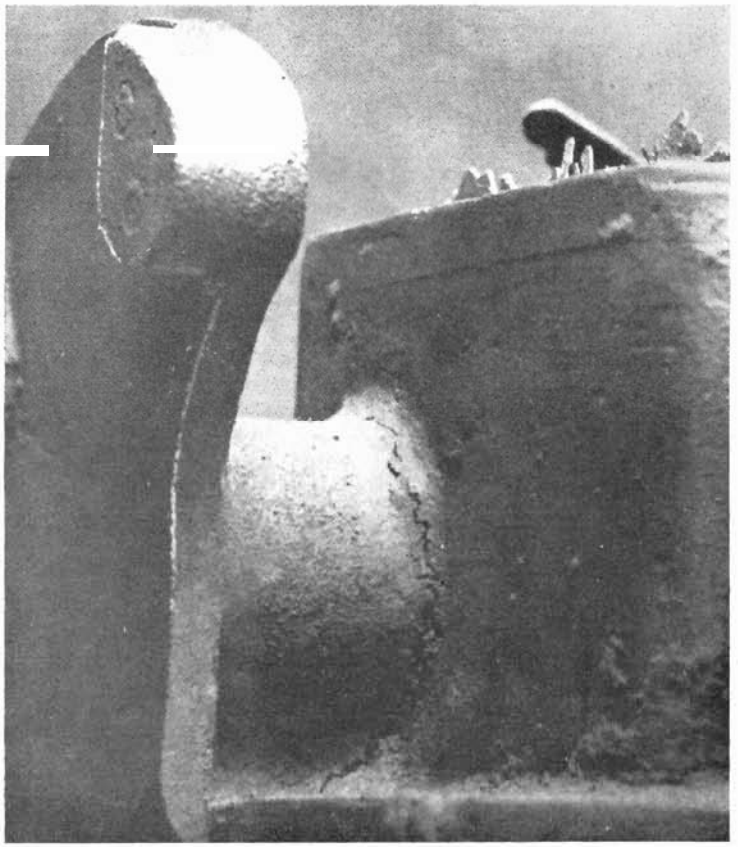

Fig. 9.14 *A contraction crack in the \$//(,1 of a small gunmetal sand ~~sting.*

In other cases contraction cracks arise during the period when the metal is solid but still at a temperature where the mechanical strength is low (Fig. 9.13).

Contraction cracks and hot tears result from the hindered contraction of the casting; this gives rise to complex internal stresses.

Local hot spots or high thermal gradients contribute to these high stresses, particularly if the mould or core is rigid enough to restrict relative movement of the different parts of the casting.

Scvcral steps are necessary if this type of defect is to be avoided. First, the cores and mould should be made more collapsible, for instance by incorporation of elastically soft material, ***e.g.*** cellulose, into the mould material or by minimising the compaction during moulding. In addition, alterations in design to avoid *abrupt* changes in section may be necessary. Hot spots can be eliminated, and thermal gradients controlled, by modification of the gating system or by the use of chills.

It should be noted that contraction cracks often have an external appearance very similar to a shrinkage cavity (see Section 9.6). They can be differentiated from the latter because there is no cavity or porous area beneath the surface. Furthermore, contraction cracks are normally located in positions clearly related to the geometry of the casting and to the restriction of free contraction by parts of the mould. A good example of this is shown in Fig. 9.14, where cracking has occurred in the fillet region between two parts of the casting.

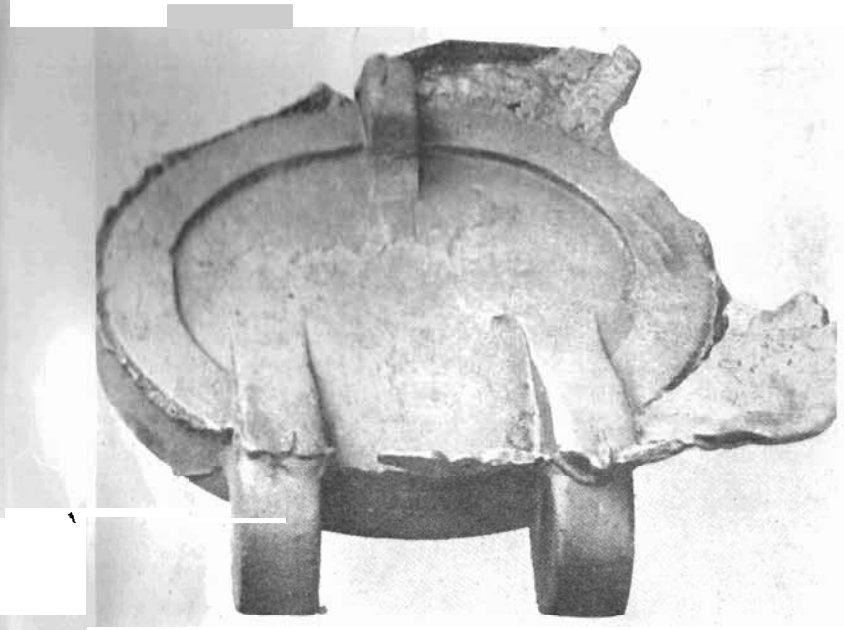

Fig. 9.15 *Excessive flash or fin along the parting line of a grey-iron casting.*

9.4 FLASH

The development of 'flash' (or 'fin') involves the formation of a run of metal around the parting line of the mould caused by the flow of liquid metal into the space between the halves of the mould. This

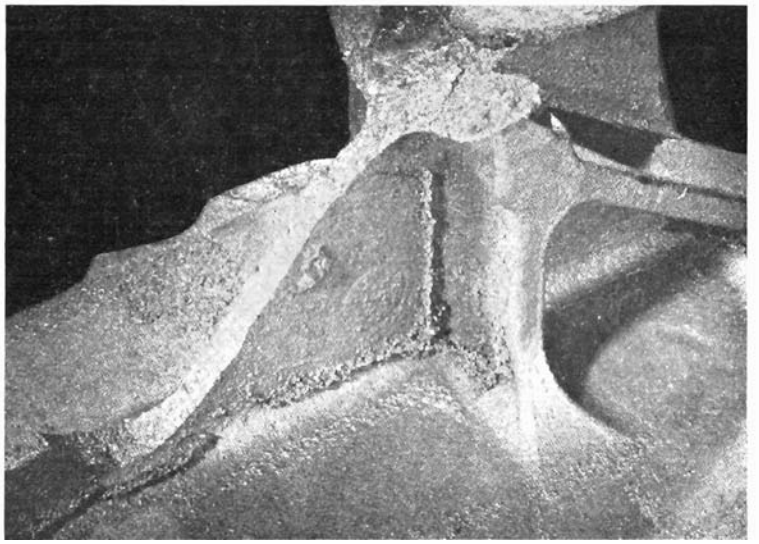

Fig. 9.16 Veining caused by the penetration of cast high-duty iron into cracks in an oil-bonded core.

defect is known as 'veining' when liquid metal penetrates into cracks in the mould or core. Examples of these are shown in Fig. **9.15** and 9.16.

Rigid clamping of the mould boxes and hardening of the mould and core faces will usually overcome this type of defect. In some instances **a** lowering of the pouring temperature is necessary since the appearance of finning or veining is accentuated by the high fluidity of liquid metals cast with high degrees of superheat.

If the two parts of the mould are displaced relative to each other, this produces a different but associated defect known as a 'crossjoint' (Fig. **9.17).** Here the remedy is obvious.

9.5 OXIDE AND DROSS INCLUSIONS

These result from the entrapment of surface oxide or other foreign matter during pouring. Often they are not immediately apparent and

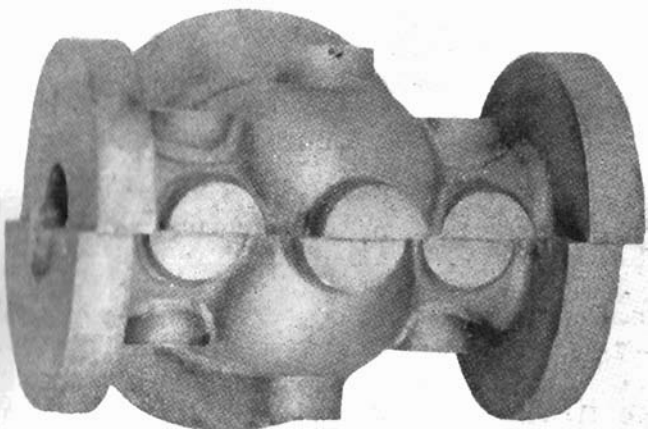

Fig. 9.17 A crossjoint in a large grey-iron valve body casting produced by mismatch of the top and bottom parts of the mould.

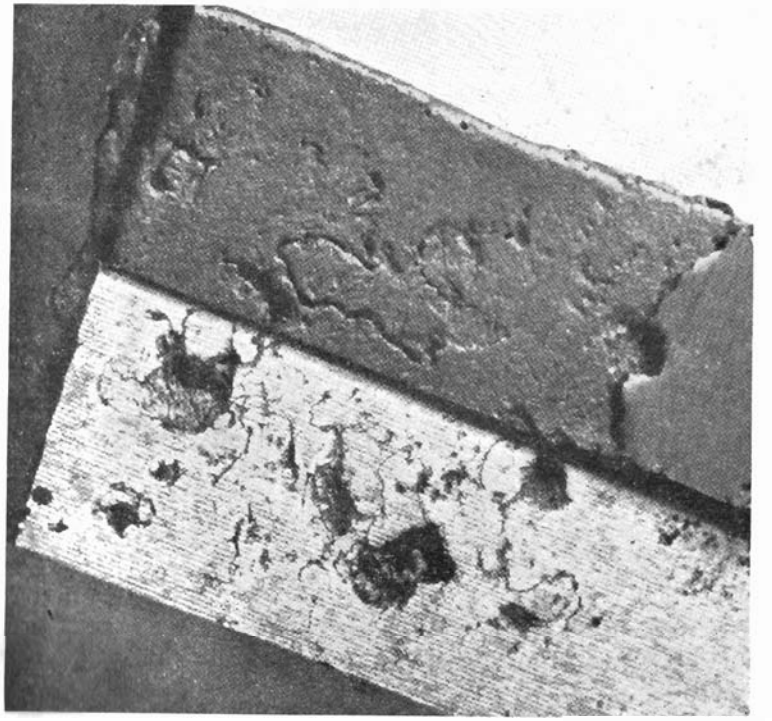

Fig. 9.18 Inclusions in an spheroidal graphite iron casting. Part of the surface has been machined away to show the nature of the defect more clearly.

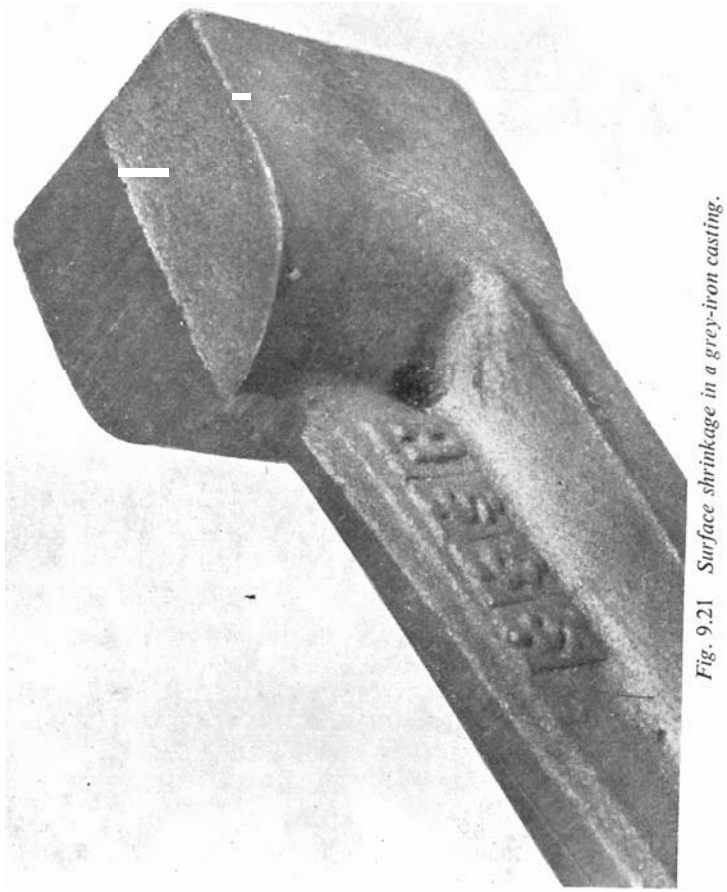

Fig. 9.21 Surface shrinkage in a grey-iron casting.

These cavities are frequently widely dispersed and located below the surface, and thus difficult to detect. Examples are shown in Figs. 9.19 and 9.20. If the shrinkage occurs near the surface, the cavities can be detected because of the presence of small depressions in the surface of the casting (Fig. 9.21). A similar case to this latter form is

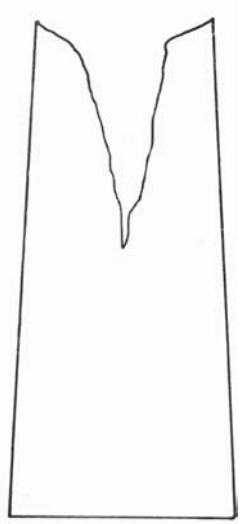

***Fig. 9.22** Cross section of a killed steel ingot showing pipe development (schematic). The piped region must be cut / / 1 , thus giving a low useful metal yield.*

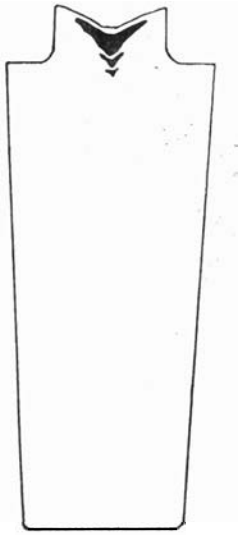

***Fig. 9.23** Cross section of a killed steel ingot cast into a mould with a refractory hot top (schematic). Shrinkage is confined to the top of the ingot and yield is increased.*

the large conical depression observed in the top of some ingots, and known as *pipe* (Fig. 9.22).

The major cause is the failure to obtain directional solidification towards desired heat centres such as risers or ingates. If the location of these feed points is bad, then shrinkage is much more likely. Relocation of feeding can help considerably. The use of higher pouring temperatures is also normally an advantage. Often proprietary methods involving exothermic heating in the mould cavity can be used to encourage directional solidification. When these are used together with judicious location of refractory inserts and chills to control heat transfer to the mould, shrinkage defects can largely be

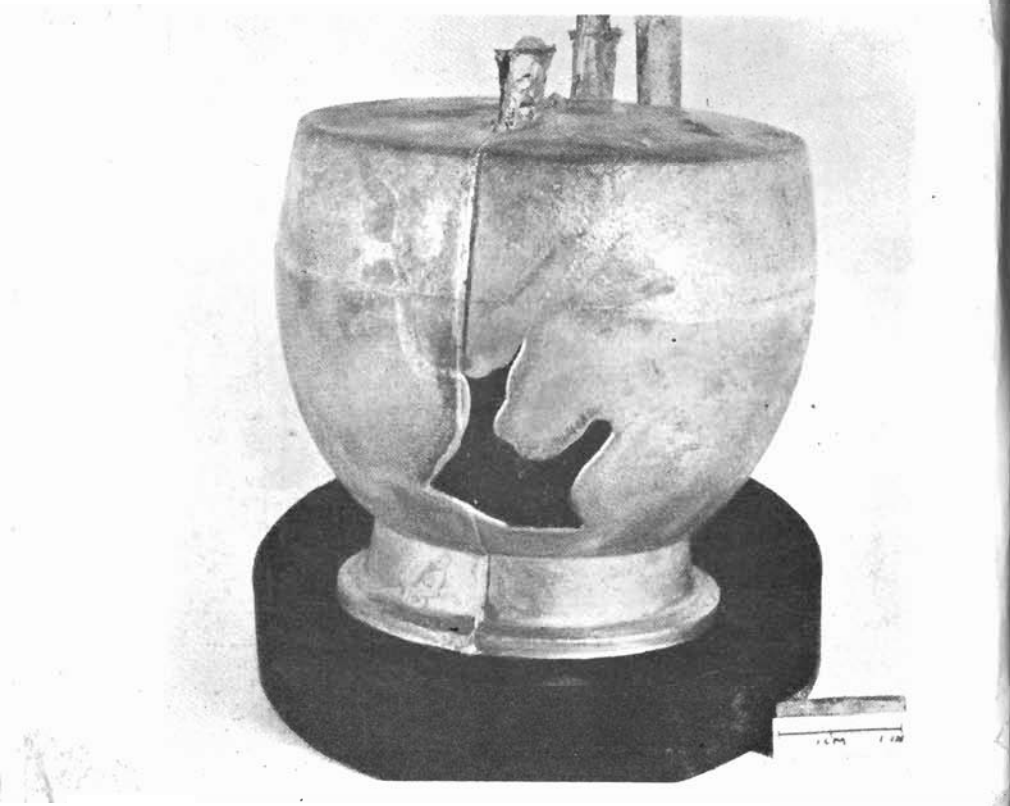

Fig. 9.24 A misrun in a brass gravity die casting.

overcome. With ingots, the use of refractory hot-tops will increase yield (Fig. 9.23).

9.7 MISRUNS

An exaggerated form of shut is the 'misrun' ***(see*** Figs. 9.24 and 9.25). These are produced when the liquid metal fails to fill the mould either because of low fluidity or if the methods of running are

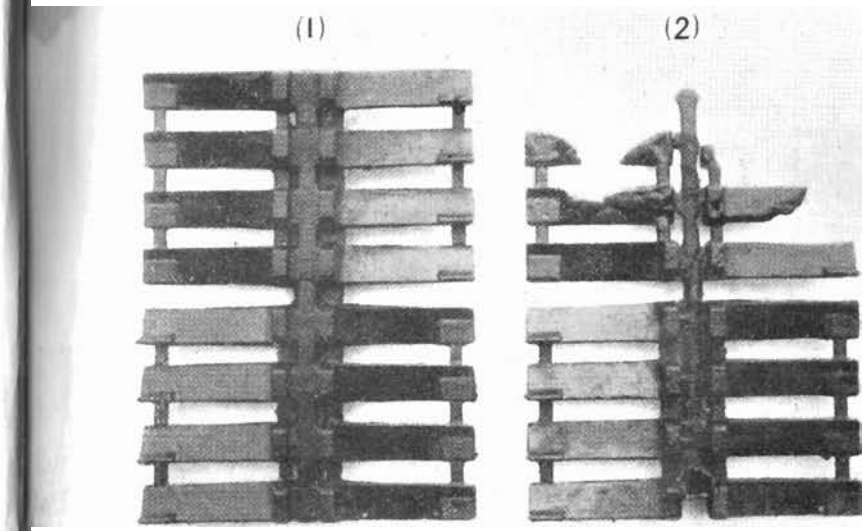

*Fig. 9.25 A striking example of a **misrun** which resulted in an incompletely filled mould (a 'short run'). Both a complete (1) and a **misrun** casting (2) are shown.*

unsatisfactory. They are evident as smooth irregular-shaped holes, with rounded edges, through the casting wall. Poor venting of moulds and cores can have a contributory effect. Raising the pouring temperature and reconsidering the position, size and number of ingates and vents will usually eliminate this defect.

0.8 SUMMARY

The sections preceding this summary describe the major defects that occur in castings. These are summarised in Table 9.1. Details of

APPENDIX 1

The Relationship Between the Interfacial Energies and the Contact Angle in Heterogeneous Nucleation

In Chapter 2 it was given that under stable conditions the contact angle, θ (*see* Fig. A1.1), was related to the surface energies of the liquid–crystal interface, γ_{LC}, the crystal–substrate interface, γ_{CS}, and the liquid–substrate interface, γ_{LS}, by

$$\cos\theta = \frac{\gamma_{LS} - \gamma_{CS}}{\gamma_{LC}}$$

A superficial examination of Fig. A1.1 might suggest that this relation is an obvious consequence of the force balance. This appendix

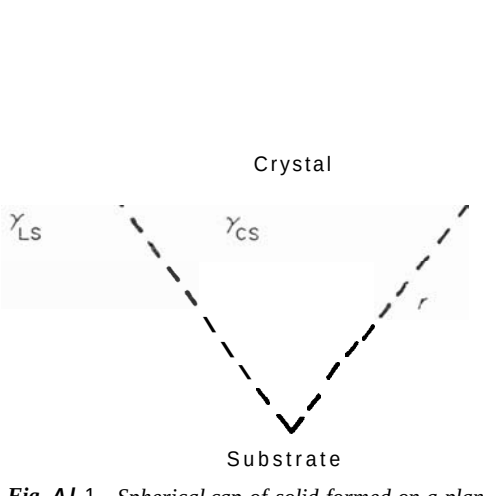

Fig. A1.1 *Spherical cap of solid formed on a planar substrate.*

gives a rigorous proof based on a method of virtual displacements. The proof depends on the assumption that the condition for stability is that the total surface energy should remain unchanged for a virtual displacement at constant volume.

Considering a spherical cap of radius r (Fig. A1.1), the area of the cap in contact with the surface is

$$A_1 = \pi r^2 \sin^2\theta \qquad \text{(A1.1)}$$

The area of the cap in contact with the liquid is

$$A_2 = 2\pi r^2(1 - \cos\theta) \qquad \textbf{(A1.2)}$$

Total excess surface energy introduced into the system by the formation of the spherical cap equals

$$A_1(\gamma_{CS} - \gamma_{LS}) + A_2 \cdot \gamma_{LC}$$

For a small displacement the assumption above means that

$$dA_1(\gamma_{CS} - \gamma_{LS}) + dA_2 \cdot \gamma_{LC} = 0$$

that is

$$\frac{\gamma_{LS} - \gamma_{CS}}{\gamma_{LC}} = \frac{dA_2}{dA_1}$$

Differentiating eqns. **(A1.1)** and (A1.2) and substituting gives, after simplification,

$$\frac{\gamma_{LS} - \gamma_{CS}}{\gamma_{LC}} = \frac{r \cdot \sin\theta + 2(1 - \cos\theta)(dr/d\theta)}{r \cdot \sin\theta\cos\theta + \sin^2\theta(dr/d\theta)} \qquad \textbf{(A1.3)}$$

The volume of a spherical cap is

$$V = \tfrac{1}{3}\pi r^3(2 - 3\cos\theta + \cos^3\theta)$$

For constant volume, $dV = 0$. Thus

$$\frac{dr}{d\theta} = -\frac{r \cdot \sin\theta(1 + \cos\theta)}{(1 - \cos\theta)(2 + \cos\theta)}$$

Substituting this in eqn. **(A1.3)** leads to

$$\frac{\gamma_{LS} - \gamma_{CS}}{\gamma_{LC}} = \cos\theta$$

in the liquid will play an important part.† There is at present no theoretical treatment for this problem. However, experimental observations[10] on copper–nickel alloys showed that the undercooling required for homogeneous nucleation was ~0·2 of the liquidus temperature.

The form of the nucleation rate equation is such that at very large undercoolings there should be a decrease in the rate of nucleation resulting from a decreased mobility of atoms. We might thus expect the curve of Fig. 2.5 to tend towards a maximum as indicated. For most metallic systems, however, it is not possible to cool through the range of temperature at which copious nucleation occurs at a rate fast enough to suppress nucleation. Quench rates of the order of 10^6 °C sec^{-1} have been used unsuccessfully with melts of pure liquid metals. In binary alloy systems where redistribution of solute must occur as part of the nucleation process, some amorphous solids have been produced using rapid quenching techniques.[11–13]

The occurrence of amorphous phases results from the combined influence of two exponential factors, one related to the transfer of

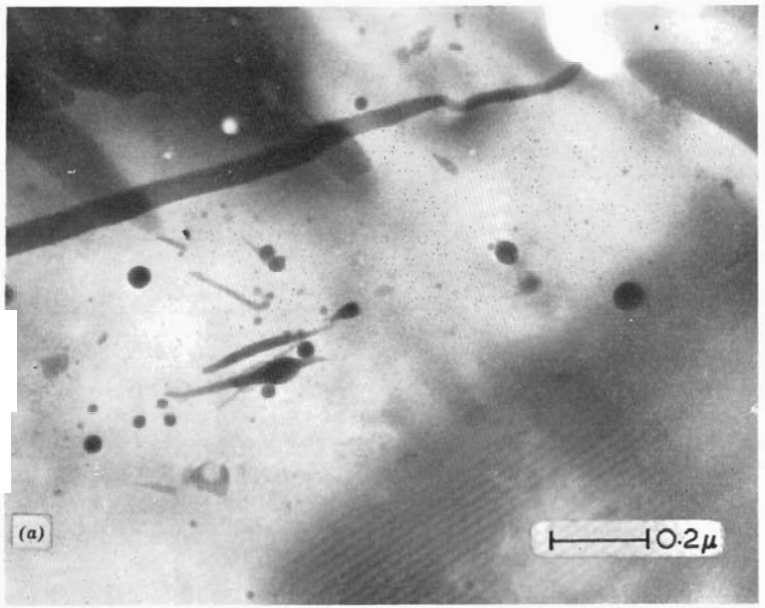

Fig. 2.6 (*a*)

† There is some evidence that in special cases the *earliest* stages of nucleation and growth take place without solute redistribution.[35]

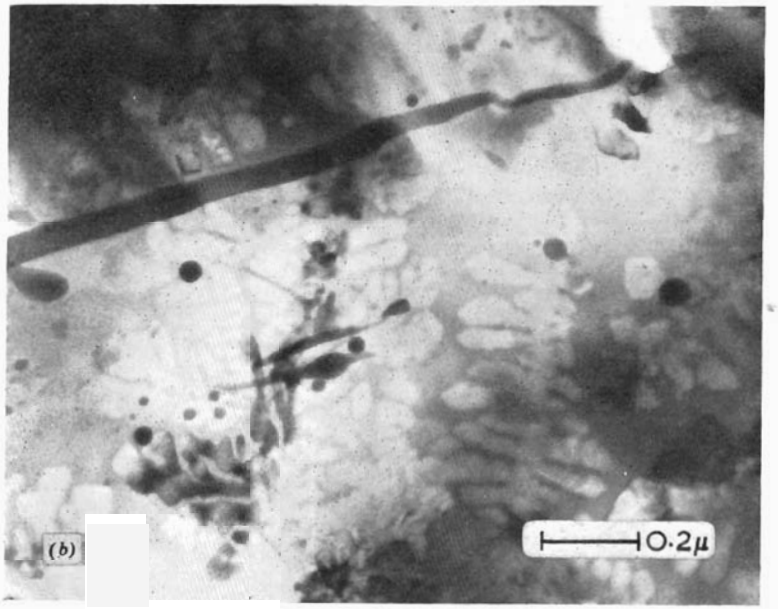

Fig. 2.6 *The electron microstructure of splat-cooled tellurium–15 at. 90 germanium in (a) the amorphous state and (b) after heating. The growth of dendrites can be seen clearly in the latter micrograph (Willens[13]).*

atoms from the liquid to the solid and the other associated with bulk diffusion in the liquid. On reheating, transformation to the crystalline state occurs quite rapidly, as shown in Fig. 2.6.

It should be noted that the treatment given assumed a spherical nucleus. Simple modifications result from considering nuclei of other shapes. One of the more realistic shapes may be that described by Chalmers[14] in which it was proposed that the nucleus was bounded by planes of high atomic density (Fig. 2.7).

Before considering heterogeneous nucleation it is interesting to question how the liquid structure affects homogeneous nucleation. This has been considered by Walton.[15] The structure of the liquid influences the nucleation rate firstly through ΔG^*, since this term contains the volume free energy change ΔG_v. If clustering occurs in the liquid this will aid nucleation. Oriani and Sundquist[16] have estimated that for most metals supercoolings of more than 10°C will be sufficient to promote embryo formation as the liquid structure orders. The structure of the liquid also has a direct effect on ΔG_A, the diffusion term, and on the liquid–crystal interfacial energy, γ_{LC}.

or a few unoccupied sites. The first type of interface was classified as 'rough' and the second type of interface as 'smooth' or 'faceted'. Further analysis showed that most metals had $\alpha \lesssim 2$, in which case they were expected to grow with a rough interface whose position was approximately determined by the isotherm fractionally below T_m. Inorganic and organic liquids normally have $\alpha \gtrsim 5$, in which case the growing nucleus rapidly becomes bounded by crystallographic faces. A small group of materials exist, *e.g.* silicon, bismuth, which occupy the middle ground in that $\alpha = 2$–5 for different faces. In these materials the behaviour is more complex and often a mixed growth form results.[3,4] It must be emphasised that the analysis of Jackson considers the relative free energy change with the fraction of sites occupied on the surface, and thus in essence it does not predict the true minimum energy form of a stationary equilibrated interface. This latter point has been examined by Miller and Chadwick.[5]

Nevertheless, the treatment has been of considerable value in increasing the understanding of the factors influencing the interface form during solidification. The studies of Jackson and Hunt[6] and Jackson *et al.*[4]—in which transparent organic crystals, chosen with a range of α-factors and thus analogous to a range of materials both metallic and non-metallic, were observed during solidification—were largely in agreement with Jackson's original predictions.[1] Figure 3.2 shows examples of the different types of interface.

There are inadequacies in the theory of Jackson, particularly those associated with kinetic influences and related to details of the crystal structure, *e.g.* the anisotropy of growth.

One approach to the problem of the relation between the interface structure and the growth of the interface was that of Cahn[7] (*see also* Cahn *et al.*[8]) who considered in detail the 'diffuseness' of the interface, *i.e.* the number of atomic layers comprising the transition from solid to liquid. Cahn concluded that the degree of diffuseness was dependent on both the material and the driving force for transformation. The driving force is determined by the undercooling at the interface. As a result it was predicted that at low driving forces the interface would be discrete and propagation would take place by the transverse motion of interface steps, while at large driving forces the growth would be normal with the interface diffuse. This theory was examined in detail by Jackson *et al.*,[4] who compared the predictions with experimental data for a considerable range of materials. The examination showed that the evidence did not support the predictions.

Jackson[9] followed up his earlier work with a more general theory of crystal growth which related both structure and growth rate. This led to reasonable predictions for growth rate anisotropy. The theory

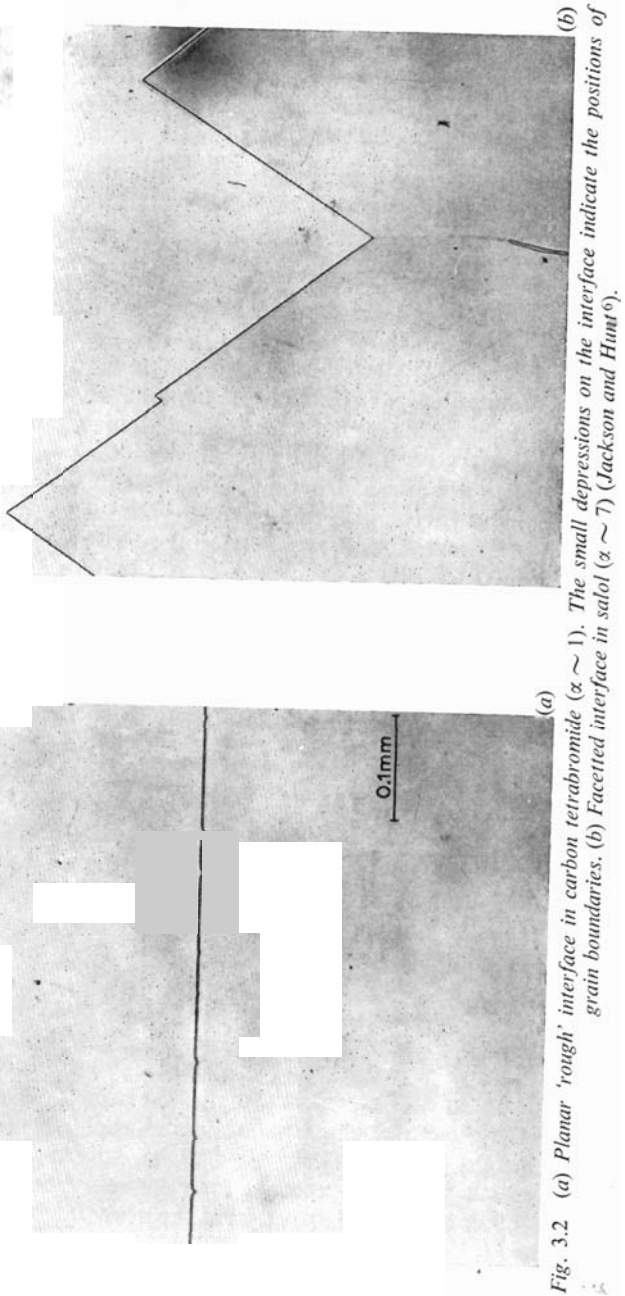

Fig. 3.2 (a) Planar 'rough' interface in carbon tetrabromide ($\alpha \sim 1$). The small depressions on the interface indicate the positions of grain boundaries. (b) Facetted interface in salol ($\alpha \sim 7$) (Jackson and Hunt[6]).

(v) low diffusivity in the liquid;
(vi) very low k_0 for $k_0 < 1$ or very high k_0 for $k_0 > 1$.

In the presence of constitutional supercooling the undercooling is,

$$\Delta T = T_L - T$$

Thus

$$\Delta T = \frac{mC_0(1 - k_0)}{k_0}\left[1 - \exp\left(-\frac{Rx}{D}\right)\right] - Gx \qquad (4.8)$$

This is as shown in Fig. 4.16. The maximum undercooling can be determined from eqn. (4.8) and is,

$$\Delta T_{max} = \frac{mC_0(1 - k_0)}{k_0} - \frac{GD}{R}\left[1 + \ln\frac{(mC_0(1 - k_0)R)}{GDk_0}\right] \qquad (4.9)$$

This maximum undercooling occurs at a point given by

$$x = \frac{D}{R}\log_e\left[\frac{mC_0(1 - k_0)R}{GDk_0}\right] \qquad (4.10)$$

The above treatment assumes that solute mixing in the liquid is the result of diffusion only. It can be modified to allow for partial or complete mixing in the liquid (*see* Chalmers[12]). In these circumstances long-range segregation will still occur.

4.5 STRUCTURAL EFFECTS RESULTING FROM SOLUTE REDISTRIBUTION IN ALLOYS

In the absence of constitutional supercooling, the behaviour during growth is essentially the same as that of pure materials with the exception that long-range segregational effects occur which are associated with the initial and final transients in the solidification process (Fig. 4.13).

The existence of a zone of constitutional supercooling, and thus a negative gradient of free energy, ahead of the interface will make an initially planar interface unstable to perturbations in shape. At low degrees of supercooling a cellular interface develops (Fig. 4.17) from the planar interface after first becoming pock-marked and then showing elongated cells. The breakdown from the planar to the cellular form can be shown experimentally to be governed by eqn. (4.7).[13,14] As the degree of supercooling increases the cell caps becomes extended and eventually branch to form cellular dendrites

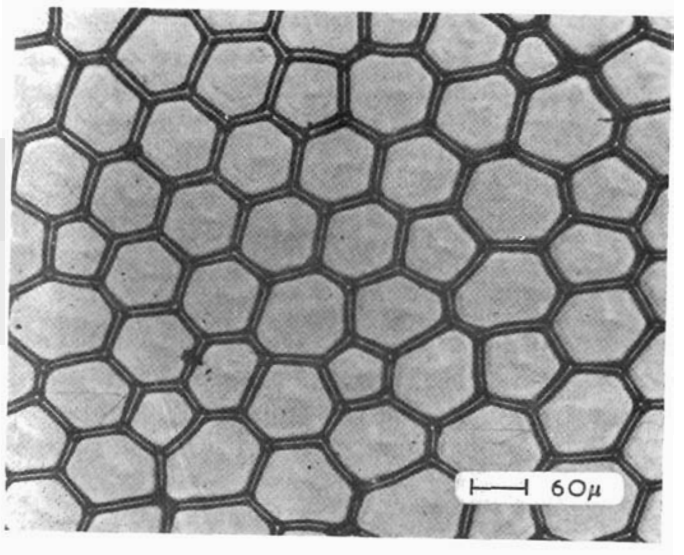

(*a*)

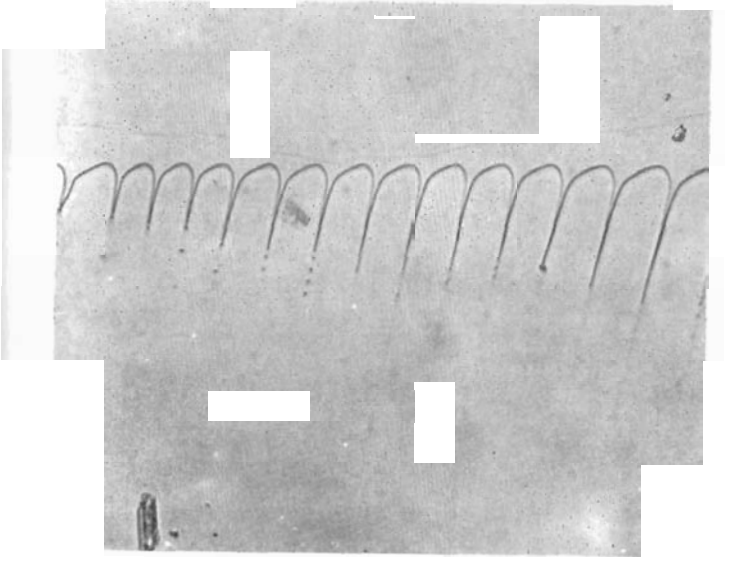

(*b*)

Fig. 4.17 *The cellular interface structure: (a) normal view of a decanted interface; (b) view of growing interface in impure carbon tetrabromide (Jackson and Hunt*[15]*).*

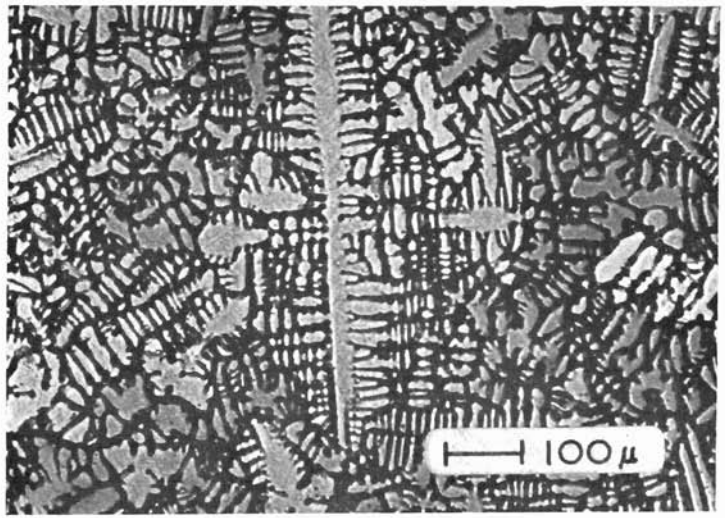

(*a*)

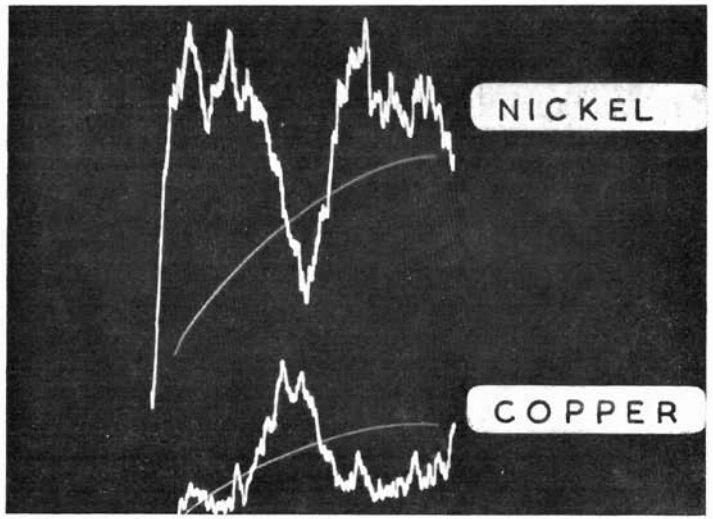

(*b*)

Fig. 4.20 *Coring in chill-cast cupronickel* ($k_0 < 1$)*: (a) as-cast structure; and (b) electron-beam microanalyser trace across the boundary between two dendrite arms. The qualitative nature of the segregation is apparent as a maximum and a minimum in the copper and nickel respectively.*

(Fig. 4.18). There is no clear criterion for the transition from cells to cellular dendrites.[14] The overall transition sequence is as shown in Fig. 4.19. In the case of both cells and cellular dendrites, microsegregation occurs. The intercellular regions are rich in solute for $k_0 < 1$ and depleted of solute for $k_0 > 1$. Under these conditions, long-range segregation effects similar to those shown in Fig. 4.13 are also bound to occur.

On a macroscopic scale this mean that a dendrite will show a variation in composition from inside to out, *i.e.* the phenomenon of *coring*. This is illustrated in Fig. 4.20; in this figure the dendritic structure is clearly evident. Although it cannot be resolved, the dendrite arms would undoubtedly show microscopic cellular segregation. Both forms of segregation can be eliminated by a homogenising heat treatment although, of course, macrosegregation effects involve long diffusion distances and thus long heat-treatment times. The effect of homogenisation is shown in Fig. 4.21.

A quite different approach to the problem of interface breakdown is that of Mullins and Sekerka,[16] who considered the stability of the interface in the presence of shape fluctuations. This treatment has some advantages, particularly since it predicts some of the parameters, *e.g.* cell size, which were not treated in the original analysis of constitutional supercooling. The treatment is mathematically complex and details can be obtained from the original paper.

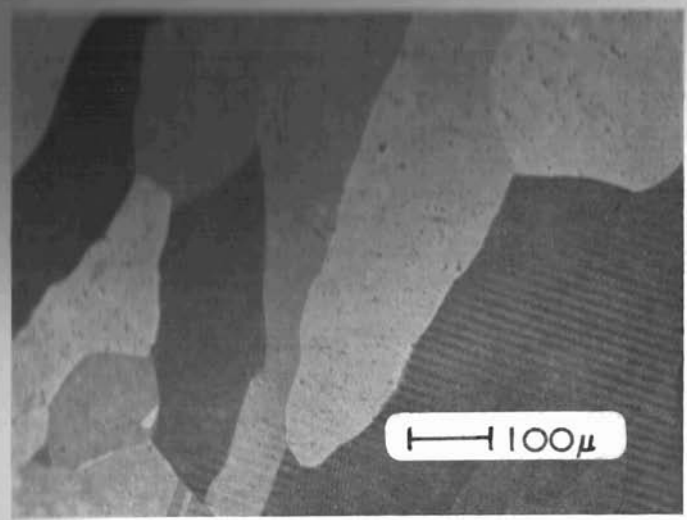

Fig. 4.21 (*a*)

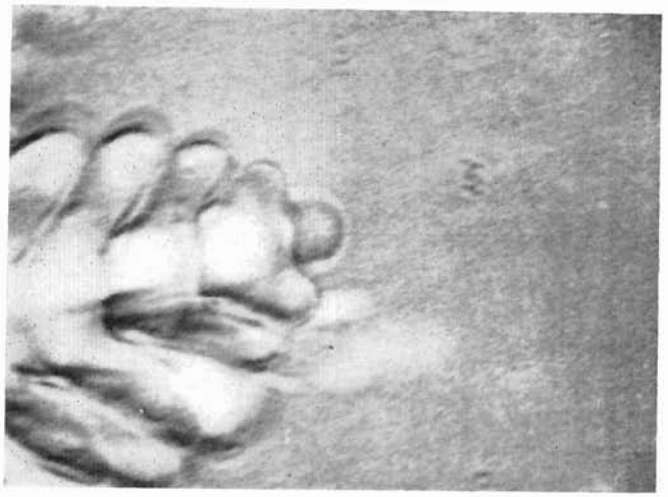

Fig. 4.22 (*a*)

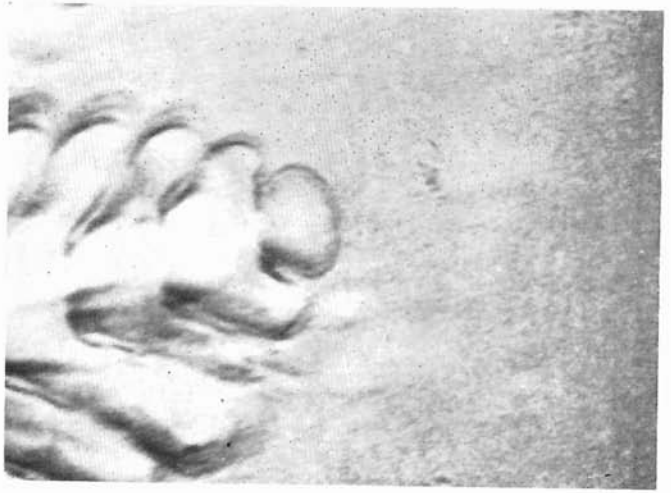

Fig. 4.22 (*b*)

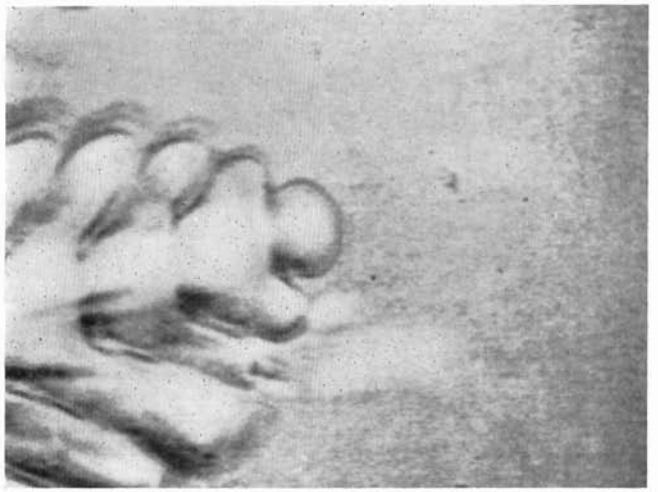

(*c*)

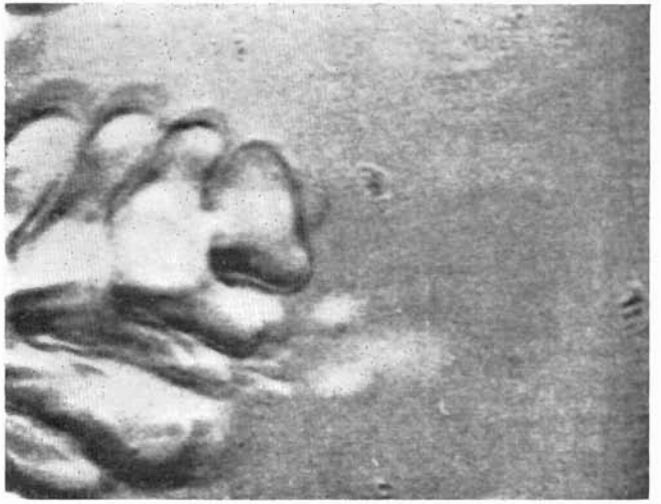

(*d*)

Fig. 4.22 *Tip of a growing dendrite showing progressive steps in tip morphology. The time interval between* (*a*) *and* (*b*) *was* 1·2 *sec; between* (*b*) *and* (*c*) 1·2 *sec; and between* (*c*) *and* (*d*) 2·1 *sec* (*Morris and Winegard*[23]).

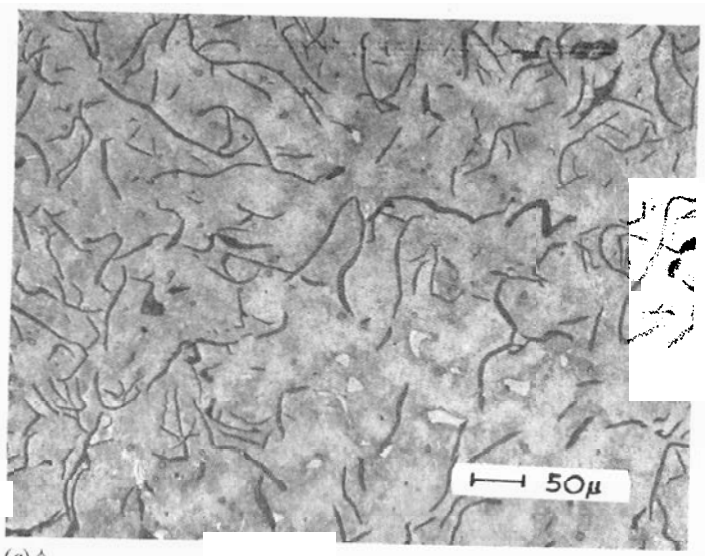

(a) ↑

(b) ↓

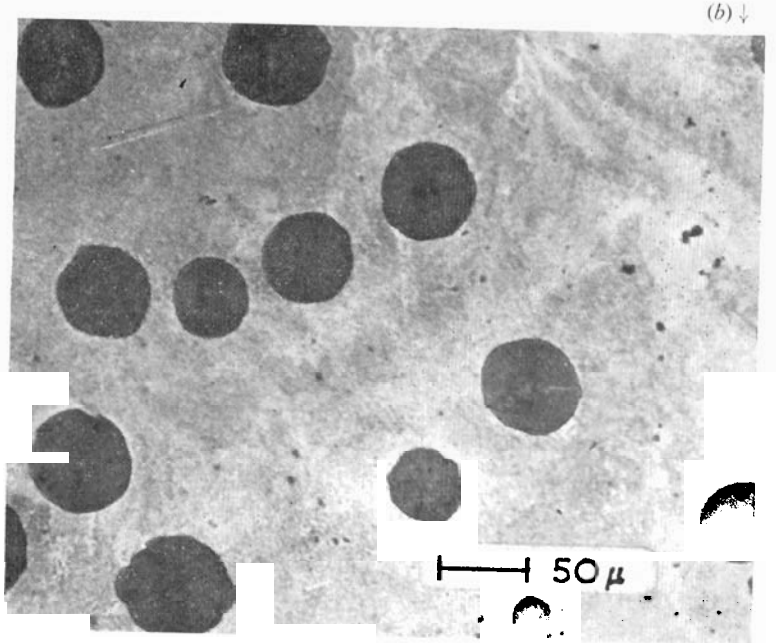

Fig. 5.11 (*a*) *Normal as-cast grey cast iron showing flake graphite.* (*b*) *Modified spheroidal graphite cast iron.*

are both examples of important structural modifications in the development of microstructure.

The recent work of Day[22] has confirmed that this modified structure is the result of a change in the mode of growth and not the result of a change in nucleation behaviour as was earlier proposed.[23,24] The coarse silicon structure of slow-cooled alloys is altered if rapid growth rates are used. A similar effect is produced by adding a modifier (sodium) to the slow-cooled alloy. These are illustrated in Fig. 5.10. The silicon morphology is basically the same in *both* the growth rate-modified *and* the additive-modified alloys.

The modification that occurs in the iron–carbon system is even more striking, as shown in Fig. 5.11. Here the normal structure of grey cast iron, graphite flakes in a pearlitic matrix, is altered to graphite spheroids in a pearlitic matrix. In this case also there is a dramatic increase in mechanical properties, particularly toughness. The bulk of the evidence[25] indicates that the spherulites separate directly from the melt without the simultaneous formation of any other solid. Solidification appears to proceed by the growth of the spherulite surrounded by an envelope of austenite, although this hypothesis has been questioned.[26] The reasons for the change in graphite morphology on the addition of magnesium are far from clear, although it has been established[27] that the additive influences the growth of the graphite rather than affecting the nucleation behaviour.

5.1.4 Other eutectic systems

There are a number of other aspects of eutectic solidification, particularly the divorced eutectics,[28] and the pseudo-binary eutectics[29] which occur in multicomponent systems. These are both very specialised topics and will not be dealt with further here.

5.2 PERITECTICS

Figure 5.12 gives the phase diagram for the almost ideal peritectic system, silver–platinum. As discussed by Uhlmann and Chadwick[30] in the first detailed study of peritectic reactions, for virtually all compositions except those near the limits of the system, the microstructure after casting will consist of cored dendrites of one phase surrounded by the second phase. Thus with reference to Fig. 5.12 we would expect this structure for compositions from 30 to 90 wt % platinum. Furthermore, the peritectic reaction should seldom proceed to completion. When the primary phase has cooled to the peritectic

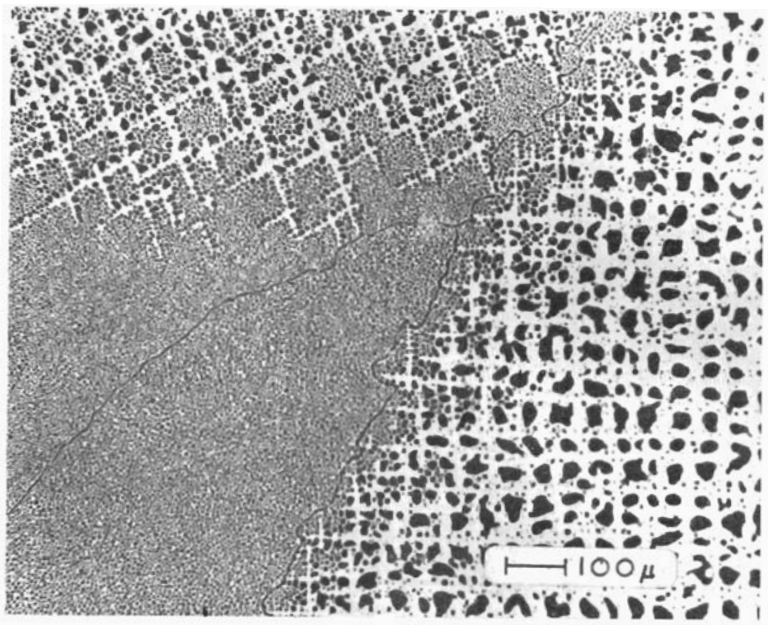

(*b*)

***Fig.* 5.16** (*a*) *Composition–velocity plot showing regions over which different microstructure types were observed.* (*b*) *Transverse section of transition regions showing composite and dendritic structures: copper—light phase, lead—dark phase. The characteristic alignment of the dendritic structure resulting from the crystallography of dendritic growth is clear* (*Livingston and Cline*[34]).

5.4 PARTICLES AND INCLUSIONS IN MELTS

Foreign particles which do not dissolve in either the liquid or the solid are often present during solidification. These insoluble particles are usually classified as *exogeneous* if they come from external sources (*e.g.* mould and ladle materials, dross) or *endogeneous* if they arise from reactions within the solidifying metal. The interaction between solid particles suspended in the liquid and the solid–liquid interface has been studied comprehensively by Uhlmann *et al.*[35] Using transparent materials, direct observations of particle–interface behaviour were made. For each system it was found that there was a critical growth rate below which the particles were 'pushed' by the interface and above which they were trapped in the solid. Figure 5.17 shows the pile-up of zinc particles at a solid–liquid thymol interface at low growth rate. The rate-controlling step was determined to be

the rate of diffusion of liquid to the growing solid behind the particle. A sufficient flux of liquid is needed to continuously replenish the solidifying material immediately behind the particle and thus keep the particle ahead of the interface. In the main, the critical growth

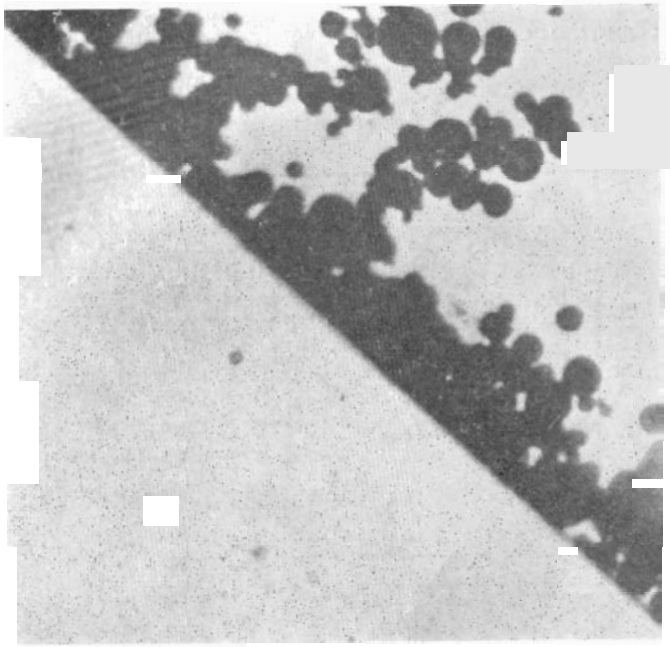

Fig. 5.17 *Pile-up of particles at a solid–liquid interface at low growth rate in the system thymol–zinc* (*Uhlmann* et al.[35]).

rates were all low ($\sim 10^{-3}$ cm sec^{-1}). It is thus expected that entrapment will occur in most practical cases. Towards the end of a solidification process, however, as the growth rates slow down, it is possible for particles to be swept together to produce quite deleterious accumulations of inclusions.

It is also possible for the solid inclusions to act as sites for heterogeneous nucleation (*see* Section 2.3) and it is recognised that they have an important role in ingot solidification.[36–38] To a large extent the segregation patterns observed in ingots (*see* Section 7.3) are influenced by the presence of inclusions.

In some cases the particles appear to have become grown-in because they have been trapped in isolated regions of liquid by the growth of dendrite branches. The constraints imposed on particle

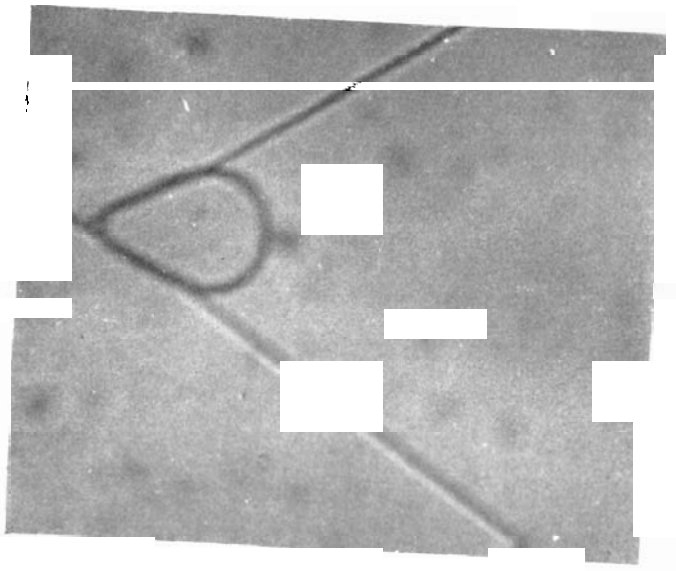

(a)

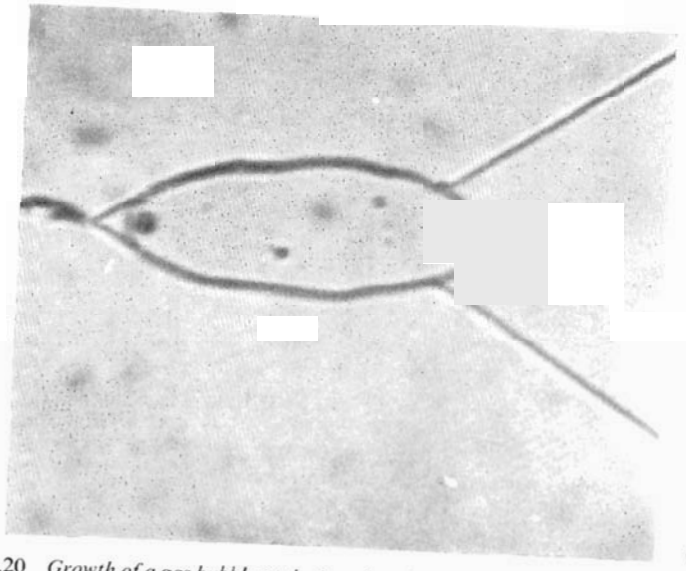

(b)

Fig. 5.20 Growth of a gas bubble at the interface in solidifying salol: (a) nucleation and incorporation into the interface; (b) formation of the elongated blowhole (Woodruff[42]).

There are few reports of investigations dealing with the factors influencing the number, form and distribution of pores in solidified metals. McNair[43] and Jordan *et al.*,[44] for instance, give some data on the effects of gas content, ingot size and solidification conditions on porosity. It is to be hoped that more fundamental work of this type will be carried out. In the meantime it should be noted that effective empirical methods have been developed for the *control* of porosity in ingots and castings (*see* Section 9.1).

REFERENCES

1. Chadwick, G. A. (1963). *Prog. Mat. Sci.*, **12,** 97.
2. Bell, J. A. E. and Winegard, W. C. (1965). *J. Inst. Met.*, **93,** 457.
3. Rumball, W. M. and Kondic, V. (1966). *Trans. Met. Soc. AIME,* **236,** 586.
4. Hunt, J. D. and Jackson, K. A. (1966). *Trans. Met. Soc. AIME,* **236,** 843.
5. Hunt, J. D. and Chilton, J. P. (1962–63). *J. Inst. Met.*, **91,** 338.
6. Chadwick, G. A. (1962–63). *J. Inst. Met.*, **91,** 169.
7. Tiller, W. A. (1958). *Liquid Metals and Solidification,* ASM, Cleveland, p. 276.
8. Jackson, K. A. and Hunt, J. D. (1966). *Trans. Met. Soc. AIME,* **236,** 1129.
9. Chadwick, G. A. (1963–64). *J. Inst. Met.*, **92,** 18.
10. Moore, A. and Elliott, R. (1968). *The Solidification of Metals,* ISI Publication 110, p. 167.
11. Day, M. G. and Hellawell, A. (1968). *Proc. Roy. Soc.*, **A305,** 473.
12. Day, M. G. (1969). *J. Metals,* **21**(4), 31.
13. Cooksey, D. J. S., Munson, D., Wilkinson, M. P. and Hellawell, A. (1964). *Phil. Mag.*, **10,** 745.
14. Hunt, J. D. (1968). *J. Crystal Growth,* **3–4,** 82.
15. Hellawell, A. (1967). *Met. and Materials,* **1,** 361.
16. Davies, G. J. (1971). *Strengthening Methods in Crystals* (Ed. by A. Kelly and R. B. Nicholson), Applied Science, Barking, p. 485.
17. Mollard, F. R. and Flemings, M. C. (1967). *Trans. Met. Soc. AIME,* **239,** 1526.
18. Mollard, F. R. and Flemings, M. C. (1967). *Trans. Met. Soc. AIME,* **239,** 1534.
19. Chadwick, G. A. (1968). *The Solidification of Metals,* ISI Publication 110, p. 138.
20. Kerr, H. W., Plumtree, A. and Winegard, W. C. (1964–65). *J. Inst. Met.*, **93,** 63.
21. Cooksey, D. J. S. and Hellawell, A. (1967). *J. Inst. Met.*, **95,** 183.
22. Day, M. G. (1970). *J. Inst. Met.*, **98,** 57.
23. Plumb, R. C. and Lewis, J. E. (1957–58). *J. Inst. Met.*, **86,** 393.
24. Kim, C. B. and Heine, R. W. (1963–64). *J. Inst. Met.*, **92,** 367.

evolved from moisture in the moulding sand. This can give rise to localised patches of cavities of considerable size on the surface (Fig. 9.2) which are often coloured with oxidation tints, or to sub-surface cavities (Fig. 9.3). In other cases fumes are generated when the molten metal comes into contact with

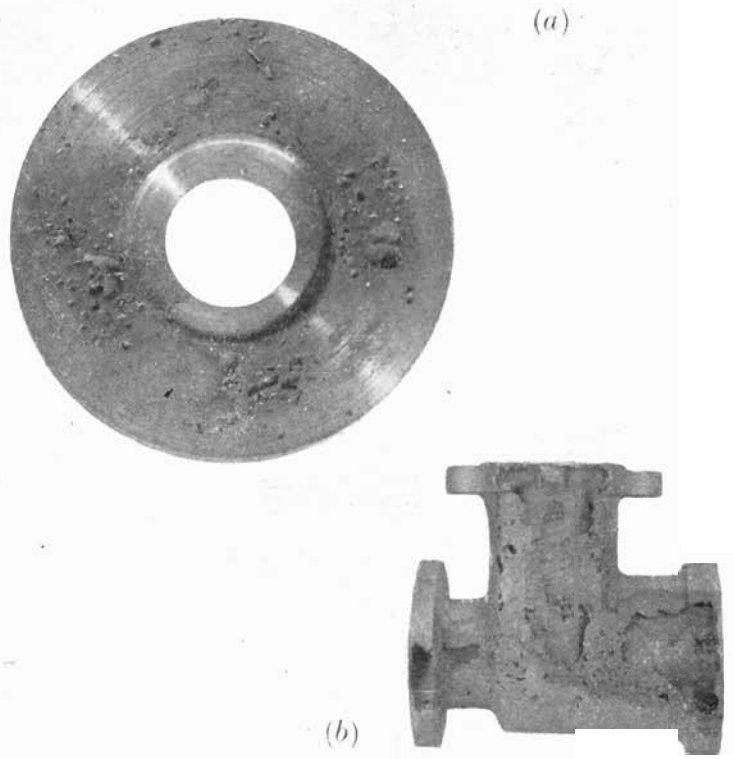

Fig. 9.2 Surface blowholes on (a) a gunmetal flange connection and (b) a grey-iron valve-body casting. In each case the cause was excessive moisture in the moulding sand.

the oil-binder of the core (Fig. 9.4). With investment castings, incomplete removal of residues from the wax pattern can cause trouble (Fig. 9.5).

(iii) As the result of chemical reactions taking place in the molten metal during cooling and solidification. Among the best-known

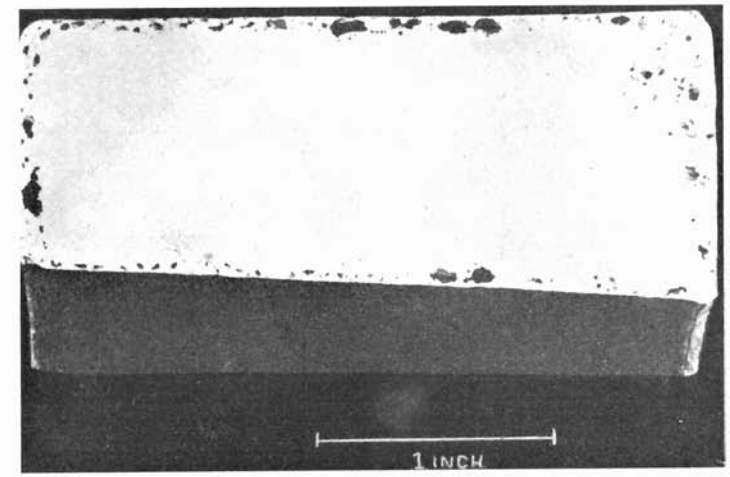

Fig. 9.3 Cross section of a cast gunmetal ring showing sub-surface pores produced by reaction of the molten metal with wet sand.

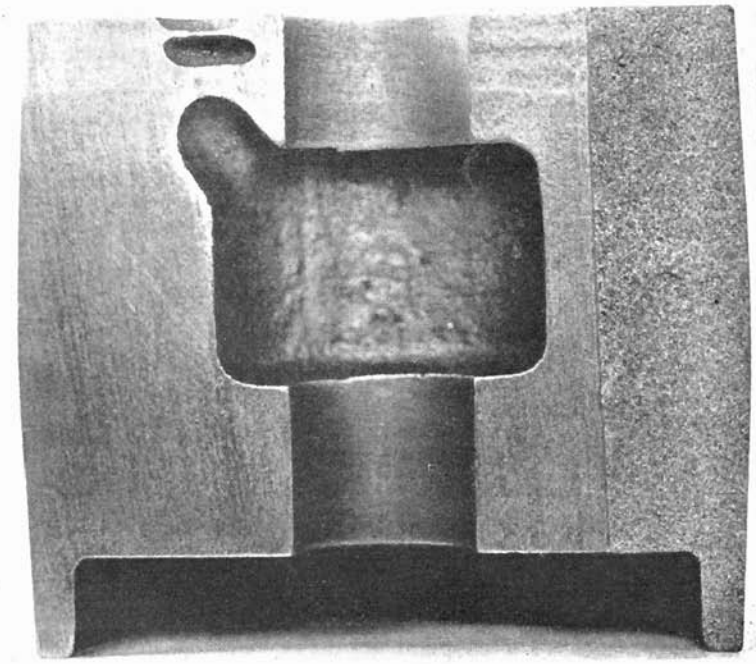

Fig. 9.4 Large blowholes produced in a grey-iron pulley wheel casting by gas evolved from a core.

9.2 COLD SHUTS

A 'cold shut' is produced when two streams of metal flowing from different regions in the casting meet without union. The shuts appear as apparent cracks or wrinkles in the surface, together with oxide

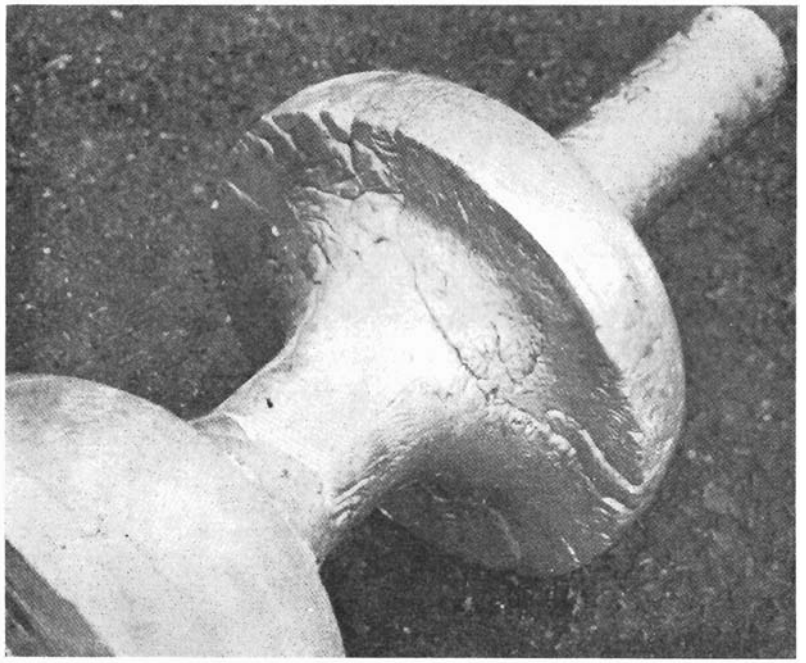

Fig. 9.11 *Cold shuts in an alloy steel casting.*

films (Figs. 9.10 and 9.11). This defect is usually the result of insufficient fluidity in the metal or the use of unsatisfactory methods of running and gating. Interrupted pouring can also give rise to cold shut formation.

The remedy is to increase fluidity either by raising the pouring temperature or by preheating the mould. Relocation of runners and ingates can often be equally effective.

9.3 CONTRACTION CRACKS

These are irregularly shaped cracks formed when the metal pulls itself apart while cooling in the mould or after removal from the

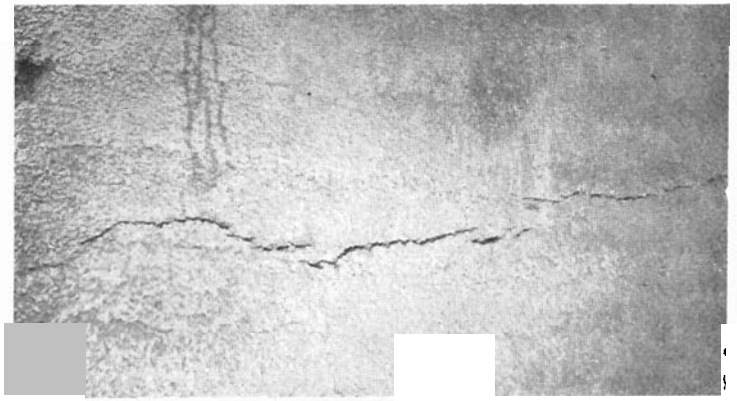

Fig. 9.12 *A hot tear in a steel casting.*

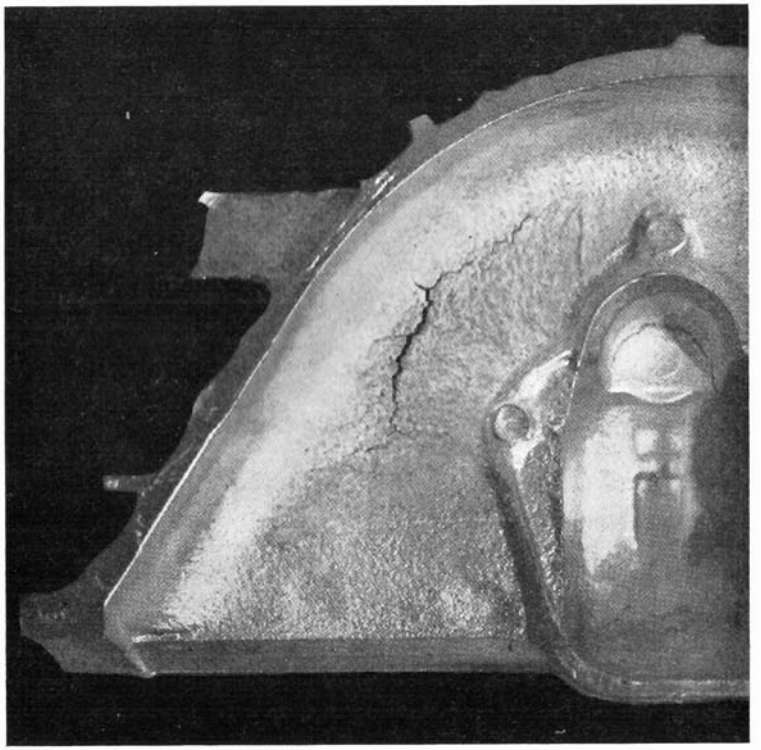

Fig. 9.13 *A contraction crack formed in an aluminium alloy die casting during cooling in the mould after solidification was complete.*

mould. When the crack appears during the last stages of solidification it is known as a 'hot tear' or a 'pull' (Fig. 9.12). In this case the crack faces are usually heavily oxidised. Hot tearing is most common in metals and alloys that have a wide freezing range, for then isolated regions of liquid become subjected to thermal stresses during cooling and fracture results.

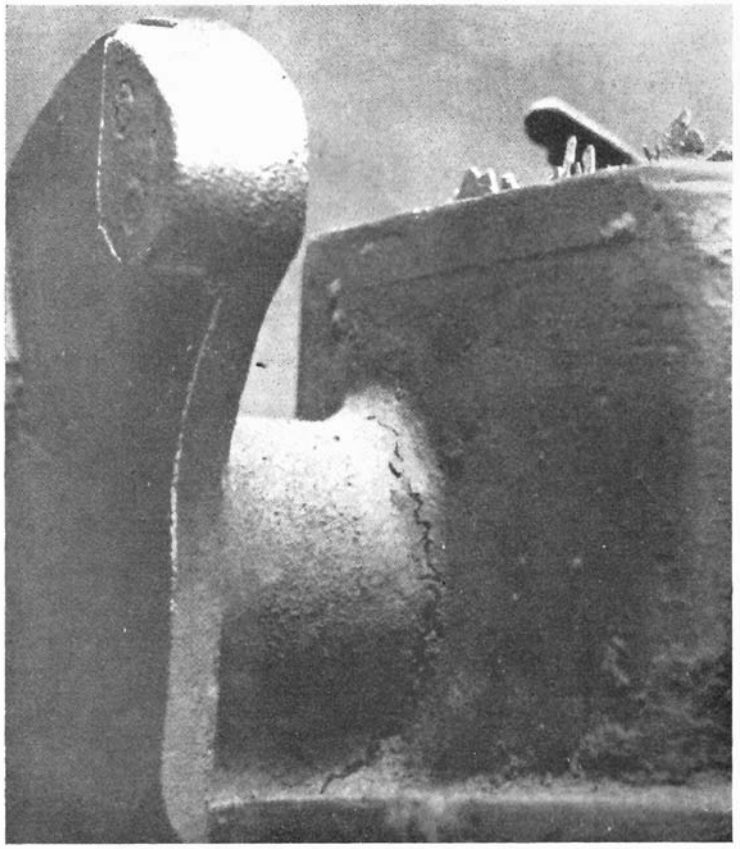

Fig. 9.14 *A contraction crack in the fillet of a small gunmetal sand casting.*

In other cases contraction cracks arise during the period when the metal is solid but still at a temperature where the mechanical strength is low (Fig. 9.13).

Contraction cracks and hot tears result from the hindered contraction of the casting; this gives rise to complex internal stresses.

Local hot spots or high thermal gradients contribute to these high stresses, particularly if the mould or core is rigid enough to restrict relative movement of the different parts of the casting.

Several steps are necessary if this type of defect is to be avoided. First, the cores and mould should be made more collapsible, for instance by incorporation of elastically soft material, *e.g.* cellulose, into the mould material or by minimising the compaction during moulding. In addition, alterations in design to avoid *abrupt* changes in section may be necessary. Hot spots can be eliminated, and thermal gradients controlled, by modification of the gating system or by the use of chills.

It should be noted that contraction cracks often have an external appearance very similar to a shrinkage cavity (*see* Section 9.6). They can be differentiated from the latter because there is no cavity or porous area beneath the surface. Furthermore, contraction cracks are normally located in positions clearly related to the geometry of the casting and to the restriction of free contraction by parts of the mould. A good example of this is shown in Fig. 9.14, where cracking has occurred in the fillet region between two parts of the casting.

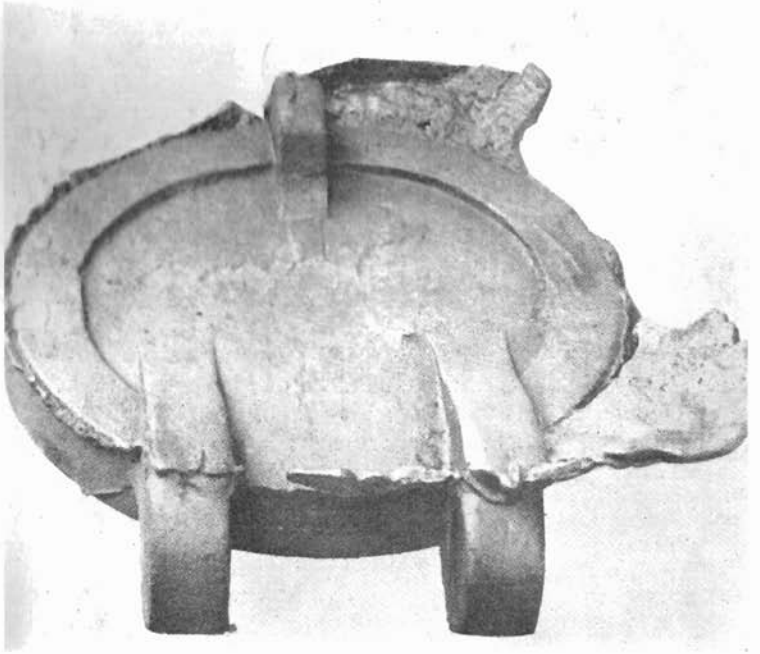

Fig. 9.15 *Excessive flash or fin along the parting line of a grey-iron casting.*

mould. When the crack appears during the last stages of solidification it is known as a 'hot tear' or a 'pull' (Fig. 9.12). In this case the crack faces are usually heavily oxidised. Hot tearing is most common in metals and alloys that have a wide freezing range, for then isolated regions of liquid become subjected to thermal stresses during cooling and fracture results.

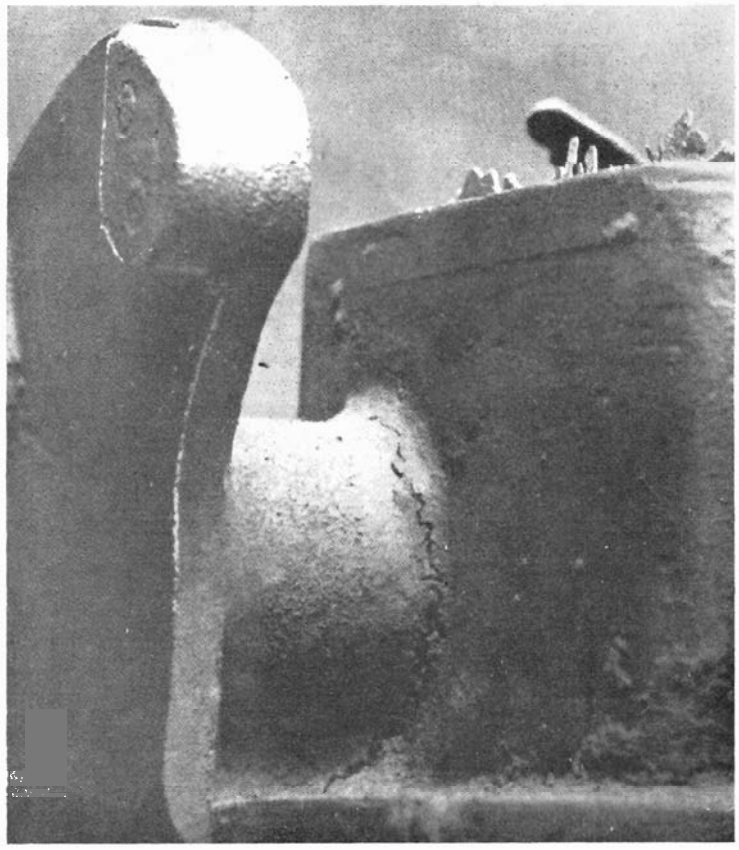

Fig. 9.14 *A contraction crack in the fillet of a small gunmetal sand casting.*

In other cases contraction cracks arise during the period when the metal is solid but still at a temperature where the mechanical strength is low (Fig. 9.13).

Contraction cracks and hot tears result from the hindered contraction of the casting; this gives rise to complex internal stresses.

Local hot spots or high thermal gradients contribute to these high stresses, particularly if the mould or core is rigid enough to restrict relative movement of the different parts of the casting.

Several steps are necessary if this type of defect is to be avoided. First, the cores and mould should be made more collapsible, for instance by incorporation of elastically soft material, *e.g.* cellulose, into the mould material or by minimising the compaction during moulding. In addition, alterations in design to avoid *abrupt* changes in section may be necessary. Hot spots can be eliminated, and thermal gradients controlled, by modification of the gating system or by the use of chills.

It should be noted that contraction cracks often have an external appearance very similar to a shrinkage cavity (*see* Section 9.6). They can be differentiated from the latter because there is no cavity or porous area beneath the surface. Furthermore, contraction cracks are normally located in positions clearly related to the geometry of the casting and to the restriction of free contraction by parts of the mould. A good example of this is shown in Fig. 9.14, where cracking has occurred in the fillet region between two parts of the casting.

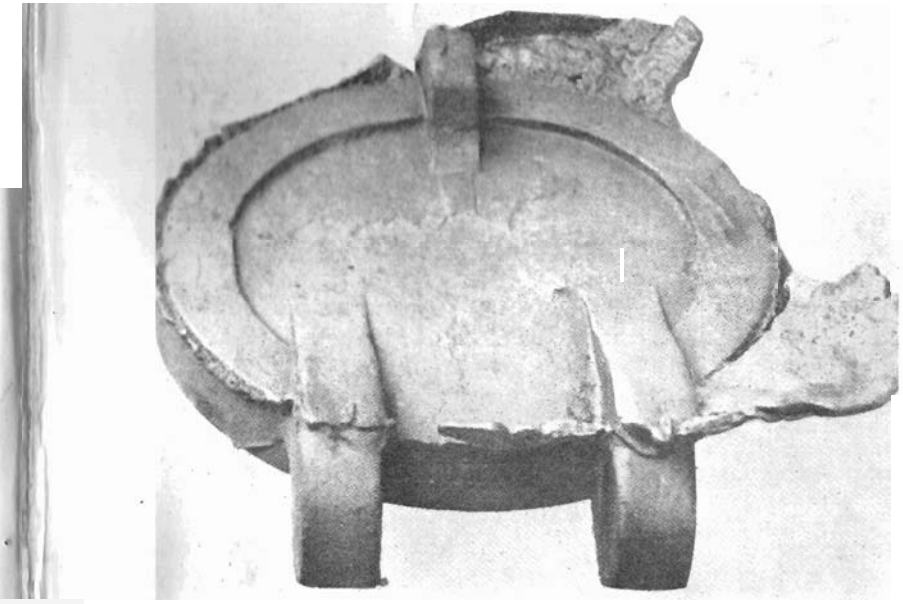

Fig. 9.15 *Excessive flash or fin along the parting line of a grey-iron casting.*

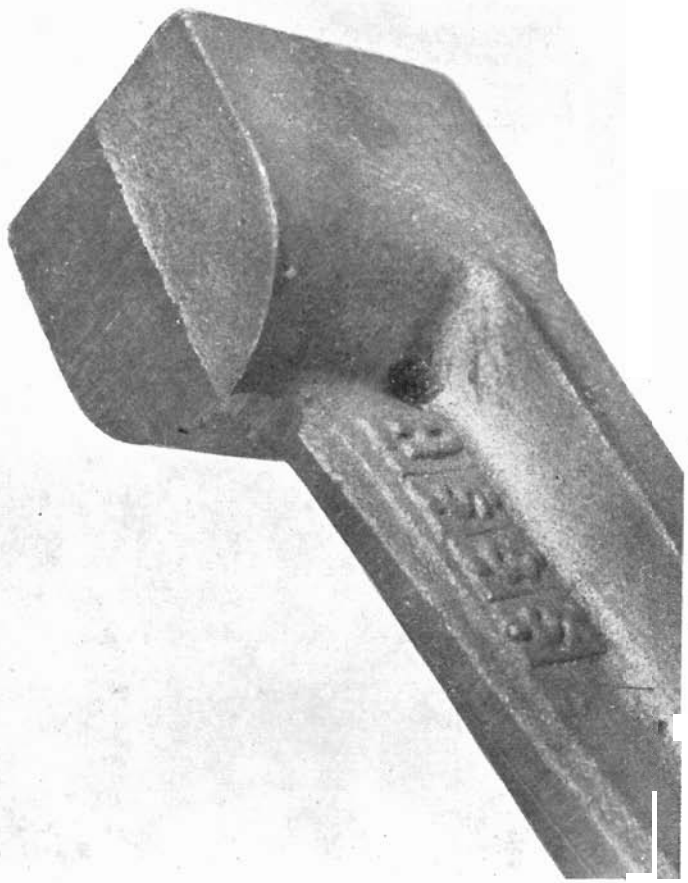

Fig. 9.21 Surface shrinkage in a grey-iron casting.

These cavities are frequently widely dispersed and located below the surface, and thus difficult to detect. Examples are shown in Figs. 9.19 and 9.20. If the shrinkage occurs near the surface, the cavities can be detected because of the presence of small depressions in the surface of the casting (Fig. 9.21). A similar case to this latter form is

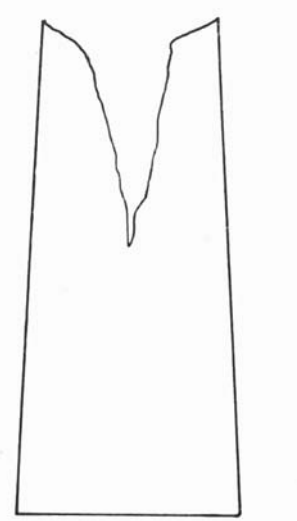

Fig. 9.22 Cross section of a killed steel ingot showing pipe development (schematic). The piped region must be cut off before working, thus giving a low useful metal yield.

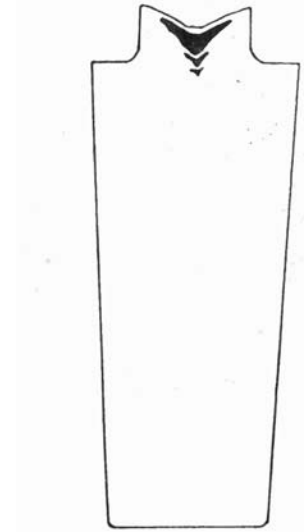

Fig. 9.23 Cross section of a killed steel ingot cast into a mould with a refractory hot top (schematic). Shrinkage is confined to the top of the ingot and yield is increased.

the large conical depression observed in the top of some ingots, and known as *pipe* (Fig. 9.22).

The major cause is the failure to obtain directional solidification towards desired heat centres such as risers or ingates. If the location of these feed points is bad, then shrinkage is much more likely. Relocation of feeding can help considerably. The use of higher pouring temperatures is also normally an advantage. Often proprietary methods involving exothermic heating in the mould cavity can be used to encourage directional solidification. When these are used together with judicious location of refractory inserts and chills to control heat transfer to the mould, shrinkage defects can largely be

APPENDIX 1

The Relationship Between the Interfacial Energies and the Contact Angle in Heterogeneous Nucleation

In Chapter 2 it was given that under stable conditions the contact angle, θ (*see* Fig. A1.1), was related to the surface energies of the liquid–crystal interface, γ_{LC}, the crystal–substrate interface, γ_{CS}, and the liquid–substrate interface, γ_{LS}, by

$$\cos\theta = \frac{\gamma_{LS} - \gamma_{CS}}{\gamma_{LC}}$$

A superficial examination of Fig. A1.1 might suggest that this relation is an obvious consequence of the force balance. This appendix

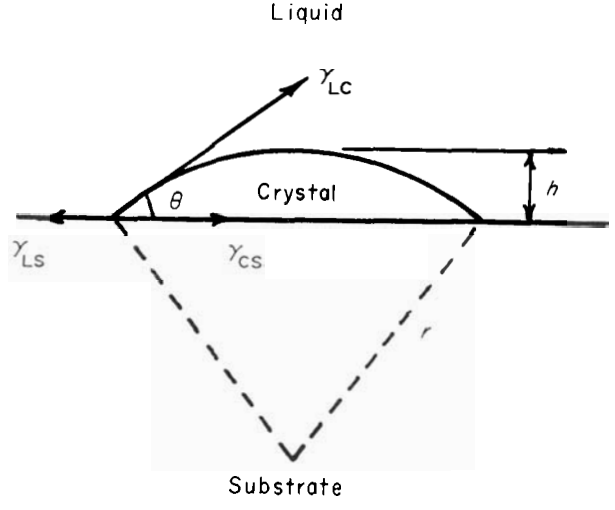

Fig. A1.1 Spherical cap of solid formed on a planar substrate.

gives a rigorous proof based on a method of virtual displacements. The proof depends on the assumption that the condition for stability is that the total surface energy should remain unchanged for a virtual displacement at constant volume.

Considering a spherical cap of radius r (Fig. A1.1), the area of the cap in contact with the surface is

$$A_1 = \pi r^2 \sin^2\theta \tag{A1.1}$$

The area of the cap in contact with the liquid is

$$A_2 = 2\pi r^2(1 - \cos\theta) \tag{A1.2}$$

Total excess surface energy introduced into the system by the formation of the spherical cap equals

$$A_1(\gamma_{CS} - \gamma_{LS}) + A_2 \cdot \gamma_{LC}$$

For a small displacement the assumption above means that

$$dA_1(\gamma_{CS} - \gamma_{LS}) + dA_2 \cdot \gamma_{LC} = 0$$

that is

$$\frac{\gamma_{LS} - \gamma_{CS}}{\gamma_{LC}} = \frac{dA_2}{dA_1}$$

Differentiating eqns. (A1.1) and (A1.2) and substituting gives, after simplification,

$$\frac{\gamma_{LS} - \gamma_{CS}}{\gamma_{LC}} = \frac{r \cdot \sin\theta + 2(1 - \cos\theta)(dr/d\theta)}{r \cdot \sin\theta\cos\theta + \sin^2\theta(dr/d\theta)} \tag{A1.3}$$

The volume of a spherical cap is

$$V = \tfrac{1}{3}\pi r^3(2 - 3\cos\theta + \cos^3\theta)$$

For constant volume, $dV = 0$. Thus

$$\frac{dr}{d\theta} = \frac{r \cdot \sin\theta(1 + \cos\theta)}{(1 - \cos\theta)(2 + \cos\theta)}$$

Substituting this in eqn. (A1.3) leads to

$$\frac{\gamma_{LS} - \gamma_{CS}}{\gamma_{LC}} = \cos\theta$$